**Title**

Organometallic Au(III) Reagents for the Modular Preparation of Macromolecular Conjugates



**Author**

Kunkel, Grace

**Publication Date**

2024

Peer reviewed|Thesis/dissertation

UNIVERSITY OF CALIFORNIA

Los Angeles

# Organometallic Au(III) Reagents for the Modular Preparation of Macromolecular Conjugates

A dissertation submitted in partial satisfaction of the requirements for the degree Doctor of Philosophy in Chemistry

by

Grace Elizabeth Kunkel

2024

ABSTRACT OF THE DISSERTATION

Organometallic Au(III) Reagents for the Modular

Preparation of Macromolecular Conjugates

by

Grace Elizabeth Kunkel

Doctor of Philosophy in Chemistry

University of California, Los Angeles, 2024

Professor Heather D. Maynard, Chair

The vast applications realized through polymer chemistry are in part due to the numerous possible polymeric architectures that contribute to distinct structure-property relationships. Despite the utility of designed polymeric scaffolds, their synthesis can pose a significant challenge. In the case of macromolecular targets not polymerizable by similar methods, post-polymerization conjugation is required. This synthetic strategy necessitates a highly efficient conjugation due to the low concentration of reactive units and the steric hindrance caused by polymer chains.

The Maynard and Spokoyny labs have developed isolable and bench-stable (Me-DalPhos)Au(III)Aryl (Me-DalPhos = ($Ad_2P(o\text{-}C_6H_4)NMe_2$) reagents for the application of cysteine *S*-arylation. This *S*-arylation chemistry is highly chemoselective, pH tolerant (0.5-14), and rapid at room temperature. These Au(III)-oxidative addition complexes were hypothesized to be excellent facilitators of complex polymer architecture synthesis *via* ligand exchange and subsequent reductive elimination with a thiol-containing macromolecular coupling partner. The selectivity of (Me-DalPhos)Au(I)Cl for aryl iodide oxidative addition and the thiophilicty of Au(III) permits the use of many desirable side-chain functional groups without concern of cross-reactivity. Furthermore, the efficiency of this reaction was hypothesized to obviate the necessity of large excess equivalents needed for polymer conjugations.

First, polymer functionalization was achieved *via* Au(III)-mediated direct conjugation of thiol-containing small molecule and polymer coupling partners (**Chapter 2**). Controlled synthesis of both thiol- and aryl iodide-capped polymers was achieved by synthetically modifying small molecule initiators and termination moieties for polymers prepared by reversible addition fragmentation chain-transfer (RAFT) polymerization, ring opening polymerization (ROP), ring opening metathesis polymerization (ROMP), and atom transfer radical polymerization (ATRP). All aryl iodide polymers underwent oxidative addition with (Me-DalPhos)Au(I)Cl at room temperature under ambient conditions to afford Au(III)-polymer precursors. Complete conversion was observed by $^1$H NMR. Reductive elimination reactions between thiol- and Au(III)-capped polymers occurred in one hour, in open air, and using an equimolar ratio of polymer precursors. Complete conversion to block copolymer products was observed by size exclusion chromatography (SEC), $^1$H NMR, and 2D Diffusion Ordered Spectroscopy (DOSY) NMR.

Next, cyclic polymer-protein conjugates were prepared using Au(III)-chemistry and compared to linear polymer-protein counterparts (**Chapter 3**). Cyclic polymers were synthesized *via* a Williamson etherification bimolecular ring closure strategy. This was followed by oxidative addition with Au(I) to yield a cyclic Au(III)-PEG reagent with minimal linear contaminants. Cyclic Au(III) PEG was conjugated to a model protein containing one thiol, DARPin. For direct comparison, a linear Au(III) PEG reagent of the same molecular weight also underwent DARPin reductive elimination. We compared activity, thermal stability, secondary structure *via* circular dichroism (CD), and hydrodynamic radii *via* SDS-PAGE and FPLC for cyclic polymer-DARPin conjugates with their linear polymer counterparts. While biophysical differences were minimal for these bioconjugates, the hydrodynamic radius was smaller for that of the cyclic polymer conjugate which may be useful for drug formulations. Furthermore, molecular dynamics calculations demonstrated that the cyclic polymer interacted less frequently with the protein active site. This work adds to the scientific understanding of the effect of polymer architecture on protein-polymer conjugate properties.

Then, polymeric Au(III) reagents mediated the regioselective formation of block copolymer proteins and protein heterodimers (**Chapter 4**). Small molecule competition studies *via* LCMS and buried volume calculations were used to determine aryl-iodide substrates that could impart *S*-arylation regioselectivity for Au(III) reagents. A *meta*-xylene derivative was determined to be the optimal substrate, as it provided steric hindrance that slowed the kinetic rate of *S*-arylation. Subsequently, a heterotelechelic PEG reagent (2 kDa) was synthesized, where one terminus contained a *para* aryl-iodide and the remaining termini contained a *meta*-xylene aryl-iodide. Oxidative addition yielded a regioselective and bifunctional *S*-arylation PEG reagent. This PEG reagent underwent reductive elimination with DARPin to produce a monopegylated product,

with no observable formation of protein homodimer *via* SDS-PAGE and LCMS. Without further purification, a second reductive elimination with a thiol-terminated pNIPAM and a thiolated glucagon was performed, highlighting the practicality of this one-pot method.

Finally, electrospun polymer fibers were functionalized using Au(III) organometallic complexes (**Chapter 5**). Polyesters were prepared with aryl-iodide end-groups and electrospun into fiber mats under positive voltage. Upon discovery that the polyester fiber morphology was not maintained during oxidative addition due to solubility in DCM, a copolymer of norbornene imide derivatives containing hydrophilic amines and aryl iodides for conjugation was prepared by ROMP. However, gold nanoparticles were observed during oxidative addition of these polyimide fibers in DCM, despite a more compatible solubility relationship. As an alternative, a copolymer of norbornene imide derivatives containing thiols and hydrophobic butyl groups was synthesized for reductive elimination with pre-made Au(III) oxidative addition complexes in water. Surprisingly, fiber morphology was disturbed as observed by SEM, and successful conjugation could not be verified when compared to negative controls.

This dissertation of Grace Elizabeth Kunkel is approved.

Timothy J. Deming

Jose A. Rodriguez

Yi Tang

Heather D. Maynard, Committee Chair

University of California, Los Angeles

2024

*This dissertation is dedicated to me, as I was to it. May we all pursue our dreams, despite our fear, with stubborn tenacity. The time will pass anyway.*

## Table of Contents

**ABSTRACT OF THE DISSERTATION** ..... **ii**

**Table of Contents** ..... **viii**

**List of Figures** ..... **xii**

**List of Tables** ..... **xxv**

**List of Abbreviations** ..... **xxvi**

**Acknowledgments** ..... **xxviii**

**Vita** ..... **xxxi**

**Chapter 1: Techniques for the Preparation of Macromolecular Structures†** ..... **1**

**1.1 Introduction** ..... **2**

**1.2 Polymerization Strategies** ..... **3**

1.2.1 Graft-to ..... 3

1.2.2 Graft-from ..... 4

**1.3 Common Targets for Biomolecule Conjugation** ..... **5**

1.3.1 Natural Nucleophilic Amino Acid Residues ..... 5

1.3.2 C- and N- Terminus ..... 6

1.3.3 Unnatural Amino Acids ..... 7

**1.4 Outlook: Conjugation *via* Organometallic Au(III) Reagents** ..... **8**

**1.5 References** ..... **9**

**Chapter 2: Efficient End-Group Functionalization and Diblock Copolymer Synthesis *via* Au(III) Polymer Reagents[†] ..... 18**

**2.1 Introduction ..... 19**

**2.2 Results and Discussion ..... 21**

2.2.1 Synthesis of Aryl Iodide and Au(III) OAC Heterotelechelic Polymers ..... 21

2.2.2 End-group modification and DBCP Synthesis *via* Au(III) OAC Polymers ..... 23

**2.3 Conclusion ..... 26**

**2.4 Experimental ..... 27**

2.4.1 Materials ..... 27

2.4.2 Analytical Techniques ..... 27

2.4.3 Methods ..... 29

**2.6 Appendix I ..... 64**

**2.5 References ..... 132**

**Chapter 3: Comparison of Cyclic and Linear PEG Conjugates[†] ..... 138**

**3.1 Introduction ..... 139**

**3.2 Results and Discussion ..... 140**

3.2.1 Synthesis of Cyclic and Linear 2 kDa PEG-Au(III) Reagents ..... 140

3.2.2. Preparation of PEG-T4L Conjugates ..... 143

3.2.3 Characterization of PEG-T4L Conjugates ..... 145

**3.3 Conclusion ..... 148**

**3.4 Experimental ..... 148**

3.4.1 Materials ..... 148

3.4.2 Analytical Techniques ..... 148

3.4.3 Methods ..... 151

**3.6 Appendix II ..... 164**

**3.5 References ..... 186**

**Chapter 4: Access to Biomacromolecular Heterodimers *via* Regioselective Au(III) *S*-Arylation PEG Reagents ..... 195**

**4.1 Introduction ..... 196**

**4.2 Results and Discussion ..... 199**

4.2.1 Synthesis of a PEG (2 kDa) Heterobifunctional Linker ..... 199

4.2.2 Construction of Block Copolymer-Protein Conjugates and Protein Heterodimers ..... 200

**4.3 Conclusion ..... 203**

**4.4 Experimental ..... 203**

4.4.1 Materials ..... 203

4.4.2 Analytical Techniques ..... 204

4.4.3 Methods ..... 205

**4.6 Appendix III ..... 215**

**4.5 References ..... 224**

**Chapter 5: Functionalization of Electrospun Polymer Fibers *via* Organometallic Au(III) Reagents ..... 228**

**5.1 Introduction ..... 229**

**5.2 Results and Discussion ..... 231**

5.2.1. Preparation of Au(III) Functionalized Electrospun Fibers via Aryl Iodide Polyesters ..... 231

5.2.2. Preparation of Au(III) Functionalized Electrospun Fibers *via* Aryl Iodide Polynorbornene Imides ..... 233

5.2.3. Preparation of Au(III)-mediated Functionalized Electrospun Fibers *via* Thiol Polynorbornene Imides ..... 234

**5.3 Conclusion ..... 237**

**5.4 Experimental ..... 238**

5.4.1 Materials ..... 238

5.4.2 Analytical Techniques ..... 238

5.4.3 Methods ..... 241

**5.6 Appendix IV ..... 249**

**5.5 References ..... 260**

## List of Figures

**Figure 1.1:** Summary of protein-polymer conjugation strategies: A) Graft-to, B) Graft-from, C) Graft-through……...2

**Figure 2.1** A) General Au(III) polymer reagent synthesis (Au(III)=[(Me-DalPhos)Au(III)Cl]$^{+}$ $SbF_6^{-}$). B) Ring opening polymerization of caprolactone and synthesis of OAC. C) Ring opening metathesis polymerization of N-butylnorbornene imide and synthesis of OAC. D) Atom transfer radical polymerization of pentafluorostyrene and synthesis of OAC…….....21

**Figure 2.2** A) Scheme of modified mono-telechelic polymer synthesis *via S*-arylation of thiolated biotin (**8a**), thiolated coumarin (**9a**), and sodium thioglucose (**TG**) with **1a** or **3a**. B) MALDI-TOF mass spectra of **1** and **1a-8a** with magnified inset. Expected and calculated Δ*m/z* differences between repeat units of **1a** and end groups of **1a** and **1a-8a**……..22

**Figure 2.3** A) pCL-*b*-pBNI (**18**) *S*-arylation scheme B) DOSY NMR spectrum of pCL-*b*-pBNI (**18**) in $CD_3CN$……25

**Figure 2.4** $^{1}H$ NMR spectrum of *exo-n*-butylnorborneneimide (**19**) in $CDCl_3$ at 25 ºC……64

**Figure 2.5** $^{13}C$ NMR spectrum of exo-n-butylnorborneneimide (**19**) in $CDCl_3$ at 25 ºC……..65

**Figure 2.6** $^{1}H$ NMR spectrum of 3-O (**20**) in acetone-$d_6$ at 25 ºC…….66

**Figure 2.7** $^{19}F\{^{1}H\}$ NMR spectrum of 3-O (**20**) in acetone-$d_6$ at 25 ºC……67

**Figure 2.8** $^{13}C$ NMR spectrum of 3-O (**20**) in acetone-$d_6$ at 25 ºC……68

**Figure 2.9** $^{1}H$ NMR spectrum of 2-(tritylthio)ethan-1-ol (**11**) in $CD_2Cl_2$ at 25 ºC……69

**Figure 2.10** $^{13}C$ NMR spectrum of 2-(tritylthio)ethan-1-ol (**11**) in $CD_2Cl_2$ at 25 ºC…….70

**Figure 2.11** $^{1}H$ NMR spectrum of 2-(4-iodophenoxy)ethan-1-ol (**2**) in DMSO-$d_6$ at 25 ºC……..71

**Figure 2.12** $^{13}C$ NMR spectrum of 2-(4-iodophenoxy)ethan-1-ol (**2**) in DMSO-$d_6$ at 25 ºC……72

**Figure 2.13** $^{1}H$ NMR spectrum of 2-(4-iodophenoxy)ethyl 2-bromo-2-methylpropanoate (**5**) in $CDCl_3$ at 25 ºC……73

**Figure 2.14** $^{13}C$ NMR spectrum of 2-(4-iodophenoxy)ethyl 2-bromo-2-methylpropanoate (**5**) in $CDCl_3$ at 25 ºC……74

**Figure 2.15** $^{1}H$ NMR spectrum of (*Z*)-1,4-bis(4-iodophenoxy)but-2-ene (**4**) in $CDCl_3$ at 25 ºC..75

**Figure 2.16** $^{13}C$ NMR spectrum of (*Z*)-1,4-bis(4-iodophenoxy)but-2-ene (**4**) in $CDCl_3$ at 25 ºC..76

**Figure 2.17** $^{1}H$ NMR spectrum of 2-iodo-*N*,*N*-dimethylaniline (**21**) in $CDCl_3$ at 25 ºC……77

**Figure 2.18** $^{13}C$ NMR spectrum of 2-iodo-*N*,*N*-dimethylaniline (**21**) in $CDCl_3$ at 25 ºC……..78

**Figure 2.19** $^{1}H$ NMR spectrum of Me-DalPhos (**22**) in $CD_2Cl_2$ at 25 ºC……..79

**Figure 2.20** $^{31}P\{^{1}H\}$ NMR spectrum of Me-DalPhos (**22**) in $CD_2Cl_2$ at 25 ºC……80

**Figure 2.21** $^{1}H$ NMR spectrum of (Me-DalPhos)$Au^{I}Cl$ (**7**) in $CD_2Cl_2$ at 25 ºC……....81

**Figure 2.22** $^{31}P\{^{1}H\}$ NMR spectrum of (Me-DalPhos)$Au^{I}Cl$ (**7**) in $CD_2Cl_2$ at 25 ºC……82

**Figure 2.23** $^{1}H$ NMR spectrum of 2-(tritylthio)ethan-1-ammonium trifluoroacetate (**23**) in MeOD at 25 ºC……...83

**Figure 2.24** $^{13}C$ NMR spectrum of 2-(tritylthio)ethan-1-ammonium trifluoroacetate (**23**) in $CD_3CN$ at 25 ºC.....84

**Figure 2.25** $^{1}H$ NMR spectrum of 2-oxo-N-(2-(tritylthio)ethyl)-2H-chromene-3-carboxamide (**9**) in $CD_2Cl_2$ at 25 ºC……..85

**Figure 2.26** $^{13}C$ NMR spectrum of 2-oxo-N-(2-(tritylthio)ethyl)-2H-chromene-3-carboxamide (**9**) in $CD_2Cl_2$ at 25 ºC……..86

**Figure 2.27** $^{1}H$ NMR spectrum of *N*-(2-mercaptoethyl)-2-oxo-2*H*-chromene-3-carboxamide (**9a**) in $CDCl_3$ at 25 ºC……87

**Figure 2.28** $^{13}C$ NMR spectrum of *N*-(2-mercaptoethyl)-2-oxo-2*H*-chromene-3-carboxamide (**9a**) in $CDCl_3$ at 25 ºC……88

**Figure 2.29** $^{1}H$ NMR spectrum of 5-((3a*S*,4*S*,6a*R*)-2-oxohexahydro-1*H*-thieno[3,4-*d*]imidazol-4-yl)-*N*-(2-(tritylthio)ethyl)pentanamide (**8**) in $CD_2Cl_2$ at 25 ºC……89

**Figure 2.30** $^{13}C$ NMR spectrum of 5-((3a*S*,4*S*,6a*R*)-2-oxohexahydro-1*H*-thieno[3,4-*d*]imidazol-4-yl)-*N*-(2-(tritylthio)ethyl)pentanamide (**8**) in $CD_2Cl_2$ at 25 ºC……..…..90

**Figure 2.31** $^{1}H$ NMR spectrum of N-(2-mercaptoethyl)-5-((3aS,4S,6aR)-2-oxohexahydro-1H-thieno[3,4-d]imidazol-4-yl)pentanamide (**8a**) in MeOD at 25 ºC……..91

**Figure 2.32** $^{13}C$ NMR spectrum of N-(2-mercaptoethyl)-5-((3aS,4S,6aR)-2-oxohexahydro-1H-thieno[3,4-d]imidazol-4-yl)pentanamide (**8a**) in MeOD at 25 ºC……..92

**Figure 2.33** $^{1}H$ NMR spectrum of pCL-aryl iodide (**1**) in $CD_3CN$ at 25 ºC……..93

**Figure 2.34** DMF SEC trace of pCL-aryl iodide (**1**)……93

**Figure 2.35** $^{1}H$ NMR spectrum of pCL-Au(III) (**1a**) in $CD_3CN$ at 25 ºC……94

**Figure 2.36** $^{31}P\{^{1}H\}$ NMR spectrum of pCL-Au(III) (**1a**) in $CD_3CN$ at 25 ºC……95

**Figure 2.37** $^{1}H$ NMR spectrum of pBNI-aryl iodide (**3**) in $CD_3CN$ at 25 ºC. Peak "c" contains both cis- and trans- alkene protons……....96

**Figure 2.38** DMF SEC trace of pBNI-aryl iodide (**3**). ……..96

**Figure 2.39** $^{1}H$ NMR spectrum of pBNI-Au(III) (**3a**) in $CD_3CN$ at 25 ºC……97

**Figure 2.40** $^{31}P\{^{1}H\}$ NMR spectrum of pBNI-Au(III) (**14a**) in $CD_2Cl_2$ at 25 ºC……..…98

**Figure 2.41** $^{1}H$ NMR spectrum of pBNI-aryl iodide (**16**) in $CD_3CN$ at 25 ºC……..99

**Figure 2.42** DMF SEC trace of pBNI-aryl iodide (**16**)……99

**Figure 2.43** $^{1}H$ NMR spectrum of pBNI-Au(III) (**16a**) in $CD_3CN$ at 25 ºC……100

**Figure 2.44** $^{31}P\{^{1}H\}$ NMR spectrum of pBNI-Au(III) (**16a**) in $CD_2Cl_2$ at 25 ºC……101

**Figure 2.45** $^{1}H$ NMR spectrum of pPFS-aryl iodide (**6**) in $CD_2Cl_2$ at 25 ºC……102

**Figure 2.46** $^{19}F\{^{1}H\}$ NMR spectrum of pPFS-aryl iodide (**6**) in acetone-$d_6$ at 25 ºC…….103

**Figure 2.47** THF SEC trace of pPFS-aryl iodide (**6**). ……104

**Figure 2.48** $^{1}H$ NMR spectrum of pPFS-Au(III) (**6a**) in $CD_2Cl_2$ at 25 ºC……105

**Figure 2.49** $^{19}F\{^{1}H\}$ NMR spectrum of pPFS-Au(III) (**6a**) in $CD_2Cl_2$ at 25 ºC……..106

**Figure 2.50** $^{31}P\{^{1}H\}$ NMR spectrum of pPFS-Au(III) (**6a**) in $CD_2Cl_2$ at 25 ºC……..107

**Figure 2.51** $^{1}H$ NMR spectrum of biotin-p(CL) (**1a-8a**) in $CD_3CN$ at 25 ºC……..108

**Figure 2.52** $^{31}P\{^{1}H\}$ NMR spectrum of biotin-p(CL) (**1a-8a**) in $CD_3CN$ at 25 ºC……..108

**Figure 2.53** MALDI of biotin-p(CL) (**1a-8a**)……..109

**Figure 2.54** $^{1}H$ NMR spectrum of coumarin-pCL (**1a-9a**) in $CD_3CN$ at 25 ºC……110

**Figure 2.55** $^{31}P\{^{1}H\}$ NMR spectrum of coumarin-p(CL) (**1a-9a**) in $CD_3CN$ at 25 ºC……110

**Figure 2.56** $^{1}H$ NMR spectrum of glucose-p(CL) (**1a-TG**) in $CD_3CN$ at 25 ºC……111

**Figure 2.57** $^{31}P\{^{1}H\}$ NMR spectrum of glucose-p(CL) (**1a-TG**) in $CD_3CN$ at 25 ºC…….112

**Figure 2.58** $^{1}H$ NMR spectrum of biotin-p(BNI) (**3a-8a**) in DMSO-$d_6$ at 25 ºC……112

**Figure 2.59** $^{31}P\{^{1}H\}$ NMR spectrum of biotin-p(BNI) (**3a-8a**) in DMSO-$d_6$ at 25 ºC……113

**Figure 2.60** $^{1}H$ NMR spectrum of coumarin-p(BNI) (**3a-9a**) in DMSO-$d_6$ at 25 ºC……113

**Figure 2.61** $^{31}P\{^{1}H\}$ NMR spectrum of coumarin-p(BNI) (**3a-9a**) in DMSO-$d_6$ at 25 ºC……..114

**Figure 2.62** $^{1}H$ NMR spectrum of glucose-p(BNI) (**3a-TG**) in DMSO-$d_6$ at 25 ºC……114

**Figure 2.63** $^{31}P\{^{1}H\}$ NMR spectrum of glucose-p(BNI) (**3a-TG**) in DMSO-$d_6$ at 25 ºC……115

**Figure 2.64** $^{1}H$ NMR spectrum of pNIPAM (**10**) in $CDCl_3$ at 25 ºC……115

**Figure 2.65** DMF SEC trace of pNIPAM (**10**)……116

**Figure 2.66** $^{1}H$ NMR spectrum of pNIPAM-SH (**10a**) in $CDCl_3$ at 25 ºC……116

**Figure 2.67** UV-vis spectroscopy of dithiobenzoate-containing p(NIPAM) (**10**) (black) and the resulting reduced thiol end-group pNIPAM-SH (**10a**) (green)……..117

**Figure 2.68** $^{1}$H NMR spectrum of pCL-Trt (**12**) in $CD_3CN$ at 25 ºC……117

**Figure 2.69** DMF SEC trace of pCL-Trt (**12**)……..118

**Figure 2.70** $^{1}$H NMR spectrum of pCL-SH (**12a**) in $CD_3CN$ at 25 ºC……118

**Figure 2.71** $^{1}$H NMR spectrum of p(CL)-Trt (**17**) in $CDCl_3$ at 25 ºC……..119

**Figure 2.72** DMF SEC trace of p(CL)-Trt (**17**)……119

**Figure 2.73** $^{1}$H NMR spectrum of p(CL)-SH (**17a**) in $CDCl_3$ at 25 ºC……120

**Figure 2.74** $^{1}$H NMR spectrum of p(NIPAM)-*b*-p(CL) (**13**) in $CD_2Cl_2$ at 25 ºC……..121

**Figure 2.75** $^{31}$P{$^{1}$H} NMR spectrum of p(NIPAM)-*b*-p(CL) (**13**) in $CD_2Cl_2$ at 25 ºC…….121

**Figure 2.76** DOSY spectrum of p(NIPAM)-*b*-p(CL) (**13**) in $CD_2Cl_2$ at 25 ºC…….122

**Figure 2.77** DMF SEC trace of p(NIPAM)-*b*-p(CL) (**13**)……122

**Figure 2.78** $^{1}$H NMR spectrum of p(CL)-*b*-p(BNI) (**14**) in $CD_3CN$ at 25 ºC……123

**Figure 2.79** $^{31}$P{$^{1}$H} NMR spectrum of p(CL)-*b*-p(BNI) (**14**) in $CD_3CN$ at 25 ºC……..124

**Figure 2.80** DOSY NMR spectrum of p(CL)-*b*-p(BNI) (**14**) in $CD_3CN$ at 25 ºC……125

**Figure 2.81** DMF SEC trace of p(CL)-*b*-p(BNI) (**14**)……..125

**Figure 2.82** $^{1}$H NMR spectrum of p(CL)-*b*-p(BNI) (**18**) in $CDCN_3$ at 25 ºC. Peak "a" contains both cis- and trans- alkene protons……...126

**Figure 2.83** $^{31}$P{$^{1}$H} NMR spectrum of p(CL)-*b*-p(BNI) (**18**) in $CDCN_3$ at 25 ºC…….127

**Figure 2.84** DOSY NMR spectrum of p(CL)-*b*-p(BNI) (**18**) in $CDCN_3$ at 25 ºC……128

**Figure 2.85** DMF SEC trace of p(CL)-*b*-p(BNI) (**18**)……..128

**Figure 2.86** $^{1}$H NMR spectrum of p(CL)-*b*-p(PFS) (**15**) in $CD_2Cl_2$ at 25 ºC……129

**Figure 2.87** $^{31}$P{$^{1}$H} NMR spectrum of p(CL)-*b*-p(PFS) (**15**) in $CD_3CN$ at 25 ºC……..129

**Figure 2.88** $^{19}F\{^{1}H\}$ NMR spectrum of p(CL)-*b*-p(PFS) (**15**) in $CD_3CN$ at 25 ºC……..130

**Figure 2.89** DOSY NMR spectrum of p(CL)-*b*-p(PFS) (**15**) in $CD_2Cl_2$ at 25 ºC……..131

**Figure 2.90** THF SEC trace of p(CL)-*b*-p(PFS) (**15**)……131

**Figure 3.1** A) Williamson ether synthesis of cyclic 2 kDa PEG-aryl iodide (2). B) DMF SEC of linear 2 kDa PEG and **2**. C) $^{1}H$ NMR of **2** in $CD_3CN$. D) Oxidative addition of **2** with (Me-DalPhos)AuCl and $AgSbF_6$ to yield **3**. E) $^{31}P\{^{1}H\}$ NMR of **3** in $CD_3CN$……141

**Figure 3.2** A) Synthetic scheme representing T4L bioconjugation (PDB ID: 2HUK) to 2 kDa cyclic PEG (**3**) and 2 kDa linear mPEG (**4**), resulting in conjugates **5** and **6**, respectively. B) Coomassie-stained SDS-PAGE gel of T4L, **6**, and **5**. By ImageJ optical densitometry, **6** and **5** are 96% and 98% converted from T4L starting material, respectively. C) LCMS of **5**. Calculated mass is 20661.6 Da, observed mass is 20662.3 Da. D) LCMS of **6**. Calculated mass is 20693.6 Da, observed mass is 20694.7 Da. E) SEC FPLC spectrum for **5** and **6**…….143

**Figure 3.3** A) Normalized CD spectrum of T4L, **5**, and **6** at 23 ºC showing no observable difference in helicity. B) Lysozyme activity fluorescence assay of T4L, **5**, and **6**. N = 3 for each group. An ordinary one-way ANOVA statistical analysis was performed. **$p < 0.005$. ns = not significantly different……....145

**Figure 3.4** Average polymer distribution isosurfaces resulting from three independent 1000 ns molecular dynamic simulations for A) **6** and B) **5.** Although there is no protein conformational difference induced by the polymer chain architecture, the cyclic PEG interacts less frequently with the T4L binding site compared to its linear counterpart……147

**Figure 3.5** $^{1}H$ NMR of (5-iodo-1,3-phenylene)dimethanol (**7**) in $CD_3CN$ at 23 ºC…….164

**Figure 3.6** $^{13}C$ NMR of (5-iodo-1,3-phenylene)dimethanol (**7**) in $CD_3CN$ at 23 ºC……165

**Figure 3.7** $^{1}H$ NMR of 1,3-bis(bromomethyl)-5-iodobenzene (**1**) in $CD_3CN$ at 23 ºC……166

**Figure 3.8** $^{13}C$ NMR of 1,3-bis(bromomethyl)-5-iodobenzene (**1**) in $CD_3CN$ at 23 ºC……167

**Figure 3.9** $^{1}H$ NMR of cyclic PEG (2 kDa)-aryl iodide (**2**) in $CD_3CN$ at 23 ºC. Note that this data is shown in Figure 3.1 within Chapter 3 but is also shown larger here for easier viewing…….168

**Figure 3.10** DMF SEC of cyclic PEG (2 kDa)-aryl iodide (**2**) and commercial linear PEG (2 kDa). Note that this data is shown in Figure 3.1 within Chapter 3 but is also shown larger here for easier viewing. The SEC analysis for **2** is as follows: $M_n$ – 2.3 kDa, $M_w$ – 2.6 kDa, $Đ$ – 1.15…….169

**Figure 3.11** Analytical HPLC of cyclic PEG (2 kDa)-aryl iodide (**2**) at 280 nm…….169

**Figure 3.12** Intrinsic viscosity of cyclic PEG (2 kDa)-aryl iodide (**2**) and linear mPEG (2 kDa)-aryl iodide. The y-intercepts represent the intrinsic viscosity [η] for **2** and linear mPEG (2 kDa)-aryl iodide as 0.003 and 0.007 mL/mg, respectively…….170

**Figure 3.13** $^{1}H$ NMR of cyclic PEG (2 kDa) [(Me-DalPhos)AuCl][$SbF_6$] (**3**) in $CD_3CN$ at 23 ºC……..171

**Figure 3.14** $^{31}P\{^{1}H\}$ NMR of cyclic PEG (2 kDa) [(Me-DalPhos)AuCl][$SbF_6$] (**3**) in $CD_3CN$ at 23 ºC. The desired Au(III) resonance occurs at 75 ppm. The resonance at 52 ppm corresponds to residual (Me-DalPhos)Au(I)Cl starting material. Note that this data is shown in Figure 3.1 of within Chapter 3 but is also shown larger here for easier viewing……172

**Figure 3.15** A) SDS-PAGE gel of T4 lysozyme following purification. B) LCMS total ion chromatogram (TIC) of T4 lysozyme following purification. C) LCMS deconvoluted mass of T4 lysozyme following purification. Expected mass: 18605.27 Da. Observed mass: 18604.95 Da..173

**Figure 3.16** SDS-PAGE of T4 lysozyme (T4L) in PBS buffer (pH 6.5) reduced with 4, 6, or 8 eq TCEP·HCl for 1 hour at either 23 ºC or 37 ºC. These samples were run in conventional Laemmli buffer (non-reducing)……...174

**Figure 3.17** SDS-PAGE of crude T4L-PEG conjugates synthesized in PBS buffer (pH 6.5) for 3 hours, utilizing either 1.3 or 3 equivalents of **3** and **4** at either 23 ºC or 37 ºC. These samples were run in a reducing Laemmli buffer…….175

**Figure 3.18** SDS-PAGE of crude T4L-PEG conjugates synthesized in PBS buffer (pH 6.5) for 18 hours, utilizing 1.3 or 3 equivalents of **3** and **4** at either 23 ºC or 37 ºC. These samples were run in a reducing Laemmli buffer……...175

**Figure 3.19** SDS-PAGE of crude T4L-PEG conjugates **6** and **5** synthesized in PBS buffer (pH 6.5) for 18 hours at 23 ºC, utilizing 3 equivalents of **4** and **3**, respectively. These samples were run in a reducing Laemmli buffer. Based on ImageJ optical densitometry, conversion to conjugate **6** is 80% and conversion to **5** is 84%.....176

**Figure 3.20** LCMS total ion chromatogram (TIC) of T4L-cyclic PEG (**5**) following purification. The major peak at 8 min corresponds to the deconvoluted mass spectra shown in Figure 3.2 C. The minor peak at 10 min corresponds to 2 kDa PEG……177

**Figure 3.21** LCMS total ion chromatogram (TIC) of T4L-linear PEG (**6**) following purification. The major peak at 7.5 min corresponds to the deconvoluted mass spectra shown in Figure 3.2 D……...177

**Figure 3.22** CD spectrum of T4L and T4L conjugates (**5** and **6**) at 25 ºC showing no significant difference in helicity. Data has been normalized to the global minimum for each sample. Local minima for each sample are as follows – T4L: 210 and 223 nm, **5**: 209 and 223 nm, **6**: 210 and 223 nm. Note that this data is shown in Figure 3.3 but is also shown larger here for easier viewing…….178

**Figure 3.23** CD thermal denaturation curves at 223 nm of T4L and T4L conjugates (**5** and **6**) showing no significant difference in melting temperature ($T_m$) between 20 – 100 °C. Specifically, $T_m$ values for each sample are as follows – T4L: 56.8 ºC, **5**: 63.2 ºC, **6**: 62.6 ºC……179

**Figure 3.24** Lysozyme activity assay fluorescence output of T4L, **5**, and **6**. N = 3 for each group. Ordinary one-way ANOVA statistical analysis was performed. **p < 0.005. ns = not significantly different. Note that this data is shown in Figure 3.4 but is also shown larger here for easier viewing…….179

**Figure 3.25** ICP-OES Au calibration curve…….180

**Figure 3.26** Model systems used for RESP charge calculations. (A) Model system for C131 and phenyl linker in simulations for **6**. (B) Model system for C131 and phenyl linker in simulations for **5**. (C) Model system for PEG polymer. The RESP charges of the two units in the middle (shown in red box) were average and assigned to all the PEG units in the system. All the structures are optimized with B3LYP-D3/6-31G(d)……..….181

**Figure 3.27** Overlay of the trajectories. (A) Trajectories for **6**. (B) Trajectories for **5**. Left: front view, right: side view. Linear PEG polymer demonstrates more conformational flexibility in MD simulations compared to cyclic PEG conjugate……182

**Figure 3.28** Spatial distribution functions of linear PEG (Shown in light blue isosurface) and representative structures of simulations for **6**……...182

**Figure 3.29** Spatial distribution functions of cyclic PEG (Shown in light blue isosurface) and representative structures of simulations for **5**……...183

**Figure 3.30** Illustration of the minimum distance studied in Figures 3.28 and 3.29. The minimum distance is defined as the smallest distance between any pair of atoms from the active site and PEG

polymer. As the picture shows, the minimum distance for this structure is the distance between the carboxylic oxygen in D20 and a hydrogen in PEG (labeled by yellow dashed line)…….184

**Figure 3.31** (A) Minimum distance between active site (E11, D20, and T26) and PEG polymer along the simulations of **6**. Distribution of each is shown in the right panel. (B) Averaged distance distribution of three replicas, where 4.65% of the frames are considered having interaction between active site and PEG polymer (Minimum distance < 7.0 Å)…….185

**Figure 3.32** (A) Minimum distance between active site (E11, D20, and T26) and PEG polymer along the simulations of **5**. Distribution of each replica is shown in the right panel. (B) Averaged distance distribution of three replicas, where 0.04% of the frames are considered having interaction between active site and PEG polymer (Minimum distance < 7.0 Å)…….185

**Figure 4.1** A) Rapid PEGylation of DARPin using organometallic Au(III) PEG reagents. B) Construction of hetero-conjugates using bis-Au(III) reagents. C) Formation of heterodimeric block copolymer protein conjugates using polymeric bis-Au(III) reagents……198

**Figure 4.2** Synthetic scheme for the preparation of the heterobifunctional Au(III) PEG linker **4**. Additional synthetic detail can be obtained in experimental section……199

**Figure 4.3** A) Synthetic scheme of regioselective DARPin PEGylation with **4**. X = Cl or $HCO_2$ due to formic acid in the LC-MS mobile phase. B) Extracted total ion chromatogram of **5**. Calculated mass is 18602.0 Da with formate anion exchange. Observed mass is 18602.1 Da….201

**Figure 4.4** A) Reductive elimination scheme of **5** with p(NIPAM) (**6**) or thiolated glucagon (**GCG-SH**). B) SDS-PAGE gel of *S*-arylation of **5** with **6** to produce a DARPin block copolymer conjugate. Lane 1 - protein ladder. Lane 2 - DARPin (non-reducing conditions). Lane 3 - **5**. Lane 4 - **7**. C) **S**DS-PAGE gel of *S*-arylation of **5** with **GCG-SH** to produce a DARPin-GCG heterodimer. Lane 1 - protein ladder. Lane 2 - DARPin (non-reducing conditions). Lane 3 - **GCG-**

**SH**. Lane 4 - **5**. Lane 5 - **8**. Unless otherwise noted, all gel lanes were prepared under reducing conditions (5% mercaptoethanol v/v). See the experimental section for additional details…….202

**Figure 4.5** $^{1}H$ NMR of **1** in $CD_3CN$ at 298 K……..215

**Figure 4.6** $^{1}H$ NMR of **2** in $CD_3CN$ at 298 K……..216

**Figure 4.7** $^{1}H$ NMR of **3** in $CD_3CN$ at 298 K……..217

**Figure 4.8** $^{1}H$ NMR of **4** in $CD_3CN$ at 298 K……..218

**Figure 4.9** $^{31}P\{^{1}H\}$ NMR of **4** in $CD_3CN$ at 298 K……..219

**Figure 4.10** $^{1}H$ NMR of **7** in $CDCl_3$ at 298 K……..220

**Figure 4.11** DMF SEC spectrum of **7**. $M_n$ is 10.6 kDa, $M_w$ is 14.0 kDa, $Đ$ is 1.32…….220

**Figure 4.12** $^{1}H$ NMR of **6** in $CDCl_3$ at 298 K……..221

**Figure 4.13** A) SDS-PAGE gel of DARPin following purification. Lane 1 - protein ladder. Lane 2 - DARPin (non-reducing conditions). Lane 3 - DARPin (reducing conditions, 5% mercaptoethanol by volume). B) LCMS total ion chromatogram (TIC) of DARPin following purification. C) LCMS deconvoluted mass of DARPin following purification. Expected mass: 15,866.84 Da. Observed mass: 15,866.23 Da. * denotes the parent mass……222

**Figure 4.14** A) Regioselective DARPin PEGylation scheme. B) SDS-PAGE gel results from conventional Au(III)-mediated PEGylation conditions (70 μM DARPin, 1.3 eq Au(III) reagent) and the corresponding products. Lane 1 - protein ladder. Lane 2 - DARPin (non-reducing conditions). Lane 3 - DARPin PEGylation with **4**……223

**Figure 5.1** A) Aryl-I polymerization scheme for Au(III)-mediated electrospun fiber functionalization. B) Thiol polymerization scheme for Au(III)-mediated electrospun fiber functionalization……..…230

**Figure 5.2** A) ROP scheme for aryl iodide initiated **1** and **2**. B) Electrospinning process. C) Fiber mat consisting of **1** and commercial pCL (80 kDa) D) SEM of **1** and commercial pCL (80 kDa) co-spun fibers. Scale bar is 20 μm. E) SEM of **2** fiber mats. Scale bar is 20 μm. SEM images in this figure were collected by collaborators from the University of Auckland……..232

**Figure 5.3** A) ROMP of **3** and **4** to produce random copolymer **5**. B) SEM of **5** fiber mats. Scale bar is 5 μm. C) **5** fiber mats suspended in DCM. D) **5** fiber mats suspended in DCM under oxidative addition conditions (see experimental section for additional detail). SEM images in this figure were collected by collaborators from the University of Auckland……233

**Figure 5.4** A) ROMP of **6** and **BNI** to produce random copolymer **7**. B) SEM of **7** fiber mats. Scale bar is 10 μm. Images in this figure were collected by collaborators from the University of Auckland……..…234

**Figure 5.5** A) Reductive elimination of **8** with **7** fiber mats to produce functionalized fiber mat **9**. B) SEM of **9** fiber mats. Scale bar is 10 μm. C) EDS spectrum of **9** fiber mats. SEM and EDS images in this figure were collected by staff from UCLA CNSI……..……235

**Figure 5.6** A) Reductive elimination of **10** with **7** fiber mats to produce functionalized fiber mat **11**. B) Fluorescence image of **11**. C) Fluorescence image of Trt-protected **11**……..…236

**Figure 5.7** $^{1}$H NMR of pCL-aryl I (**1**) in $CDCl_3$ at 23 ºC…….249

**Figure 5.8** DMF SEC of pCL-aryl I (**1**)……250

**Figure 5.9** $^{1}$H NMR of Trt-protected thiol norbornene imide monomer (**6**) in DMSO-$d_6$ at 23 ºC……..251

**Figure 5.10** $^{1}$H NMR of p(BNI-*co*-$NI_{SH}$) (**7**) in DMSO-$d_6$ at 23 ºC. Note that in the absence of a defined end-group, the trityl group is integrated to 15 to observe the ratio between the monomer types (~10:1 BNI to **6**, respectively)…….252

**Figure 5.11** DMF SEC of p(BNI-*co*-$NI_{SH}$) (**7**)……..…253

**Figure 5.12** $^{1}H$ NMR of *para*-bromobenzene Au(III)-$Ad_2$ OAC (**8**) in $CD_2Cl_2$ at 23 ºC……254

**Figure 5.13** $^{31}P\{^{1}H\}$ NMR of *para*-bromobenzene Au(III)-$Ad_2$ OAC (**8**) in $CD_2Cl_2$ at 23 ºC…255

**Figure 5.14** $^{1}H$ NMR of p(BNI-*co*-$NI_{Aryl\ Br}$) (**9**) in $CD_2Cl_2$ at 23 ºC. Note that in the absence of a defined end-group, an aryl Br peak is integrated to 2 to observe the ratio between BNI and aryl Br (~8:1 BNI to Aryl Br, respectively)……..256

**Figure 5.15** $^{1}H$ NMR of BODIPY-Au(III) OAC **(10)** in $CD_2Cl_2$ at 23 ºC……257

**Figure 5.16** $^{31}P\{^{1}H\}$ NMR of BODIPY-Au(III) OAC **(10)** in $CD_2Cl_2$ at 23 ºC……258

## List of Tables

**Table 2.1** Functionality, precursor, synthesis strategy, NMR molecular weight ($M_n$), SEC molecular weight ($M_n$), and dispersity ($Đ$) reported for polymer precursors and DBCP (BCP). Expected $M_n$ is calculated from $^1$H NMR observed conversion…….24

**Table 5.1:** Electrospinning Solution Conditions…….. 259

## List of Abbreviations

| | |
|---|---|
| Ad | Adamantyl |
| ATRP | Atom Transfer Radical Polymerization |
| Boc | tert-Butyloxycarbonyl |
| Bpy | 2,2-bipyridine |
| CD | Circular Dichroism |
| CL | Caprolactone |
| CTA | Chain Transfer Agent |
| Cy | Cyclohexyl |
| DCM | Dichloromethane |
| DI | Deionized |
| DMF | Dimethylformamide |
| DPBS | Dulbeco's Phosphate Buffered Saline |
| ESI | Electrospray Ionization |
| $Et_2O$ | Diethyl ether |
| EtOAc | Ethyl Acetate |
| Eq. | Equivalents |
| FDA | Food and Drug Administration |
| Fmoc | Fluorenylmethyloxycarbonyl |
| FPLC | Fast Protein Liquid Chromatography |
| G1/G3 | Grubbs' 1$^{st}$ and 3$^{rd}$ Catalyst |
| GPC | Gel Permeation Chromatography |
| HPLC | High Performance Liquid Chromatography |

| | |
|---|---|
| LCMS | Liquid Chromatography-Mass Spectrometry |
| MALDI-TOF | Matrix-Assisted Laser Desorption/Ionization-Time of Flight |
| MD | Molecular Dynamics |
| MeCN | Acetonitrile |
| MeOH | Methanol |
| mPEG | Monomethyl Ether Poly(Ethylene Glycol) |
| NI | Norbornene Imide |
| NIPAM | N-isopropyl acrylamide |
| NMR | Nuclear Magnetic Resonance |
| OCDS | Organization for Cultural Diversity in Science |
| PEG | Poly(Ethylene Glycol) |
| PFS | Pentafluorostyrene |
| RAFT | Reversible Addition Fragmentation Chain Transfer |
| ROMP | Ring Opening Metathesis Polymerization |
| ROP | Ring Opening Polymerization |
| SDS-PAGE | Sodium Dodecylsulfate-Polyacrylamide Gel Electrophoresis |
| SEC | Size Exclusion Chromatography |
| tBu | tert-Butyl Ether |
| TCEP | Tris(2-carboxyethyl)phosphine |
| TEA | Triethylamine |
| TFA | Trifluoroacetic Acid |
| THF | Tetrahydrofuran |
| VL | Valerolactone |

**Acknowledgments**

There are many people without whom this would not have been possible. It takes a village, after all, and my village overflows with love.

First, I want to thank my academic advisor Professor Heather Maynard for the opportunities and guidance she has provided me these past five years. I am also grateful for Professor Alex Spokoyny, who adopted me into his group and made me feel at home there. Thank you to Ricky Ruiz—our department would not function without this friendly and caring individual. I must thank my professors at Hope College, who instilled in me a love for science. Finally, I want to acknowledge my gratitude for Professor Beth Anderson, who taught me that I am not my sample, all data is useful data, and of course—scientists can wear fun pants.

I am thankful for every single lab mate that I had the privilege of overlapping with at UCLA. To the students and postdocs that came before me—Dr. Daniele Vinciguerra, Dr. Kathryn Messina, Dr. Priera Panescu, Dr. Kyle Tamshen, Dr. Madeline Gelb, Dr. Douglas Rose, Dr. Neil Forsythe, Dr. Jane Yang, Dr. Mikayla Tan, and Nik Theopold—thank you for answering my incessant questions with patience and empathy. I am a better chemist for having worked alongside these individuals. Specifically, to Kyle—thank you for being an amazing mentor to me both at UCLA and Gilead. To the postdocs that arrived during my graduate school experience— Dr. Pedro Salas, Dr. Théo Pesenti, Dr. Rajalakshmi Pallathery, Dr. Panos Georgiou, and Dr. Tony Zhang—I am grateful to have learned from each of your diverse backgrounds. Thank you for putting up with my loud music and chaotic personality. To my girls—Haillie Lower, Ellie Puente, and Katie Snell—you are all brilliant scientists and even better friends. My graduate education would have been poorer without our coffee walks, griddle days, and yoga sessions. Thank you for being girls

together with me. To Felix Fu—if you have no fans, I'm dead. I can't wait to see all that you accomplish. To the younger crew—Ryan Lai, Mia Rose Kayaian, Maggie Polite, Elaine Chao, Brock Hosier, and Alex Meckes—thank you for reminding me of what it felt like to start. There are so many possibilities for each of you, and I wish you all success and peace. Thank you also to Ashley Julio and Nik Burton—I am so glad for the fun memories of pickle ball, concerts, ski trips, Halloween parties, and so much more with you both. Finally thank you to Lily K. Sloan—my first friend at UCLA. You are a loyal and committed friend, and I am so thankful for all our laughs, rant sessions, and gossip dinners.

I must thank Team Gold—I can't imagine any of this without you all. Thank you to Dr. Evan Doud and Dr. James Tilden for your advice and friendship. I know that our team is in capable hands moving forward thanks to Ellie and Maggie. Of course, there is also the original Team Gold—Dr. Hayden Montgomery and Dr. Joseph (Billy) Treacy. Hayden—you are the best friend a girl could ask for. I will never forget the tears you wiped, the hugs you gave, or the pep-talks you imparted. I am honored to be your friend, from now until we're castaways. Billy—grad school was a long road with many hurdles, but I couldn't have done it without you. I wouldn't have wanted to. I was glad to have someone like you alongside me on this journey, hurdles and all.

Thank you to my Hope College girls—Lauren Hilt, Caitlin Skiba, and Ashley Klepac. Thank you for the McFlurries delivered at midnight to the library, for the laughs after difficult exams, and for the visits during these past five years. It has been a beautiful thing, to watch each of you bloom into adulthood. I can't wait to keep growing together. To Sara Hudson, my longest friend—you are so kind, understanding, and thoughtful. Thank you for being a shoulder to cry on, even 3000 miles away.

Finally, I am overwhelmed with gratitude for my family. To my cousins, uncles, aunts, grandparents—thanks for rooting for me. The impossible becomes manageable when I have so many people uplifting me. To Amanda and Rachel—thank you for being my fiercest supporters. I am so thankful to have had built-in best friends from the very beginning. To my bonus siblings—Jessi Kunkel and Nick Rodriguez—thank you for keeping me (and my whole family) on this side of insane. It's so much fun to flirt with the line though, isn't it? I am so grateful you have entered our lives; we are better for it. To my brother, Daniel—words cannot express all the wisdom I have treasured from our conversations. I am so blessed to have a brother that is equal parts goofy and profound. I have always looked up to you and am grateful that your mind and your heart can both be heard in your love. To my sister, Jane—we've come a long, long way from rolling marbles in the attic, and thank God for that. I am so grateful to have someone who knows my heart so completely. We may not be twins, but we are two pieces cut from the same cloth, and the comfort of that makes me feel at ease even during the darkest days. To my parents, Sharon and Bob—I have won the parents lotto. You both are generous, loving, and all together exceptional people. Thank you for raising me to launch, even despite fear, and always, always giving me a safe place to land. I love you both and am so proud to be on the Kunkel Team.

Finally, I want to acknowledge the girls who are curious, of which I am one. Anyone can be a scientist. There is no mold to fit in and no personality test. You can wear ribbons in your hair and safety glasses on your face. You belong here.

## Vita

Education

*University of California, Los Angeles, Los Angeles, CA*

Doctor of Philosophy in Chemistry — Expected: 2024

Master of Science in Chemistry — May 2021

*Hope College, Holland, MI*

Bachelor of Science in Chemistry — May 2019

Publications

- **Kunkel, G. E.**; Zhou, Q.; Treacy, J. W.; Montgomery, H. R.; Salas-Ambrosio, P.; Ready, A. D.; Spokoyny, A. M.; Houk, K. N.; Maynard, H. D. Comparison of Cyclic and Linear PEG Conjugates. *Bioconjugate Chem.* **2024**, *35* (6), 744–749.
- Sivasankaran, R.P.; Snell, K.; **Kunkel, G.E.**; Georgiou, P.; Puente, E. G.; Maynard, H. D. Polymer- mediated Protein/Peptide Therapeutic Stabilization: Current Progress and Future Directions. *Prog. Polym. Sci.* **2024**, *accepted*.
- Doud, E. A.; Tilden, J. A. R.; Treacy, J. W.; Chao, E. Y.; Montgomery, H. R.; **Kunkel, G. E.**; Olivares, E. J.; Adhami, N.; Kerr, T. A.; Chen, Y.; Rheingold, A. L.; Loo, J. A.; Frost, C. G.; Houk, K. N.; Maynard, H. D.; Spokoyny, A. M. Ultrafast Au(III)-Mediated Arylation of Cysteine. *J. Am. Chem. Soc.* **2024**. *146* (18), 12365–12374.
- **Kunkel, G. E.**; Treacy, J. W.; Montgomery, H. R.; Puente, E. G.; Doud, E. A.; Spokoyny, A. M.; Maynard, H. D. Efficient End-Group Functionalization and Diblock Copolymer Synthesis via Au(III) Polymer Reagents. *Chem. Commun.* **2023**, *60* (1), 79–82.
- Fasana, C. D.; Jensen, M. S.; Ponte, G. E. G.; MacAlister, T. R.; **Kunkel, G. E.**; Rogers, J. P.; Ochs, A. M.; Stevens, D. L.; Weller, D. P.; Morelli, D. T.; Anderson, M. E. Synthetic Versatility, Reaction Pathway, and Thermal Stability of Tetrahedrite Nanoparticles. *J. Mater. Chem. C* **2020**, *8* (40), 14219– 14229.
- Weller, D. P.; **Kunkel, G. E.**; Ochs, A. M.; Morelli, D. T.; Anderson, M. E. Observation of N-Type Behavior in Fe-Doped Tetrahedrite at Low Temperature. *Materials Today Physics* **2018**, *7*, 1–6.

- Weller, D. P.; Stevens, D. L.; **Kunkel, G. E.**; Ochs, A. M.; Holder, C. F.; Morelli, D. T.; Anderson, M. E. Thermoelectric Performance of Tetrahedrite Synthesized by a Modified Polyol Process. *Chem. Mater.* **2017**, *29* (4), 1656–1664.

Presentations

- "Efficient Preparation of Macromolecular Structures and Bioconjugates *via* Au(III) Reagents", Gordon Research Conference "Biotherapeutics and Vaccines Development", Galveston, TX, March 17-22, 2024 (poster).
- "Efficient Synthesis of Discrete Polymer Architectures *via* Organometallic Reagents", ACS National Meeting, Chicago, Illinois, August 21-25, 2022 (poster).
- "Modified Polyol Synthesis and Thermoelectric Characterization of Tetrahedrite", ACS National Meeting, Washington D.C., August 20-August 25, 2017 (poster).

Awards

- UCLA Dissertation Year Fellowship, 2023-2024.
- NIH Chemistry-Biology Interface Training Grant, 2020-2023.
- NSF GRFP Honorable Mention, 2020.
- Beckman Scholar, 2017-2018.

Teaching Experience

*UCLA Department of Chemistry and Biochemistry Teaching Assistant*

- General and Organic Chemistry, Laboratory II (Chem 14CL)
  - Fall 2019
  - Spring 2020 (remote)
- General and Organic Chemistry, Laboratory I (Chem 14BL)
  - Winter 2020

Leadership and Service

- Organization for Cultural Diversity in Science (OCDS)
  - *Internal Coordinator* 2022 – 2023
  - *Professional Development Chair* 2021 – 2022
  - *Social and Recruitment Chair* 2020 – 2021

# Chapter 1

# Techniques for the Preparation of Macromolecular Structures[†]

## 1.1 Introduction

As proteins become increasingly sought after for their medicinal relevance, the need for precise chemical modifications to enhance their stability has become more pronounced. Following the seminal peptide modification work by Wilchek et al. in 1965, the concept of protein labeling has received staggering attention and has been the focus of several comprehensive reviews.[1–5] The challenges introduced by proteins in a chemical reaction context such as instability, requirement of aqueous media, and chemically competing functional groups has brought forth biorthogonal click chemistry as a groundbreaking field of study that continues to evolve.[6]

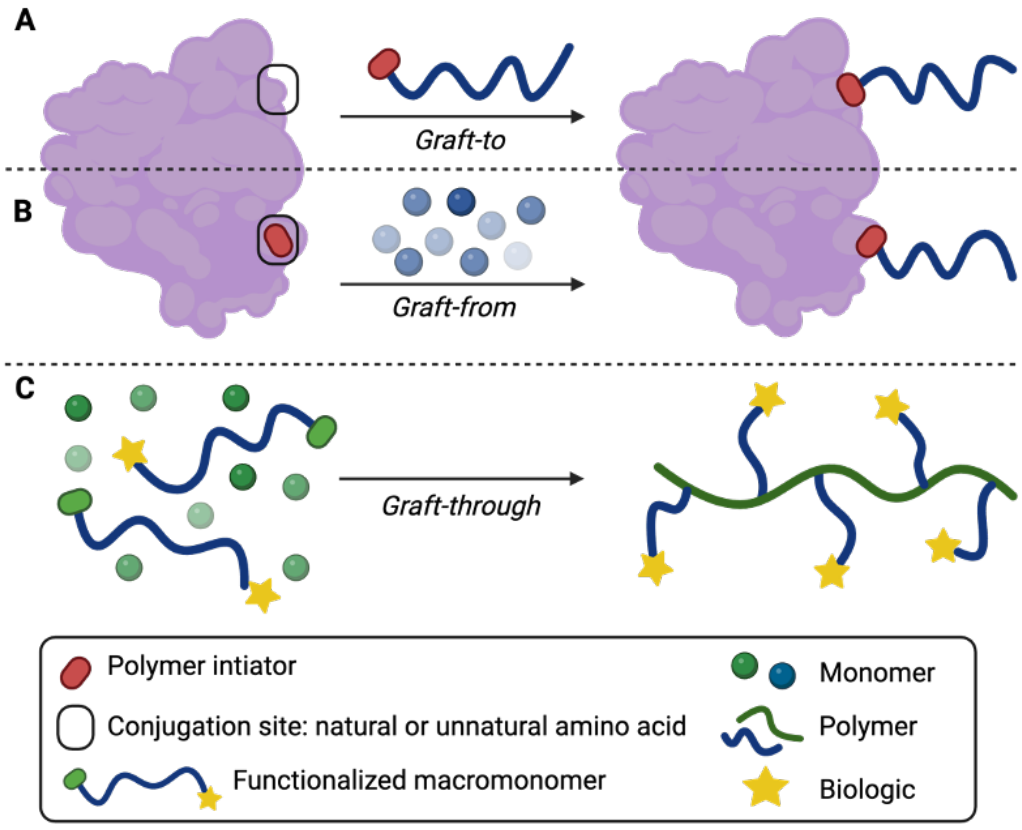


**Figure 1.1** Summary of protein-polymer conjugation strategies: A) Graft-to, B) Graft-from, C) Graft-through.

Among substrates for bioconjugation in therapeutics, polymers are attractive candidates due to their ability to provide proteins with stealth properties, increased circulation time, and stability.[7] However, polymers present new obstacles towards effective bioconjugation including steric bulk, low relative concentration of reactive units, and difficulty in removing unreacted starting materials. In this section, we will focus on strategies for site-selective polymer bioconjugation that address these concerns.

## 1.2 Polymerization Strategies

### 1.2.1 Graft-to

In the graft-to polymer bioconjugation strategy, polymers are first synthesized to contain a reactive conjugation handle, purified and characterized, and then attached to a biomolecule of interest (**Figure 1.1 A**). This approach is attractive in that polymer synthesis is relatively straightforward and can accommodate conventional reaction conditions such as organic solvents and elevated temperatures. Additionally, the characterization of polymer precursors can be thorough, such as the use of size exclusion chromatography (SEC) and nuclear magnetic spectroscopy (NMR), which can provide a clearer understanding of bioconjugation products. In the 1970s, the first example of protein-polymer bioconjugation was performed in which polyethylene glycol (PEG) was covalently attached to bovine serum albumin (BSA) using cyanuric acid as a coupling agent. [8,9] Since this discovery, many common synthetic organic reactions have been utilized to prepare graft-to protein-polymer conjugates, such as amidation between lysine residues and activated ester containing polymers or Michael addition between cysteine-residues and maleimide polymers.[10–13] While effective in creating protein-polymer conjugation, these methods suffer from nucleophile non-specificity, low conversion, and reversibility in biologically relevant media. It is documented that conjugation specificity in protein-polymer conjugates

improves protein circulation time and retention of activity.[14,15] Additionally, complete conversion is critical in the graft-to strategy due to the difficulties of purifying macromolecules from one another. One way to mitigate these concerns is the introduction of click-chemistry, though this also necessitates incorporation of a click handle into the biomolecule.[16,17] Another area of graft-to conjugation receiving attention is the use of self-immolative linkers to return proteins to their native form and thereby rescue protein activity.[18,19]

### 1.2.2 Graft-from

As an alternative strategy, graft-from bioconjugation involves the coupling of a small-molecule reactive polymerization handle to a biomolecule of interest to create a macroinitiator (**Figure 1.1 B**). Then, polymerization proceeds from the biomolecule to produce a protein-polymer conjugate. This method is advantageous due to the efficiency of small molecule bioconjugation and the relative ease of purification. However, graft-from bioconjugation requires benign polymerization conditions that are compatible with biomolecules. In 2005, our group utilized a biotinylated ATRP initiator to conjugate a reactive polymerization handle to the surface of streptavidin.[20] Following ATRP polymerization of *N*-isopropylacrylamide (NIPAM), this resulted in first example of graft-from bioconjugation. Shortly thereafter, the Matyjaszewski and Russell groups also performed ATRP from the surface of 2-bromoisobutyramide functionalized chymotrypsin.[21] Since these discoveries, graft-from bioconjugation has enabled the preparation of many impressive and therapeutically relevant biomacromolecules. In most cases, ATRP and RAFT are used in this strategy as they utilize mild reaction conditions for the polymerization of vinyl monomers to produce well-defined polymer conjugates.[22,23] In 2020, our group detailed many of these reports in a review focused on graft-from bioconjugations [24]

### 1.2.3 Graft-through

In graft-through bioconjugation, monomers containing a secondary bio-reactive unit, thus named "macromonomers", are polymerized (**Figure 1.1 C**). This technique is most often used with ring opening metathesis polymerization (ROMP) and offers tunability of polymer size and branching. Examples of grafting-through polymerization wherein oligopeptides and oligonucleotides are the biomolecules of interest were also covered in our 2020 bioconjugation review.[24] In addition, the Minko group has demonstrated the use of enzymes as macromonomers, which improved biocatalytic activity due to the crowding effect and enhanced the thermal stability of the enzyme.[25,26]

## 1.3 Common Targets for Biomolecule Conjugation

### 1.3.1 Natural Nucleophilic Amino Acid Residues

Perhaps the most common mode of bioconjugation occurs through naturally occurring nucleophilic residues, such as lysine and cysteine. The abundance of lysine makes it a convenient target for conjugation with electrophiles such as *N*-hydroxysuccinimide (NHS)-esters, acid-halides, nitrophenyl carbonates, and squaric acid moieties.[27–30] However, the promiscuous nature of these electrophiles and the relative abundance of lysine in the proteome leads to a lack of bioconjugation selectivity. To mediate this concern, computation and tertiary structure modeling can be utilized to predict and restrict lysine conjugation.[31,32] Another strategy to increase selectivity is to target cysteine residues, which have a far lower proteomic abundance. For example, in 2005, our group prepared a singly conjugated BSA-p(NIPAM) biomacromolecule through a disulfide linkage between an ATRP initiator and the free cysteine of BSA.[33] Other conventional cysteine-reactive bioconjugation handles include divinylsulfones and maleimides, although these can reverse *in vivo*.[13,34,35] These traditional strategies have evolved to circumvent these issues, such as

in the development of dibromomaleimides to reduce the reversibility of conjugation.[36] Nevertheless, research interests have gravitated towards discovery of fast cysteine conjugation protocols such as activated arylation reagents.[37,38] While many rapid methods are currently limited to small molecule bioconjugation, a handful of strategies have been shown to tolerate larger payloads. For example, stoichiometric organometallic Au(III)-PEG reagents have demonstrated reductive elimination with a model protein, DARPin, in one minute.[39] This method resulted in a strong *S*-aryl bond that is resistant to reversibility. Alternatively, the Ball group utilized Ni(II) catalysis to conjugate polymers to lysozyme at the cysteine residue *via* arylation.[40] Using this method, the group also prepared thermoresponsive lysozyme homodimers. When conventional nucleophilic residues are not available, do not provide sufficient specificity, or interfere too greatly with protein activity, it can be beneficial to utilize less frequently targeted residues for bioconjugation such as tyrosine, tryptophan, and methionine.[41]

### 1.3.2 C- and N- Terminus

Another approach to achieve site-selective bioconjugation is to target the C- or N terminus of the protein of interest, which by nature can only result in singly conjugated biomacromolecules and are also ubiquitous among proteins. A common approach for N-terminus conjugation is through reductive amination of an aldehyde-functionalized coupling partner at pH 5, though it is important to note that cross-reactivity with lysine moieties is possible.[42] Additionally, the Chilkoti group has demonstrated N-terminus incorporation of an amine-functionalized ATRP initiator *via* a pyridoxal-5-phosphate (PLP) transamination.[43] Following graft-from ATRP using poly(ethylene glycol) methyl ether methacrylate (PEGMA) as a monomer, they produced an N-terminal protein-polymer conjugate. The N-terminal position can also be chemically targeted through interactions with an adjacent residue as observed in native chemical ligation, oxidative coupling such as use of potassium ferricyanide, and oxime ligation with an aldehyde target.[44] Since the carboxylic acid

moiety of the C-terminus is nearly indistinguishable from other residues containing this functionality (Asp, Glu), conjugations specifically targeting this terminus rely on enzymatic coupling. A highly utilized approach involves the enzyme sortase (SrtA) from *Staphylococcus aureus*, wherein a pentapeptide sequence LPXTG is recombinantly expressed in a target protein and serves as an identifying feature for selective conjugation.[45] While SrtA is most commonly used to functionalize the C-terminus, the N-terminus can also be targeted by using sortases of varying specificity.[46] Through recombinant expression, both termini can present functionality that permits small molecule or polymer conjugation. For example, alternative to their PLP N-terminus approach, the Chilkoti group also fused an intein to the C-terminus which is excised to reveal a thioester that could react with an ATRP initiator, thereby enabling a graft-from protein polymer conjugation to occur.[47]

### 1.3.3 Unnatural Amino Acids

Rather than relying on conjugation targets found endogenously within proteins, the introduction of non-canonical amino acids and the development of biorthogonal "click" chemistry has provided an additional route toward specific bioconjugation. [6,48] In this strategy, proteins are expressed recombinantly to possess functionalized amino acids with a chemical conjugation handle. Then, the coupling partner bearing an appropriate corresponding moiety can be added to forge the conjugation. Noncanonical amino acids can be introduced to proteins by several means, including the use of auxotrophic bacteria strains, stop codon suppressor tRNAs, and orthogonal aminoacyl-tRNA synthetases.[49] Using the graft-to method, many well-known bioorthogonal reactions have been utilized to prepare protein-polymer conjugates, such as the Cu(I)-catalyzed azide−alkyne cycloaddition (CuAAC), Staudinger reactions, and Suzuki-Miyaura cross-coupling. [28,50–52] Alternatively, polymer initiators have also been incorporated in both peptides and proteins as noncanonical amino acids to perform graft-from polymerization.[53,54] For example, the

Matyjaszewski and Ryan groups designed 4-(2′-bromoisobutyramido)phenylalanine as an initiator for ATRP to prepare a GFP-oligo(ethylene oxide) monomethyl ether methacrylate polymer ($OEO_{300}MA$) conjugate.[54] Recently, the Matyjaszewski group has expanded this work to incorporate initiators into DNA and RNA sequences, thereby creating polynucleotide-polymer hybrid materials.[55,56]

## 1.4 Outlook: Conjugation *via* Organometallic Au(III) Reagents

As evidenced by the numerous developing methods and targets of bioconjugation described *vide supra*, chemists have a wide breadth of tools available to achieve complex bio-macromolecules. The remainder of this dissertation will focus specifically on the fitness of Au(III) organometallic reagents for the preparation of macromolecular constructs. Although these structures can be accessed by other means, we regard Au(III) oxidative addition complexes as privileged reagents for these transformations due to their rapid and tunable kinetics, robust chemoselectivity, and biological compatibility.[57] Though less familiar to a conventional biochemist, this work highlights the practical utility and relative ease of conjugation *via* bench-stable organometallic complexes.

## 1.5 References

†This chapter contains portions of a review article currently under revisions with the following citation: Sivasankaran, R.P.; Snell, K.; **Kunkel, G.E.**; Georgiou, P.; Puente, E. G.; Maynard, H. D. Polymer- mediated Protein/Peptide Therapeutic Stabilization: Current Progress and Future Directions. *Prog. Polym. Sci.* **2024**, *accepted.*


(1) Zioudrou, C.; Wilchek, M.; Patchornik, A. Conversion of the L-Serine Residue to an L-Cysteine Residue in Peptides*. *Biochemistry* **1965**, *4* (9), 1811–1822. https://doi.org/10.1021/bi00885a018.

(2) Boutureira, O.; Bernardes, G. J. L. Advances in Chemical Protein Modification. *Chem. Rev.* **2015**, *115* (5), 2174–2195. https://doi.org/10.1021/cr500399p.

(3) Spicer, C. D.; Davis, B. G. Selective Chemical Protein Modification. *Nat. Commun.* **2014**, *5* (1), 4740. https://doi.org/10.1038/ncomms5740.

(4) Shiraiwa, K.; Cheng, R.; Nonaka, H.; Tamura, T.; Hamachi, I. Chemical Tools for Endogenous Protein Labeling and Profiling. *Cell Chem. Biol.* **2020**, *27* (8), 970–985. https://doi.org/10.1016/j.chembiol.2020.06.016.

(5) Lieser, R. M.; Yur, D.; Sullivan, M. O.; Chen, W. Site-Specific Bioconjugation Approaches for Enhanced Delivery of Protein Therapeutics and Protein Drug Carriers. *Bioconjug. Chem.* **2020**, *31* (10), 2272–2282. https://doi.org/10.1021/acs.bioconjchem.0c00456.

(6) Sletten, E. M.; Bertozzi, C. R. Bioorthogonal Chemistry: Fishing for Selectivity in a Sea of Functionality. *Angew. Chem. Int. Ed.* **2009**, *48* (38), 6974–6998. https://doi.org/10.1002/anie.200900942.

(7) Wright, T. A.; Page, R. C.; Konkolewicz, D. Polymer Conjugation of Proteins as a Synthetic Post-Translational Modification to Impact Their Stability and Activity. *Polym. Chem.* **2019**, *10* (4), 434–454. https://doi.org/10.1039/C8PY01399C.

(8) A, A.; T, van E.; Nc, P.; Ff, D. Alteration of Immunological Properties of Bovine Serum Albumin by Covalent Attachment of Polyethylene Glycol. *J. Biol. Chem.* **1977**, *252* (11).

(9) Abuchowski, A.; McCoy, J. R.; Palczuk, N. C.; Es, T. van; Davis, F. F. Effect of Covalent Attachment of Polyethylene Glycol on Immunogenicity and Circulating Life of Bovine Liver Catalase. *J. Biol. Chem.* **1977**, *252* (11), 3582–3586.

(10) McDowall, L.; Chen, G.; Stenzel, M. H. Synthesis of Seven-Arm Poly(Vinyl Pyrrolidone) Star Polymers with Lysozyme Core Prepared by MADIX/RAFT Polymerization. *Macromol. Rapid Commun.* **2008**, *29* (20), 1666–1671. https://doi.org/10.1002/marc.200800416.

(11) Heredia, K. L.; Nguyen, T. H.; Chang, C.-W.; Bulmus, V.; Davis, T. P.; Maynard, H. D. Reversible siRNA–Polymer Conjugates by RAFT Polymerization. *Chem. Commun.* **2008**, No. 28, 3245–3247. https://doi.org/10.1039/B804812F.

(12) Vanparijs, N.; Maji, S.; Louage, B.; Voorhaar, L.; Laplace, D.; Zhang, Q.; Shi, Y.; Hennink, W. E.; Hoogenboom, R.; Geest, B. G. D. Polymer-Protein Conjugation via a 'Grafting to' Approach – a Comparative Study of the Performance of Protein-Reactive RAFT Chain Transfer Agents. *Polym. Chem.* **2015**, *6* (31), 5602–5614. https://doi.org/10.1039/C4PY01224K.

(13) Mantovani, G.; Lecolley, F.; Tao, L.; Haddleton, D. M.; Clerx, J.; Cornelissen, J. J. L. M.; Velonia, K. Design and Synthesis of N-Maleimido-Functionalized Hydrophilic Polymers

via Copper-Mediated Living Radical Polymerization: A Suitable Alternative to PEGylation Chemistry. *J. Am. Chem. Soc.* **2005**, *127* (9), 2966–2973. https://doi.org/10.1021/ja0430999.

(14) Bhattacharjee, S.; Liu, W.; Wang, W.-H.; Weitzhandler, I.; Li, X.; Qi, Y.; Liu, J.; Pang, Y.; Hunt, D. F.; Chilkoti, A. Site-Specific Zwitterionic Polymer Conjugates of a Protein Have Long Plasma Circulation. *ChemBioChem* **2015**, *16* (17), 2451–2455. https://doi.org/10.1002/cbic.201500439.

(15) Tamshen, K.; Wang, Y.; Jamieson, S. M. F.; Perry, J. K.; Maynard, H. D. Genetic Code Expansion Enables Site-Specific PEGylation of a Human Growth Hormone Receptor Antagonist through Click Chemistry. *Bioconjug. Chem.* **2020**, *31* (9), 2179–2190. https://doi.org/10.1021/acs.bioconjchem.0c00365.

(16) Le Droumaguet, B.; Velonia, K. Click Chemistry: A Powerful Tool to Create Polymer-Based Macromolecular Chimeras. *Macromol. Rapid Commun.* **2008**, *29* (12–13), 1073–1089. https://doi.org/10.1002/marc.200800155.

(17) Jung, S.; Kwon, I. Expansion of Bioorthogonal Chemistries towards Site-Specific Polymer–Protein Conjugation. *Polym. Chem.* **2016**, *7* (28), 4584–4598. https://doi.org/10.1039/C6PY00856A.

(18) Rose, D. A.; Treacy, J. W.; Yang, Z. J.; Ko, J. H.; Houk, K. N.; Maynard, H. D. Self-Immolative Hydroxybenzylamine Linkers for Traceless Protein Modification. *J. Am. Chem. Soc.* **2022**, *144* (13), 6050–6058. https://doi.org/10.1021/jacs.2c01136.

(19) Gavriel, A. G.; Sambrook, M. R.; Russell, A. T.; Hayes, W. Recent Advances in Self-Immolative Linkers and Their Applications in Polymeric Reporting Systems. *Polym. Chem.* **2022**, *13* (22), 3188–3269. https://doi.org/10.1039/D2PY00414C.

(20) Bontempo, D.; Maynard, H. D. Streptavidin as a Macroinitiator for Polymerization: In Situ Protein−Polymer Conjugate Formation. *J. Am. Chem. Soc.* **2005**, *127* (18), 6508–6509. https://doi.org/10.1021/ja042230+.

(21) Lele, B. S.; Murata, H.; Matyjaszewski, K.; Russell, A. J. Synthesis of Uniform Protein−Polymer Conjugates. *Biomacromolecules* **2005**, *6* (6), 3380–3387. https://doi.org/10.1021/bm050428w.

(22) Sumerlin, B. S. Proteins as Initiators of Controlled Radical Polymerization: Grafting-from via ATRP and RAFT. *ACS Macro Lett.* **2012**, *1* (1), 141–145. https://doi.org/10.1021/mz200176g.

(23) Grover, G. N.; Maynard, H. D. Protein-Polymer Conjugates: Synthetic Approaches by Controlled Radical Polymerizations & Interesting Applications. *Curr. Opin. Chem. Biol.* **2010**, *14* (6), 818. https://doi.org/10.1016/j.cbpa.2010.10.008.

(24) Messina, M. S.; Messina, K. M. M.; Bhattacharya, A.; Montgomery, H. R.; Maynard, H. D. Preparation of Biomolecule-Polymer Conjugates by Grafting-from Using ATRP, RAFT, or ROMP. *Prog. Polym. Sci.* **2020**, *100*, 101186. https://doi.org/10.1016/j.progpolymsci.2019.101186.

(25) Wang, X.; Yadavalli, N. S.; Laradji, A. M.; Minko, S. Grafting through Method for Implanting of Lysozyme Enzyme in Molecular Brush for Improved Biocatalytic Activity and Thermal Stability. *Macromolecules* **2018**, *51* (14), 5039–5047. https://doi.org/10.1021/acs.macromol.8b00991.

(26) Yadavalli, N. S.; Borodinov, N.; Choudhury, C. K.; Quiñones-Ruiz, T.; Laradji, A. M.; Tu, S.; Lednev, I. K.; Kuksenok, O.; Luzinov, I.; Minko, S. Thermal Stabilization of Enzymes

with Molecular Brushes. *ACS Catal.* **2017**, *7* (12), 8675–8684. https://doi.org/10.1021/acscatal.7b03138.

(27) Steinbach, T.; Wurm, F.; Klok, H.-A. Squaric Acid Mediated Bioconjugation Expanded to Polymers Prepared by ATRP. *Polym. Chem.* **2014**, *5* (13), 4039–4047. https://doi.org/10.1039/C4PY00168K.

(28) Wang, Y.; Wu, C. Site-Specific Conjugation of Polymers to Proteins. *Biomacromolecules* **2018**, *19* (6), 1804–1825. https://doi.org/10.1021/acs.biomac.8b00248.

(29) Haque, M.; Forte, N.; Baker, J. R. Site-Selective Lysine Conjugation Methods and Applications towards Antibody–Drug Conjugates. *Chem. Commun.* **2021**, *57* (82), 10689–10702. https://doi.org/10.1039/D1CC03976H.

(30) Tao, L.; Mantovani, G.; Lecolley, F.; Haddleton, D. M. α-Aldehyde Terminally Functional Methacrylic Polymers from Living Radical Polymerization: Application in Protein Conjugation "Pegylation." *J. Am. Chem. Soc.* **2004**, *126* (41), 13220–13221. https://doi.org/10.1021/ja0456454.

(31) Matos, M. J.; Oliveira, B. L.; Martínez-Sáez, N.; Guerreiro, A.; Cal, P. M. S. D.; Bertoldo, J.; Maneiro, M.; Perkins, E.; Howard, J.; Deery, M. J.; Chalker, J. M.; Corzana, F.; Jiménez-Osés, G.; Bernardes, G. J. L. Chemo- and Regioselective Lysine Modification on Native Proteins. *J. Am. Chem. Soc.* **2018**, *140* (11), 4004–4017. https://doi.org/10.1021/jacs.7b12874.

(32) Carmali, S.; Murata, H.; Amemiya, E.; Matyjaszewski, K.; Russell, A. J. Tertiary Structure-Based Prediction of How ATRP Initiators React with Proteins. *ACS Biomater. Sci. Eng.* **2017**, *3* (9), 2086–2097. https://doi.org/10.1021/acsbiomaterials.7b00281.

(33) Heredia, K. L.; Bontempo, D.; Ly, T.; Byers, J. T.; Halstenberg, S.; Maynard, H. D. In Situ Preparation of Protein−"Smart" Polymer Conjugates with Retention of Bioactivity. *J. Am. Chem. Soc.* **2005**, *127* (48), 16955–16960. https://doi.org/10.1021/ja054482w.

(34) Grover, G. N.; Alconcel, S. N. S.; Matsumoto, N. M.; Maynard, H. D. Trapping of Thiol-Terminated Acrylate Polymers with Divinyl Sulfone To Generate Well-Defined Semitelechelic Michael Acceptor Polymers. *Macromolecules* **2009**, *42* (20), 7657–7663. https://doi.org/10.1021/ma901036x.

(35) Stenzel, M. H. Bioconjugation Using Thiols: Old Chemistry Rediscovered to Connect Polymers with Nature's Building Blocks. *ACS Macro Lett.* **2013**, *2* (1), 14–18. https://doi.org/10.1021/mz3005814.

(36) Smith, M. E. B.; Schumacher, F. F.; Ryan, C. P.; Tedaldi, L. M.; Papaioannou, D.; Waksman, G.; Caddick, S.; Baker, J. R. Protein Modification, Bioconjugation, and Disulfide Bridging Using Bromomaleimides. *J. Am. Chem. Soc.* **2010**, *132* (6), 1960–1965. https://doi.org/10.1021/ja908610s.

(37) Chen, F.-J.; Gao, J. Fast Cysteine Bioconjugation Chemistry. *Chem. – Eur. J.* **2022**, *28* (66), e202201843. https://doi.org/10.1002/chem.202201843.

(38) Zhang, C.; Vinogradova, E. V.; Spokoyny, A. M.; Buchwald, S. L.; Pentelute, B. L. Arylation Chemistry for Bioconjugation. *Angew. Chem. Int. Ed.* **2019**, *58* (15), 4810–4839. https://doi.org/10.1002/anie.201806009.

(39) Montgomery, H. R.; Messina, M. S.; Doud, E. A.; Spokoyny, A. M.; Maynard, H. D. Organometallic S-Arylation Reagents for Rapid PEGylation of Biomolecules. *Bioconjug. Chem.* **2022**, *33* (8), 1536–1542. https://doi.org/10.1021/acs.bioconjchem.2c00280.

(40) Swierczynski, M. J.; Ball, Z. T. One-Step Protein–Polymer Conjugates from Boronic-Acid-Functionalized Polymers. *Bioconjug. Chem.* **2020**, *31* (11), 2494–2498. https://doi.org/10.1021/acs.bioconjchem.0c00516.

(41) Kjærsgaard, N. L.; Nielsen, T. B.; Gothelf, K. V. Chemical Conjugation to Less Targeted Proteinogenic Amino Acids. *ChemBioChem* **2022**, *23* (19), e202200245. https://doi.org/10.1002/cbic.202200245.

(42) Kinstler, O.; Molineux, G.; Treuheit, M.; Ladd, D.; Gegg, C. Mono-N-Terminal Poly(Ethylene Glycol)–Protein Conjugates. *Adv. Drug Deliv. Rev.* **2002**, *54* (4), 477–485. https://doi.org/10.1016/S0169-409X(02)00023-6.

(43) Gao, W.; Liu, W.; Mackay, J. A.; Zalutsky, M. R.; Toone, E. J.; Chilkoti, A. In Situ Growth of a Stoichiometric PEG-like Conjugate at a Protein's N-Terminus with Significantly Improved Pharmacokinetics. *Proc. Natl. Acad. Sci.* **2009**, *106* (36), 15231–15236. https://doi.org/10.1073/pnas.0904378106.

(44) Rosen, C. B.; Francis, M. B. Targeting the N Terminus for Site-Selective Protein Modification. *Nat. Chem. Biol.* **2017**, *13* (7), 697–705. https://doi.org/10.1038/nchembio.2416.

(45) Mao, H.; Hart, S. A.; Schink, A.; Pollok, B. A. Sortase-Mediated Protein Ligation: A New Method for Protein Engineering. *J. Am. Chem. Soc.* **2004**, *126* (9), 2670–2671. https://doi.org/10.1021/ja039915e.

(46) Antos, J. M.; Chew, G.-L.; Guimaraes, C. P.; Yoder, N. C.; Grotenbreg, G. M.; Popp, M. W.-L.; Ploegh, H. L. Site-Specific N- and C-Terminal Labeling of a Single Polypeptide Using Sortases of Different Specificity. *J. Am. Chem. Soc.* **2009**, *131* (31), 10800–10801. https://doi.org/10.1021/ja902681k.

(47) Gao, W.; Liu, W.; Christensen, T.; Zalutsky, M. R.; Chilkoti, A. In Situ Growth of a PEG-like Polymer from the C Terminus of an Intein Fusion Protein Improves Pharmacokinetics and Tumor Accumulation. *Proc. Natl. Acad. Sci.* **2010**, *107* (38), 16432–16437. https://doi.org/10.1073/pnas.1006044107.

(48) Kolb, H. C.; Finn, M. G.; Sharpless, K. B. Click Chemistry: Diverse Chemical Function from a Few Good Reactions. *Angew. Chem. Int. Ed.* **2001**, *40* (11), 2004–2021. https://doi.org/10.1002/1521-3773(20010601)40:11<2004::AID-ANIE2004>3.0.CO;2-5.

(49) de Graaf, A. J.; Kooijman, M.; Hennink, W. E.; Mastrobattista, E. Nonnatural Amino Acids for Site-Specific Protein Conjugation. *Bioconjug. Chem.* **2009**, *20* (7), 1281–1295. https://doi.org/10.1021/bc800294a.

(50) Dirks, A. (Ton) J.; Cornelissen, J. J. L. M.; Nolte, R. J. M. Monitoring Protein−Polymer Conjugation by a Fluorogenic Cu(I)-Catalyzed Azide−Alkyne 1,3-Dipolar Cycloaddition. *Bioconjug. Chem.* **2009**, *20* (6), 1129–1138. https://doi.org/10.1021/bc8004667.

(51) Serwa, R.; Majkut, P.; Horstmann, B.; Swiecicki, J.-M.; Gerrits, M.; Krause, E.; Hackenberger, C. P. R. Site-Specific PEGylation of Proteins by a Staudinger-Phosphite Reaction. *Chem. Sci.* **2010**, *1* (5), 596–602. https://doi.org/10.1039/C0SC00324G.

(52) Dumas, A.; Spicer, C. D.; Gao, Z.; Takehana, T.; Lin, Y. A.; Yasukohchi, T.; Davis, B. G. Self-Liganded Suzuki–Miyaura Coupling for Site-Selective Protein PEGylation. *Angew. Chem. Int. Ed.* **2013**, *52* (14), 3916–3921. https://doi.org/10.1002/anie.201208626.

(53) Broyer, R. M.; Quaker, G. M.; Maynard, H. D. Designed Amino Acid ATRP Initiators for the Synthesis of Biohybrid Materials. *J. Am. Chem. Soc.* **2008**, *130* (3), 1041–1047. https://doi.org/10.1021/ja0772546.

(54) Peeler, J. C.; Woodman, B. F.; Averick, S.; Miyake-Stoner, S. J.; Stokes, A. L.; Hess, K. R.; Matyjaszewski, K.; Mehl, R. A. Genetically Encoded Initiator for Polymer Growth from Proteins. *J. Am. Chem. Soc.* **2010**, *132* (39), 13575–13577. https://doi.org/10.1021/ja104493d.

(55) Jeong, J.; Szczepaniak, G.; Das, S. R.; Matyjaszewski, K. Expanding the Architectural Horizon of Nucleic-Acid-Polymer Biohybrids by Site-Controlled Incorporation of ATRP Initiators in DNA and RNA. *Chem* **2023**, *9* (11), 3319–3334. https://doi.org/10.1016/j.chempr.2023.07.013.

(56) Jeong, J.; Hu, X.; Murata, H.; Szczepaniak, G.; Rachwalak, M.; Kietrys, A.; Das, S. R.; Matyjaszewski, K. RNA-Polymer Hybrids via Direct and Site-Selective Acylation with the ATRP Initiator and Photoinduced Polymerization. *J. Am. Chem. Soc.* **2023**, *145* (26), 14435–14445. https://doi.org/10.1021/jacs.3c03757.

(57) Montgomery, H. R.; Spokoyny, A. M.; Maynard, H. D. Organometallic Oxidative Addition Complexes for S-Arylation of Free Cysteines. *Bioconjug. Chem.* **2024**. https://doi.org/10.1021/acs.bioconjchem.4c00222.

# Chapter 2

# Efficient End-Group Functionalization and Diblock Copolymer Synthesis *via* Au(III) Polymer Reagents†

## 2.1 Introduction

Polymers with α- and/or ω-functionalization, also known as telechelic polymers, are useful building blocks for the synthesis of unique macromolecular architectures through coordination and conjugation.[58] This type of functionality can be achieved through the post-polymerization modification of chain transfer agents (CTAs) or use of functionalized CTAs in reversible addition fragmentation chain transfer (RAFT) polymerization, the nucleophilic substitution of terminal halides in atom transfer radical polymerization (ATRP) or the use of functionalized initiators, or the synthesis of nucleophilic initiators in anionic ring opening polymerization (ROP).[58] For example, small molecules such as fluorescent probes and affinity tags are commonly conjugated to polymers post-synthetically for use in various biological and materials applications. While there are many successful examples of these strategies, the post-polymerization modification of the end-group can suffer from challenges including poor kinetics which results in moderate to low levels of conversion to product. Additionally, the resulting linkages can also be reversable (for example containing ester bonds), leading to loss of the desired functionality.[59]

In addition to appending small molecules, telechelic polymers are also well-suited for the synthesis of macromolecular architectures such as diblock copolymers (DBCP). Typically, synthesis of DBCPs is undertaken by sequential polymerization of different monomers.[60] However, when the target DBCP contains units not polymerizable by compatible methods, post-polymerization conjugation of the disparate polymer blocks is required.[60] This latter synthetic strategy has significant challenges including the necessity of a highly efficient conjugation due to the low concentration of reactive units and the steric hindrance caused by polymer chains. One method to alleviate these synthetic concerns is to use “click”-type reactions due to their enhanced kinetics and chemoselectivity.[61] Effective examples of using “click”-type reactions for the

construction of DBCPs include thiol-ene reactions,[62,63] Cu(I)-catalyzed azide-alkyne cycloadditions (CuAAC),[64–66] Diels-Alder cycloadditions,[67,68] and more recently developed selective routes such as Sulfur(VI) Fluoride Exchange (SuFEx) reactions.[69] Thus, "click"-type chemistry allows for the facile synthesis of these DBCPs that otherwise would be synthetically inaccessible.[68,70–73] In each case, careful design and successful installation of reactive polymer end-groups is critical to achieve the desired product. Despite enabling impressive macromolecular structures, it is important to note that traditional "click"-chemical routes face some limitations. For example, these aforementioned methods have been known to exhibit low conversion when coupling partners are used at equimolar ratios due to kinetic limitations.[74] These methods can also place restrictions on monomer scope such as the need for the repeat units to be thermal- or photo-stable.[75] "Click"-type reactions can also lack certain chemical orthogonality; for example, acetylenic Glaser coupling is a possible side reaction for CuAAC conjugations.[76] Alternatively, the termination of living polymerizations with macromolecules has been utilized for the synthesis of these architectures, but this strategy generally requires a large excess of the terminating macromolecule, necessitating purification *via* time-intensive fractionation.[77] There remains a need for additional rapid and mild methodologies to address these limitations in existing conjugation techniques.

We have previously developed Au(III) mediated *S*-arylation utilizing isolable and bench-stable (Me-DalPhos)Au(III)Aryl reagents.[78] Recently, this chemistry has been expanded to demonstrate sterically-driven regioselectivity as well as successful picomolar bioconjugation with reagents enabling bimolecular rate constants of up to $1.7 \times 10^4$ $M^{-1}s^{-1}$.[79] Organometallic *S*-arylation with Au(III) oxidative addition complexes (OACs) are highly chemoselective, pH tolerant, and rapid at room temperature.[78–80] With these characteristics in mind, we envisioned that Au(III)

OACs would efficiently facilitate the synthesis of both modified mono-telechelic polymers and DBCP *via* ligand exchange with a second thiol-containing species and subsequent reductive elimination (RE). The resulting *S*-aryl bond would obviate the concern of a reversible conjugation, and the rapid kinetics and chemoselectivity of the reaction would provide quantiative conversion at equimolar ratios and prevent undesired side reactions.

## 2.2 Results and Discussion

### 2.2.1 Synthesis of Aryl Iodide and Au(III) OAC Heterotelechelic Polymers

We first synthesized aryl iodide-capped polymers to serve as precursors to OACs (**Figure 2.1A**). We prepared p(ε-caprolactone) (pCL) (**1**) (**Figure 2.1B**) by anionic ROP using an aryl

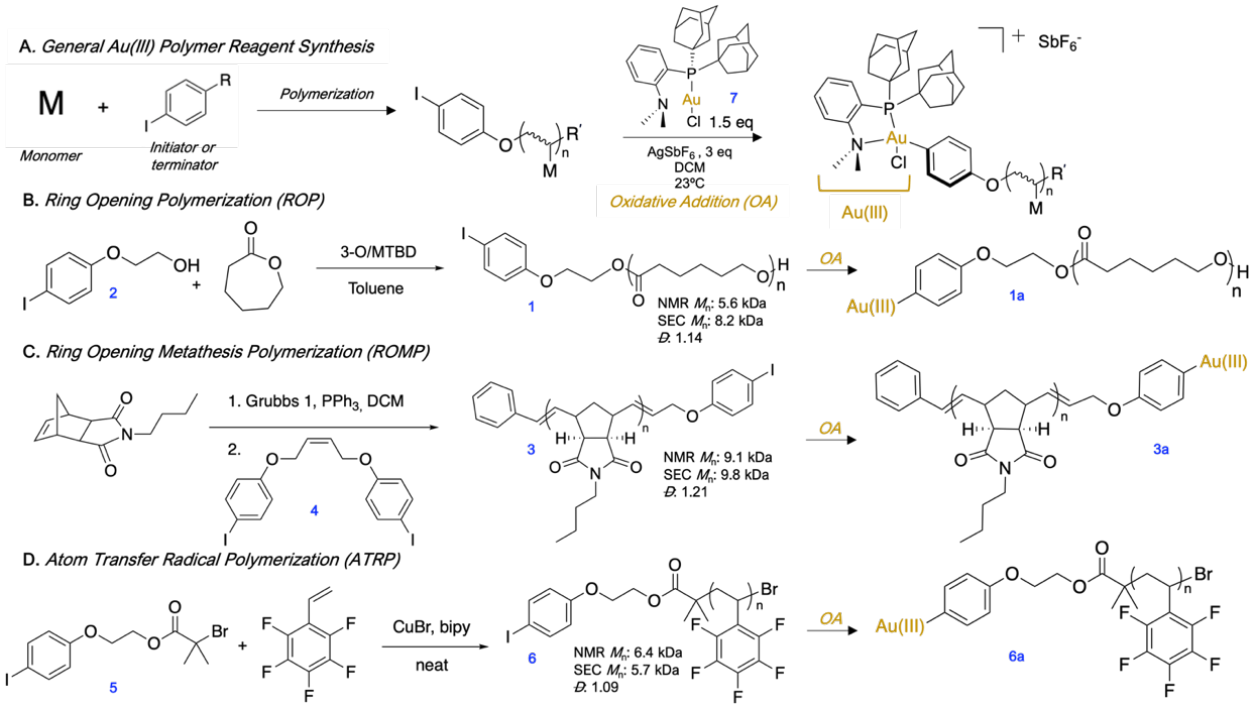


**Figure 2.1** A) General Au(III) polymer reagent synthesis (Au(III)=[(Me-DalPhos)Au(III)Cl]$^+$ $SbF_6^-$). B) Ring opening polymerization of caprolactone and synthesis of OAC. C) Ring opening metathesis polymerization of N-butylnorbornene imide and synthesis of OAC. D) Atom transfer radical polymerization of pentafluorostyrene and synthesis of OAC.

iodide-functionalized initiator (**2**) and the 3-O/MTBD cocatalyst sytem.[81] While in preliminary polymerizations we utilized a 4-iodobenzyl alcohol to initiate, we found that upon oxidative addition, the terminal ester adjacent to the Au(III) complex can be activated and cleaved. Therefore, we replaced our initiator with 4-iodophenethyl alcohol (**2**) wherein the terminal ester was no longer activated at the benzylic position and thus less likely to cleave. Next, p(*n*-

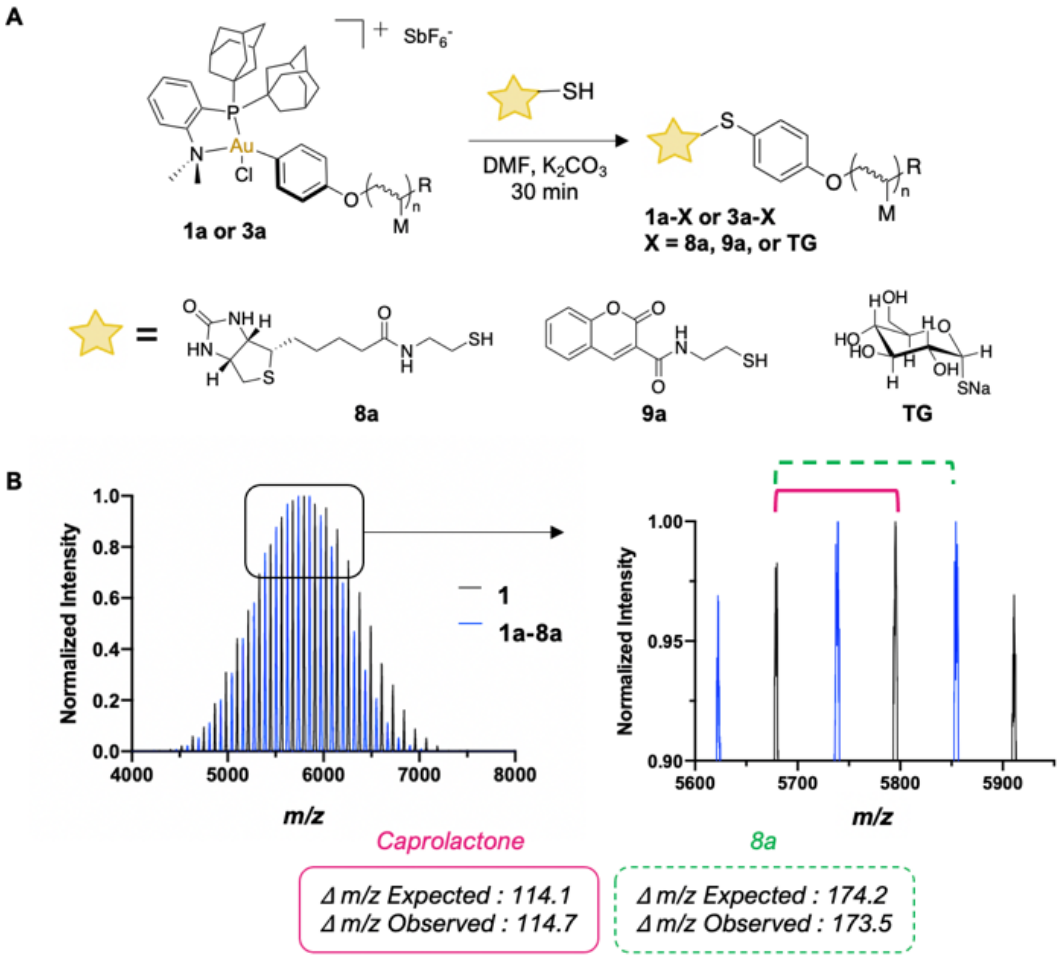


**Figure 2.2** A) Scheme of modified mono-telechelic polymer synthesis *via* *S*-arylation of thiolated biotin (**8a**), thiolated coumarin (**9a**), and sodium thioglucose (**TG**) with **1a** or **3a**. B) MALDI-TOF mass spectra of **1** and **1a-8a** with magnified inset. Expected and calculated Δ*m/z* differences between repeat units of **1a** and end groups of **1a** and **1a-8a**.

butylnorborneneimide) (pBNI) (**3**) (**Figure 2.1C**) was synthesized by ROMP and quenched using a cis-stilbene aryl iodide derivative (**4**) to incorporate an aryl iodide *via* direct end-capping.[82,83] Finally, we synthesized an aryl iodide-containing ATRP initiator (**5**) from **2** and employed it in the synthesis of p(pentafluorostyrene) (pPFS) (**6**) (**Figure 2.1D**). Many polymer conjugation strategies utilize the tertiary bromide of ATRP polymer end-groups,[84] which generally necessitates low polymer conversion to protect end-group fidelity.[85,86] In this case, the use of an aryl iodide-containing ATRP initiator ensures the presence of a functional handle without sacrificing polymer conversion. All aryl iodide polymers underwent oxidative addition in open air with (Me-DalPhos)Au(I)Cl (**7**) using $AgSbF_6$ as a halide scavenger to afford isolable and bench stable

Au(III) polymer reagents (**1a, 3a, 6a**). $^{1}H$ and $^{31}P\{^{1}H\}$ NMR spectroscopy were used to determine conversion to the Au(III) species, and it was found that the removal of excess Au(I) was not necessary, as it did not inhibit the subsequent *S*-arylation. Isolated Au(III) polymer complexes are stable for up to three months, as monitored by $^{31}P\{^{1}H\}$ NMR spectroscopy.[87]

### 2.2.2 End-group modification and DBCP Synthesis *via* Au(III) OAC Polymers

We performed *S*-arylation on a small library of biologically relevant small molecules (**Figure 2.2A**). Successful *S*-arylation of thiolated biotin (**8a**), thiolated coumarin (**9a**), and commercial sodium thioglucose (**TG**) with pCL-Au(III) (**1a**) and pBNI-Au(III) (**3a**) occurred in 30 minutes as observed *via* $^{1}H$ NMR and $^{31}P\{^{1}H\}$ NMR spectroscopy (**Figures 2.51-2.63**). MALDI-TOF characterization was also used to observe mass differences which correspond to the replacement of the iodide of **1a** with **8a,** thereby confirming that efficient *S*-arylation had occurred (**Figure 2.2B**).

In a similar approach, we hypothesized that these Au(III) polymer reagents would offer a facile and modular synthesis of DBCP utilizing thiol-modified mono-telechelic polymers (**Table 2.1**). To this end, p(*N*-isopropylacrylamide) (pNIPAM) (**10**) was synthesized *via* RAFT. The

presence of a dithioester in many CTAs affords a free thiol coupling partner following aminolysis (**10a**). This aminolysis of the CTA was monitored by UV-Vis spectroscopy and $^1$H NMR (**Figures 2.66-2.67**). To achieve thiol-functionalized polymers *via* ROP, an *S*-trityl protected thioether initiator (**11**) was used for the synthesis of pCL (**12**) and subsequently deprotected to reveal the free thiol (**12a**). This demonstrates that controlled polymerization strategies such as ROP can be utilized in either the thiol or aryl iodide block interchangeably by employing the appropriate small molecule conjugation handle in the initiator.

This thiol polymer library was subjected to various polymeric Au(III) *S*-arylation reagents to yield DBCP synthesized by disparate polymerization methods(**Table 2.1**, **Entries 13-15**, see experimental section for synthetic details). Specifically, p(NIPAM)-SH (**10a**) was reacted with

**Table 2.1** Functionality, precursor, synthesis strategy, NMR molecular weight ($M_n$), SEC molecular weight ($M_n$), and dispersity ($Đ$) reported for polymer precursors and DBCP (BCP). Expected $M_n$ is calculated from $^1$H NMR observed conversion.

| Entry | Functionality | Precursor | Strategy | Expected $M_n$ (kDa) | SEC $M_n$ (kDa) | Dispersity ($Đ$) |
|---|---|---|---|---|---|---|
| **10** | Thiol | NIPAM | RAFT | 9.6 | 9.3 | 1.11 |
| **12** | Thiol | CL | ROP | 9.6 | 10.0 | 1.20 |
| **13** | BCP | **1a** + **10a** | *S*-Arylation | 12.5 | 11.9 | 1.37 |
| **14** | BCP | **3a** + **12a** | *S*-Arylation | 25.7 | 17.7 | 1.27 |
| **15** | BCP | **6a** + **12a** | *S*-Arylation | 12.5 | 11.9 | 1.37 |
| **16** | Aryl I | BNI | ROMP | 30.2 | 27.2 | 1.27 |
| **17** | Thiol | CL | ROP | 36.4 | 37.4 | 1.13 |
| **18** | BCP | **16a** + **17a** | *S*-Arylation | 72.7 | 42.3 | 1.40 |

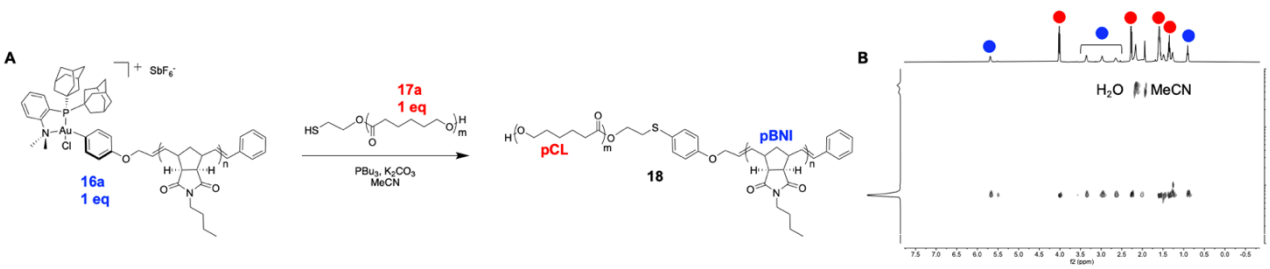


**Figure 2.3** A) pCL-*b*-pBNI (**18**) *S*-arylation scheme B) DOSY NMR spectrum of pCL-*b*-pBNI (**18**) in $CD_3CN$.

pCL-Au(III) (**1a**) to prepare a p(NIPAM)-*b*-p(CL) DBCP (**13**). Furthermore, p(CL)-SH (**12a**) was reacted with p(BNI)-Au(III) (**3a**) and p(PFS)-Au(III) (**6a**) to produce p(CL)-*b*-p(BNI) (**14**) and p(CL)-*b*-p(PFS) (**15**) DBCPs, respectively. All *S*-arylation reactions occur in one hour, in open air, using an equimolar ratio of polymer precursors, and at ambient temperature, highlighting the mild conditions and efficiency of this synthetic strategy. These reactions occur in the presence of tributylphosphine ($PBu_3$) as a disulfide reducing agent, and it was observed that $PBu_3$ did not interfere with the *S*-arylation. Conversion and product dispersity were monitored by multinuclear NMR spectroscopy, diffusion ordered spectroscopy (DOSY), and size exclusion chromatography (SEC) (**Figures 2.74-2.90**). DOSY NMR experiments indicated that, in every example, both sets of polymer peaks diffused at the same rate, suggesting one, connected DBCP species in solution. Complete conversion of precursors **6a** and **12a** to produce **15** was observed by DOSY NMR experiments (**Figure 2.89**), and $^{19}F$ NMR spectroscopy (**Figure 2.88**) indicates that the *S*-arylation outpaces any potential $S_NAr$ reactions with the side chains of **6a** despite the lower relative concentration of Au(III) in solution.[88] Since $^{1}H$, $^{31}P$, and DOSY NMR experiments indicate full conversion to DBCP products, peak shape abnormalities in SEC spectra for *S*-arylation products may be a result of secondary structure and column interaction from disparately hydrophobic blocks.

In general, quantitative conversion to DBCP products becomes more challenging as the polymer precursor size increases, as this lowers the relative concentration of reactive end-group units in solution. We hypothesized that our robust conjugation method would allow for access to large DBCP that may be challenging to obtain using other methods. To test this hypothesis, we prepared 27.2 kDa pBNI-Au(III) (**16a**) and 36.4 kDa pCL-SH (**17a**) mono-telechelic polymers (**Table 2.1**). We observed quantitative conversion to DBCP product **18** by $^{31}P\{^{1}H\}$ and DOSY NMR spectroscopy after one hour using our standard conjugation conditions, highlighting the efficiency of this method (**Figure 2.3**).

## 2.3 Conclusion

This work demonstrates the efficiency of the post-polymerization synthesis of small molecule mono-telechelic polymers and DBCP utilizing organometallic Au(III) polymer reagents. The synthetic availability of the aryl iodide and thiol coupling partners allows for their facile incorporation into small molecules and polymers. These polymers can be synthesized by common controlled polymerization techniques such as RAFT, ROP, ATRP, and ROMP. The selectivity of (Me-DalPhos)Au(I)Cl (**7**) for aryl iodides during oxidative addition and the thiophilicty of Au(III) permits the use of many desirable side-chain functional groups without concern of cross-reactivity. Au(III) polymer reagents are isolable and bench-stable, allowing for a modular approach to the rapid minute-scale synthesis of various functionalized polymers. Ultimately, this work adds to the "click"-type reaction toolbox for the synthesis of complex polymers and can be expanded for the synthesis of other polymeric applications and macromolecular architectures.

## 2.4 Experimental

### 2.4.1 Materials

Unless otherwise stated, all materials were purchased and used as received from Fisher Scientific, Combi-Blocks, Alfa Aesar, Oakwood Chemicals, or Sigma Aldrich. Silver hexafluoroantimonate ($AgSbF_6$) was stored in a nitrogen atmosphere glovebox prior to use. Anhydrous triethylamine, DCM, and toluene were prepared by distillation over calcium hydride under an argon atmosphere. Anhydrous dioxane was purchased from Sigma-Aldrich. Caprolactone and MTBD were distilled under vacuum over activated 4 Å molecular sieves prior to use.

### 2.4.2 Analytical Techniques

NMR spectra were recorded on the following: AV400 Bruker spectrometer at 400 ($^1$H), 376 ($^{19}$F{$^1$H}), 101 ($^{13}$C), and 121 MHz ($^{31}$P{$^1$H}), AV300 Bruker spectrometer at 300 (1H) and 75 MHz ($^{13}$C), and NEO600 Bruker spectrometer at 600 ($^1$H) and 243 ($^{31}$P{$^1$H}). Spectra are reported in δ (parts per million) relative to residual proteo-solvent signals for $^1$H and $H_3PO_4$ (δ 0.00 ppm) for $^{31}$P{$^1$H}. All DOSY NMR spectra were recorded on a DRX 500 Bruker spectrometer at 500 MHz ($^1$H). The following abbreviations were used to explain multiplicities: s = singlet, d = doublet, t = triplet, q = quartet, m = multiplet. Deuterated solvents were purchased from Cambridge Isotope Laboratories and used as received for all NMR experiments.

Column chromatography was performed on a Biotage Isolera One 3.0 autocolumn instrument using KP-Sil high-performance columns repacked using Silicycle silica (P60, particle size 40–63 μm, column sizes described in experimental). TLC was performed using Millipore Sigma silica plates (60F-254) using short-wave UV light or $KMnO_4$ as visualizing agents. Electrospray ionization (ESI) mass spectra were obtained using an Agilent 6530 QTOF-ESI in tandem with a 1260 Infinity LC. DART mass spectra were obtained using a Thermo Exactive Plus

Orbitrap with IonSense ID-CUBE DART source. IR spectra were obtained using a PerkinElmer Spectrum One FT-IR Spectrometer.

DMF Size Exclusion Chromatography (SEC)/Gel Permeation Chromatography (GPC) was conducted on an Agilent 1260 Infinity II high performance liquid chromatography (HPLC) system with a Wyatt Optilab (RI and MALS detection), one Polymer Laboratories PLgel guard column, and two Polymer Laboratories PLgel 5 μm mixed D columns. The eluent was DMF (HPLC Grade, 99.7+%, Thermo Scientific Chemicals) containing LiBr (0.1 M) at 40 °C (Flow rate: 0.6 mL/min). THF SEC was conducted on a Shimadzu Prominence modular HPLC system with a Shimadzu Prominence-I LC 2030 C 3D autosampler, two MZ-Gel SDplus LS 5 μm, 300 × 8 mm linear columns, Wyatt DAWN HELOS-II, and a Wyatt Optilab T-rEX. The column temperature was set to 40 °C and flow rate was set to 0.7 mL/min. Molecular weight information was determined for data collected on either SEC instrument was obtained using a PMMA (Agilent Technologies, EasiVial PMMA, pre-weighed calibration kit) conventional calibration analysis.

MALDI-TOF spectra were obtained using a Bruker Ultraflex MALDI TOF-TOF. MALDI samples were prepared by combining 1 mg/mL solution of the polymer sample, 1 mg/mL dithranol, and NaTFA (100 mM) in a 5:25:1 v/v/v ratio. All solutions were prepared in THF.

### 2.4.3 Methods

**Synthesis of *exo-n*-butylnorborneneimide (19)**

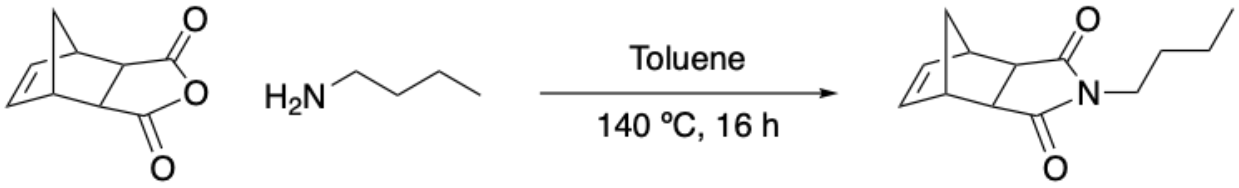


A flame dried 250 mL round bottom flask was charged with a stir bar and equipped with a Dean-Stark apparatus. Cis-5-norbornene-exo-2,3-dicarboxylic anhydride (2.0 g, 1 Eq, 12.2 mmol) was suspended in 60 mL of toluene, then *n*-butylamine (1.2 mL, 1 Eq, 12.2 mmol) was added to the flask, forming a light yellow suspension. This was heated at 140 ºC for 16 hours. The reaction was cooled to room temperature and further purified using flash column chromatography (100 g silica gel, 0-70% gradient of ethyl acetate against hexanes) to yield *exo-n*-butylnorborneneimide as an off white solid (2.52 g, 11.5 mmol, 94% yield).

**Physical state:** Off white solid

**TLC ($KMnO_4$):** $R_f$ 0.77 (1:1 hexanes-ethyl acetate)

**$^1$H NMR (300 MHz, $CDCl_3$):** δ 6.26 (t, *J* = 1.9 Hz, 2H), 3.49 – 3.39 (m, 2H), 3.25 (m, 2H), 2.65 (d, *J* = 1.4 Hz, 2H), 1.57 – 1.45 (m, 3H), 1.37 – 1.24 (m, 2H), 1.24 – 1.18 (m, 1H), 0.90 (t, *J* = 7.3 Hz, 3H).

**$^{13}$C NMR (75 MHz, $CDCl_3$):** δ 178.19, 137.93, 47.90, 45.27, 42.81, 38.60, 29.93, 20.32, 13.72.

**HRMS (ESI/QTOF):** $[M+H]^+$ calculated for $C_{13}H_{18}NO_2^+$ 220.1338, observed 220.1362.

**IR (Film):** 2960, 2876, 1768, 1689, 1435, 1394, 1358, 1341, 1286, 1263, 1190, 1137, 1103, 1017 $cm^{-1}$.

**Synthesis of 3-O Trisurea (20)**[81]

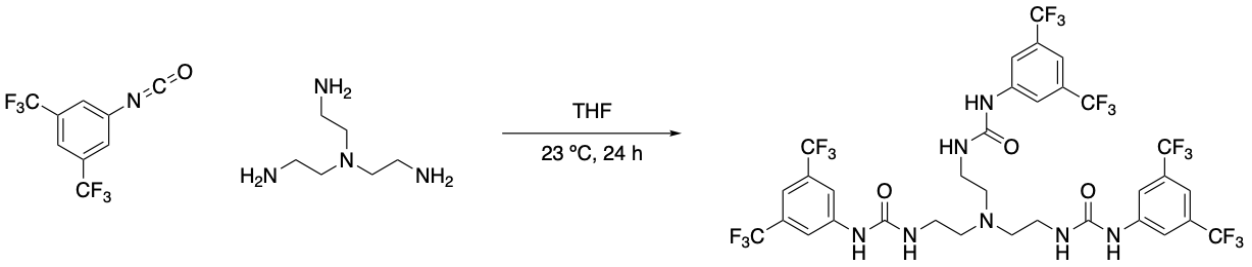


A flame dried two neck, 100 mL round bottom flask was charged with a stir bar and tris(2-aminoethyl)amine (400 mg, 1 Eq, 2.74 mmol) was dissolved in 20 mL of anhydrous THF. The 1-isocyanato-3,5-bis(trifluoromethyl)benzene (2.16 g, 1.18 mL, 3.1 Eq, 8.48 mmol) was dissolved in 5 mL of anhydrous THF and added to the round bottom flask at 23 ºC over 15 minutes *via* syringe pump. The reaction was left to stir at 23 ºC for 24 hours under an argon atmosphere. The reaction was subsequently concentrated under vacuum and purified using flash column chromatography (100 g silica gel, 0-10% gradient of methanol against DCM) to yield 3-O as a white solid (1.88 g, 2.14 mmol, 78% yield).

**Physical state:** White solid

**TLC (UV):** $R_f$ 0.40 (9:1 DCM-methanol)

**$^1$H NMR (400 MHz, Acetone-d$_6$):** δ 8.80 (br s, 3H), 8.00 (d, *J* = 1.6 Hz, 6H), 7.41 (t, *J* = 1.6 Hz, 3H), 6.49 (t, *J* = 5.3 Hz, 3H), 3.36 (q, *J* = 5.5 Hz, 6H), 2.72 (d, *J* = 5.7 Hz, 6H).

**$^{19}$F{$^1$H} NMR (376 MHz, Acetone-d$_6$):** δ -63.74.

**$^{13}$C NMR (101 MHz, Acetone-d$_6$):** δ 156.31, 143.36, 132.28 (q, *J* = 32.9 Hz), 124.39 (q, *J* = 271.9 Hz), 118.34, 114.83, 55.71, 39.16.

**HRMS (DART):** $[M+H]^+$ calculated for $C_{33}H_{28}F_{18}N_7O_3^+$ 912.1966, observed 912.1965.

**Synthesis of 2-(tritylthio)ethan-1-ol (11)**

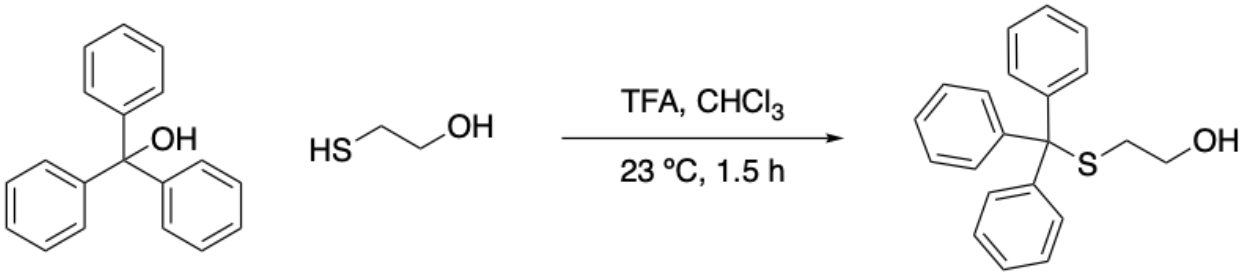


A 100 mL round bottom flask was charged with a stir bar and 30 mL of chloroform was added to the flask followed by 2-mercaptoethan-1-ol (630.2 mg, 568 µL, 1.4 Eq, 8.07 mmol). This was left to stir at 23 ºC for a minute, then triphenylmethanol (1.5 g, 1 Eq, 5.76 mmol) was added as a solid to the flask, creating a light brown solution. Trifluoroacetic acid (7.400 g, 5.000 mL, 11.3 Eq, 64.9 mmol) was then added to the solution, immediately forming a bright yellow color. This was left to stir under an open atmosphere at 23 ºC for 90 minutes. The contents of the reaction were concentrated under vacuum, then the material was carefully neutralized with a saturated sodium bicarbonate solution. The material was transferred to a separatory funnel and extracted with ethyl acetate (200 mL) then washed with brine (50 mL). The organic layer was collected, dried with anhydrous magnesium sulfate, filtered, then concentrated under vacuum. The product was further purified using flash column chromatography (100 g silica gel 0-60% gradient of ethyl acetate against hexanes) to afford 2-(tritylthio)ethan-1-ol as a white solid (1.197 g, 3.745 mmol, 65% yield).

**Physical state:** White solid

**TLC (UV):** $R_f$ 0.32 (3:1 hexanes-ethyl acetate)

**$^1$H NMR (300 MHz, $CD_2Cl_2$):** δ 7.47 – 7.40 (m, 6H), 7.34 – 7.19 (m, 9H), 3.36 (q, J = 6.2 Hz, 2H), 2.43 (t, J = 6.3 Hz, 2H), 1.59 (t, J = 6.1 Hz, 1H).

**$^{13}$C NMR (75 MHz, $CD_2Cl_2$):** δ 145.28, 129.97, 128.31, 127.12, 66.97, 61.19, 35.56.

**HRMS (DART):** $[M+H]^+$ calculated for $C_{21}H_{21}OS^+$ 321.1313, observed 321.1318.

**IR (Film):** 3357, 3056, 2948, 1595, 1488, 1443, 1183, 1034 $cm^{-1}$.

**Synthesis of 2-(4-iodophenoxy)ethan-1-ol (2)**

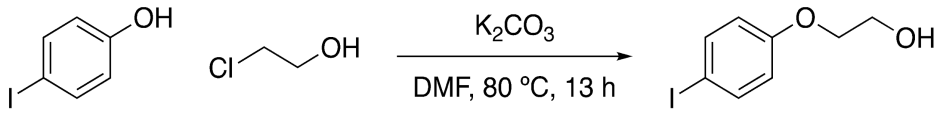


A 50 mL round bottom flask was charged with a stir bar and 4-iodophenol (750.0 mg, 1 Eq, 3.409 mmol) and potassium carbonate (1.65 g, 3.5 Eq, 11.9 mmol) were added to the flask. The solids were dissolved in 10 mL of DMF, creating a white suspension. This mixture was headed at 50 ºC for five minutes, then 2-chloroethanol (274 µL, 1.2 Eq, 4.09 mmol) was added to the solution at 50 ºC. The solution was left to heat at 80 ºC for 13 hours. The contents of the reaction were cooled down and transferred to a separatory funnel with ethyl acetate (200 mL), then the organic layer was washed with water (50 mL), saturated sodium carbonate (50 mL), and brine (50 mL). The organic layer was collected, dried with anhydrous magnesium sulfate, filtered, and concentrated under vacuum. The product was further purified using flash column chromatography (100 g silica gel, 0-60% gradient of ethyl acetate against hexanes) to afford 2-(4-iodophenoxy)ethan-1-ol as an off white solid (500 mg, 1.909 mmol, 56% yield).

**Physical state:** Off white solid

**TLC (UV):** $R_f$ 0.42 (1:1 hexanes-ethyl acetate)

**$^1$H NMR (400 MHz, DMSO-$d_6$):** δ 7.62 – 7.54 (m, 2H), 6.83 – 6.74 (m, 2H), 4.86 (t, *J* = 5.5 Hz, 1H), 3.95 (m, 2H), 3.74 – 3.64 (m, 2H).

**$^{13}$C NMR (101 MHz, DMSO-$d_6$):** δ 158.60, 137.91, 117.29, 82.90, 69.65, 59.44.

**HRMS (ESI/QTOF):** $[M+H]^+$ calculated for $C_{12}H_{10}IO_2^+$ 264.9725, observed 264.9763.

**IR (Film):** 3303, 2937, 2863, 1585, 1485, 1456, 1285, 1244, 1175, 1083, 1051 $cm^{-1}$.

**Synthesis of 2-(4-iodophenoxy)ethyl 2-bromo-2-methylpropanoate (5)**

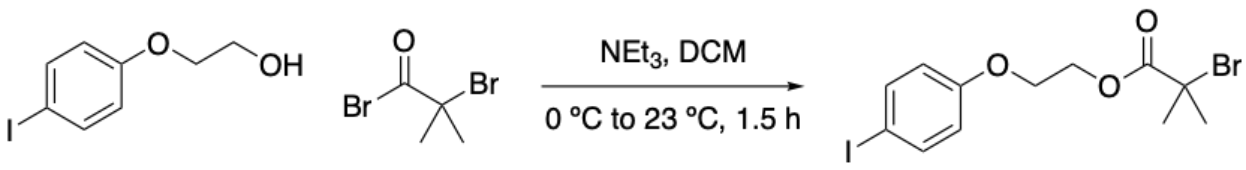


A flame dried two neck 50 mL round bottom flask was charged with a stir bar and 2-(4-iodophenoxy)ethan-1-ol (300 mg, 1 Eq, 1.14 mmol) was added to the flask and dissolved in 7 mL of anhydrous DCM, forming a clear solution. Anhydrous triethylamine (190 µL, 1.2 Eq, 1.36 mmol) was added to the flask, forming a light yellow solution. The solution was cooled to 0 ºC under an argon atmosphere. Separately, 2-bromo-2-methylpropanoyl bromide (181 µL, 1.2 Eq, 1.36 mmol) was dissolved in 3 mL of anhydrous DCM, then this was added to the solution *via* syringe pump over a period of 10 minutes with no color change. This was left to room up to 23 ºC where it was stirred for 90 minutes under an argon atmosphere. The contents of the reaction were transferred to a separatory funnel (150 mL DCM) where the organic layer was washed once with brine (50 mL). The organic layer was collected, dried with anhydrous magnesium sulfate, filtered, and concentrated under vacuum. The product was further purified using flash column chromatography (50 g silica gel, 0-50% gradient of ethyl acetate against hexanes) to afford 2-(4-iodophenoxy)ethyl 2-bromo-2-methylpropanoate as a white solid (429 mg, 1.037 mmol, 91% yield).

**Physical state:** White solid

**TLC (UV):** $R_f$ 0.67 (2:1 hexanes-ethyl acetate)

**$^1$H NMR (300 MHz, $CDCl_3$):** δ 7.61 – 7.50 (m, 2H), 6.75 – 6.65 (m, 2H), 4.55 – 4.47 (m, 2H), 4.22 – 4.14 (m, 2H), 1.93 (s, 6H).

**$^{13}$C NMR (75 MHz, $CDCl_3$):** δ 171.77, 158.52, 138.47, 117.30, 83.59, 65.89, 64.13, 55.55, 30.84.

**HRMS (ESI/QTOF):** $[M+Na]^+$ calculated for $C_{12}H_{14}BrINaO_3^+$ 434.9069, observed 434.9073.

**IR (Film):** 2970, 1735, 1586, 1485, 1461, 1388, 1371, 1275, 1242, 1161, 1108, 1073, 1058 $cm^{-1}$.

**Synthesis of (*Z*)-1,4-bis(4-iodophenoxy)but-2-ene (4)**

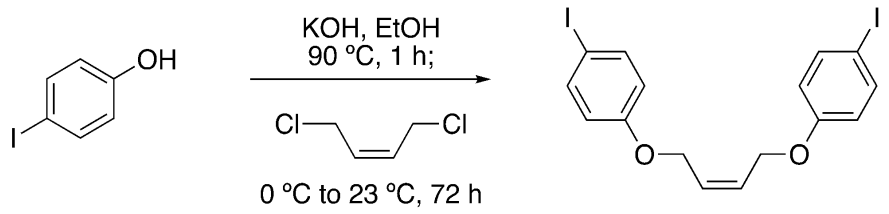


A one neck 250 mL round bottom flask was charged with a stir bar and 4-iodophenol (7.261 g, 3 Eq, 33.00 mmol) and potassium hydroxide (1.79 g, 2.9 Eq, 31.9 mmol) were added as solid to the flask. 40 mL of ethanol was added to the flask, and the solution was refluxed at 90 ºC for one hour. The flask was cooled to 0 ºC, then (Z)-1,4-dichlorobut-2-ene (1.157 mL, 1 Eq, 11.00 mmol) was added to the flask dropwise over three minutes. The solution was allowed to warm up to 23 ºC where it was left to stir for 72 hours (Product formation monitored by HPLC, near quantitative conversion after 72 hours). The contents of the reaction were diluted with ethyl acetate (300 mL) and transferred to a separatory funnel where the organic layer was washed with brine (2 x 100 mL). The organic layer was collected, dried with anhydrous magnesium sulfate, filtered, and concentrated under vacuum. The product was further purified using flash column chromatography

(350 g silica gel, 0-20% gradient of DCM against hexanes) to afford (Z)-1,4-bis(4-iodophenoxy)but-2-ene as a white solid (3.799 g, 7.700 mmol, 70% yield).

**Physical state:** White solid

**TLC (UV):** $R_f$ 0.83 (1:1 hexanes-DCM)

**$^1$H NMR (400 MHz, $CDCl_3$):** δ 7.60 – 7.51 (m, 4H), 6.74 – 6.62 (m, 4H), 5.91 (m, 2H), 4.65 – 4.60 (m, 4H).

**$^{13}$C NMR (101 MHz, $CDCl_3$):** δ 158.35, 138.46, 128.54, 117.20, 83.38, 64.38.

**HRMS (DART):** $[M]^+$ calculated for $C_{16}H_{14}I_2O_2^+$ 491.9083, observed 491.9087.

**IR (Film):** 3058, 2917, 2872, 1582, 1570, 1481, 1452, 1414, 1398, 1375, 1341, 1298, 1281, 1231, 1172, 1112, 1059, 1032 $cm^{-1}$.

**Synthesis of 2-iodo-*N*,*N*-dimethylaniline[89] (21)**

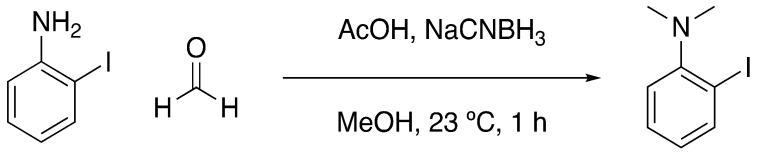


A one neck 1 L round bottom flask was charged with a stir bar, then 2-iodoaniline (10.0 g, 1 Eq, 45.656 mmol) was dissolved in 400 mL of methanol. Formaldehyde (34.1 mL, 10 Eq, 456.6 mmol, 37 wt. % in water) and acetic acid (13.1 mL, 5 Eq, 228.28 mmol) were added to the flask and left to stir for ten minutes at 23 ºC. Sodium cyanoborohydrdide (11.5 g, 4 Eq, 182.6 mmol) was added in portions over a 15 minute period, then this was left to stir for one hour at 23 ºC. The reaction was concentrated under vacuum and carefully pH adjusted to pH 8.0 using 1 M $NaHCO_3$. The product was transferred to a separatory with ethyl acetate (300 mL), then the organic layer was washed with $NaHCO_3$ (2 x 75 mL) and brine (100 mL). The organic layer was collected, dried

with anhydrous magnesium sulfate, filtered, and concentrated under vacuum. The resulting product was further purified by vacuum distillation at 85 ºC to afford a clear liquid (9.45 g, 38.4 mmol, 84% yield).

**Physical state:** Clear liquid

**TLC (UV):** $R_f$ 0.67 (5:1 hexanes-ethyl acetate)

**$^1$H NMR (400 MHz, $CDCl_3$):** δ 7.84 (dd, *J* = 7.8, 1.5 Hz, 1H), 7.31 (m, 1H), 7.10 (dd, *J* = 8.0, 1.5 Hz, 1H), 6.77 (m, 1H), 2.77 (s, 6H).

**$^{13}$C NMR (101 MHz, $CDCl_3$):** δ 155.10, 140.33, 129.19, 125.12, 120.61, 97.27, 45.12.

**HRMS (ESI/QTOF):** $[M+H]^+$ calculated for $C_8H_{11}IN^+$ 247.9936, observed 247.9963.

**IR (Neat):** 2981, 2939, 2857, 2826, 2777, 1579, 1468, 1450, 1314, 1183, 1157, 1110, 1094, 1045, 1011 $cm^{-1}$.

**Synthesis of Me-DalPhos[90] (22)**

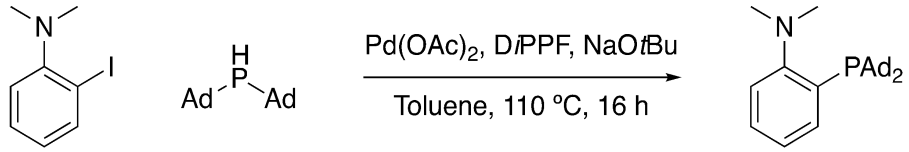


Inside of a nitrogen atmosphere in a glovebox, $Pd(OAc)_2$ (16.7 mg, 0.025 Eq, 74.4 µmol) and D*i*PPF (37.3 mg, 0.030 Eq, 89.3 µmol) were added as solids to a one dram vial charged with a stir bar, then the solids were dissolved in 400 µL of anhydrous toluene and left to stir at 23 ºC for 15 minutes. Separately, di-1-adamantylphosphine (900 mg, 1 Eq, 2.98 mmol) and NaO*t*Bu (429 mg, 1.5 Eq, 4.46 mmol) were added as solids to a scintillation vial charged with a stir bar and subsequently dissolved in 8 mL of anhydrous toluene where this was left to stir for 15 minutes. 2-iodo-*N*,*N*-dimethylaniline (757 mg, 103 Eq, 3.07 mmol) was weighed out into a scintillation vial

charged with a stir bar and diluted with 2 mL of anhydrous toluene. The $Pd(OAc)_2$/D*i*PPF solution was transferred to the scintillation vial containing the 2-iodo-*N*,*N*-diemethylaniline, then the $HPAd_2$/NaO*t*Bu suspension was transferred to the scintillation vial. Each vial was washed with 500 µL (1 mL total) of anhydrous toluene. The scintillation vial was sealed with electrical tape and removed from the glovebox where it was refluxed in a closed vial at 110 ºC for 16 hours. The reaction was cooled to 23 ºC and subsequently concentrated under vacuum. The solid was redissolved in chloroform and filtered through a plug of Celite, then the product was concentrated under vacuum. The product was suspended in cold hexanes and transferred to a medium grain fritted funnel where the product was rinsed with cold diethyl ether (2 x 5 mL), cold acetonitrile (2 x 5 mL), and cold diethyl ether (2 x 5 mL). The residual solid on the frit was then dried under vacuum to afford the product as a white solid (893 mg, 2.12 mmol, 71% yield).

**Physical state:** White solid

**$^1$H NMR (400 MHz, $CD_2Cl_2$)** δ 7.72 – 7.65 (m, 1H), 7.33 – 7.25 (m, 1H), 7.20 – 7.10 (m, 1H), 7.06 – 6.95 (m, 1H), 2.69 (s, 6H), 2.00 – 1.84 (m, 18H), 1.71 – 1.62 (m, 12H).

**$^{31}$P{$^1$H} NMR (162 MHz, $CD_2Cl_2$):** δ 20.26.

**HRMS (DART):** $[M+H]^+$ calculated for $C_{28}H_{41}NP^+$ 422.2977, observed 422.2972.

**Synthesis of (Me-DalPhos)Au$^{I}$Cl[91] (7)**

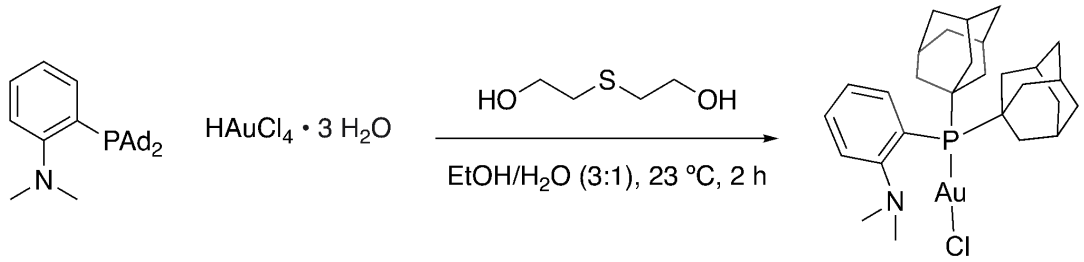


A scintillation vial was charged with a stir bar and $HAuCl_4 \bullet 3H_2O$ (322 mg, 1 Eq, 819 µmol) was added as a solid to the flask, then it was dissolved in 2 mL of DI water. Separately, Me-DalPhos (345 mg, 1 Eq, 818.6 µmol) was suspended in 3 mL of ethanol in a dram vial, then this was added to the scintillation vial. The dram vial was washed with ethanol (3 x 1 mL) and transferred to the scintillation vial. This was stirred at 23 ºC for two hours. The contents of the reaction were then transferred onto a medium grain fritted funnel where the white solid was washed with methanol (3 x 5 mL). The white solid was dissolved in DCM and filtered through a plug of Celite to remove any nanoparticles that may have formed. The eluent was then concentrated under vacuum to afford the product as a white solid (482 mg, 737 µmol, 90% yield).

**Physical state:** White solid

**$^{1}$H NMR (400 MHz, $CD_2Cl_2$)** δ 7.79 – 7.72 (m, 1H), 7.59 – 7.51 (m, 2H), 7.34 – 7.27 (m, 1H), 2.57 (s, 6H), 2.26 – 2.17 (m, 6H), 2.12 – 2.04 (m, 6H), 2.01 – 1.94 (m, 6H), 1.72 – 1.64 (m, 12H).

**$^{31}$P{$^{1}$H} NMR (162 MHz, $CD_2Cl_2$):** δ 56.70.

**HRMS (DART):** $[M+H]^+$ calculated for $C_{28}H_{41}NP^+$ 654.2331, observed 654.2325.

**Synthesis of 2-(tritylthio)ethan-1-ammonium trifluoroacetate (23)**

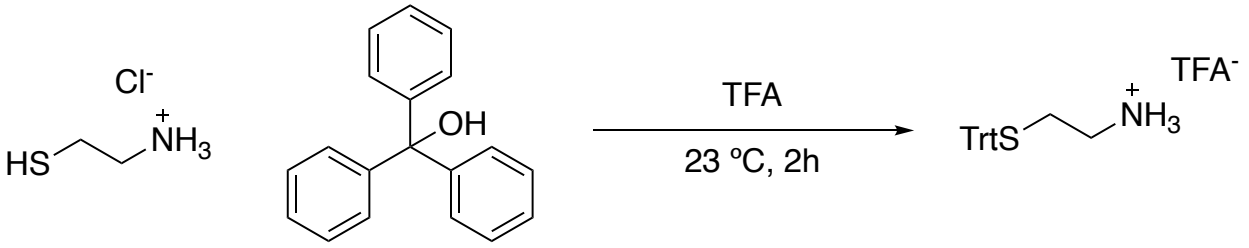


A 100 mL one neck RBF was charged with a stir bar and 2-aminoethane-1-thiol hydrochloride (1.92 g, 1.1 Eq, 16.9 mmol) and triphenylcarbinol (4.00 g, 1 Eq, 15.4 mmol) were added as solids to the flask. The materials were then dissolved in trifluoroacetic acid (22.20 g, 15.0 mL, 12.7 Eq, 195 mmol), turning the solution immediately yellow and then a dark brown color with a slight exotherm. The reaction was stirred at 23 ºC for two hours. After two hours, the reaction was dried under a stream of air. The reaction was then precipitated into diethyl ether (45 mL) upon which a white solid crashed out. The solid was filtered and washed with diethyl ether (3 x 25 mL) to yield 2-(tritylthio)ethan-1-ammonium trifluoroacetate as a white solid (3.90 g, 9.00 mmol, 59% yield).

**Physical state:** White solid

**$^{1}$H NMR (400 MHz, MeOD):** δ 7.45 – 7.38 (m, 6H), 7.29 – 7.25 (m, 6H), 7.24 – 7.18 (m, 3H), 2.40 – 2.39 (m, 2H), 2.37 – 2.31 (m, 2H).

**$^{13}$C NMR (101 MHz, $CD_3CN$):** δ 145.31, 130.28, 129.12, 127.98, 67.80, 39.34, 29.50.

**HRMS (ESI/QTOF):** $[M+Na]^+$ calculated for $C_{21}H_{21}NNaS^+$ 342.1292, observed 342.1289.

**Synthesis of 2-oxo-N-(2-(tritylthio)ethyl)-2H-chromene-3-carboxamide (9)**

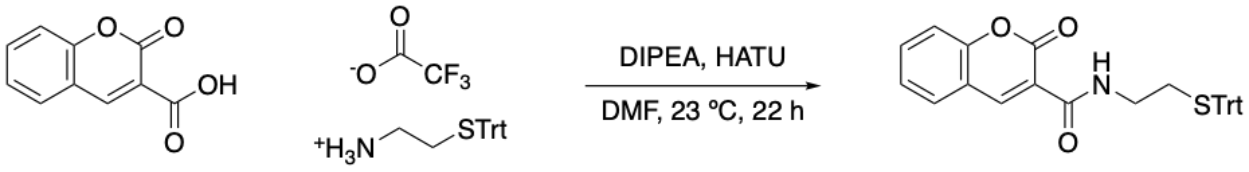


A scintillation vial was charged with a stir bar, then 2-oxo-2H-chromene-3-carboxylic acid (200 mg, 1 Eq, 1.05 mmol) and HATU (520 mg, 1.3 Eq, 1.37 mmol) were added as solids and dissolved in 4 mL of DMF to create a clear solution. DIPEA (408 mg, 550 µL, 3 Eq, 3.16 mmol) was added to the flask upon which the reaction became a yellow suspension. This was left to stir under ambient conditions for 15 minutes. Separately, 2-(tritylthio)ethan-1-ammonium trifluoroacetate (545 mg, 1.2 Eq, 1.26 mmol) was added as a solid to a dram vial and dissolved in 2 mL of DMF. After 15 minutes, the activated solution had turned gold, so the amine was added to the vial with no color change or exotherm. The reaction was stirred at 23 ºC for 22 hours. The reaction mixture was then diluted with DCM (150 mL) and washed with brine (50 mL). The organic layer was collected, dried with anhydrous magnesium sulfate, filtered, and concentrated under vacuum. The material was purified by flash column chromatography (50 g silica gel, 0-60% gradient of ethyl acetate against hexanes) to afford 2-oxo-N-(2-(tritylthio)ethyl)-2H-chromene-3-carboxamide as a white solid (236 mg, 483 µmol, 46% yield).

**Physical state:** White solid

**TLC (UV):** $R_f$ 0.70 (1:1 hexanes-ethyl acetate)

**$^1$H NMR (400 MHz, $CD_2Cl_2$):** δ 8.84 (s, 1H), 8.79 (br t, J = 5.8 Hz, 1H), 7.73 – 7.65 (m, 2H), 7.47 – 7.36 (m, 8H), 7.30 (m, 6H), 7.25 – 7.19 (m, 3H), 3.29 (q, J = 6.7 Hz, 2H), 2.47 (t, J = 6.7 Hz, 2H).

**$^{13}$C NMR (101 MHz, $CD_2Cl_2$):** δ 161.68, 161.64, 154.94, 148.54, 145.21, 134.39, 130.26, 129.99, 128.36, 127.14, 125.61, 119.13, 118.92, 116.92, 67.13, 38.91, 32.15.

**HRMS (ESI/QTOF):** $[M+Na]^+$ calculated for $C_{31}H_{25}NNaO_3S^+$ 514.1453 Da, observed 514.1446 Da

**Synthesis of *N*-(2-mercaptoethyl)-2-oxo-2*H*-chromene-3-carboxamide (9a)**

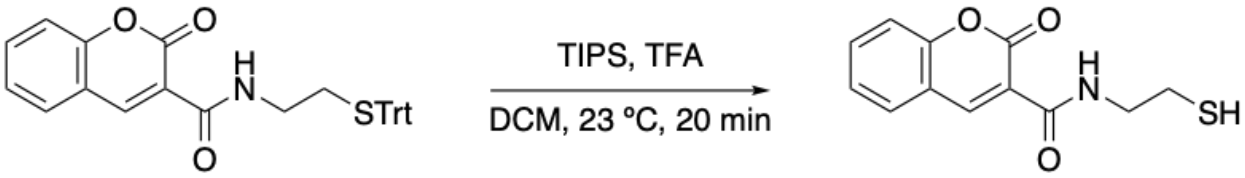


A scintillation vial was charged with a stir bar and 2-oxo-N-(2-(tritylthio)ethyl)-2H-chromene-3-carboxamide (90 mg, 1 Eq, 0.18 mmol) was added as a white solid to the flask. The solid was dissolved in 5 mL of 1:1 TFA-DCM (v/v), forming a golden solution. Subsequently, tris(propan-2-yl)silane (193 mg, 250 µL, 6.7 Eq, 1.22 mmol) was added to the solution with no observable exotherm and a color change from golden to clear and colorless. This was left to stir for 20 minutes at 23 ºC. After 20 minutes, the reaction was concentrated under vacuum. The product was purified by trituration with 8 mL of 3:1 hexanes-diethyl ether. This process was repeated three more times, then the residual white solid was concentrated under vacuum to yield N-(2-mercaptoethyl)-2-oxo-2H-chromene-3-carboxamide as a white solid (39 mg, 153 µmol, 85% yield).

**Physical state:** White solid

**TLC (UV):** $R_f$ 0.45 (1:1 hexanes-ethyl acetate)

**$^1$H NMR (400 MHz, $CDCl_3$):** δ 9.11 (s, 1H), 8.91 (s, 1H), 7.73 – 7.62 (m, 2H), 7.45 – 7.33 (m, 2H), 3.66 (q, J = 6.6 Hz, 2H), 2.78 (q, J = 8.5 Hz, 2H), 1.47 (t, J = 8.5 Hz, 1H).

**$^{13}$C NMR (101 MHz, $CDCl_3$):** δ 161.84, 161.54, 154.60, 148.69, 134.31, 129.97, 125.47, 118.73, 118.41, 116.80, 43.11, 24.42.

**HRMS (ESI/QTOF):** $[M+H]^+$ calculated for $C_{12}H_{12}NO_3S^+$ 250.0538 Da, observed 250.0567 Da.

**Synthesis of 5-((3a*S*,4*S*,6a*R*)-2-oxohexahydro-1*H*-thieno[3,4-*d*]imidazol-4-yl)-*N*-(2-(tritylthio)ethyl)pentanamide (8)**

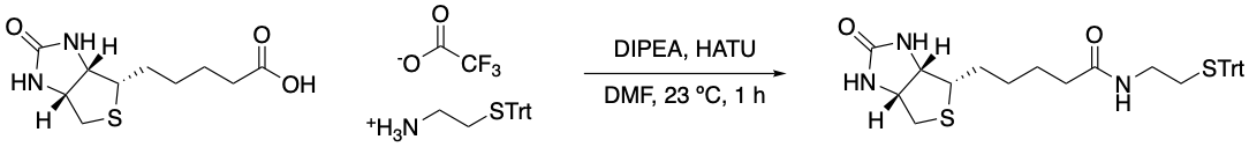


A one neck, 25 mL RBF was charged with a stir bar, then d-biotin (237 mg, 1.5 Eq, 969 µmol) and HATU (319 mg, 1.3 Eq, 840 µmol) were added as solids to the flask. These were dissolved in 4 mL of DMF to create a white suspension. After 5 minutes, DIPEA (250 mg, 338 µL, 3 Eq, 1.94 mmol) was added to the flask, creating a yellow suspension that came into solution over a few minutes. This was left to stir at 23 ºC for 15 minutes. Separately, 2-(tritylthio)ethan-1-ammonium trifluoroacetate (280 mg, 1 Eq, 646 µmol) was dissolved in 2 mL of DMF along with DIPEA (125 mg, 169 µL, 1.5 Eq, 970 µmol). After 15 minutes, the amine solution was added to the flask, retaining the yellow color. The reaction was stirred at 23 ºC for 1 hour. The reaction was then diluted with ethyl acetate (150 mL) and washed once with saturated sodium carbonate (50 mL) and once with brine (50 mL). The organic layer was collected, dried with anhydrous magnesium sulfate, filtered, and concentrated under vacuum. The product was purified by reverse phase chromatography (25 g C18 column, 10-100% acetonitrile against water, both with 0.1% TFA additive) to yield 5-((3aS,4S,6aR)-2-oxohexahydro-1H-thieno[3,4-d]imidazol-4-yl)-N-(2-(tritylthio)ethyl)pentanamide as a white solid (269 mg, 491 µmol, 76% yield).

**Physical state:** White solid

**$^1$H NMR (400 MHz, $CD_2Cl_2$):** δ 7.44 – 7.35 (m, 6H), 7.34 – 7.26 (m, 6H), 7.26 – 7.20 (m, 3H), 6.41 (s, 1H), 5.94 (s, 1H), 5.67 (s, 1H), 4.45 (dd, J = 7.9, 4.7 Hz, 1H), 4.27 (dd, J = 7.9, 4.5 Hz, 1H), 3.14 (td, J = 7.4, 4.5 Hz, 1H), 3.06 (q, J = 6.1 Hz, 2H), 2.88 (dd, J = 12.9, 4.9 Hz, 1H), 2.68 (d, J = 12.9 Hz, 1H), 2.45 – 2.34 (m, 2H), 2.21 – 2.04 (m, 2H), 1.76 – 1.54 (m, 4H), 1.48 – 1.34 (m, 2H).

**$^{13}$C NMR (101 MHz, $CD_2Cl_2$):** δ 173.50, 164.67, 145.14, 129.93, 128.36, 127.19, 67.12, 62.29, 60.92, 55.74, 40.83, 38.59, 35.96, 32.31, 28.23, 28.21, 25.86.

**HRMS (ESI/QTOF):** $[M+Na]^+$ calculated for $C_{31}H_{35}N_3NaO_2S_2^+$ 568.2068 Da, observed 568.2053 Da.

**Synthesis of N-(2-mercaptoethyl)-5-((3aS,4S,6aR)-2-oxohexahydro-1H-thieno[3,4-d]imidazol-4-yl)pentanamide (8a)**

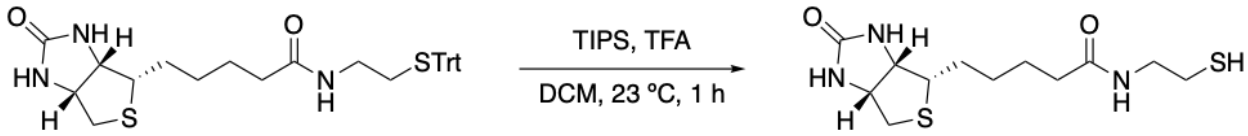


A scintillation vial was charged with a stir bar and 5-((3aS,4S,6aR)-2-oxohexahydro-1H-thieno[3,4-d]imidazol-4-yl)-N-(2-(tritylthio)ethyl)pentanamide (269 mg, 1 Eq, 493 µmol) was added. The solid was dissolved in 10 mL of 1:1 TFA-DCM (v/v), forming a bright yellow solution. Triisopropylsilane (387 mg, 500 µL, 4.95 Eq, 2.44 mmol) was then added to the solution upon which the solution turned white, then water (500 mg, 500 µL, 56.3 Eq, 27.7 mmol) was added. This was left to stir at 23 ºC for 1 hour. The reaction mixture was purified by reverse phase chromatography (25 g C18 column, 10-100% acetonitrile against water, both with 0.1% TFA) to yield N-(2-mercaptoethyl)-5-((3aS,4S,6aR)-2-oxohexahydro-1H-thieno[3,4-d]imidazol-4-yl)pentanamide as a white powder (108 mg, 355 µmol, 72% yield).

**Physical state:** White solid

**$^{1}$H NMR (400 MHz, MeOD):** δ 4.50 (ddd, J = 7.9, 5.0, 1.0 Hz, 1H), 4.31 (dd, J = 7.9, 4.5 Hz, 1H), 3.34 (t, J = 6.8 Hz, 2H), 3.21 (ddd, J = 8.9, 5.8, 4.4 Hz, 1H), 2.93 (dd, J = 12.8, 5.0 Hz, 1H), 2.71 (d, J = 12.7 Hz, 1H), 2.60 (tt, J = 6.8, 1.2 Hz, 2H), 2.26 – 2.17 (m, 2H), 1.80 – 1.53 (m, 4H), 1.51 – 1.40 (m, 2H).

**$^{13}$C NMR (101 MHz, MeOD):** δ 176.20, 166.12, 63.40, 61.66, 56.98, 43.85, 41.02, 36.72, 29.75, 29.47, 26.83, 24.50.

**HRMS (ESI/QTOF):** $[M+H]^+$ calculated for $C_{12}H_{22}N_3O_2S_2^+$ 304.1153 Da, observed 304.1161 Da.

**Synthesis of p(CL)-aryl I *via* ROP (1)**


General ROP procedure: This reaction was performed at 23ºC within a nitrogen filled glovebox. 3-O catalyst (**20**) (59.9 mg, 0.5 eq, 65.7 µmol) was weighed in a vial and a stir bar was added. Caprolactone (600 mg, 583 µL, 42 eq, 5.3 mmol) was added to a second vial. In a third vial, 2-(4-iodophenoxy)ethan-1-ol (33.1 mg, 1 Eq, 125 µmol) was measured and added to the 3-O vial using toluene to transfer. Next, MTBD (10.1 mg, 9.4 µL, 0.5 eq, 65.7 µmol) was added to the 3-O vial. Finally, the contents of the caprolactone vial were added to the 3-O reaction vial to initiate the reaction using toluene to transfer. A total of 2.5 mL toluene was added to the reaction mixture. After 60 min, the reaction was quenched with acetic acid outside of the glovebox and monomers were removed *via* precipitation with 45 mL of a cold MeOH/hexanes mixture (20:1 v/v) four times to produce a white powder. Yield: 92%

**$^1$H NMR (300 MHz, $CD_3CN$):** δ 7.59 (d, *J* = 9.0 Hz, 2H), 6.75 (d, *J* = 9.0 Hz, 2H), 4.39 – 4.29 (m, 2H), 4.18 – 4.11 (m, 2H), 4.02 (t, *J* = 6.6 Hz, 99 H), 2.27 (t, *J* = 7.4 Hz, 100H), 1.67 – 1.50 (m, 200H), 1.46 – 1.22 (m, 101H).

**SEC analysis:** $M_n$ is 8.2 kDa, $M_w$ is 9.4 kDa, $Đ$ is 1.14.

**Synthesis of p(CL)-Au(III) *via* oxidative addition (1a)**

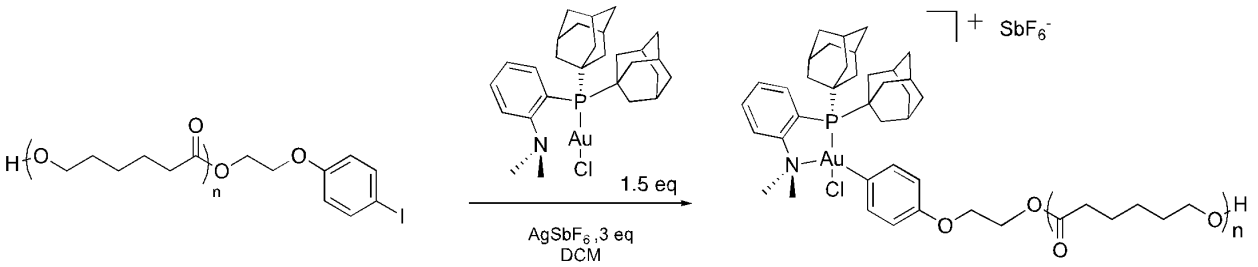


General Oxidative Addition Procedure[78,92]: For every oxidative addition, molecular weight of the precursor aryl iodide polymer was determined *via* $^1$H NMR analysis. $AgSbF_6$ was removed from a glovebox with a nitrogen atmosphere, dissolved in DCM, blocked from the light with electrical tape, and placed in a -20 ºC freezer. Next, (Me-DalPhos)AuCl (18.5 mg, 1.5 eq, 28.2 μmol) was dissolved in 2 mL DCM and placed in a -20 ºC freezer. pCL-aryl iodide (103.5 mg, 1 eq, 18.8 μmol) was weighed into a dram vial, and the (Me-DalPhos)AuCl solution was added. Finally, the pCL-aryl iodide and (Me-DalPhos)AuCl mixture was added to the $AgSbF_6$ (9.1 mg, 1.4 eq, 26.4 μmol) dram vial and mixed. Precipitates immediately crashed out of solution and the solution became yellow. The reaction was stirred at room temperature for 30 minutes. Next, $AgSbF_6$ (3.2 mg, 0.5 eq, 9.4 μmol) was added and stirred for 30 minutes. Then, $AgSbF_6$ (3.9 mg, 0.6 eq, 11.3 μmol) was added and stirred for 30 minutes. Finally, AgSbF6 (3.2 mg, 0.5 eq, 9.4 μmol) was added and stirred for 15 hours. The reaction solution was run through a Celite plug with DCM, triturated with diethyl ether, and dried to produce a white or pale yellow powder. Complete conversion was determined by the disappearance of aryl-I peaks in the $^1$H NMR. This reaction was

carried forward without further purification. Product Yield: 61%. Product purity by weight was determined to be 93% based on $^{1}$H NMR.

**$^{1}$H NMR (300 MHz, $CD_3CN$):** δ 8.06 – 7.88 (m, 2H), 7.73 – 7.63 (m, 2H), 7.45 (d, *J* = 8.8 Hz, 2H), 6.94 (d, *J* = 8.9 Hz, 2H), 4.42 – 4.35 (m, 2H), 4.22 – 4.15 (m, 2H), 4.02 (t, *J* = 6.6 Hz, 122H), 2.27 (t, *J* = 7.4 Hz, 137H), 1.71 – 1.46 (m, 244H), 1.42 – 1.23 (m, 126H).

**$^{31}$P{$^{1}$H} NMR (121 MHz, $CD_3CN$):** δ 75.31.

**Synthesis of p(BNI)-aryl I *via* ROMP (3)**

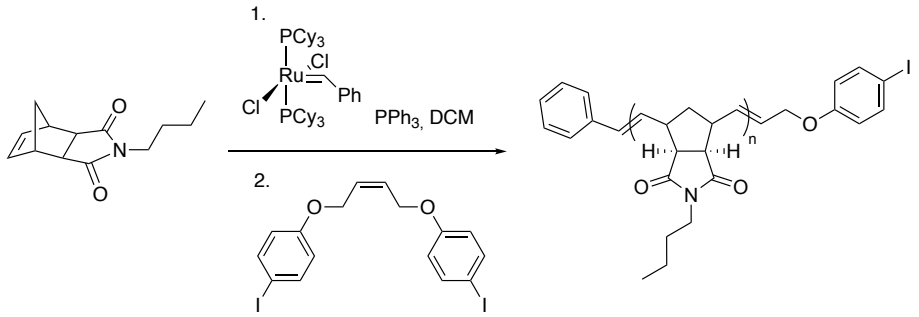


General ROMP procedure: This reaction occurred within a nitrogen atmosphere glovebox. N-butylimide norbornene (296 mg, 37 eq, 1.3 mmol) was measured into a dram vial equipped with a stir bar in the glovebox and dissolved in DCM. Triphenylphosphine (9.6 mg, 1 eq, 36.5 μmol) was dissolved into DCM and added to the monomer vial. Grubbs' 1 catalyst (30.0 mg, 1 eq, 36.5 μmol) was measured and dissolved into a separate dram vial with DCM and then transferred to the monomer vial. The reaction solution was dark purple. The reaction stirred for 5 hours. Next, (Z)-1,4-bis(4-iodophenoxy)but-2-ene (179 mg, 10 eq, 365 μmol) was added and the reaction stirred for 16 hours. The polymer was precipitated four times in 45 mL of a diethylether/THF (2:1 v/v) and then dried to produce a tan powder. Yield: 51%

**$^{1}$H NMR (400 MHz, $CD_3CN$):** δ 7.58 (d, *J* = 8.7 Hz, 2H), 7.45 – 7.21 (m, 5H), 6.76 (d, *J* = 8.9 Hz, 2H), 5.77 – 5.48 (m, 97H), 4.50 (d, *J* = 5.3 Hz, 2H), 3.42 – 3.27 (m, 97H), 3.08 – 2.90 (m,

113H), 2.75 – 2.57 (m, 81H), 1.56 – 1.44 (m, 112H), 1.28 (q, $J$ = 7.5 Hz, 100H), 0.90 (t, $J$ = 7.3 Hz, 147H).

**SEC analysis:** $M_n$ is 9.8 kDa, $M_w$ is 11.8 kDa, ~~$Đ$~~ is 1.21.

**Synthesis of p(BNI)-Au(III) *via* oxidative addition (3a)**

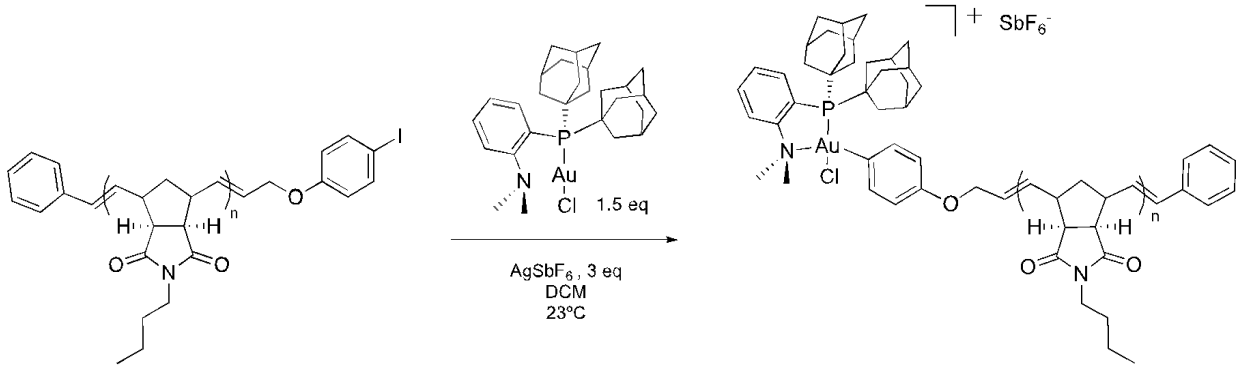


Following general oxidative addition procedure using $AgSbF_6$ (12.3 mg, 3 eq, 33.8 μmol) over four additions, (Me-DalPhos)AuCl (11.6 mg, 1.5 eq, 17.9 μmol), and p(BNI)-aryl I (100.0 mg, 1 eq, 11.3 μmol). The product is a yellow powder. Yield: 69%. Product purity by weight was determined to be 92% based on $^1$H NMR.

**$^1$H NMR (600 MHz, $CD_3CN$):** δ 8.06 – 8.01 (m, 1H), 7.98 – 7.80 (m, 3H), 7.71 – 7.64 (m, 2H), 7.49 – 7.12 (m, 8H), 6.95 (d, $J$ = 8.8 Hz, 2H), 5.75 – 5.50 (m, 102H), 4.58 – 4.53 (m, 2H), 3.39 – 3.33 (m, 101H), 3.05 – 2.93 (m, 111H), 2.71 – 2.58 (m, 88H), 1.52 – 1.47 (m, 115H), 1.31 – 1.22 (m, 106H), 0.90 (t, $J$ = 7.4 Hz, 153H).

**$^{31}$P{$^1$H} NMR (243 MHz, $CD_3CN$):** δ 75.11.

**Synthesis of p(BNI)-aryl I *via* ROMP (16)**

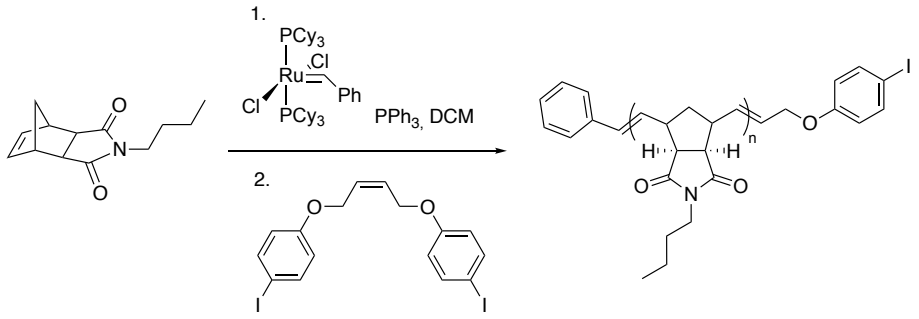


Following general ROMP procedure using N-butylimide norbornene (329 mg, 137 eq, 1.5 mmol), triphenylphosphine (2.87 mg, 1 eq, 10.9 μmol), 1st generation Grubbs Catalyst (9.0 mg, 1 eq, 10.9 μmol), and (Z)-1,4-bis(4-iodophenoxy)but-2-ene (53.8 mg, 10 eq, 109 μmol) to produce a tan powder. Yield: 89%

**$^1$H NMR (400 MHz, $CD_3CN$):** δ 7.58 (d, *J* = 9.0 Hz, 2H), 7.44 – 7.21 (m, 5H), 6.76 (d, *J* = 9.0 Hz, 2H), 5.74 – 5.48 (m, 276H), 4.50 (d, 2H), 3.41 – 3.30 (m, 275H), 3.01 – 2.93 (m, 325H), 2.72 – 2.57 (m, 227H), 1.54 – 1.43 (m, 317H), 1.28 (q, *J* = 7.5 Hz, 280H), 0.90 (t, *J* = 7.3 Hz, 416H).

**SEC analysis:** $M_n$ is 27.2 kDa, $M_w$ is 34.4 kDa, $Đ$ is 1.27.

**Synthesis of p(BNI)-Au(III) *via* oxidative addition (16a)**

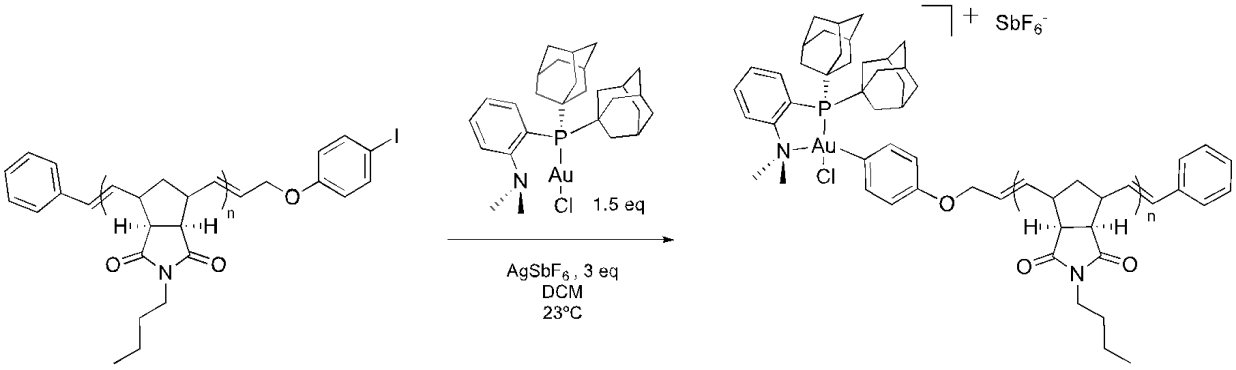


Following general oxidative addition procedure using $AgSbF_6$ (3.41 mg, 3 eq, 9.93 μmol) over four additions, (Me-DalPhos)AuCl (3.25 mg, 1.5 eq, 4.96 μmol), and p(BNI)-aryl I (100.0 mg, 1 eq, 3.31 μmol). The product is a yellow powder. Yield: 93%. Product purity by weight was determined to be 98% based on $^1$H NMR.

**$^1$H NMR (600 MHz, $CD_3CN$):** δ 8.06 – 8.01 (m, 1H), 7.97 – 7.81 (m, 3H), 7.35 – 7.29 (m, 7H), 6.99 – 6.90 (m, 2H), 5.76 – 5.42 (m, 312H), 4.57 – 4.51 (m, 2H), 3.41 – 3.25 (m, 306H), 3.02 – 2.91 (m, 361H), 2.70 – 2.60 (m, 253H), 1.48 (t, *J* = 7.7 Hz, 343H), 1.28 (q, *J* = 7.5 Hz, 313H), 0.90 (t, *J* = 7.4 Hz, 466H).

**$^{31}$P{$^1$H} NMR (243 MHz, $CD_3CN$):** δ 75.11.

**Synthesis of p(PFS)-aryl I *via* ATRP (6)**

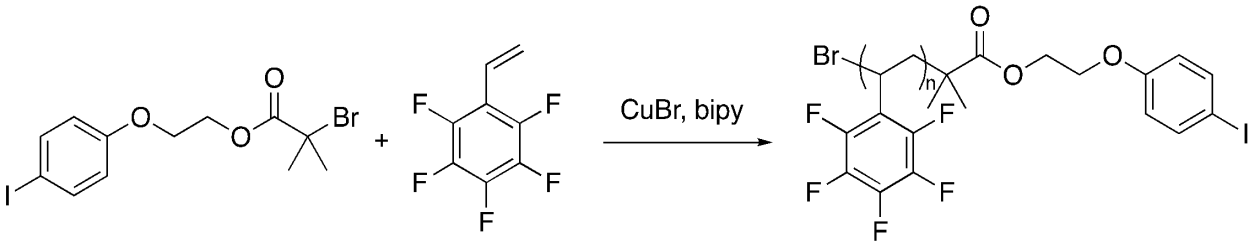


2,2'-Bipyridine (26.8 mg, 2 eq, 171.7 μmol), copper(I) bromide (12.3 mg, 1 eq, 85.9 μmol), neat 1,2,3,4,5-pentafluoro-6-vinylbenzene (500.0 mg, 354 μL, 30 eq, 2.6 mmol) and 2-(4-iodophenoxy)ethyl 2-bromo-2-methylpropanoate (35.5 mg, 1 eq, 85.9 μmol) were measured and added to a Schlenk flask. The reaction was freeze-pump-thawed 3 times. The reaction solution was blue/green. After 1 hour, the reaction was diluted in THF, filtered through a pad of neutral alumina, then precipitated in cold hexanes (45 mL) three times to produce a white solid. Yield: 54%

**$^{1}$H NMR (400 MHz, $CD_2Cl_2$):** δ 7.55 (d, 2H), 6.66 (d, 2H), 2.87 – 2.27 (m, 34H), 2.11 – 1.89 (m, 64H).

**$^{19}$F NMR (376 MHz, Acetone-$d_6$):** δ -140.24 – -146.85 (m), -155.50 – -160.20 (m), -162.64 – -166.37 (m).

**SEC analysis:** $M_n$ is 5.7 kDa, $M_w$ is 6.2 kDa, $Đ$ is 1.09.

**Synthesis of p(PFS)-Au(III) *via* oxidative addition (6a)**

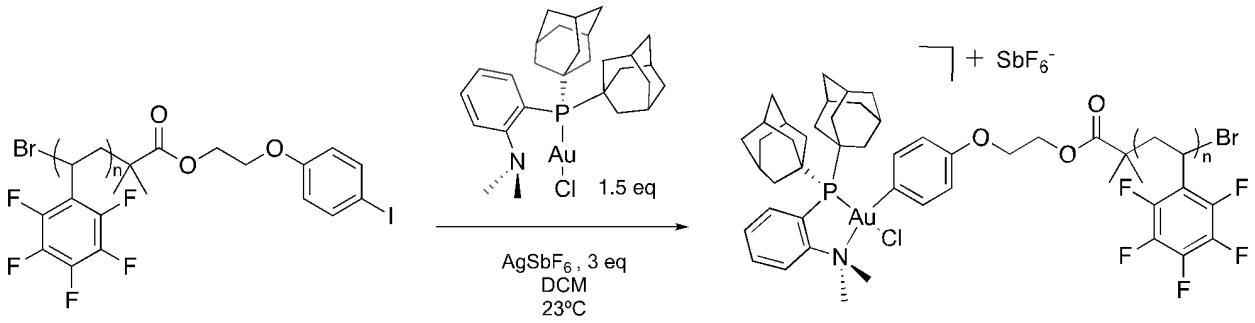


Following general oxidative addition procedure using $AgSbF_6$ (16.1 mg, 3 eq, 46.8 μmol) over four additions, (Me-DalPhos)AuCl (15.3 mg, 1.5 eq, 23.4 μmol), and p(PFS)-aryl I (100.0 mg, 1 eq, 15.6 μmol). The product is a yellow powder. Yield: 58%. Product purity by weight was determined to be 94% based on $^1$H NMR.

**$^1$H NMR (600 MHz, $CD_2Cl_2$):** δ 8.07 – 7.68 (m, 4H), 7.33 (d, *J* = 1.2 Hz, 2H), 6.90 (d, *J* = 1.2 Hz, 2H), 2.84 – 2.25 (m, 54H), 2.14 – 1.88 (m, 90H).

**$^{19}$F NMR (376 MHz, $CD_2Cl_2$):** δ -143.47 (d, *J* = 329.6 Hz), -155.33, -162.09.

**$^{31}$P{$^1$H} NMR (243 MHz, $CD_2Cl_2$):** δ 74.53, 59.88, 57.44, 51.70.

**Synthesis of mono-telechelic biotin-p(CL) *via* reductive elimination (1a-8a)**

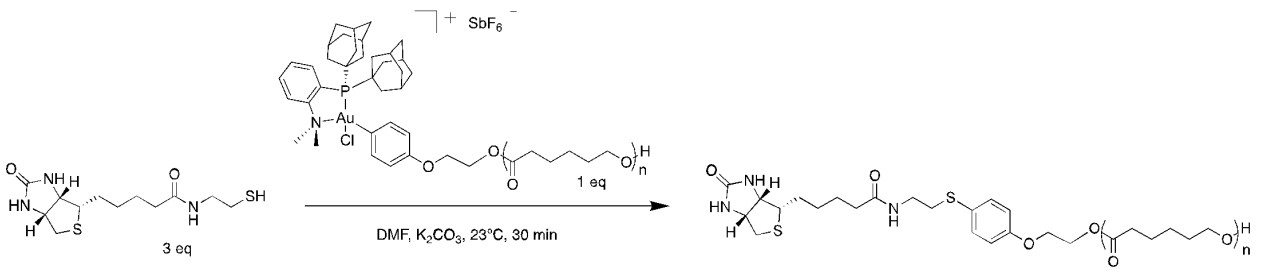


General Small Molecule Reductive Elimination Procedure: Thiolated biotin (1.4 mg, 3 eq, 4.7 μmol), potassium carbonate (1.5 mg, 7 eq, 10.9 μmol), and pCL-Au(III) (**1a**) (10.3 mg, 93% wt, 1 eq, 1.6 μmol) was added to a vial with 500 μL DMF. The reaction proceeded for 30 minutes before one precipitation in 15 mL of cold methanol to produce a white powder. Yield: 47%.

**$^1$H NMR (400 MHz, $CD_3CN$):** δ 7.38 (d, *J* = 8.8 Hz, 1H), 6.89 (d, *J* = 8.9 Hz, 1H), 6.56 – 6.48 (m, 0H), 5.19 – 5.07 (m, 1H), 4.95 – 4.89 (m, 1H), 4.42 – 4.38 (m, 1H), 4.38 – 4.31 (m, 2H), 4.25 – 4.20 (m, 1H), 4.18 – 4.13 (m, 2H), 4.02 (t, *J* = 6.6 Hz, 101H), 3.47 (t, *J* = 6.5 Hz, 2H), 3.31 – 3.22 (m, 2H), 2.91 (s, 2H), 2.27 (t, *J* = 7.4 Hz, 105H), 1.72 – 1.46 (m, 217H), 1.45 – 1.28 (m, 110H).

**Synthesis of mono-telechelic coumarin-p(CL) *via* reductive elimination (1a-9a)**

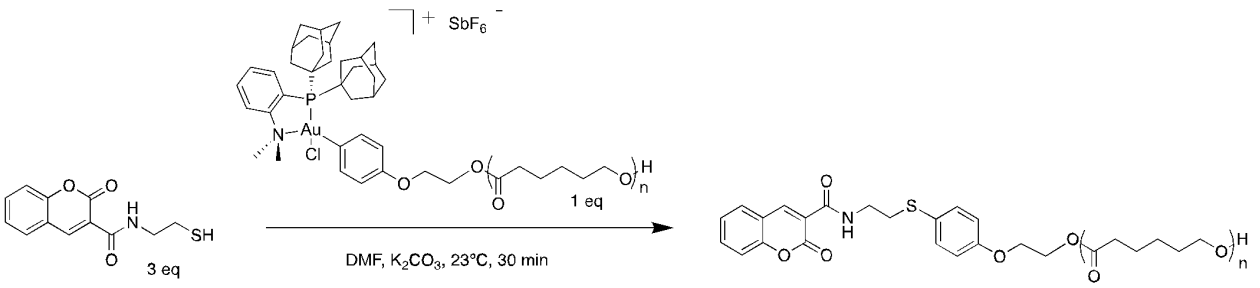


Following the general small molecule reductive elimination procedure with potassium carbonate (1.5 mg, 7 eq, 11.0 μmol), thiolated coumarin (1.2 mg, 3 eq, 4.7 μmol), pCL-Au(III) (**1a**) (10.4 mg, 93% wt, 1 eq, 1.6 μmol), and one precipitation in 15 mL of cold diethyl ether to produce a white powder. Yield: 82%.

**$^1$H NMR (400 MHz, $CD_3CN$):** δ 8.89 (d, *J* = 1.6 Hz, 1H), 8.82 (s, 1H), 7.82 (d, *J* = 8.0 Hz, 1H), 7.76 – 7.66 (m, 1H), 7.48 – 7.30 (m, 4H), 6.86 (d, *J* = 8.9 Hz, 2H), 4.38 – 4.22 (m, 2H), 4.09 (d, *J* = 4.8 Hz, 2H), 4.01 (t, *J* = 6.6 Hz, 134H), 3.59 – 3.51 (m, 2H), 3.51 – 3.42 (m, 2H), 3.06 (t, *J* = 6.7 Hz, 2H), 2.27 (t, *J* = 7.4 Hz, 113H), 1.71 – 1.50 (m, 230H), 1.44 – 1.21 (m, 116H).

**Synthesis of mono-telechelic glucose-p(CL) *via* reductive elimination (1a-TG)**

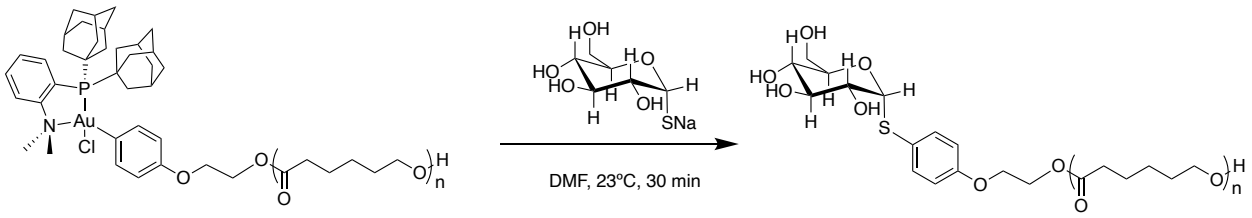


Following the general small molecule reductive elimination procedure with 1-Thio-b-D-glucose sodium salt dihydrate (1.0 mg, 3 eq, 4.7 μmol) and pCL-Au(III) (**1a**) (10.4 mg, 93% wt, 1 eq, 1.6 μmol) to produce a white powder. Potassium carbonate was not required with use of a thiol salt. Yield: 49%.

**$^1$H NMR (400 MHz, $CD_3CN$):** δ 7.49 (d, *J* = 8.8 Hz, 2H), 6.89 (d, *J* = 8.8 Hz, 2H), 5.72 – 5.67 (m, 1H), 4.43 (d, *J* = 9.7 Hz, 2H), 4.39 – 4.33 (m, 2H), 4.22 – 4.13 (m, 3H), 4.02 (t, *J* = 6.6 Hz, 141H), 3.87 – 3.80 (m, 1H), 3.76 – 3.70 (m, 1H), 3.62 – 3.53 (m, 1H), 3.33 – 3.28 (m, 1H), 3.10 – 3.01 (m, 1H), 2.27 (t, *J* = 7.4 Hz, 154H), 1.68 – 1.51 (m, 285H), 1.44 – 1.26 (m, 150H).

**Synthesis of mono-telechelic biotin-p(BNI) *via* reductive elimination (3a-8a)**

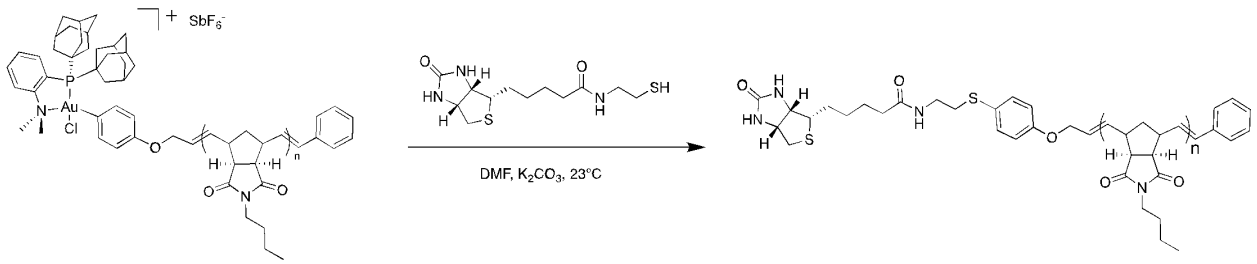


Following the general small molecule reductive elimination procedure with potassium carbonate (682 μg, 7 eq, 4.9 μmol), thiolated biotin (642 μg, 3 eq, 2.1 μmol), and pBNI-Au(III) (**2a**) (6.6 mg, 92% wt, 1 eq, 0.7 μmol) to produce a white powder. Yield: 62%.

**$^1$H NMR (400 MHz, DMSO-d$_6$):** δ 7.98 – 7.91 (m, 1H), 7.45 – 7.19 (m, 7H), 6.92 (d, 2H), 6.01 – 5.91 (m, 1H), 5.69 – 5.36 (m, 78H), 4.51 (d, *J* = 5.6 Hz, 2H), 4.36 – 4.27 (m, 1H), 4.15 – 4.10 (m, 1H), 3.11 – 2.96 (m, 87H), 2.70 – 2.58 (m, 64H), 2.03 – 1.93 (m, 36H), 1.54 – 1.49 (m, 27H), 1.43 (t, *J* = 7.3 Hz, 97H), 1.32 – 1.15 (m, 88H), 0.86 (t, *J* = 7.4 Hz, 123H).

**Synthesis of mono-telechelic coumarin-p(BNI) *via* reductive elimination (3a-9a)**

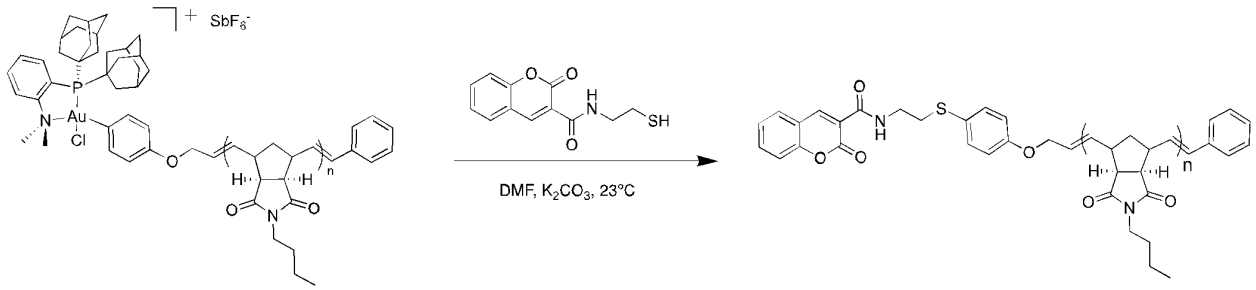


Following the general small molecule reductive elimination procedure with potassium carbonate (820 μg, 7 eq, 5.9 μmol), thiolated coumarin (634 μg, 3 eq, 2.5 μmol), pBNI-Au(III) (**2a**) (7.9 mg, 92% wt, 1 eq, 0.8 μmol), and one precipitation in 15 mL cold diethyl ether to produce a white powder. Yield: 40%.

**$^1$H NMR (400 MHz, DMSO-d$_6$):** δ 8.95 – 8.88 (m, 1H), 8.00 – 7.91 (m, 1H), 7.79 – 7.71 (m, 1H), 7.50 (d, 1H), 7.46 – 7.29 (m, 7H), 7.25 – 7.18 (m, 1H), 6.90 (d, *J* = 8.8 Hz, 2H), 5.73 – 5.39 (m, 76H), 3.10 – 2.96 (m, 87H), 2.70 – 2.54 (m, 62H), 2.06 – 1.90 (m, 37H), 1.60 – 1.49 (m, 26H), 1.49 – 1.37 (m, 86H), 1.28 – 1.15 (m, 95H), 0.86 (t, *J* = 7.3 Hz, 122H).

**Synthesis of mono-telechelic glucose-p(BNI) *via* reductive elimination (3a-TG)**

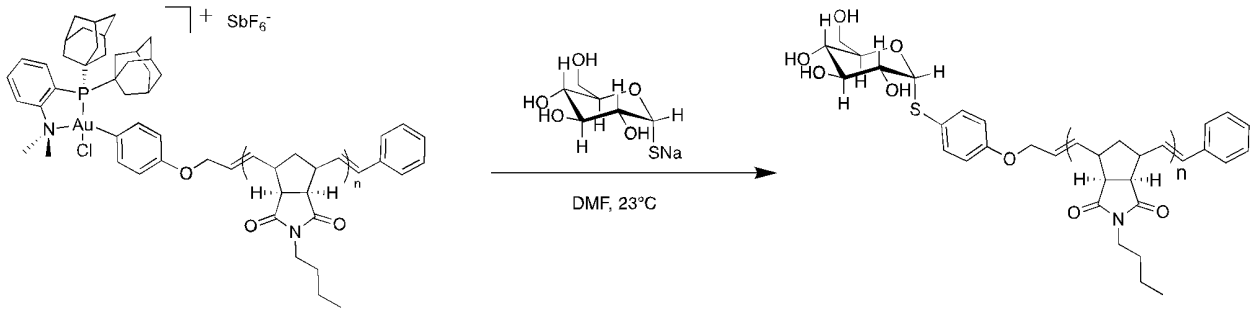


Following the general small molecule reductive elimination procedure 1-thio-b-D-glucose sodium salt dihydrate (528 μg, 3 eq, 2.4 μmol) and pBNI-Au(III) (**2a**) (7.5 mg, 92% wt, 1 eq, 0.8 μmol). Yield: 82%.

**$^1$H NMR (400 MHz, DMSO-d$_6$):** δ 7.47 – 7.20 (m, 7H), 6.90 (d, *J* = 8.9 Hz, 2H), 5.72 – 5.43 (m, 80H), 5.20 – 5.12 (m, 1H), 5.06 – 5.02 (m, 1H), 4.95 – 4.89 (m, 1H), 4.55 – 4.47 (m, 3H), 4.38 (d, *J* = 10.0 Hz, 1H), 3.70 – 3.63 (m, 2H), 3.06 – 2.99 (m, 95H), 2.69 – 2.57 (m, 65H), 2.02 – 1.93 (m, 50H), 1.67 – 1.49 (m, 28H), 1.48 – 1.39 (m, 97H), 1.22 (q, *J* = 7.2 Hz, 98H), 0.86 (t, *J* = 7.4 Hz, 131H).

**Synthesis of p(*N*-isopropylacrylamide) *via* RAFT (10)**

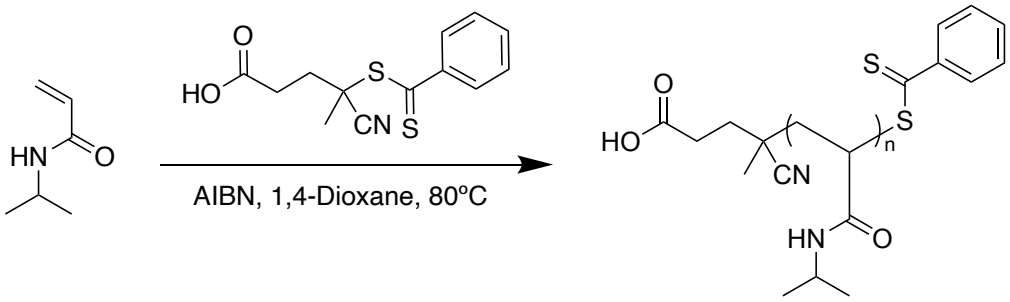


N-Isopropylacrylamide (NIPAM) (700.0 mg, 140 eq, 6.2 mmol) and 4-cyano-4-((phenylcarbonothioyl)thio)pentanoic acid (12.3 mg, 1 eq, 44.2 μmol), and azobisisobutyronitrile (2.2 mg, 0.3 eq, 13.3 μmol) were dissolved in a Schlenk flask with 2 mL of anhydrous 1,4-dioxane. The reaction underwent three freeze-pump-thaw cycles to remove oxygen. The reaction was exposed to an argon atmosphere. The reaction progressed at 80 °C while stirring for 4 hours, at which time the reaction was precipitated into 45 mL of cold diethyl ether three times to produce a pink solid. Yield: 20%

**$^1$H NMR (400 MHz, $CDCl_3$):** δ 7.95 (t, *J* = 8.2 Hz, 2H), 7.54 (t, 1H), 7.39 (t, 2H), 6.30 (s, 1H), 4.24 – 3.83 (m, 69H), 2.69 – 1.28 (m, 492H), 1.21 – 1.01 (m, 408H).

**SEC analysis:** $M_n$ is 9.3 kDa, $M_w$ is 10.4, $Đ$ is 1.11.

**Aminolysis of p(*N*-isopropylacrylamide) (10a)**

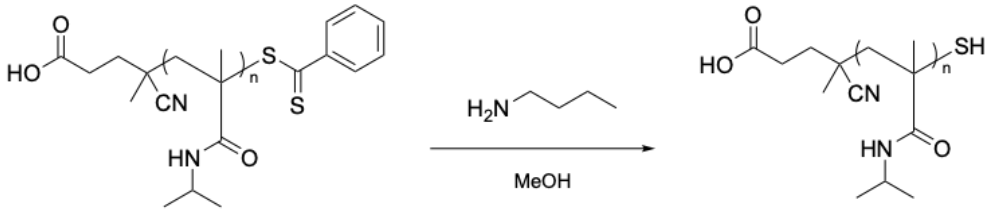


p(*N*-isopropylacrylamide) (51.5 mg, 1 eq, 4.5 μmol) was added to a dram vial and dissolved in 500 μL of methanol. The reaction solution was pink and translucent. *n*-butylamine (13.2 mg, 17.9 μL, 40 eq, 181 μmol) was added to the dram vial and the reaction was stirred at 23 ºC for 30 minutes. The reaction became yellow, indicating that the dithioester end group had been cleaved. Next, the reaction was precipitated three times into cold diethyl ether (45 mL) to produce a white solid. Yield: 64%

**$^1$H NMR (400 MHz, $CDCl_3$):** δ 6.86 – 6.03 (m, 67H), 4.22 – 3.76 (m, 69H), 2.57 – 1.29 (m, 278H), 1.30 – 0.96 (m, 401H).

**Synthesis of Trt-p(CL) *via* ROP (12)**

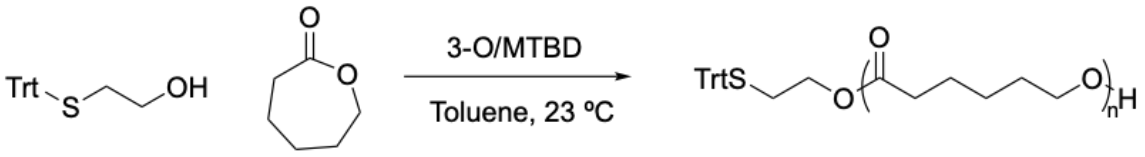


Following the general ROP procedure, 3-O catalyst (9.983 mg, 1.1 eq, 10.951 μmol), caprolactone (100.0 mg, 97.0 μL, 88 eq, 876.1 μmol), 2-(tritylthio)ethan-1-ol (3.2 mg, 1 eq, 10.0 μmol), MTBD (1.7 mg, 1.6 μL, 1.1 eq, 11.0 μmol), and 1.75 mL toluene. Yield: 93%

**$^1$H NMR (300 MHz, $CD_3CN$):** δ 7.52 – 7.19 (m, 15H), 4.07 (t, $J$ = 6.7 Hz, 168H), 2.32 (t, $J$ = 7.5 Hz, 171H), 1.84 – 1.50 (m, 345H), 1.54 – 1.31 (m, 173H).

**SEC analysis:** $M_n$ is 10.0 kDa, $M_w$ is 12.0 kDa, ~~$Đ$~~ is 1.20.

**Deprotection of Trt-p(CL) (12a)**

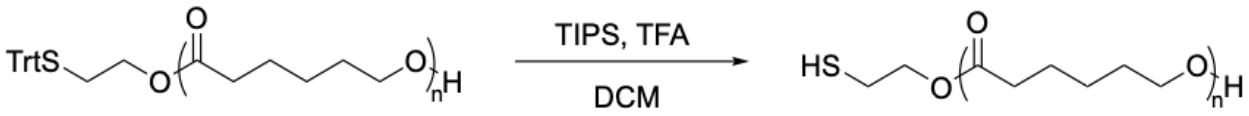


General Trt deprotection procedure: The polymer was dissolved in 0.5 mL DCM and TFA (0.7 g, 0.5 mL, 700 eq, 6 mmol) was added. The solution turned bright yellow. Next, tris(propan-2-yl)silane (70.9 mg, 91.9 µL, 45 eq, 448 µmol)was added and the reaction became clear and colorless. After 10 minutes, the reaction solution was precipitated into cold diethyl ether (45 mL) to produce a white powder. Yield: 85%

**$^1$H NMR (300 MHz, $CD_3CN$):** δ 4.07 (t, *J* = 6.6 Hz, 168H), 2.32 (t, *J* = 7.5 Hz, 181H), 1.78 – 1.56 (m, 337H), 1.52 – 1.30 (m, 171H).

**Synthesis of p(CL)-Trt *via* ROP (17)**

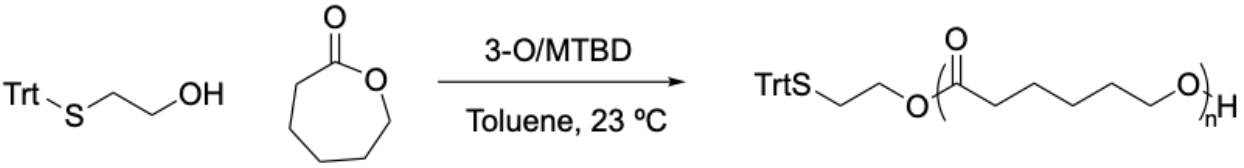


Following general ROP procedure using 3-O catalyst (30.0 mg, 3.8 eq, 32.9 µmol), caprolactone (300 mg, 291 µL, 307 Eq, 2.6 mmol, 2-(tritylthio)ethan-1-ol (2.7 mg, 1 eq, 8.6 µmol) and MTBD (5.0 mg, 4.7 µL, 3.8 eq, 32.9 µmol). Yield: 72%.

**$^1$H NMR (400 MHz, $CDCl_3$):** δ 7.41 – 7.37 (m, 2H), 7.30 – 7.27 (m, 10H), 7.24 – 7.19 (m, 5H), 4.32 (t, *J* = 6.6 Hz, 2H), 4.05 (t, *J* = 6.7 Hz, 708H), 2.29 (t, *J* = 7.5 Hz, 714H), 1.70 – 1.54 (m, 1450H), 1.43 – 1.29 (m, 718H).

**SEC analysis:** $M_n$ is 37.4 kDa, $M_w$ is 42.3 kDa, ~~*Đ*~~ is 1.13.

**Deprotection of p(CL)-Trt (17a)**

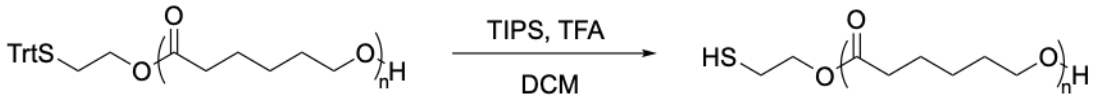


Following the general trityl deprotection procedure using pCL-Trt (**17**) (100.0 mg, 1 eq, 2.70 μmol)). TFA (92.4 mg, 62.5 μL, 300 eq, 811 μmol) and tris(propan-2-yl)silane (19.3 mg, 24.9 μL, 45 eq, 122 μmol) to produce a white powder. Yield: 87%.

**$^1$H NMR (400 MHz, $CDCl_3$):** δ 4.06 (t, 708H), 2.30 (t, *J* = 7.5 Hz, 736H), 1.77 – 1.54 (m, 1464H), 1.44 – 1.29 (m, 776H).

**Synthesis of p(NIPAM)-*b*-p(CL) (13) *via* reductive elimination of pNIPAM-SH (10a) and pCL-Au(III) (1a)**

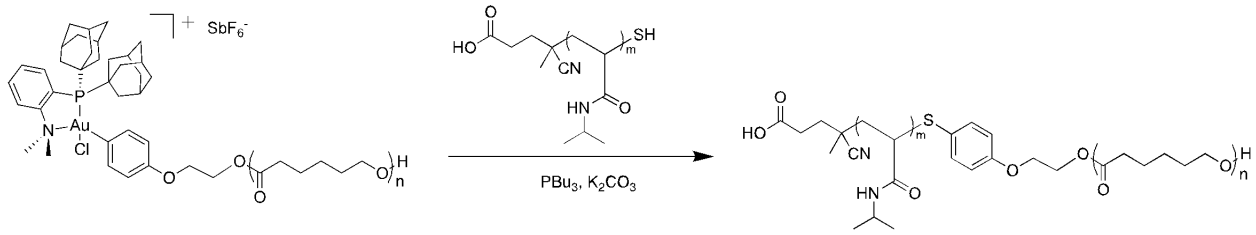


General Polymer Reductive Elimination Procedure: For every reductive elimination, molecular weight of each precursor polymer was determined *via* $^1$H NMR analysis. pNIPAM-SH (**10a**) (7.31 mg, 1 eq, 0.76 μmol) and a stir bar were added to a 1 mL vial and dissolved in 250 μL DMF. After preparation of a tributyl phosphine ($PBu_3$) solution, pNIPAM-SH was reduced with $PBu_3$ (308 μg, 2 eq, 1.52 μmol) for 20 minutes at room temperature. Next, potassium carbonate (1.9 mg, 10 eq, 13.7 μmol) was added to the vial. Finally, pCL-Au(III) (**1a**) (4.47 mg, 93% wt, 1 eq, 0.76 μmol) was dissolved with an additional 250 μL DMF and added to the solution. The

reaction was stirred for 1 hour at room temperature, where it was then precipitated in 15 mL of cold diethyl ether and dried under vacuum to produce a white powder. Yield: 53%.

**$^1$H NMR (500 MHz, $CD_2Cl_2$):** δ 6.51 (s, 73H), 4.03 (t, *J* = 6.7 Hz, 113H), 3.99 (s, 59H), 2.29 (t, *J* = 7.5 Hz, 100H), 2.11 – 1.78 (m, 163H), 1.67 – 1.57 (m, 308H), 1.46 – 1.29 (m, 166H), 1.13 (s, 495H), 0.99 – 0.86 (m, 75H).

**SEC analysis:** $M_n$ is 11.9 kDa, $M_w$ is 16.3 kDa, $Đ$ is 1.37

**Synthesis of p(CL)-*b*-p(BNI) (14) *via* reductive elimination of pCL-SH (12a) and pBNI-Au(III) (3a)**

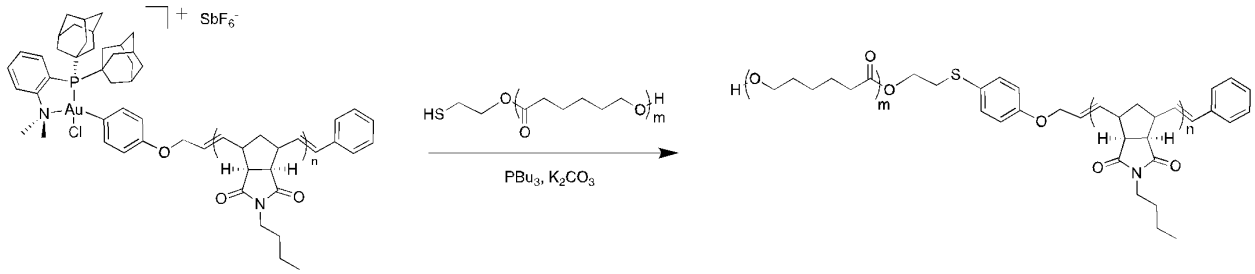


Following the general polymer reductive elimination procedure using pCL-SH (4.62 mg, 1 eq, 0.5 μmol) (**12a**), $PBu_3$ (187 μg, 2 eq, 0.9 μmol), potassium carbonate (447 μg, 7 eq, 3.2 μmol), and pBNI-Au(III) (**3a**) (4.30 mg, 92% wt, 1 eq, 0.5 μmol). The product is a white powder. Yield: 57%.

**$^1$H NMR (500 MHz, $CD_3CN$):** δ 5.72 – 5.46 (m, 102H), 4.52 – 4.49 (m, 2H), 4.01 (t, 256H), 3.42 – 3.32 (m, 104H), 3.04 – 2.94 (m, 119H), 2.69 – 2.61 (m, 88H), 2.27 (t, 268H), 1.65 – 1.53 (m, 556H), 1.52 – 1.46 (m, 120H), 1.40 – 1.32 (m, 266H), 1.31 – 1.23 (m, 101H), 0.91 (t, *J* = 7.4 Hz, 155H).

**$^{31}$P{$^1$H} NMR (243 MHz, $CD_3CN$):** δ 67.91, 57.32.

**SEC analysis:** $M_n$ is 17.7 kDa, $M_w$ is 22.5 kDa, $Đ$ is 1.27.

**Synthesis of p(CL)-*b*-p(BNI) (18) *via* reductive elimination of pCL-SH (17a) and pBNI-Au(III) (16a)**

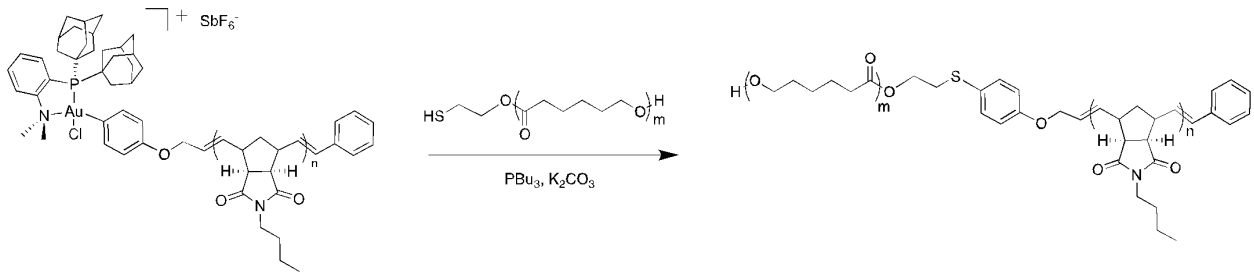


Following general polymer reductive elimination procedure using pCL-SH (10.0 mg, 1 eq, 0.3 μmol) (**17a**), $PBu_3$ (118 μg, 2 eq, 0.6 μmol), potassium carbonate (283 μg, 7 eq, 2.0 μmol), and pBNI-Au(III) (8.4 mg, 98% wt, 1 eq, 0.3 μmol) (**16a**). The product is a white powder. Yield: 85%.

**$^1$H NMR (500 MHz, $CD_3CN$):** δ 5.76 – 5.38 (m, 276H), 4.00 (t, *J* = 6.6 Hz, 745H), 3.40 – 3.28 (m, 271H), 3.04 – 2.87 (m, 332H), 2.63 (s, 232H), 2.26 (t, *J* = 7.4 Hz, 812H), 1.64 – 1.52 (m, 1568H), 1.47 (t, *J* = 7.6 Hz, 350H), 1.38 – 1.29 (m, 772H), 1.29 – 1.21 (m, 342H), 0.88 (t, *J* = 7.4 Hz, 408H).

**$^{31}$P{$^1$H} NMR (243 MHz, $CD_3CN$):** δ 61.78, 57.23.

**SEC analysis:** $M_n$ is 42.3 kDa, $M_w$ is 59.1 kDa, ~~$Đ$~~ is 1.40.

**Synthesis of p(CL)-*b*-p(PFS) (15) *via* reductive elimination of pBNI-SH (12a) and pPFS-Au(III) (6a)**

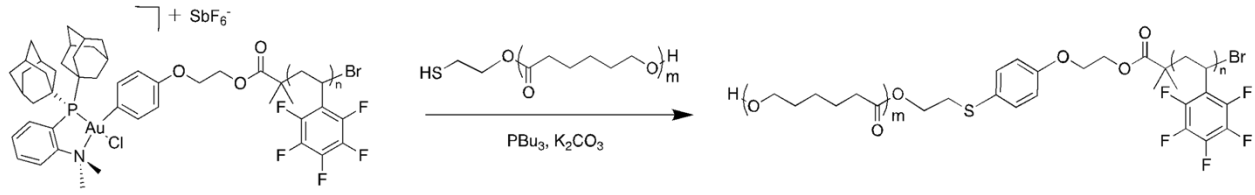


Following general polymer reductive elimination procedure using pCL-SH (**12a**) (11.4 mg, 1 eq, 1.2 μmol), tributyl phosphine (967 μg, 1.19 μL, 4 eq, 4.8 μmol), potassium carbonate (1.7

mg, 10 eq, 11.9 μmol), and pPFS-Au(III) (**6a**) (9.1 mg, 94% wt, 1 eq, 1.2 μmol). The product is a white powder. Yield: 66%.

**$^{1}$H NMR (600 MHz, $CD_2Cl_2$):** δ 7.40 (d, *J* = 8.6 Hz, 2H), 6.86 (d, *J* = 8.2 Hz, 2H), 4.07 (t, *J* = 6.7 Hz, 223H), 2.89 – 2.40 (m, 28H), 2.33 (t, *J* = 7.5 Hz, 231H), 2.19 – 1.92 (m, 71H), 1.74 – 1.52 (m, 545H), 1.50 – 1.37 (m, 235H).

**$^{19}$F NMR (376 MHz, $CD_3CN$):** δ -141.40 – -145.97 (m), -156.88 – -158.79 (m), -163.19 – -166.18 (m).

**SEC analysis:** $M_n$ is 9.77 kDa, $M_w$ is 15.6 kDa, and ~~$Đ$~~ is 1.60.

# 2.6 Appendix I

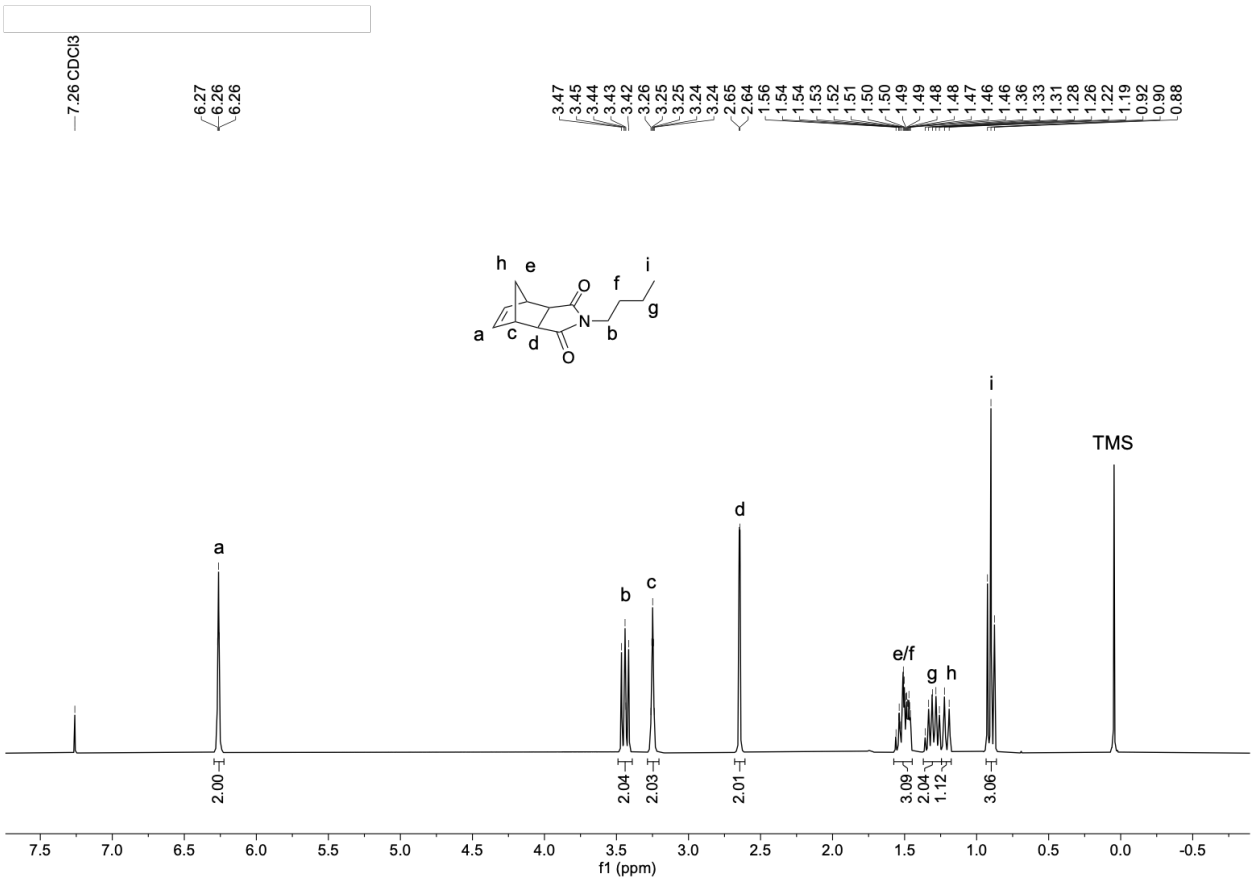


**Figure 2.4** $^{1}$H NMR spectrum of *exo*-*n*-butylnorborneneimide (**19**) in $CDCl_3$ at 25 ºC.

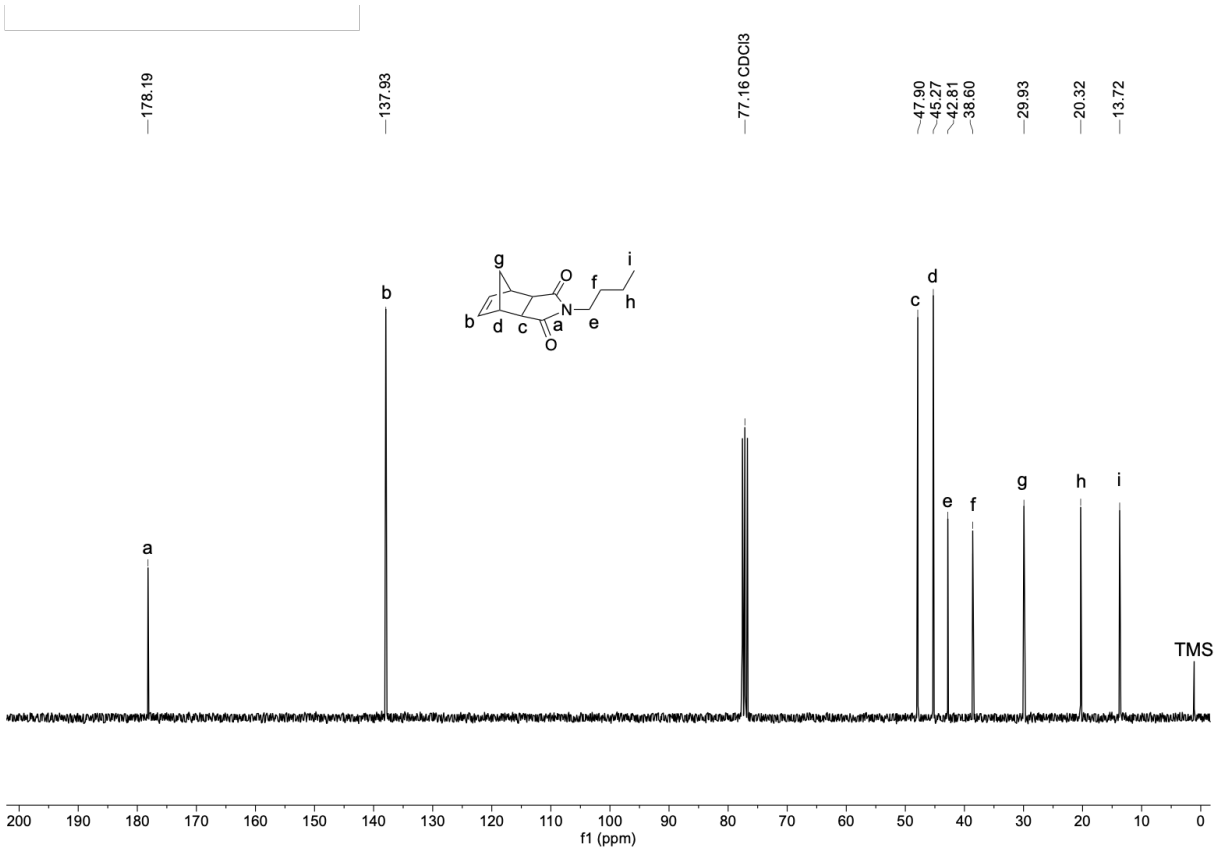


**Figure 2.5** $^{13}C$ NMR spectrum of exo-n-butylnorborneneimide (**19**) in $CDCl_3$ at 25 ºC.

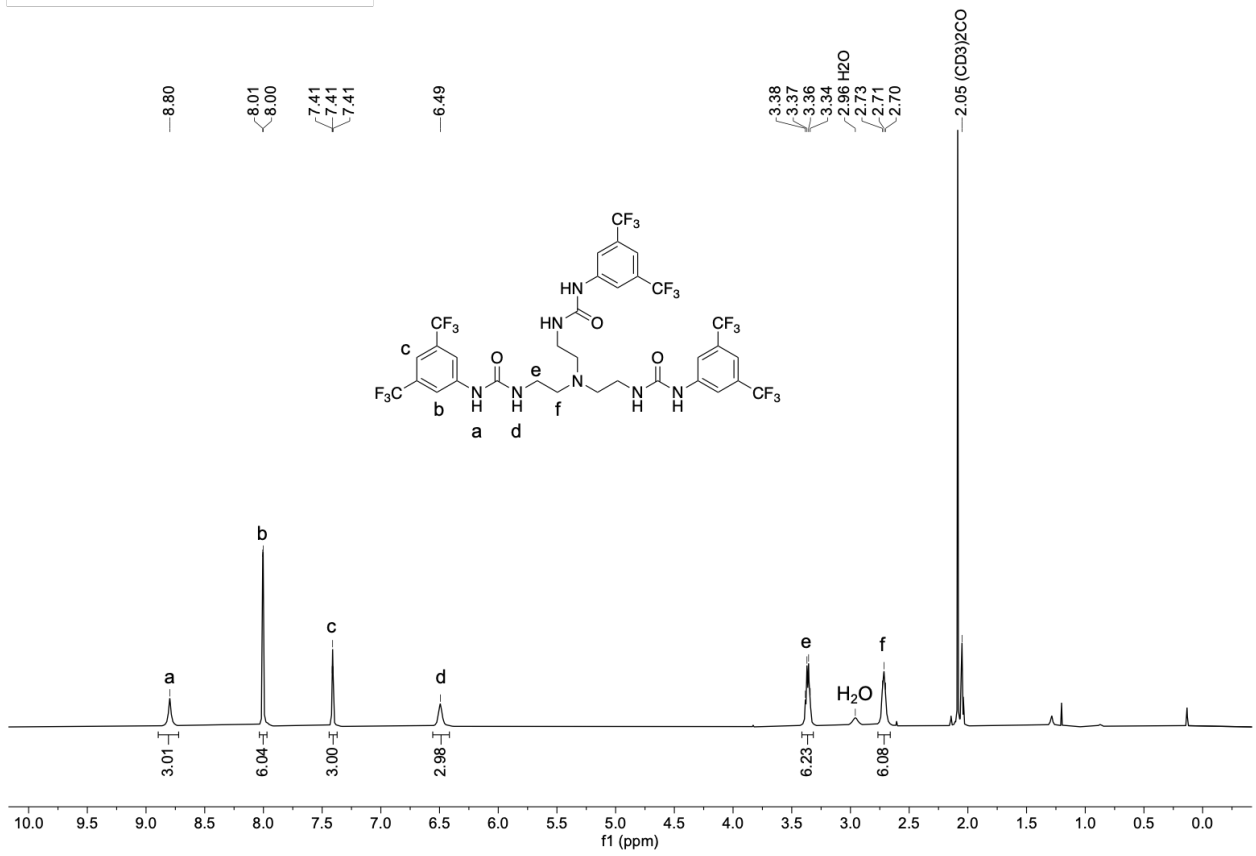


**Figure 2.6** $^{1}$H NMR spectrum of 3-O (**20**) in acetone-$d_6$ at 25 ºC.

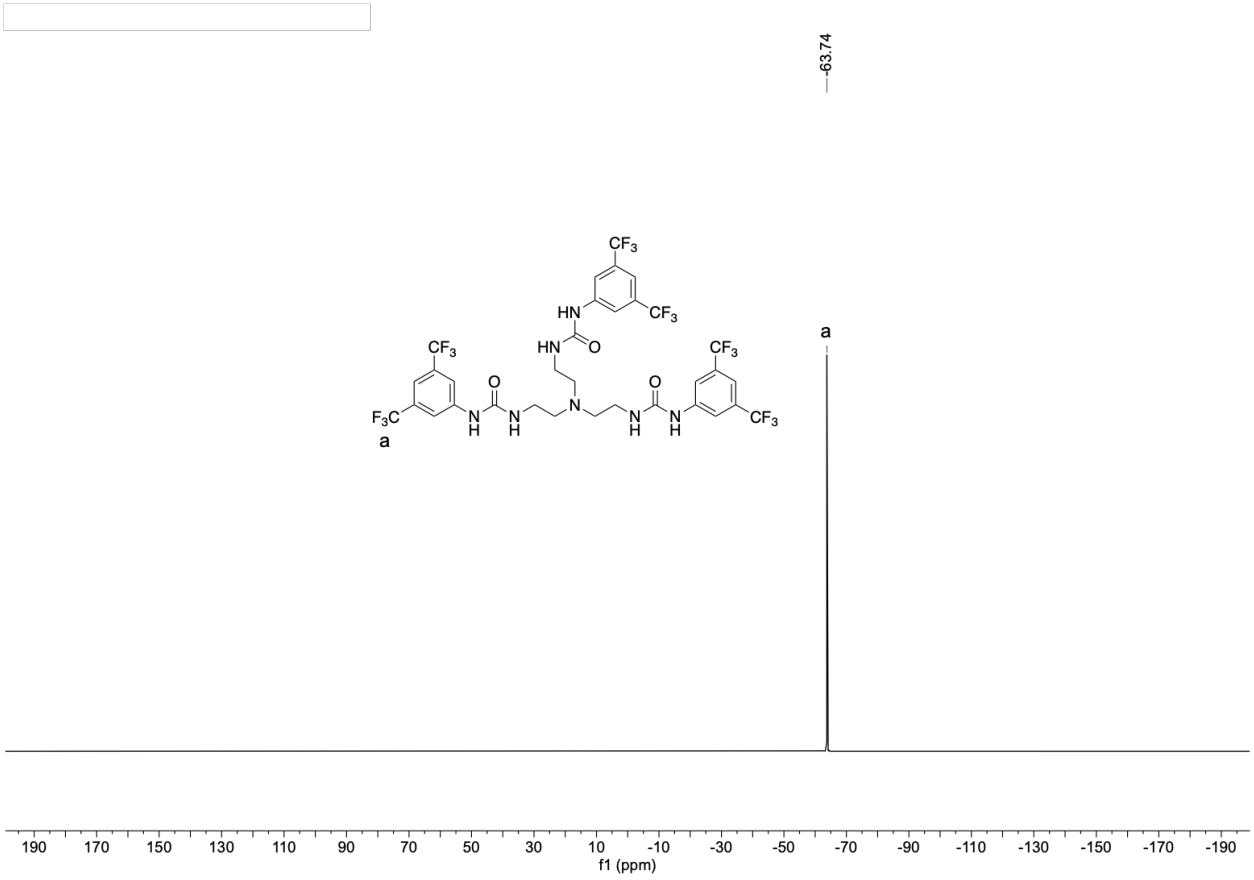


**Figure 2.7** $^{19}F\{^{1}H\}$ NMR spectrum of 3-O (**20**) in acetone-$d_6$ at 25 ºC.

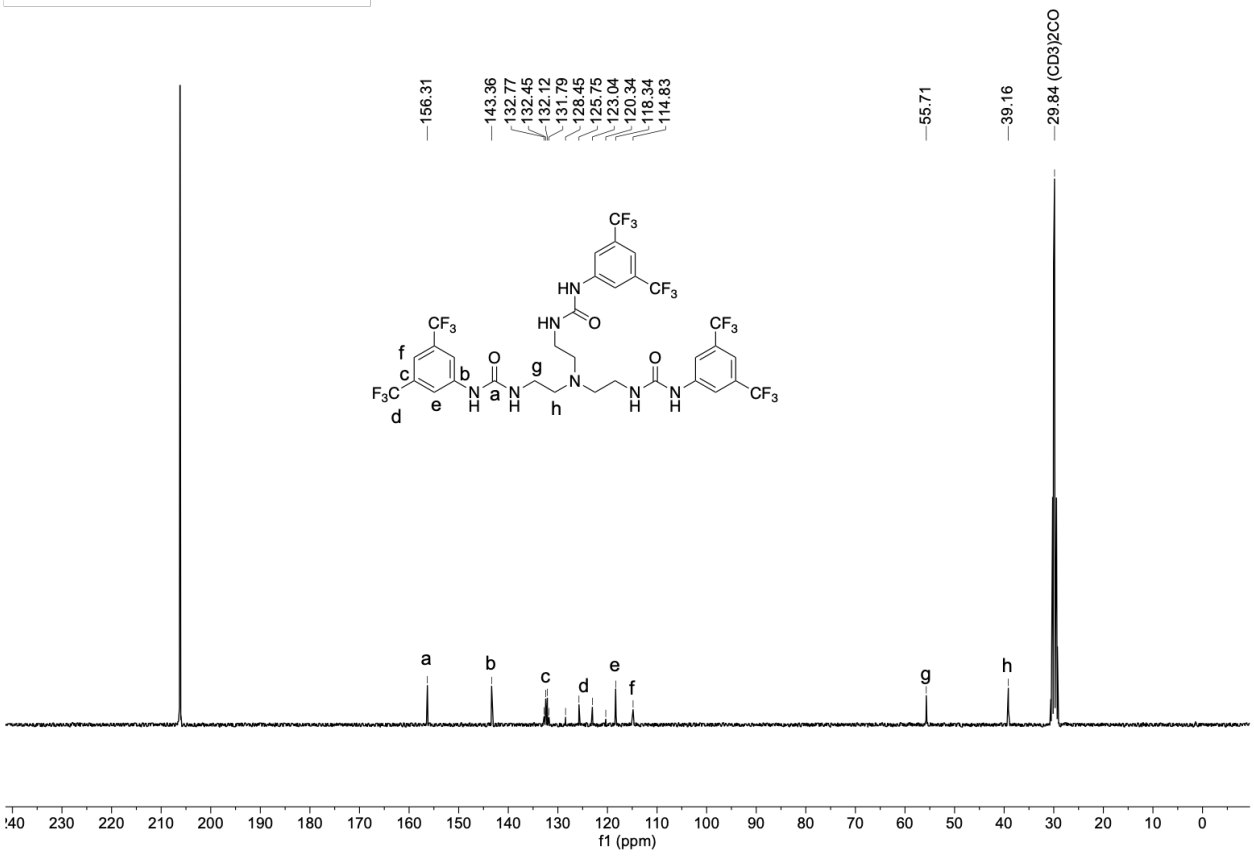


**Figure 2.8** $^{13}C$ NMR spectrum of 3-O (**20**) in acetone-$d_6$ at 25 ºC.

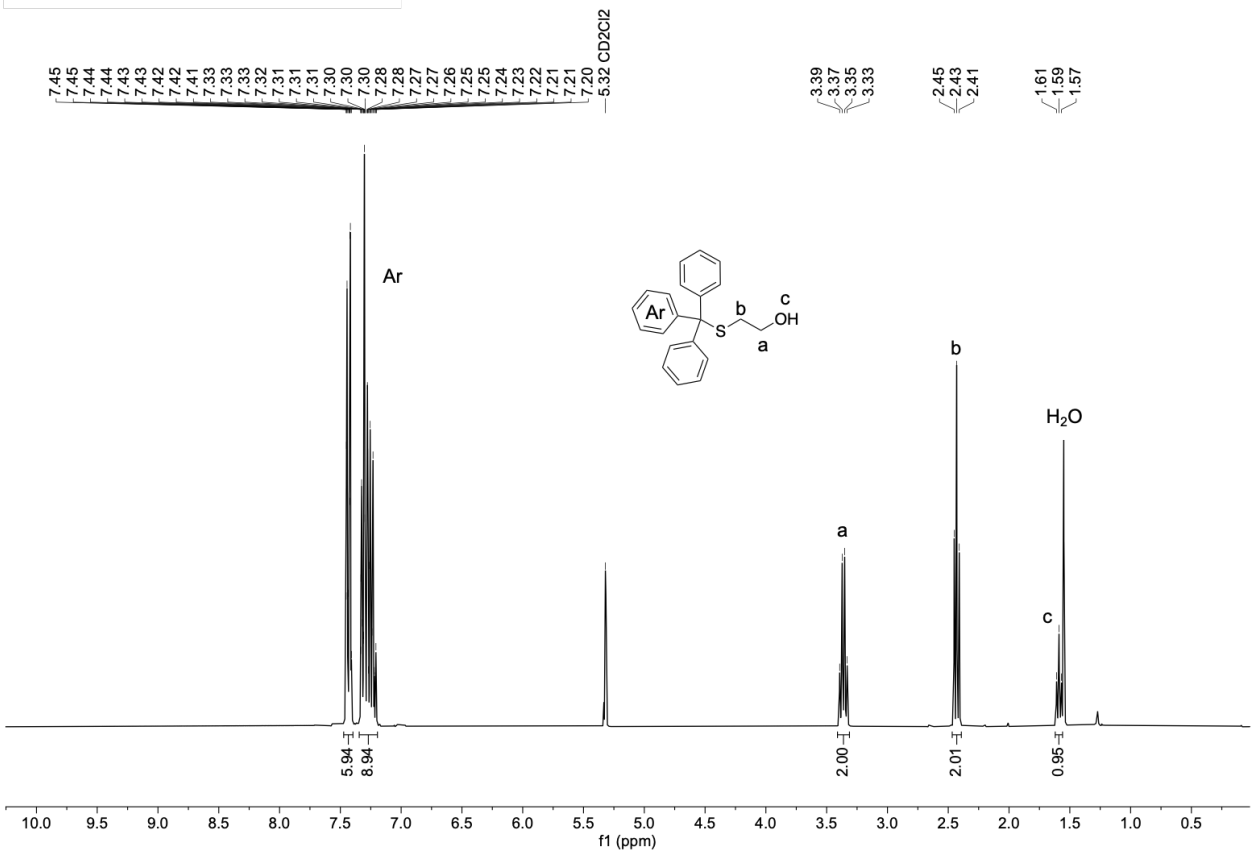


**Figure 2.9** $^{1}$H NMR spectrum of 2-(tritylthio)ethan-1-ol (**11**) in $CD_2Cl_2$ at 25 ºC.

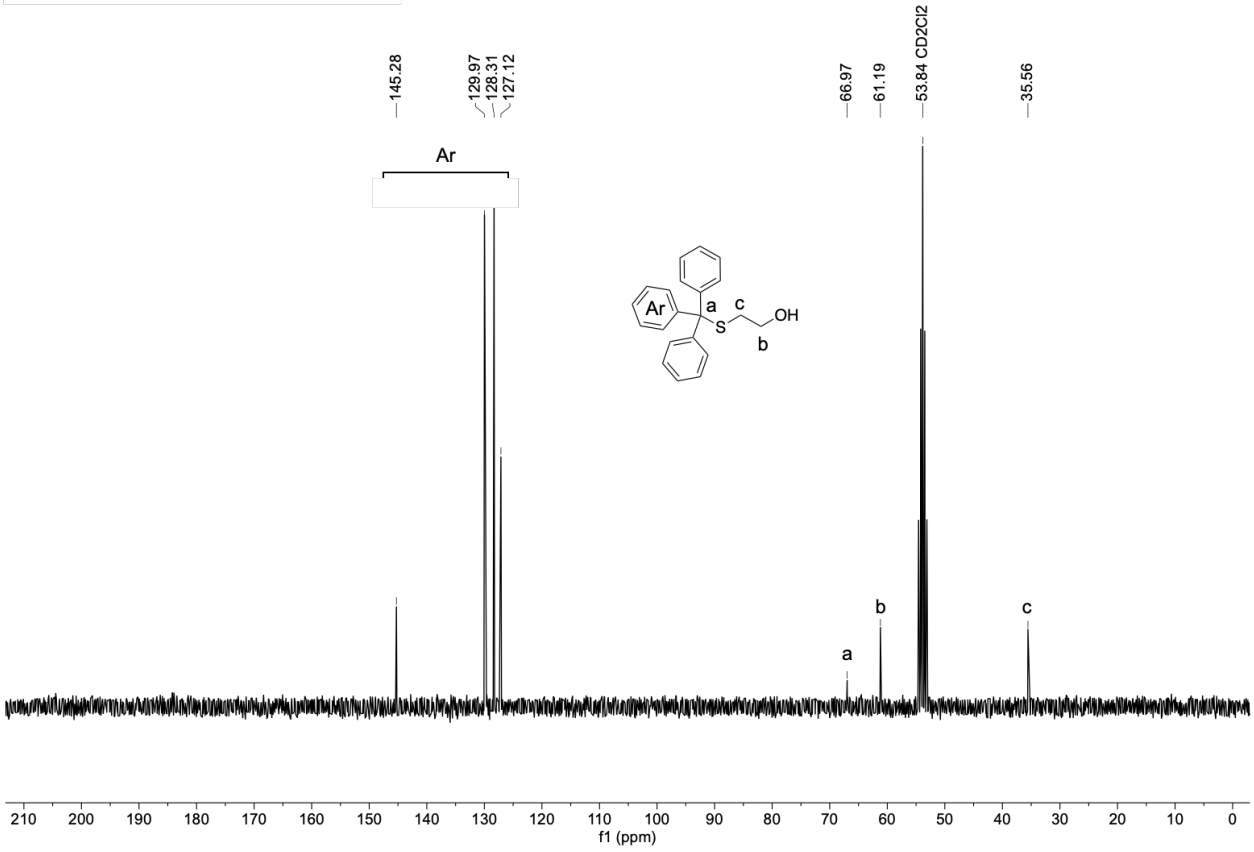


**Figure 2.10** $^{13}C$ NMR spectrum of 2-(tritylthio)ethan-1-ol (**11**) in $CD_2Cl_2$ at 25 ºC.

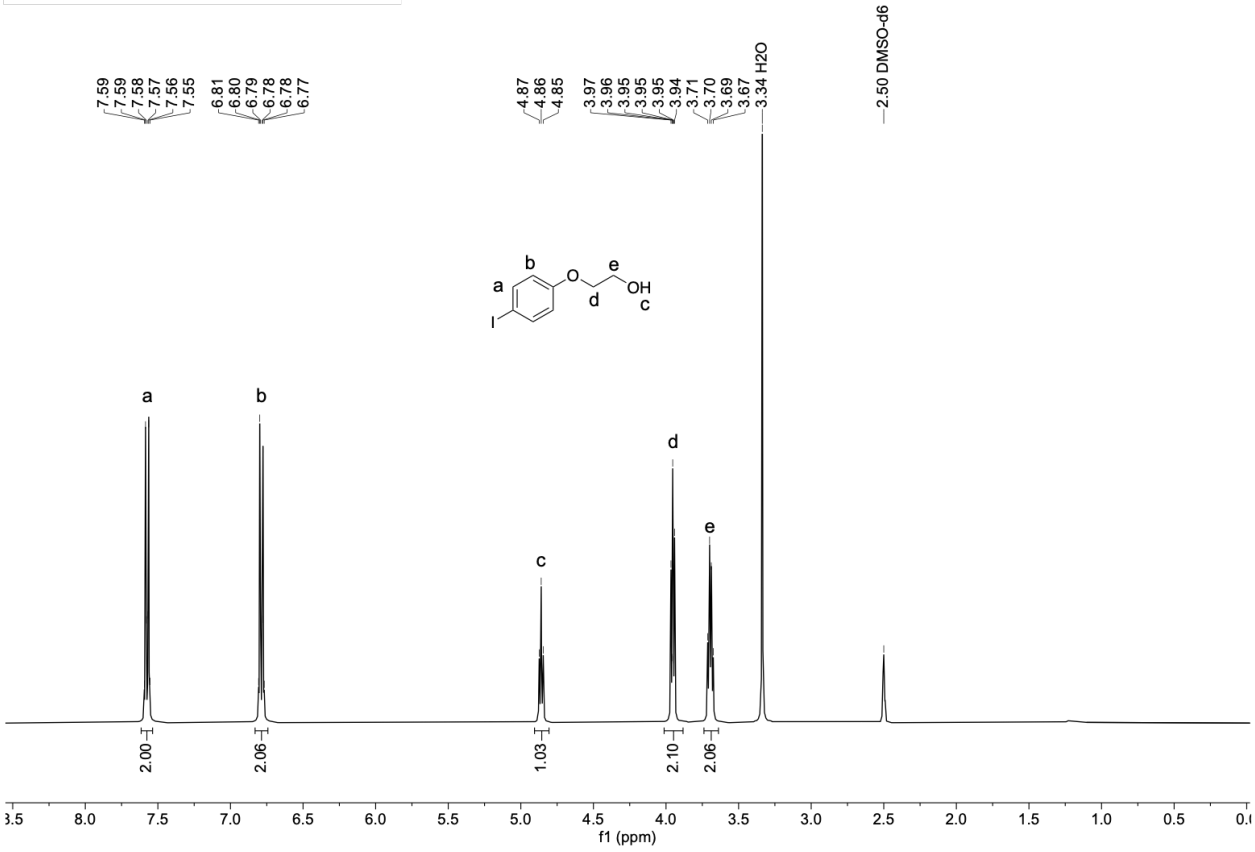


**Figure 2.11** $^{1}$H NMR spectrum of 2-(4-iodophenoxy)ethan-1-ol (**2**) in DMSO-$d_6$ at 25 ºC.

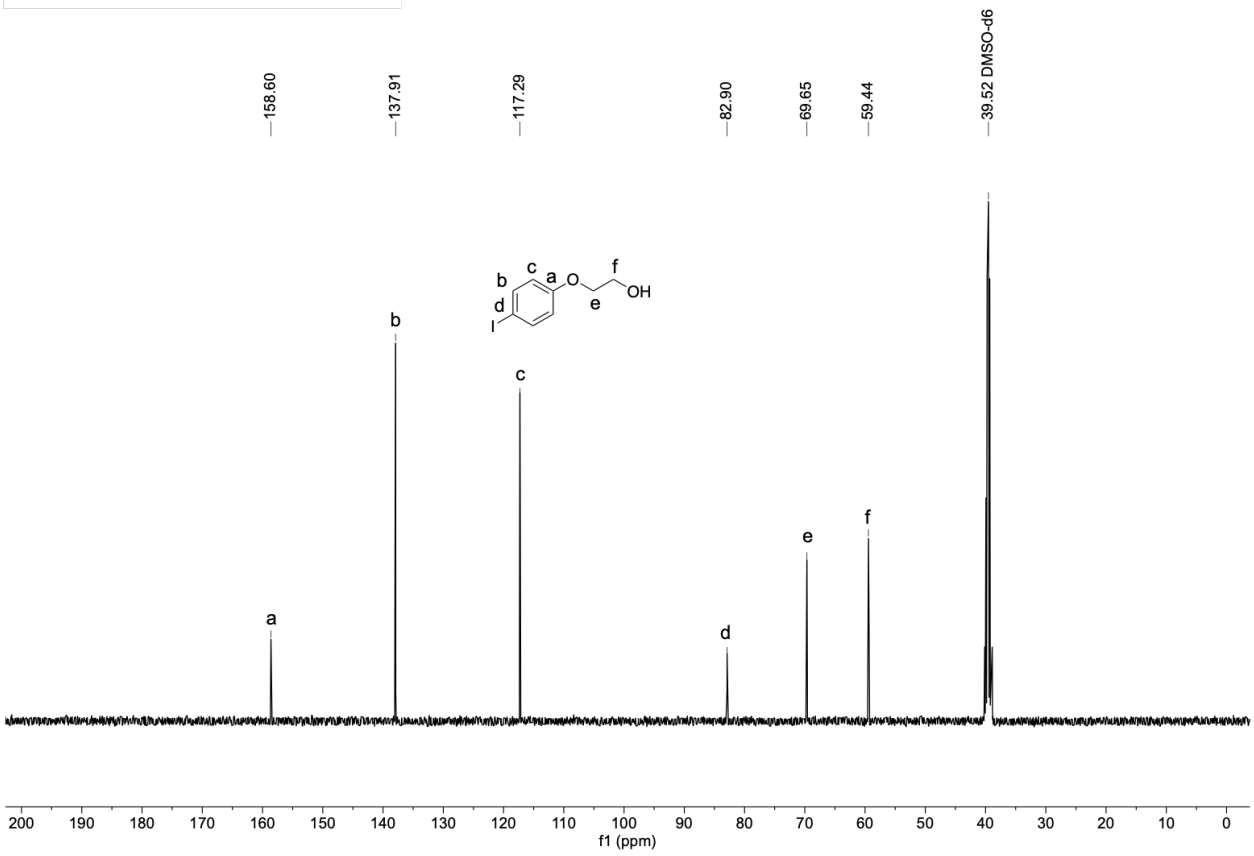


**Figure 2.12** $^{13}$C NMR spectrum of 2-(4-iodophenoxy)ethan-1-ol (**2**) in DMSO-$d_6$ at 25 ºC.

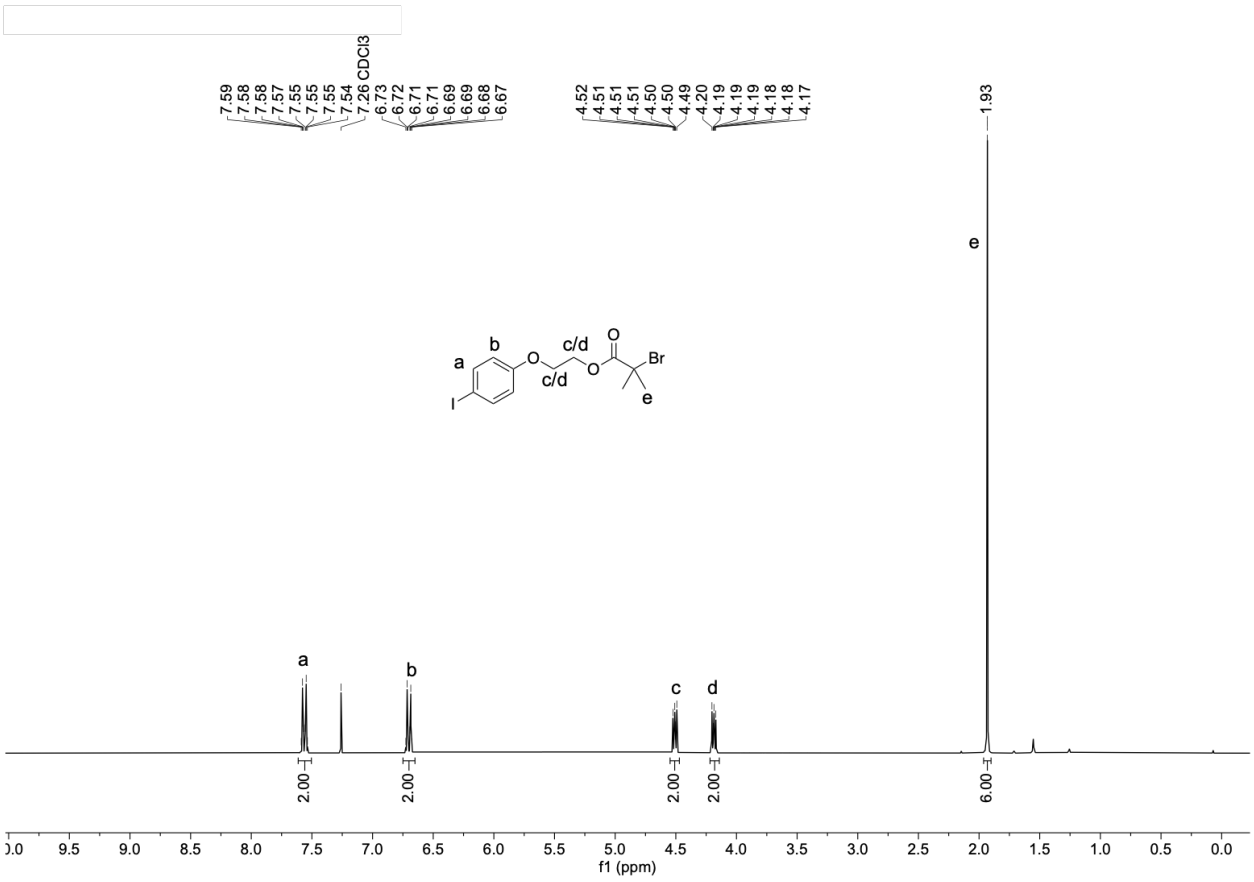


**Figure 2.13** $^{1}$H NMR spectrum of 2-(4-iodophenoxy)ethyl 2-bromo-2-methylpropanoate (**5**) in $CDCl_3$ at 25 ºC.

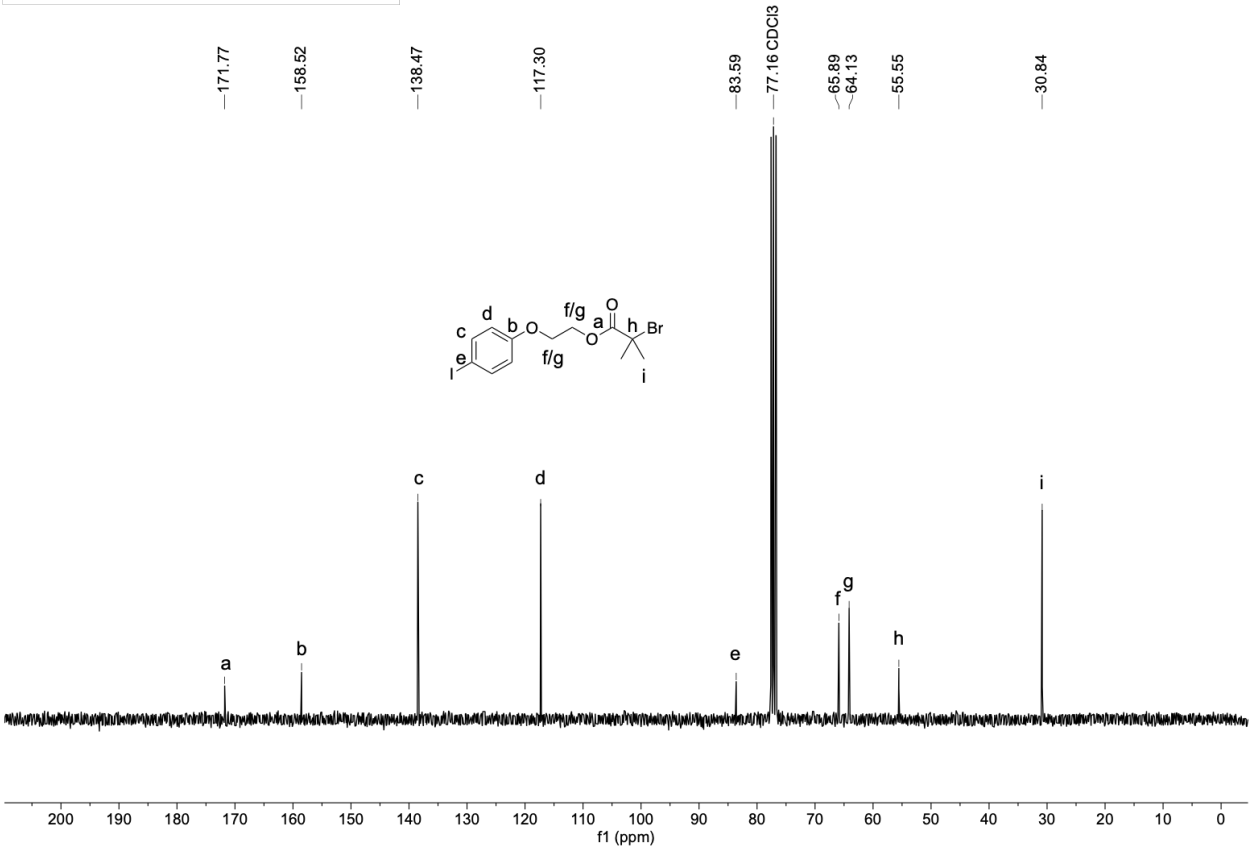


**Figure 2.14** $^{13}C$ NMR spectrum of 2-(4-iodophenoxy)ethyl 2-bromo-2-methylpropanoate (**5**) in $CDCl_3$ at 25 ºC.

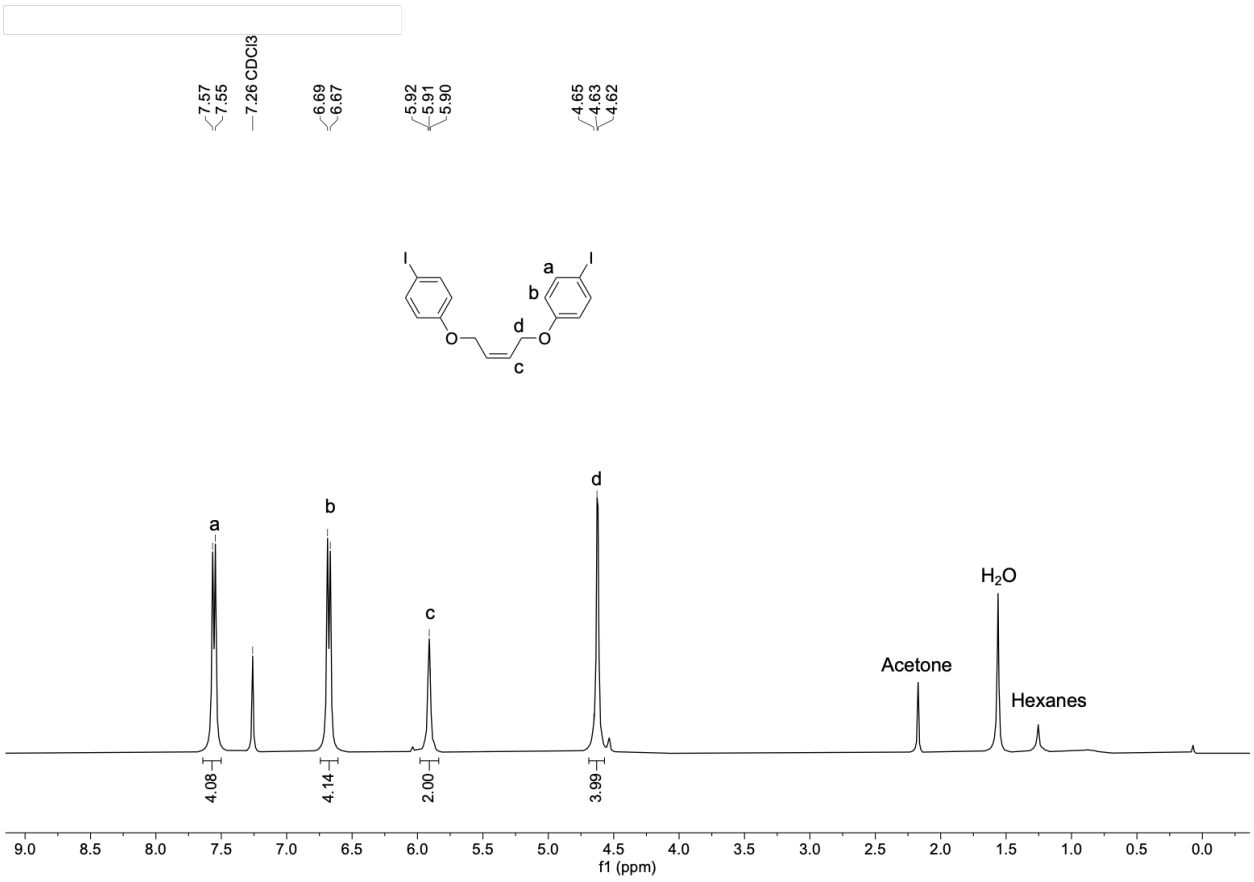


**Figure 2.15** $^{1}$H NMR spectrum of (*Z*)-1,4-bis(4-iodophenoxy)but-2-ene (**4**) in $CDCl_3$ at 25 ºC.

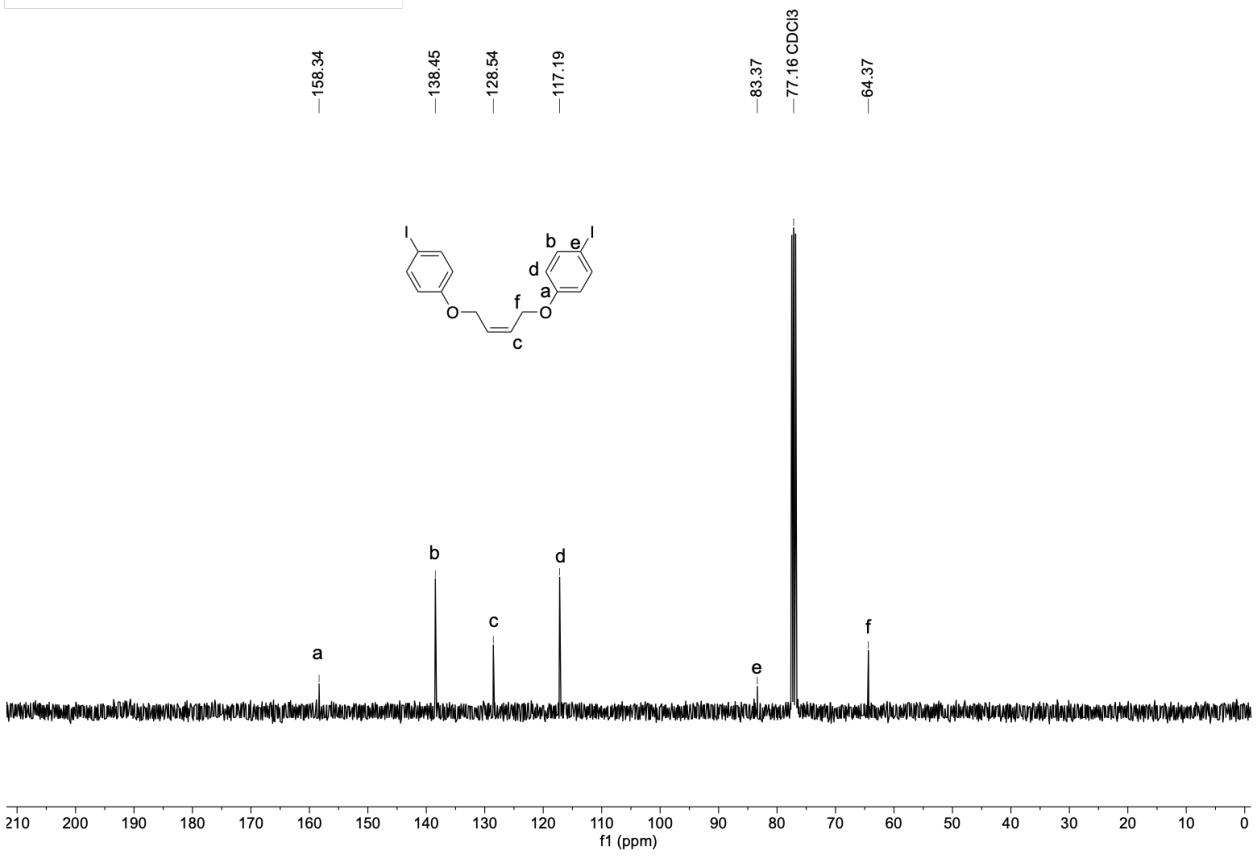


**Figure 2.16** $^{13}$C NMR spectrum of (*Z*)-1,4-bis(4-iodophenoxy)but-2-ene (**4**) in $CDCl_3$ at 25 ºC.

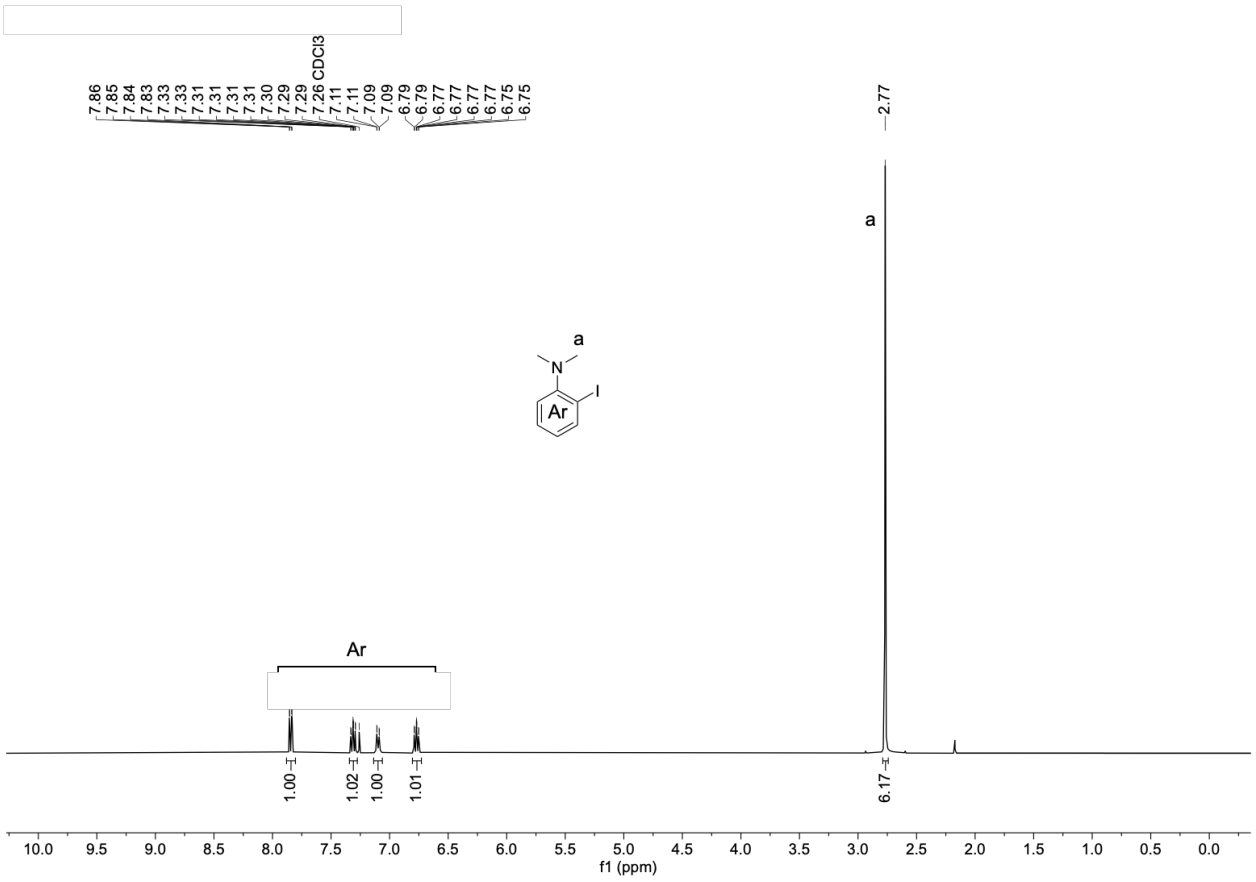


**Figure 2.17** $^{1}$H NMR spectrum of 2-iodo-*N*,*N*-dimethylaniline (**21**) in $CDCl_3$ at 25 ºC.

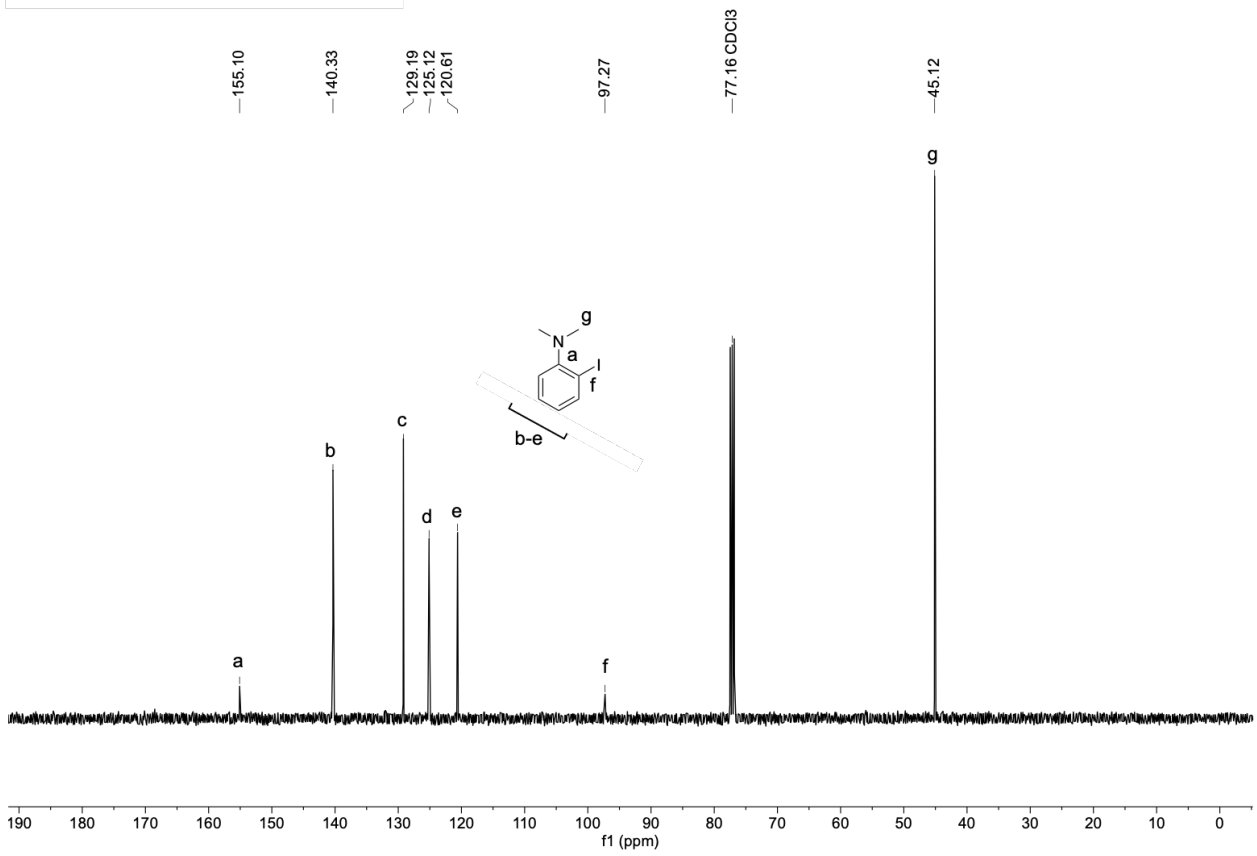


**Figure 2.18** $^{13}$C NMR spectrum of 2-iodo-*N*,*N*-dimethylaniline (**21**) in $CDCl_3$ at 25 ºC.

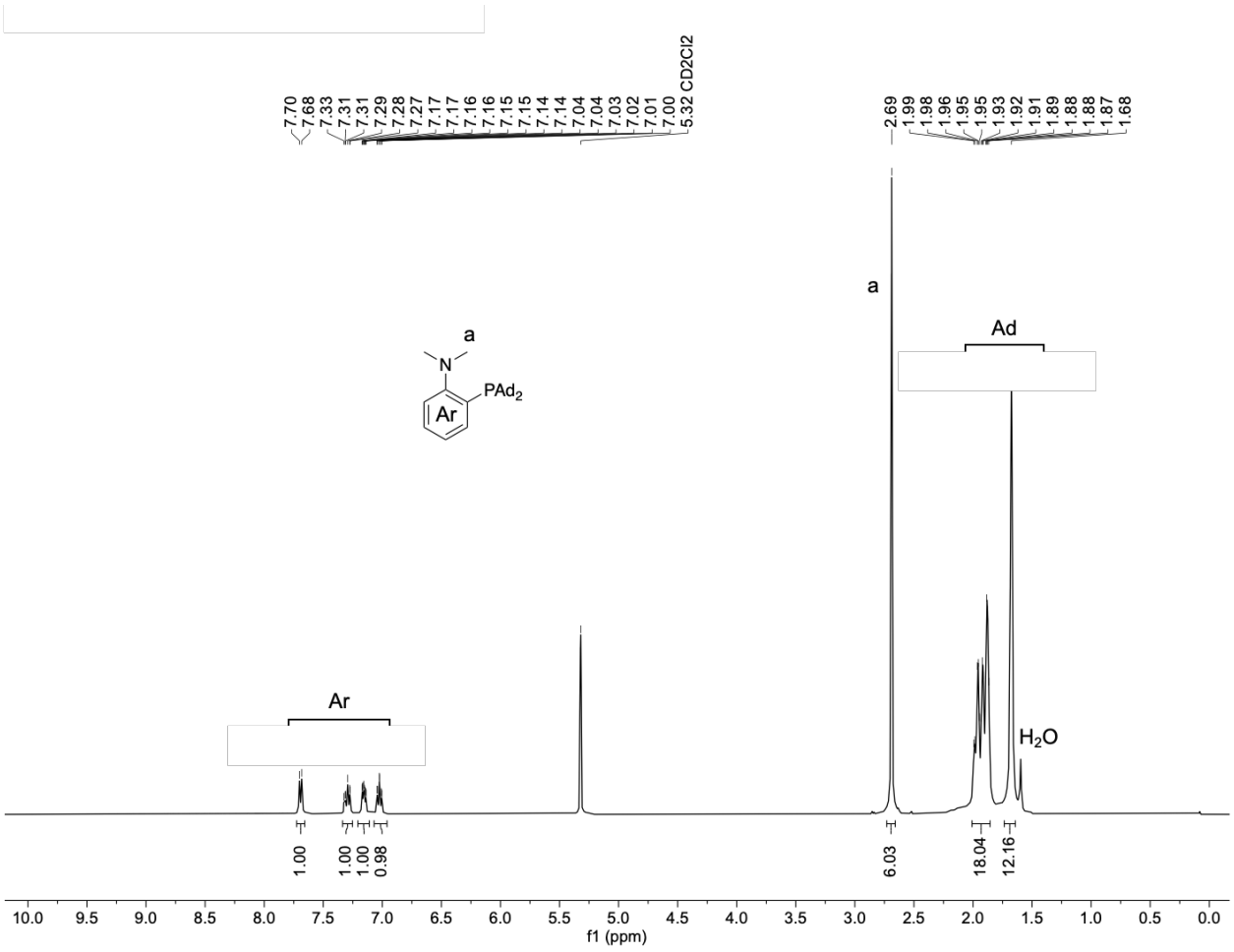


**Figure 2.19** $^{1}$H NMR spectrum of Me-DalPhos (**22**) in $CD_2Cl_2$ at 25 ºC.

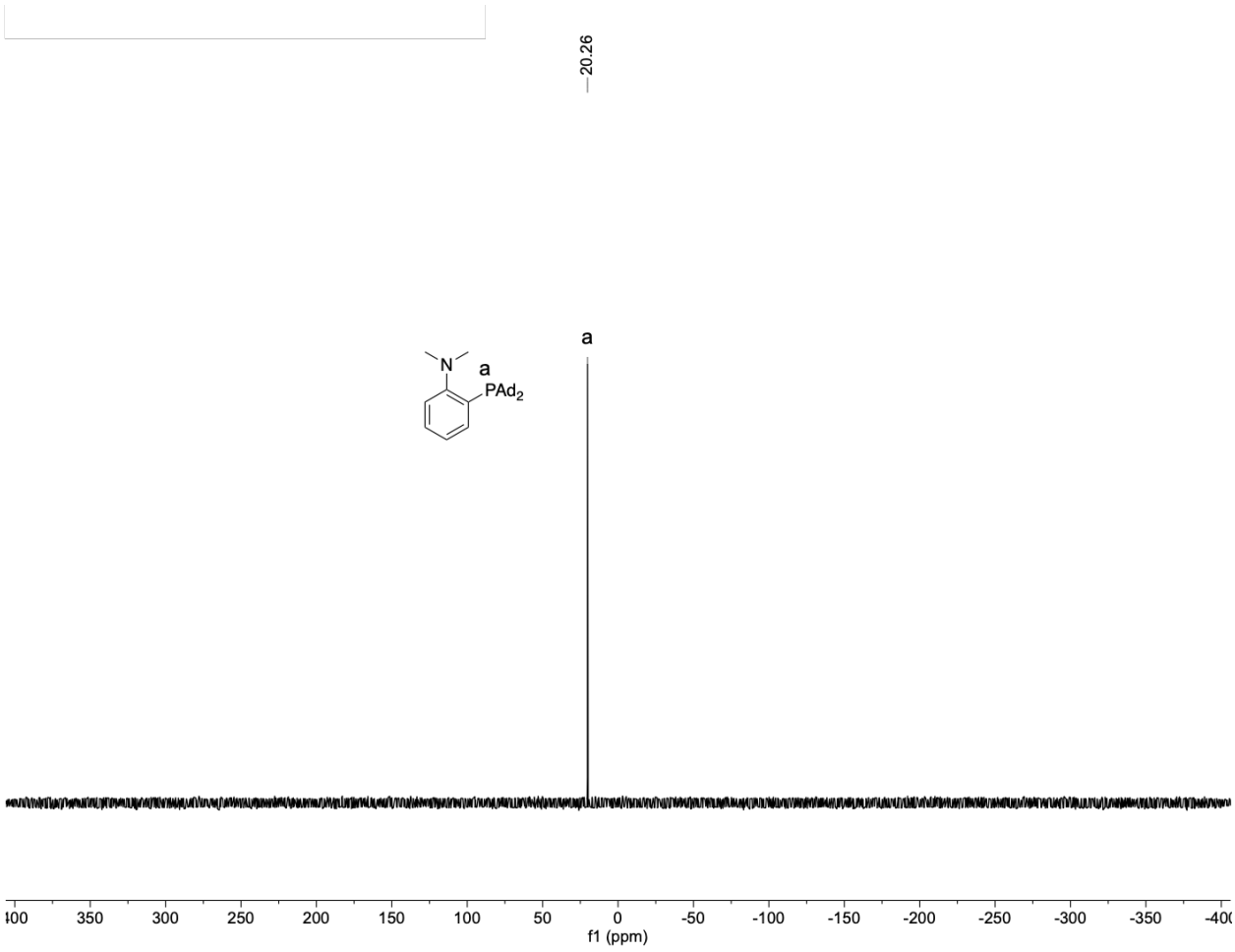


**Figure 2.20** $^{31}P\{^{1}H\}$ NMR spectrum of Me-DalPhos (**22**) in $CD_2Cl_2$ at 25 ºC.

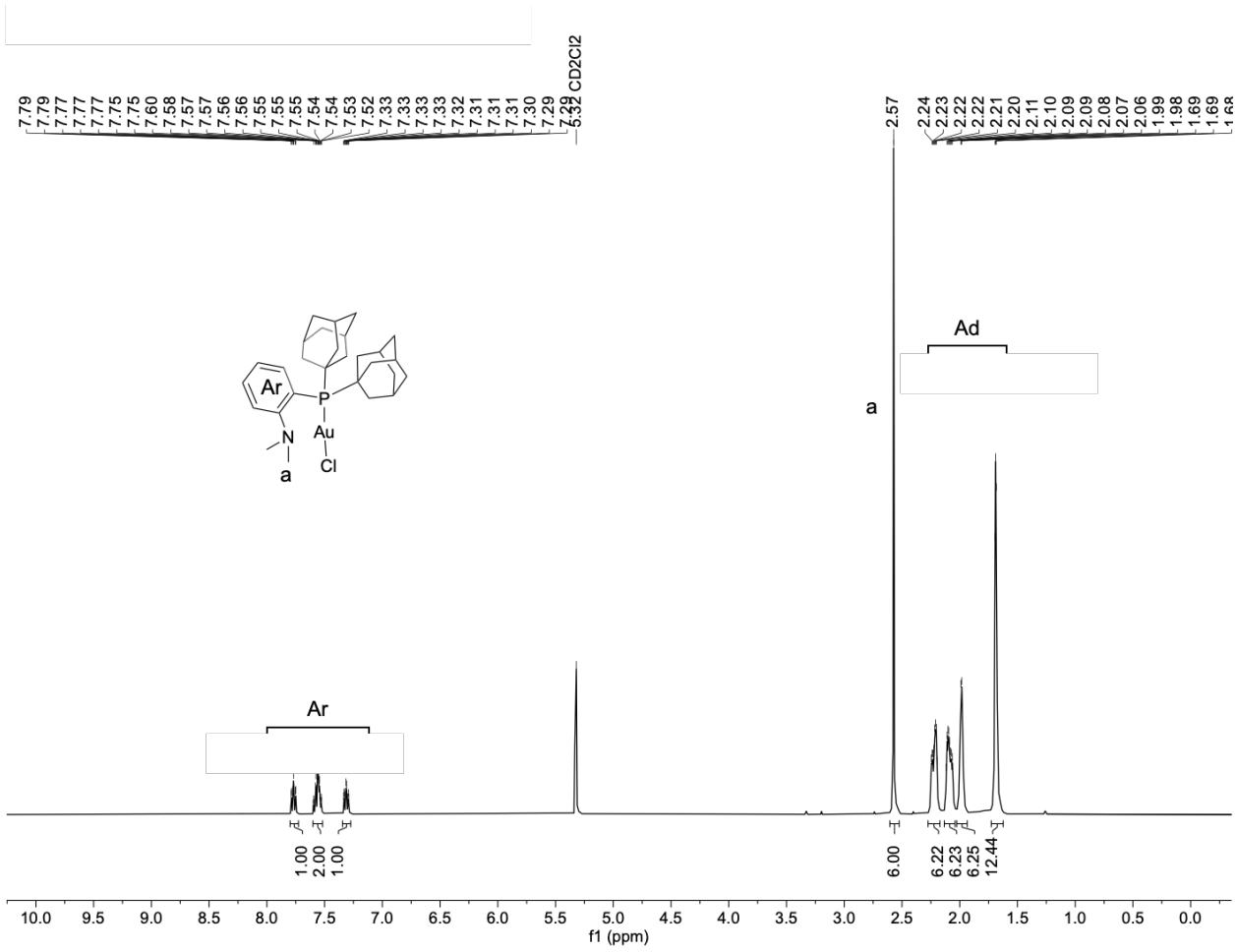


**Figure 2.21** $^{1}$H NMR spectrum of (Me-DalPhos)Au$^{I}$Cl (**7**) in $CD_2Cl_2$ at 25 ºC.

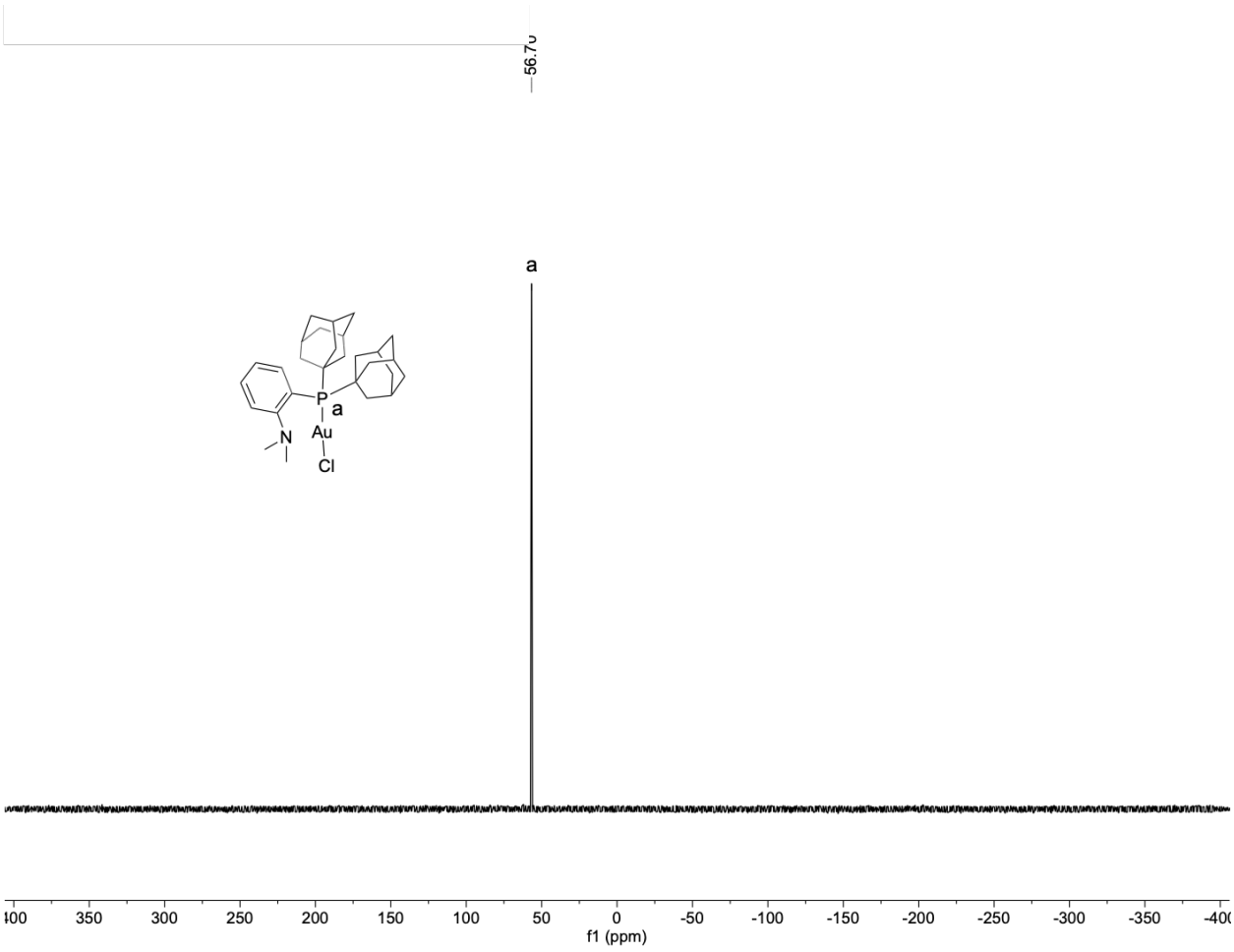


**Figure 2.22** $^{31}P\{^{1}H\}$ NMR spectrum of (Me-DalPhos)$Au^{I}Cl$ (**7**) in $CD_2Cl_2$ at 25 ºC.

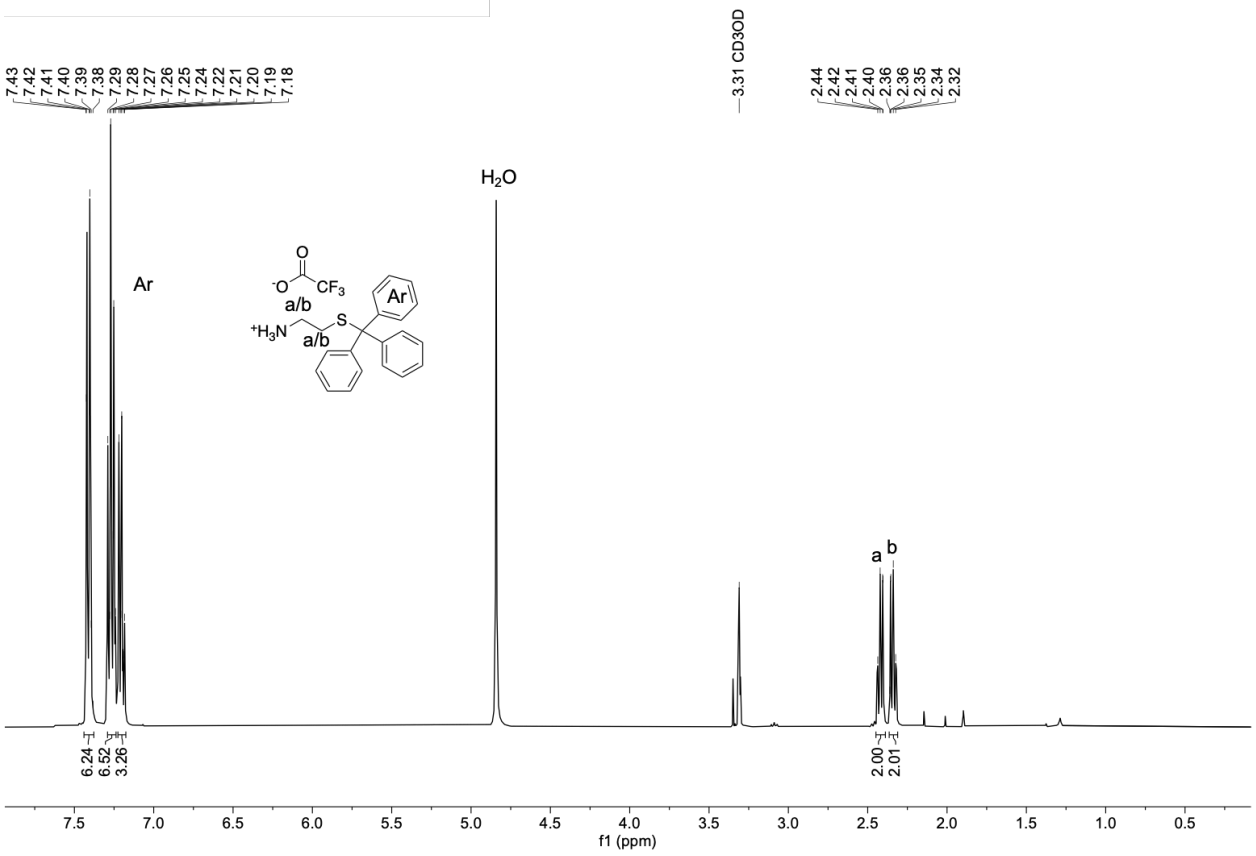


**Figure 2.23** $^{1}$H NMR spectrum of 2-(tritylthio)ethan-1-ammonium trifluoroacetate (**23**) in MeOD at 25 ºC.

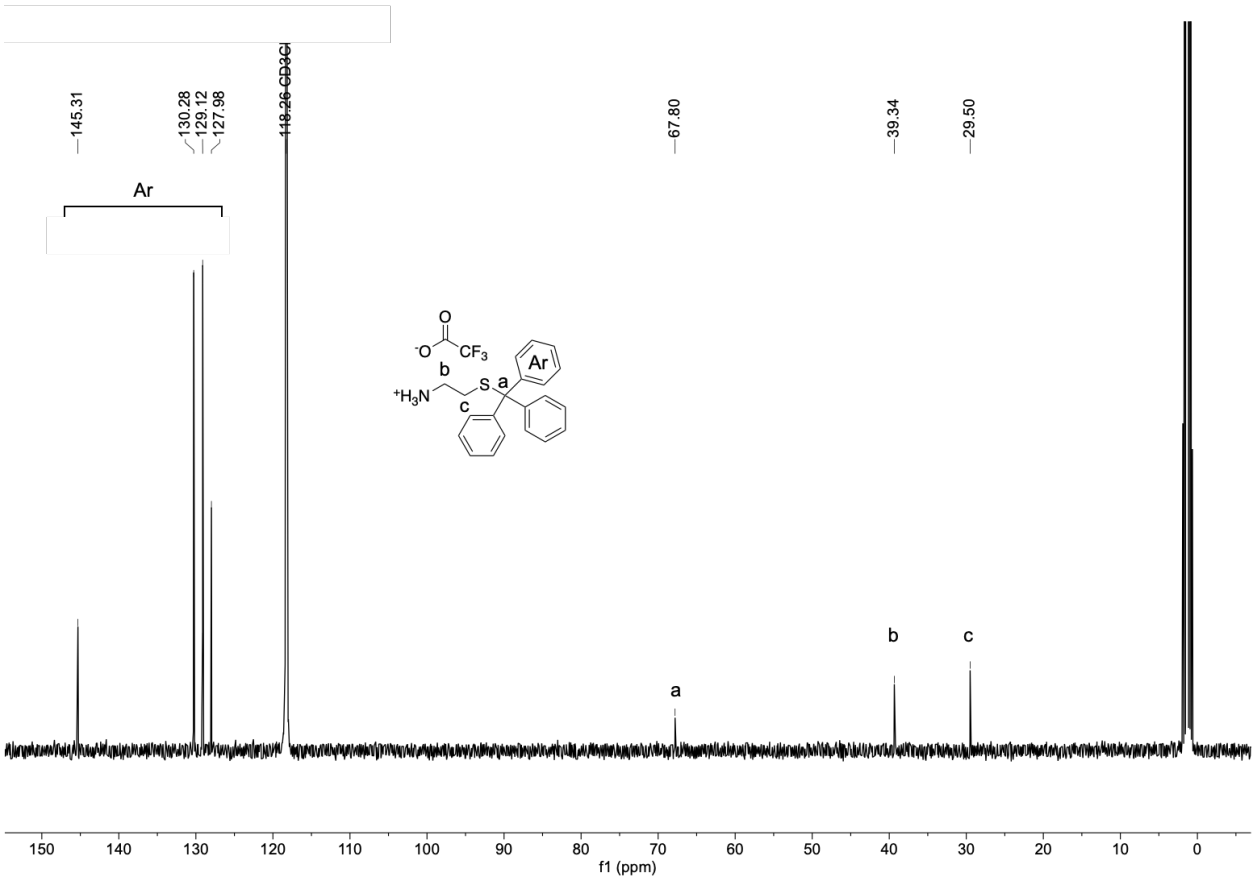


**Figure 2.24** $^{13}C$ NMR spectrum of 2-(tritylthio)ethan-1-ammonium trifluoroacetate (**23**) in $CD_3CN$ at 25 ºC. *$CD_3CN$ used to prevent overlap of the product signals with the solvent signals.

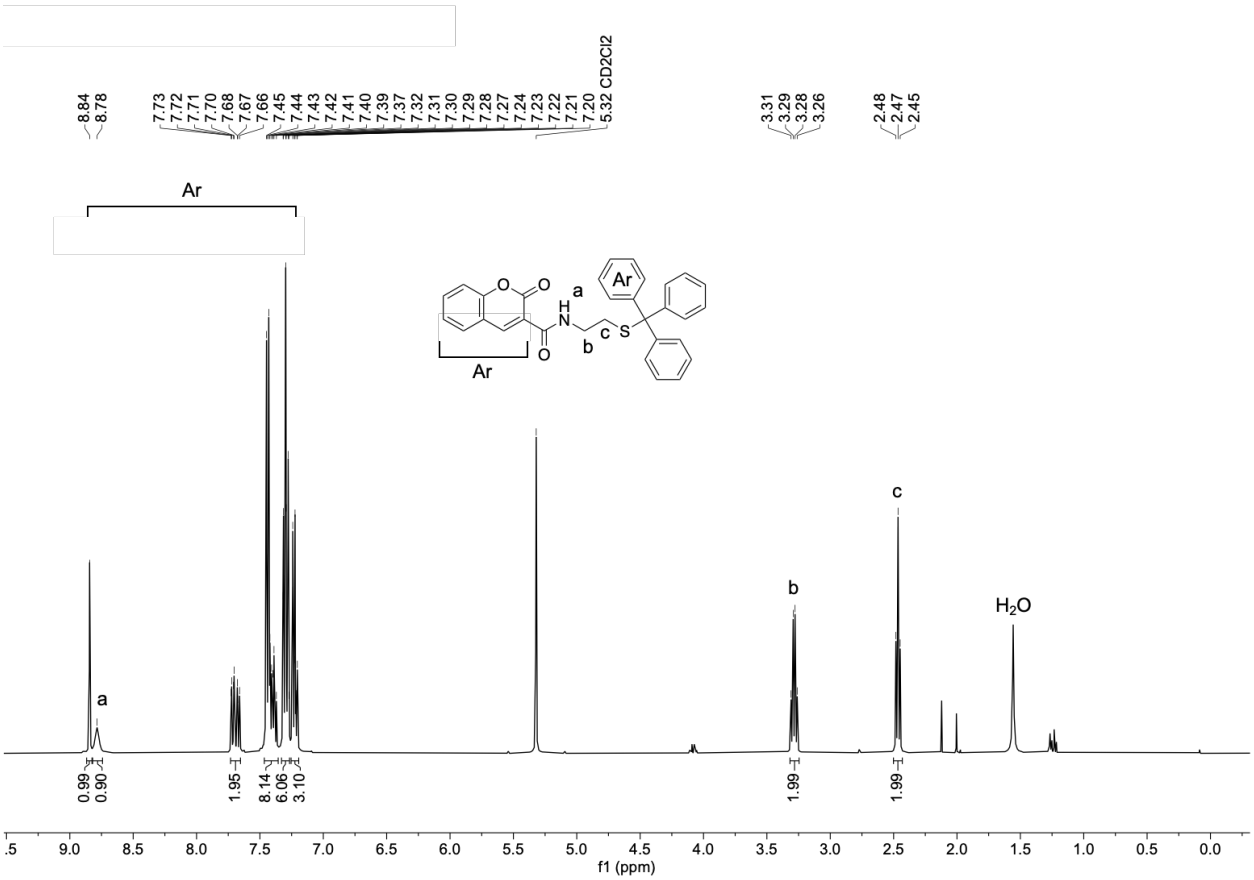


**Figure 2.25** $^{1}$H NMR spectrum of 2-oxo-N-(2-(tritylthio)ethyl)-2H-chromene-3-carboxamide (**9**) in $CD_2Cl_2$ at 25 ºC.

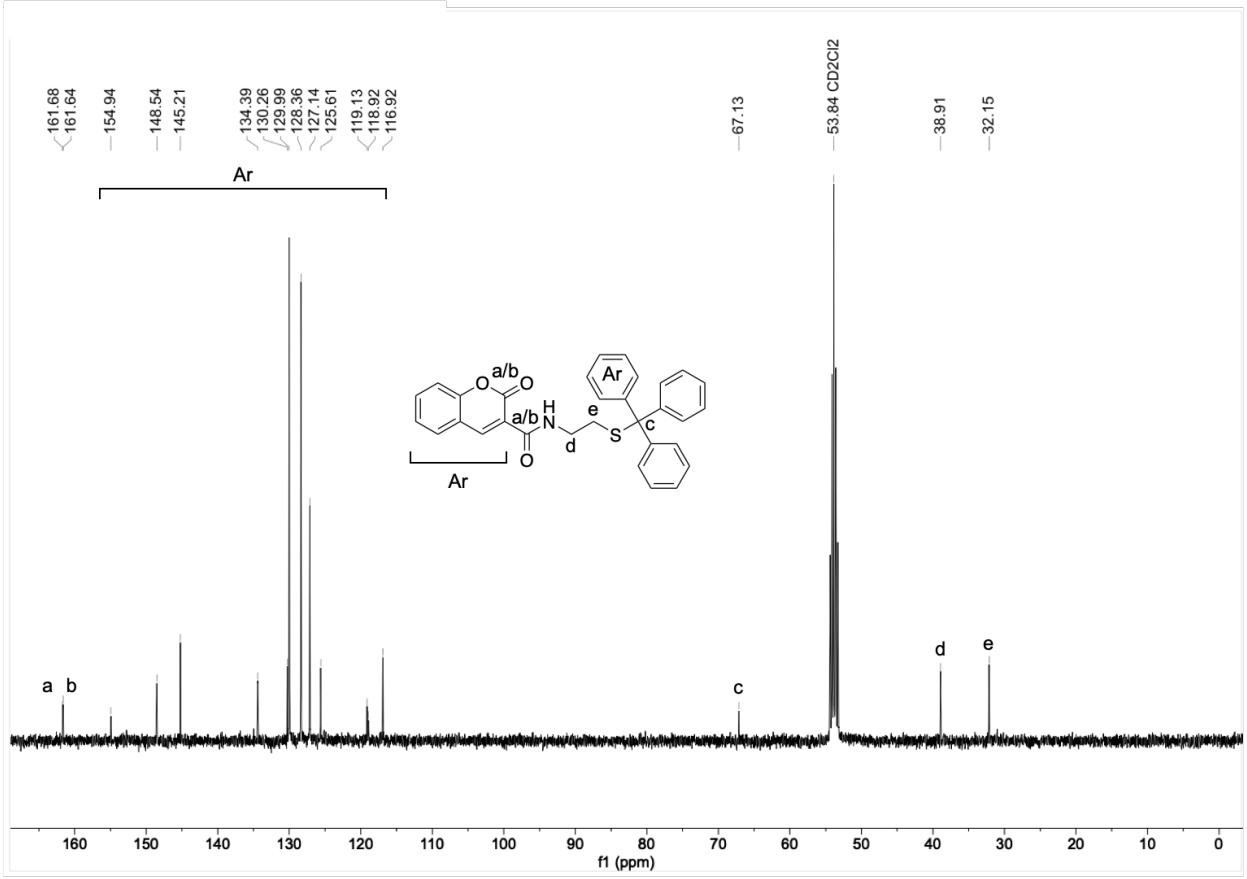


**Figure 2.26** $^{13}C$ NMR spectrum of 2-oxo-N-(2-(tritylthio)ethyl)-2H-chromene-3-carboxamide (**9**) in $CD_2Cl_2$ at 25 ºC.

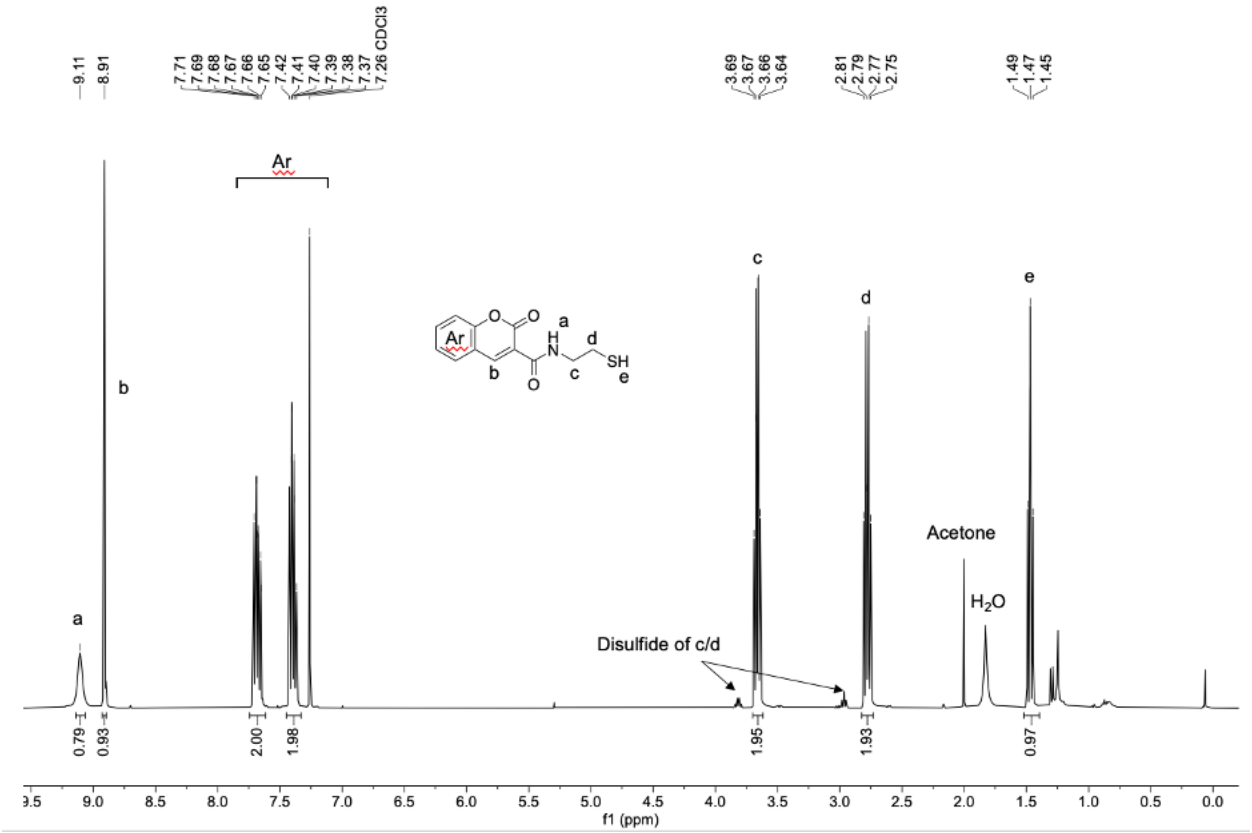


**Figure 2.27** $^{1}$H NMR spectrum of *N*-(2-mercaptoethyl)-2-oxo-2*H*-chromene-3-carboxamide (**9a**) in $CDCl_3$ at 25 ºC.

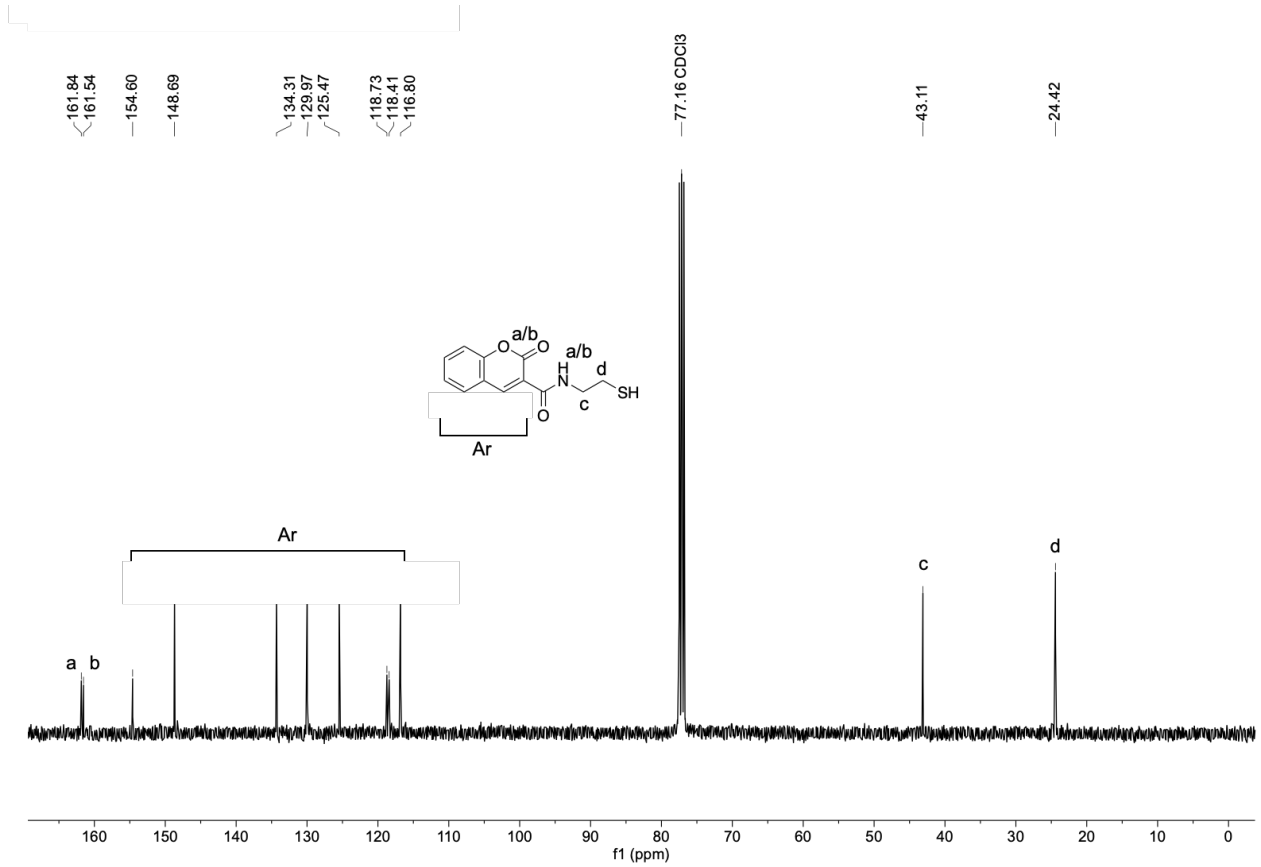


**Figure 2.28** $^{13}$C NMR spectrum of *N*-(2-mercaptoethyl)-2-oxo-2*H*-chromene-3-carboxamide (**9a**) in $CDCl_3$ at 25 ºC.

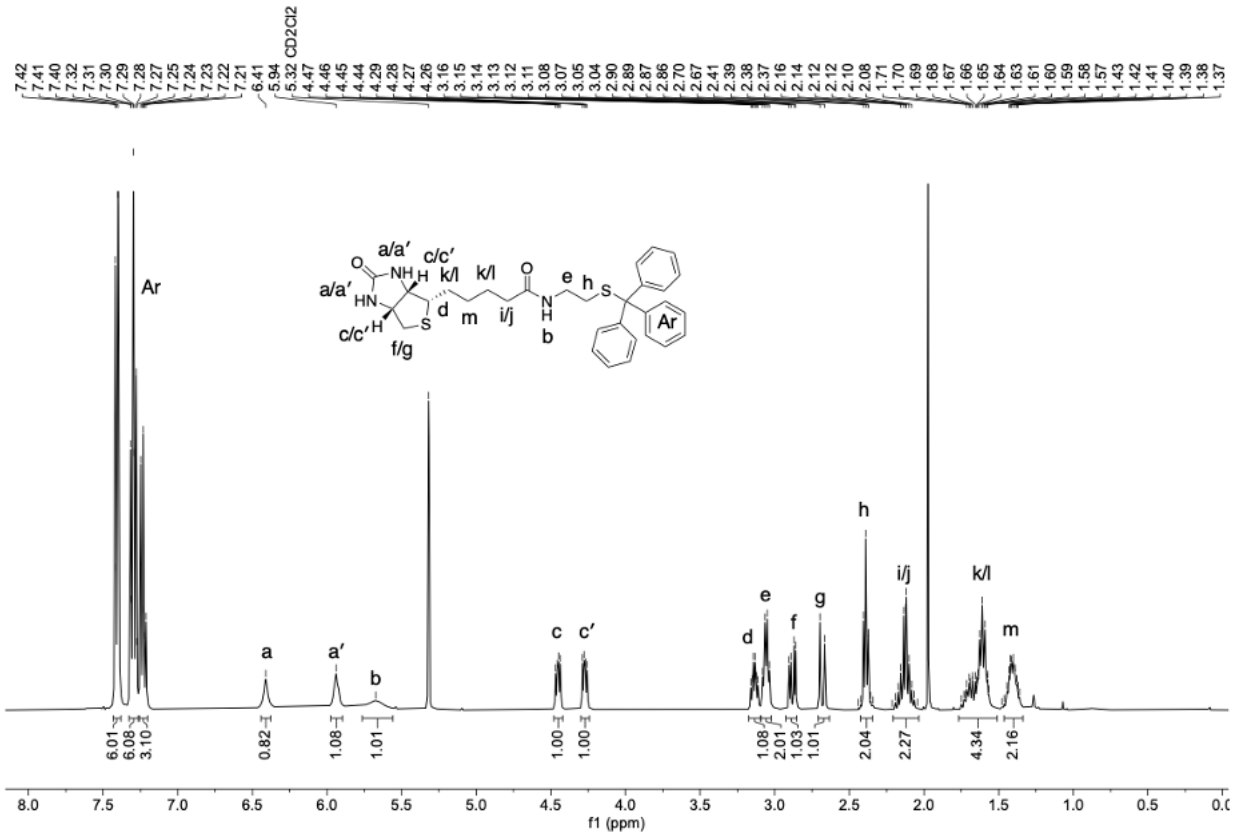


**Figure 2.29** $^{1}$H NMR spectrum of 5-((3a*S*,4*S*,6a*R*)-2-oxohexahydro-1*H*-thieno[3,4-*d*]imidazol-4-yl)-*N*-(2-(tritylthio)ethyl)pentanamide (**8**) in $CD_2Cl_2$ at 25 ºC.

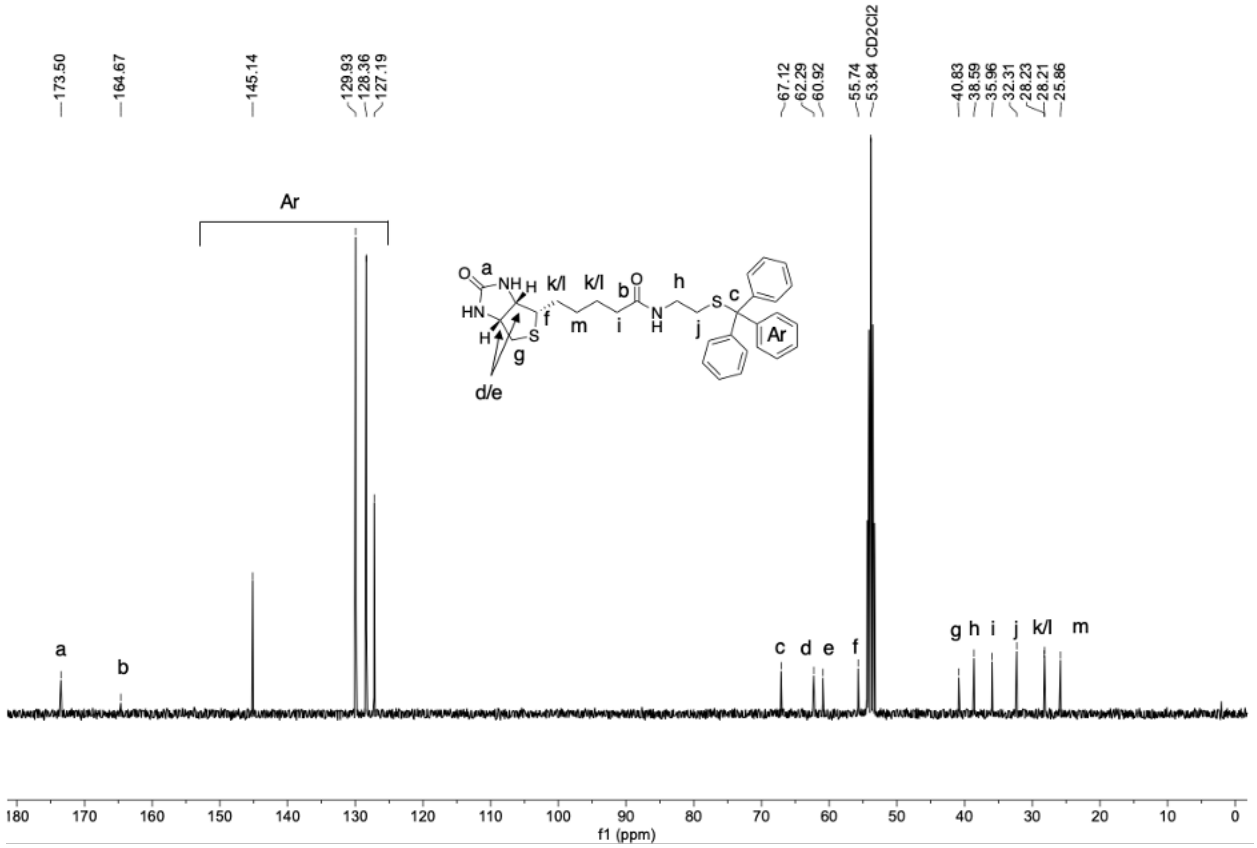


**Figure 2.30** $^{13}$C NMR spectrum of 5-((3a*S*,4*S*,6a*R*)-2-oxohexahydro-1*H*-thieno[3,4-*d*]imidazol-4-yl)-*N*-(2-(tritylthio)ethyl)pentanamide (**8**) in $CD_2Cl_2$ at 25 ºC.

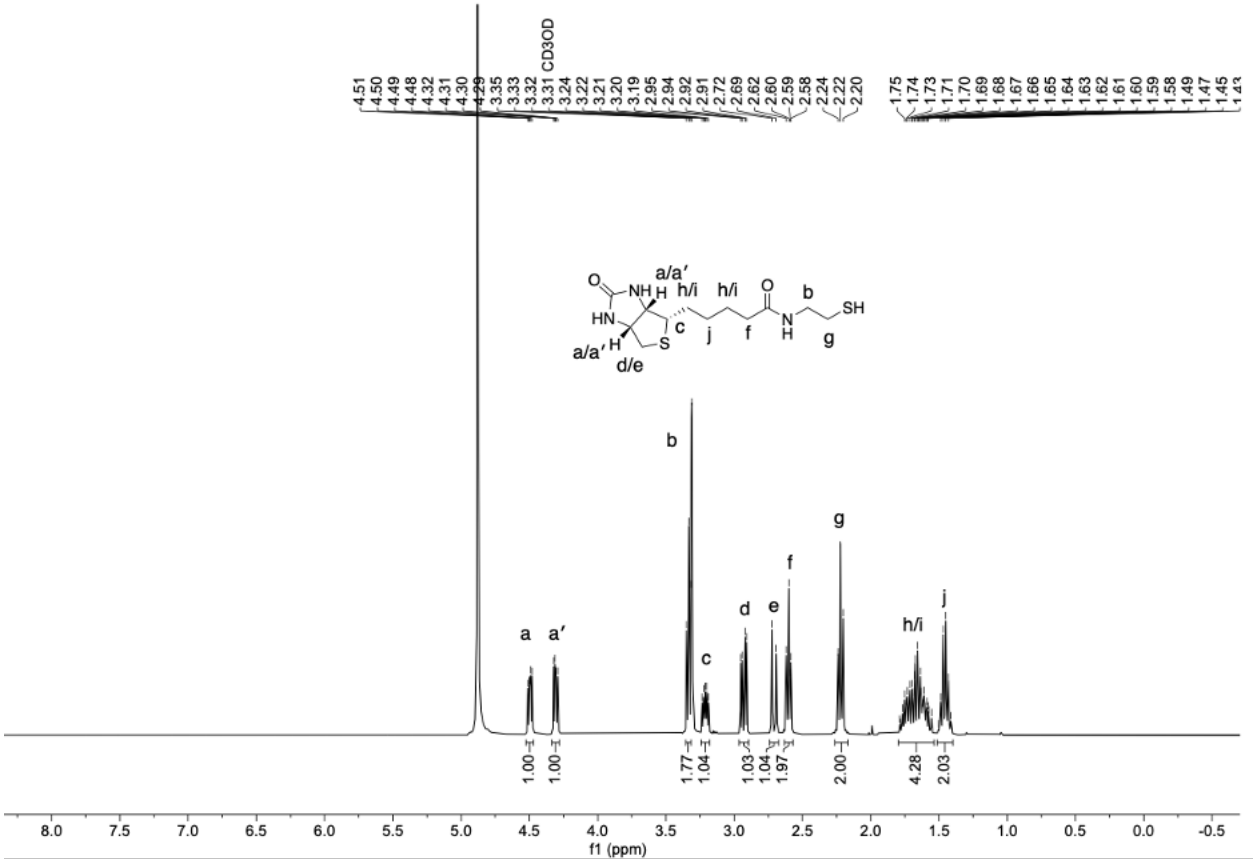


**Figure 2.31** $^{1}$H NMR spectrum of N-(2-mercaptoethyl)-5-((3aS,4S,6aR)-2-oxohexahydro-1H-thieno[3,4-d]imidazol-4-yl)pentanamide (**8a**) in MeOD at 25 ºC.

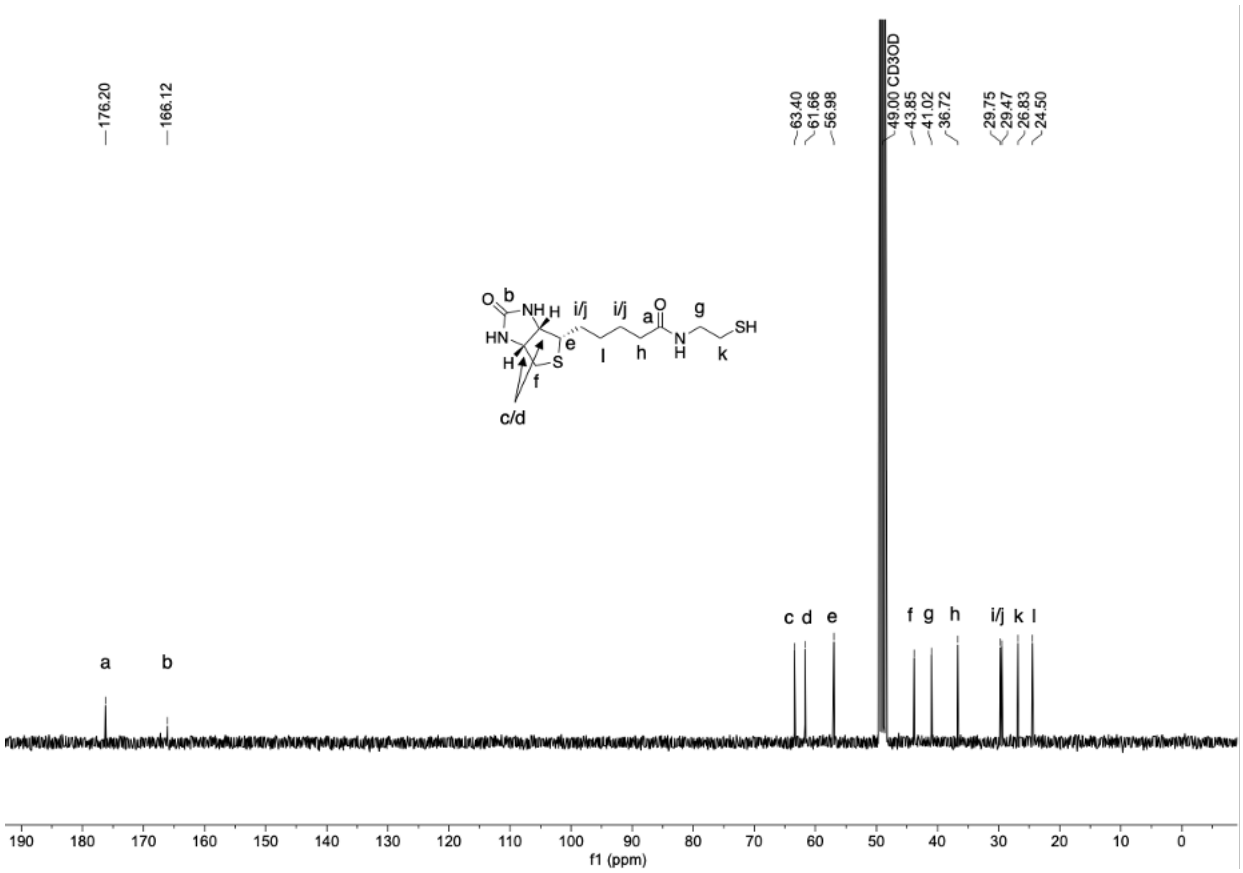


**Figure 2.32** $^{13}$C NMR spectrum of N-(2-mercaptoethyl)-5-((3aS,4S,6aR)-2-oxohexahydro-1H-thieno[3,4-d]imidazol-4-yl)pentanamide (**8a**) in MeOD at 25 ºC.

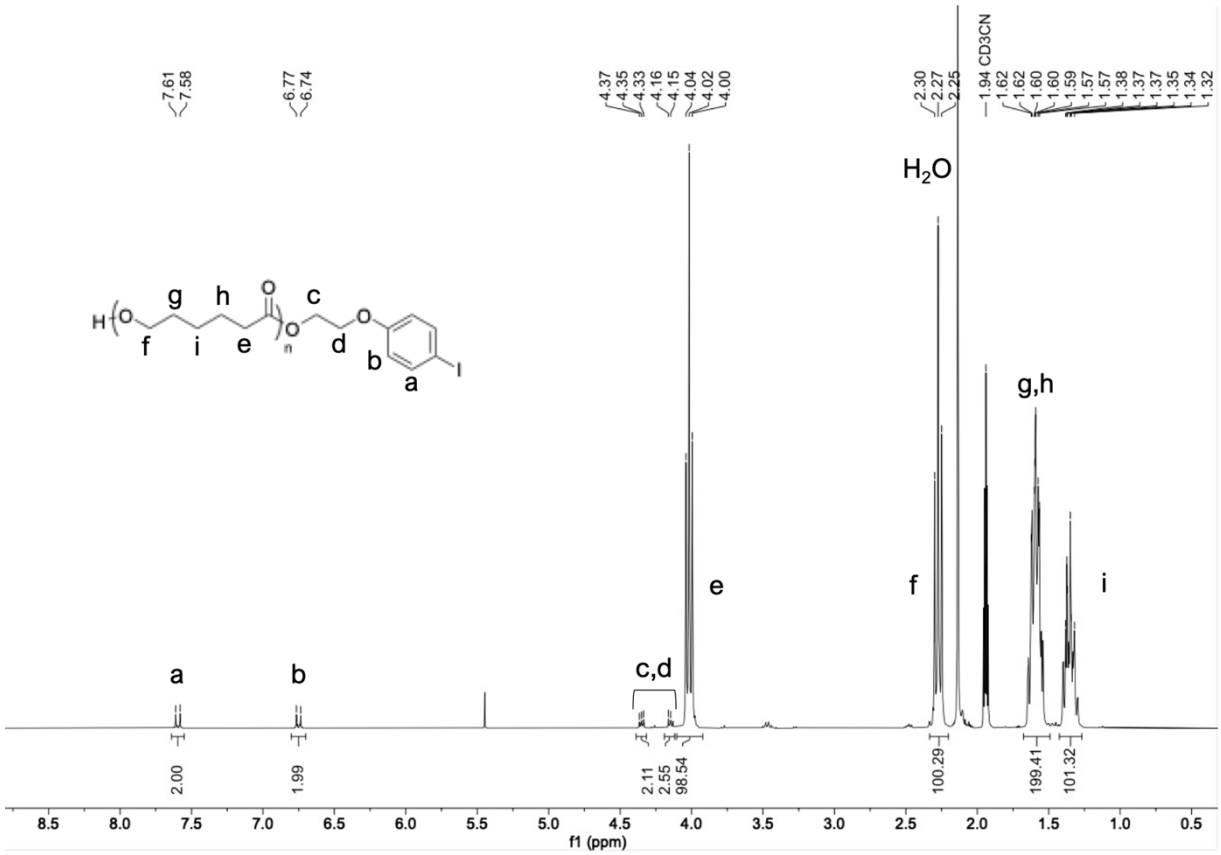


**Figure 2.33** $^{1}$H NMR spectrum of pCL-aryl iodide (**1**) in $CD_3CN$ at 25 ºC.

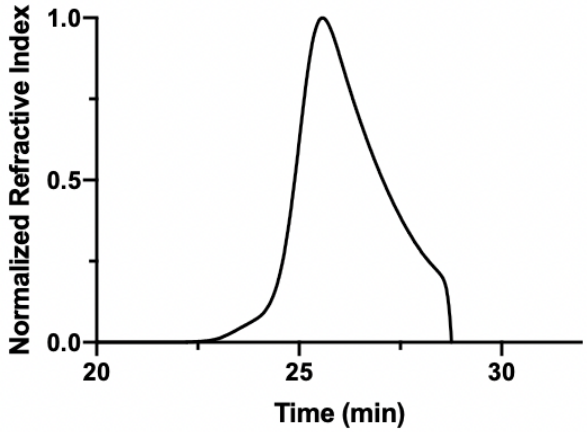


**Figure 2.34** DMF SEC trace of pCL-aryl iodide (**1**).

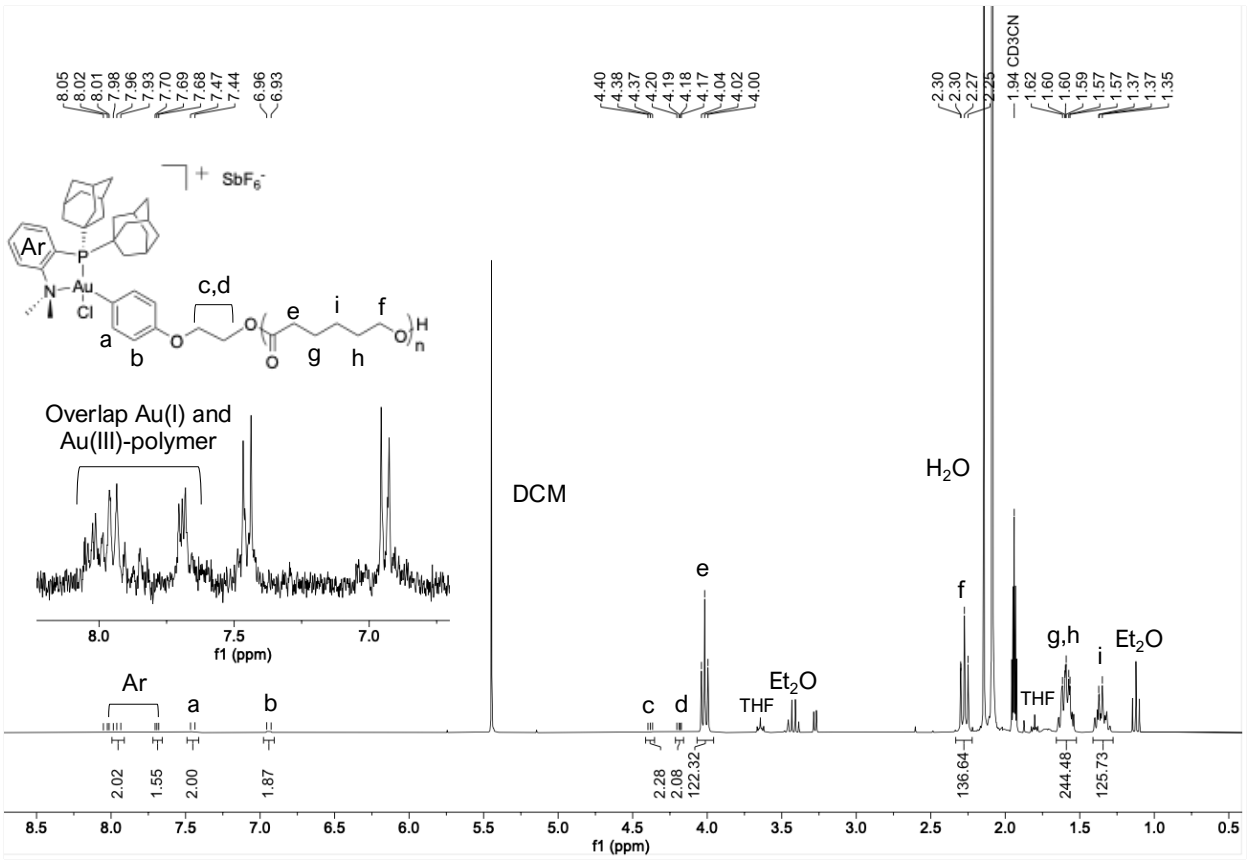


**Figure 2.35** $^{1}$H NMR spectrum of pCL-Au(III) (**1a**) in $CD_3CN$ at 25 ºC.

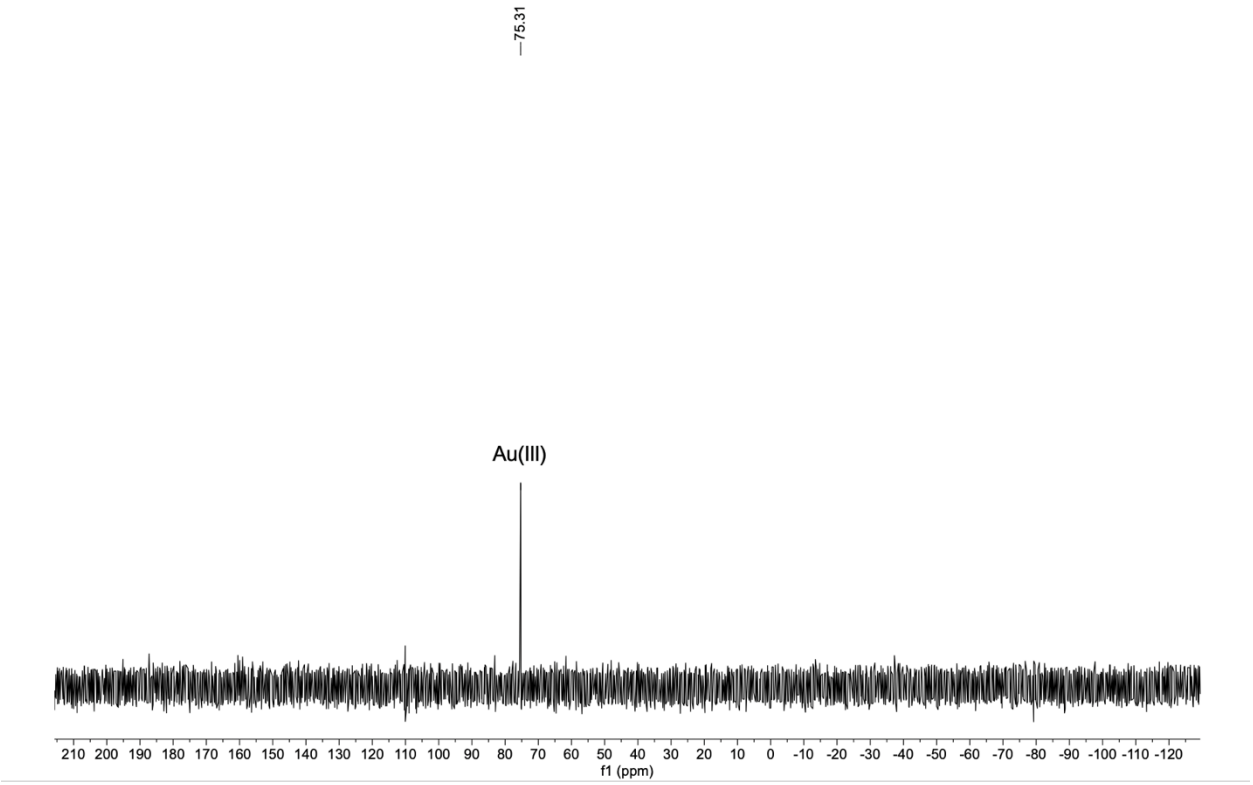


**Figure 2.36** $^{31}P\{^{1}H\}$ NMR spectrum of pCL-Au(III) (**1a**) in $CD_3CN$ at 25 ºC.

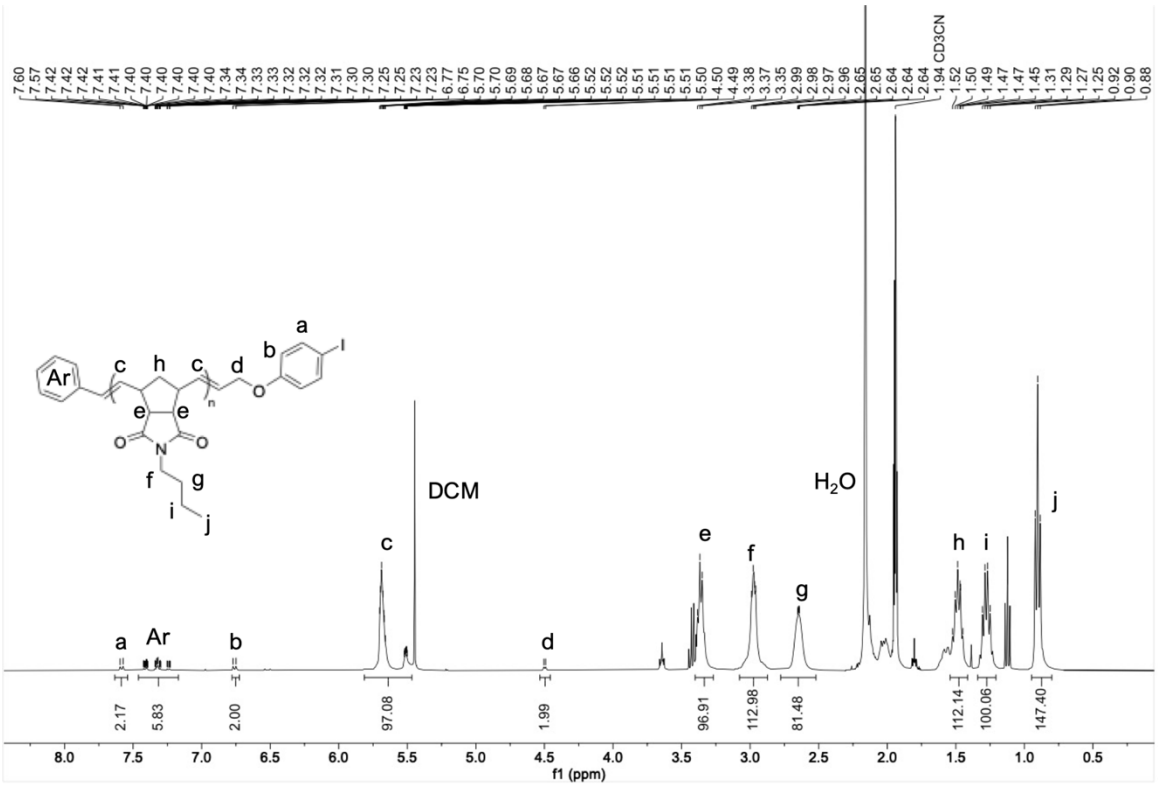


**Figure 2.37** $^{1}$H NMR spectrum of pBNI-aryl iodide (**3**) in $CD_3CN$ at 25 ºC. Peak "c" contains both cis- and trans- alkene protons.

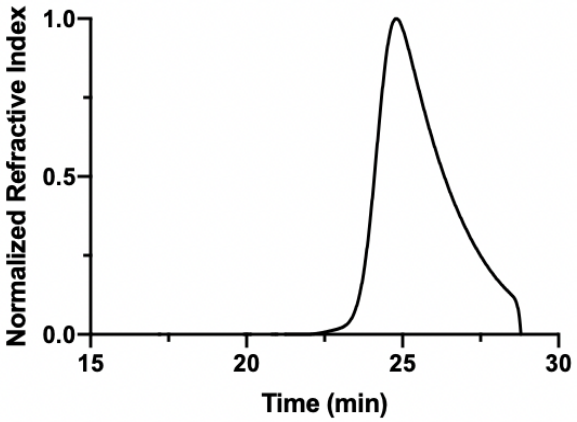


**Figure 2.38** DMF SEC trace of pBNI-aryl iodide (**3**).

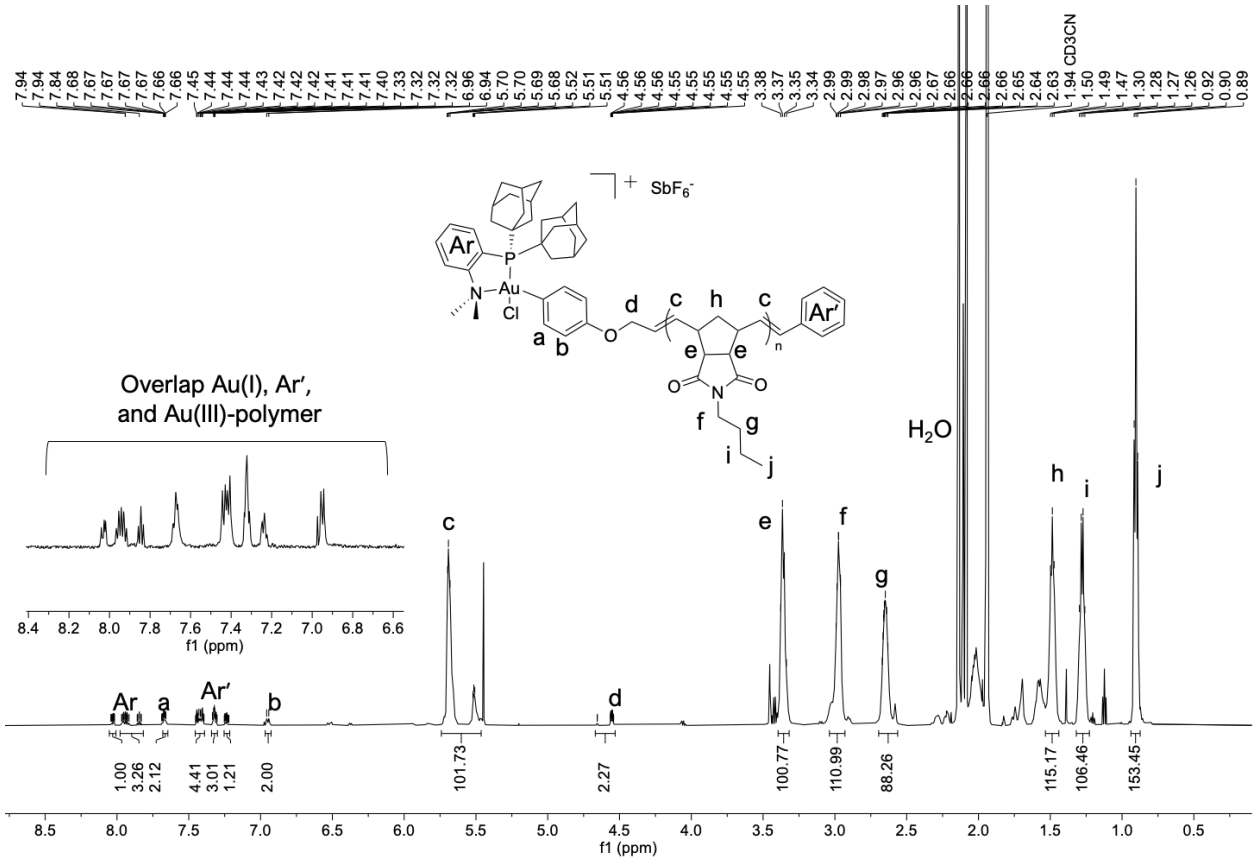


**Figure 2.39** $^{1}$H NMR spectrum of pBNI-Au(III) (**3a**) in $CD_3CN$ at 25 ºC.

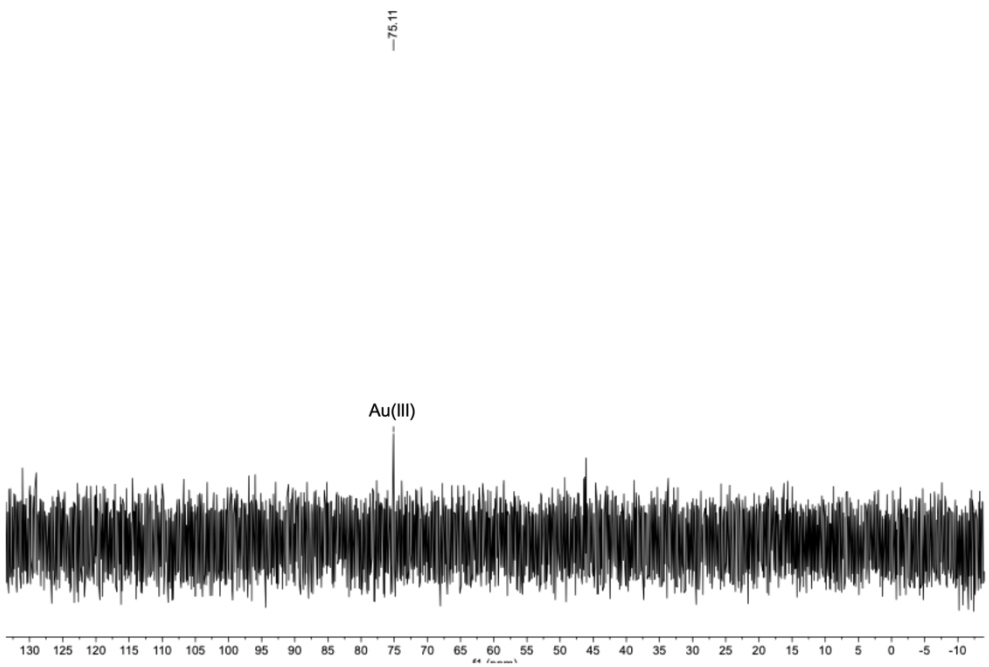


**Figure 2.40** $^{31}P\{^{1}H\}$ NMR spectrum of pBNI-Au(III) (**14a**) in $CD_2Cl_2$ at 25 ºC.

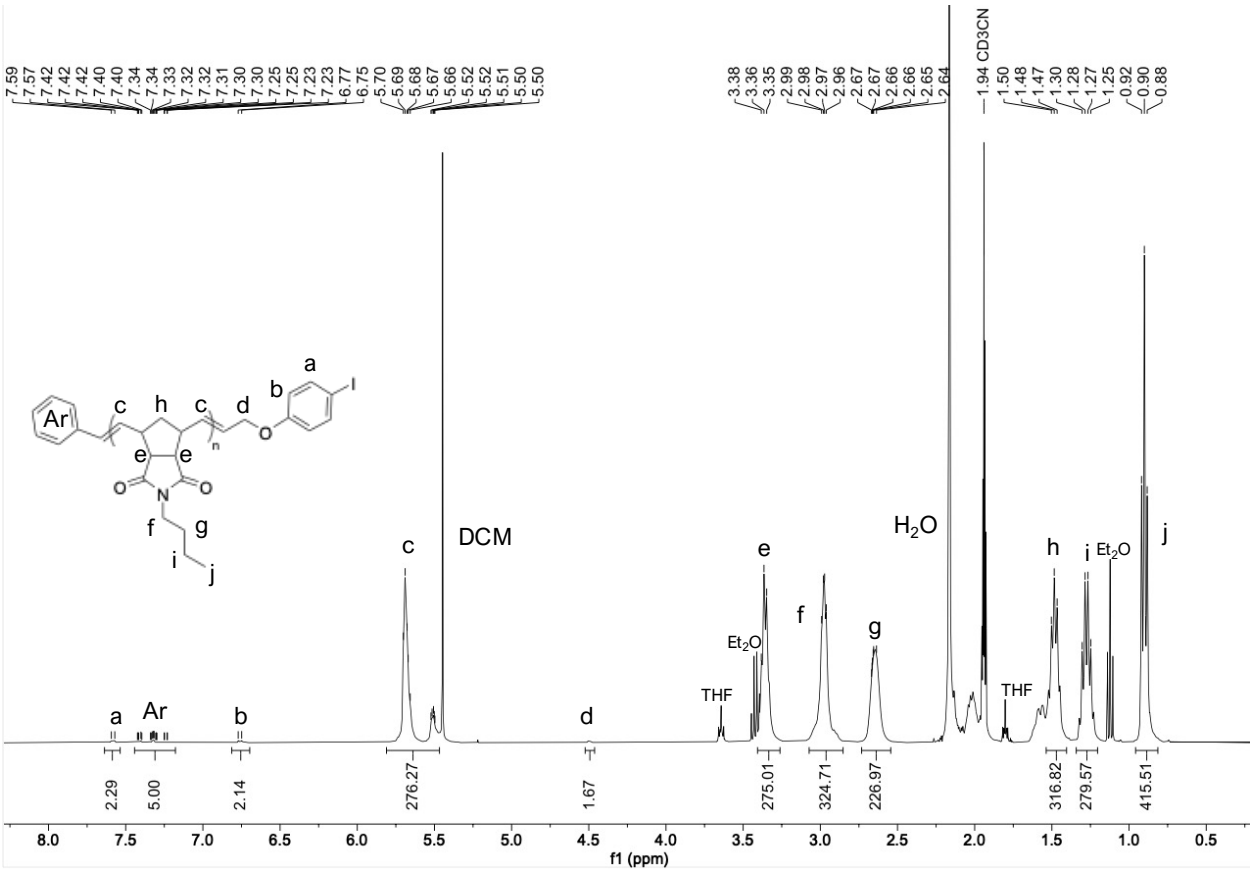


**Figure 2.41** $^1$H NMR spectrum of pBNI-aryl iodide (**16**) in $CD_3CN$ at 25 ºC.

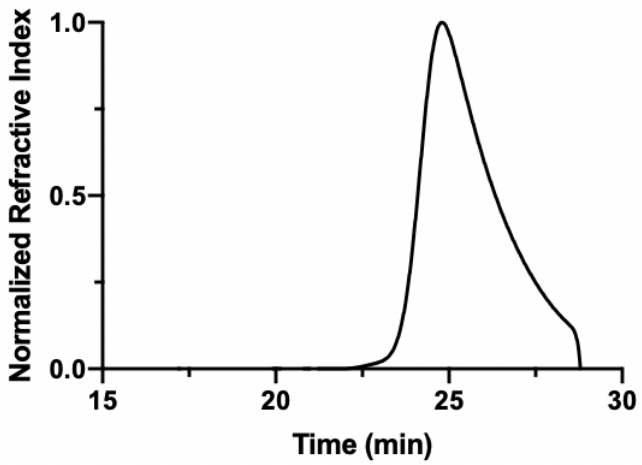


**Figure 2.42** DMF SEC trace of pBNI-aryl iodide (**16**).

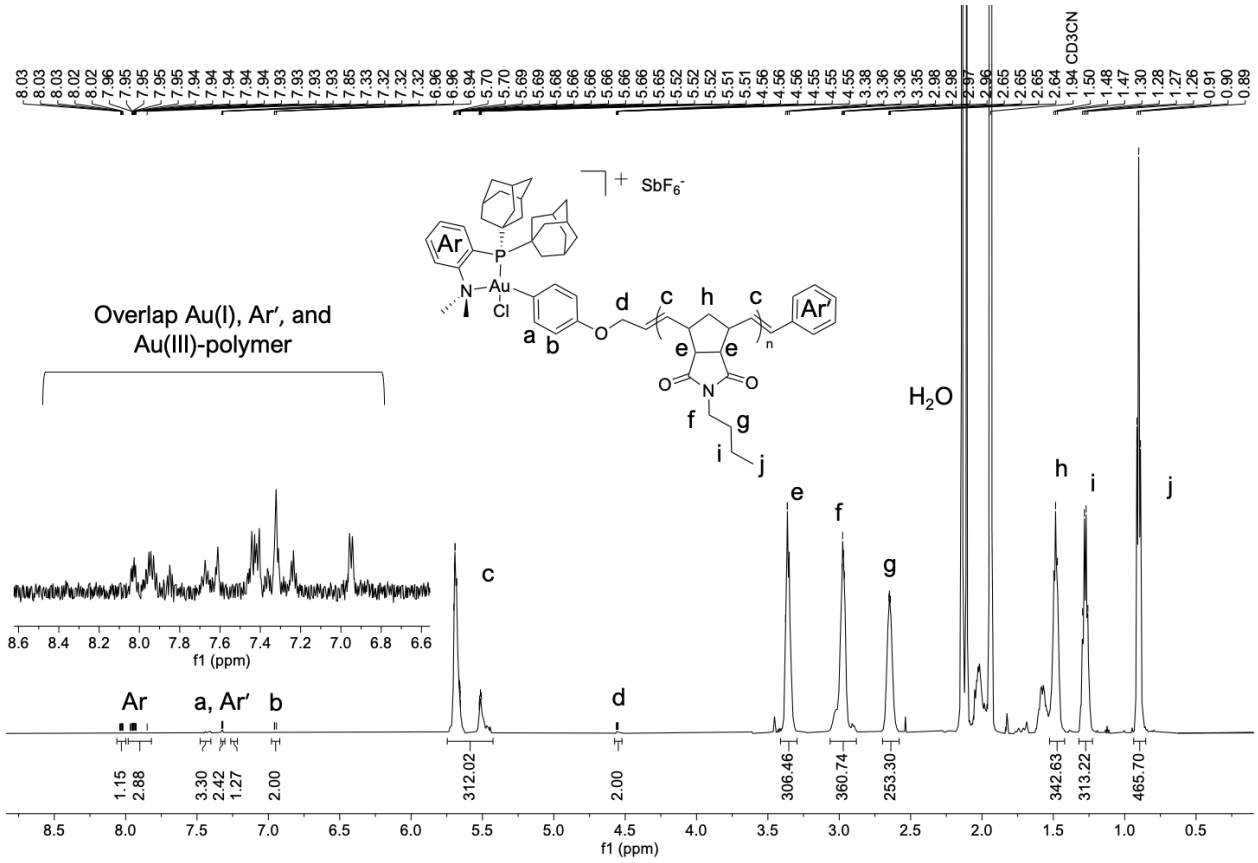


**Figure 2.43** $^{1}$H NMR spectrum of pBNI-Au(III) (**16a**) in $CD_3CN$ at 25 ºC.

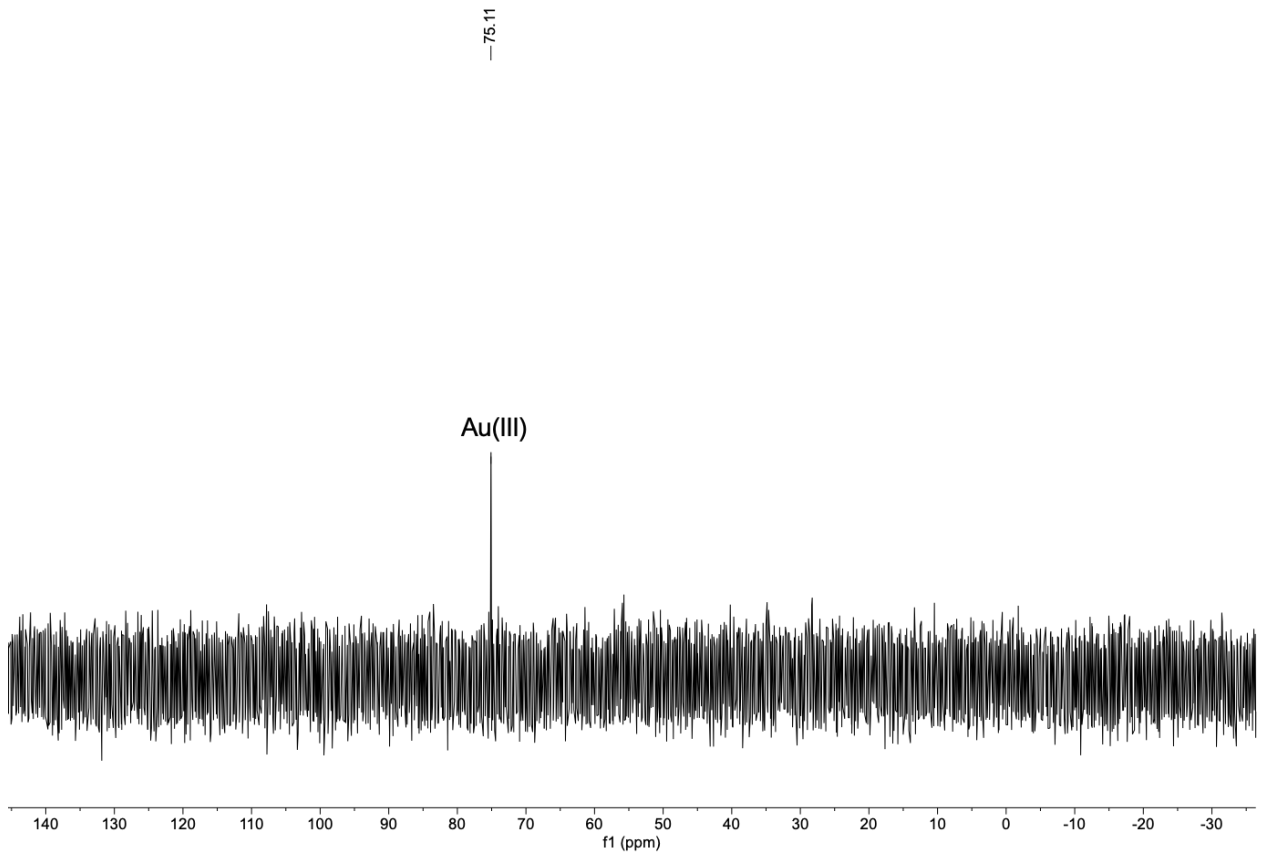


**Figure 2.44** $^{31}P\{^{1}H\}$ NMR spectrum of pBNI-Au(III) (**16a**) in $CD_2Cl_2$ at 25 ºC.

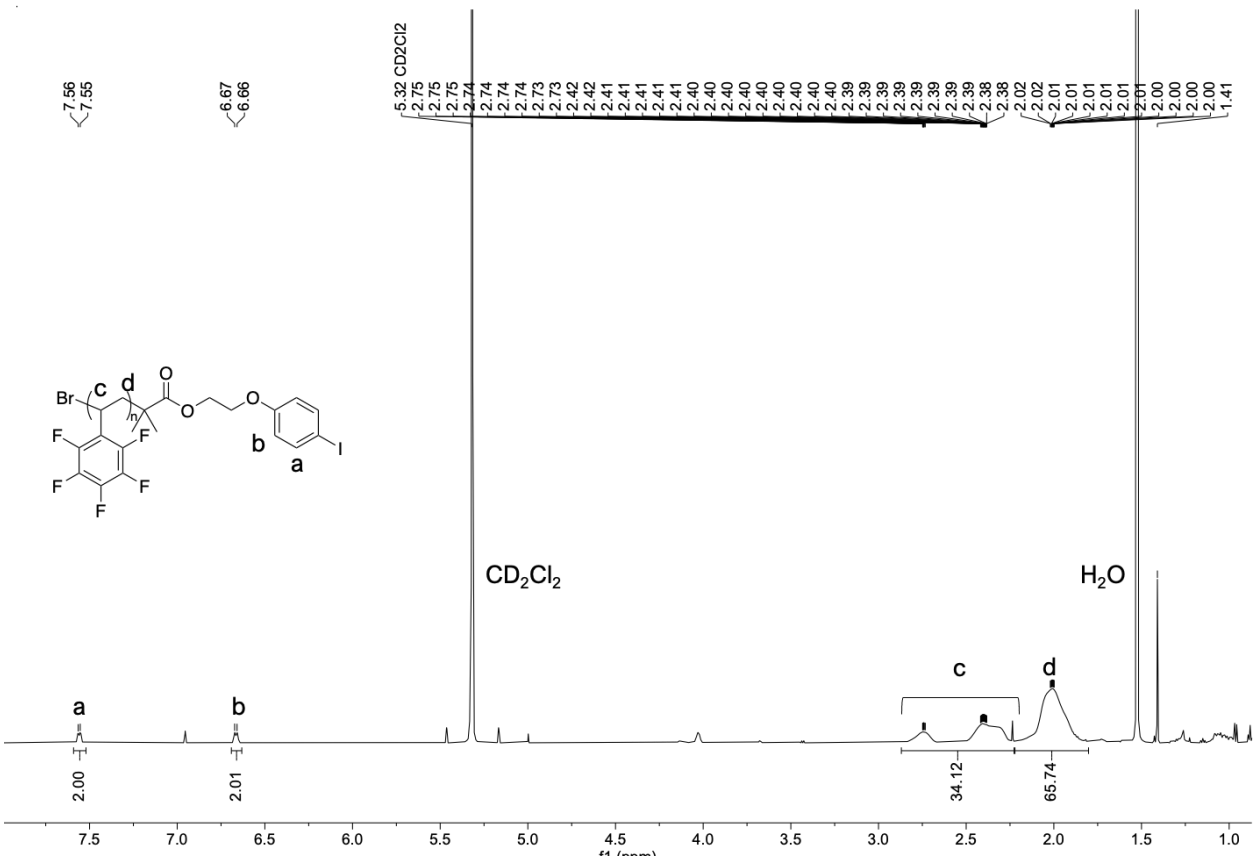


**Figure 2.45** $^{1}$H NMR spectrum of pPFS-aryl iodide (**6**) in $CD_2Cl_2$ at 25 ºC.

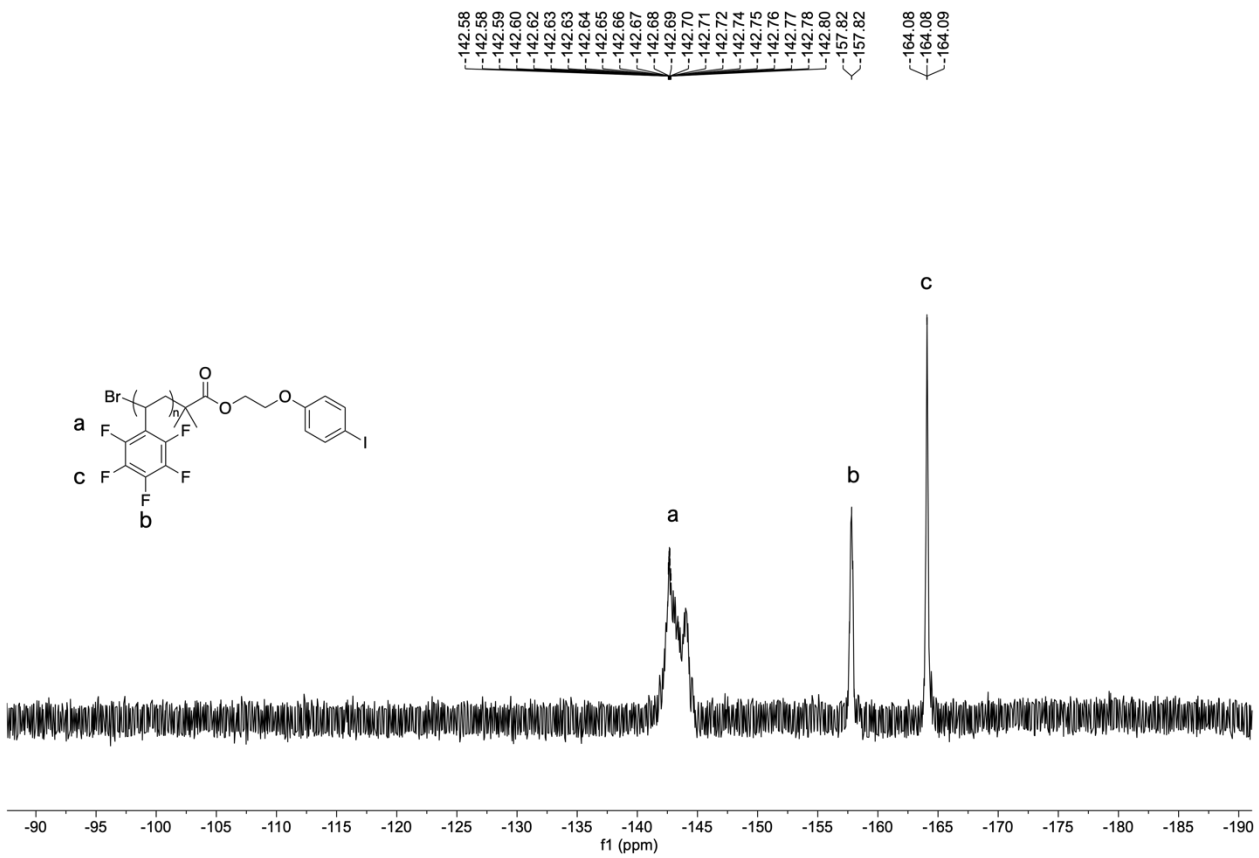


**Figure 2.46** $^{19}F\{^{1}H\}$ NMR spectrum of pPFS-aryl iodide (**6**) in acetone-$d_6$ at 25 ºC.

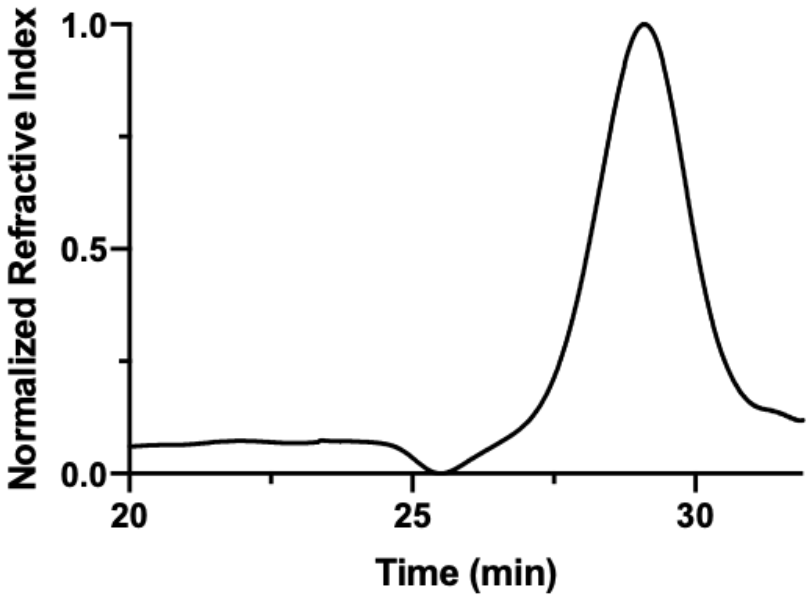


**Figure 2.47** THF SEC trace of pPFS-aryl iodide (**6**).

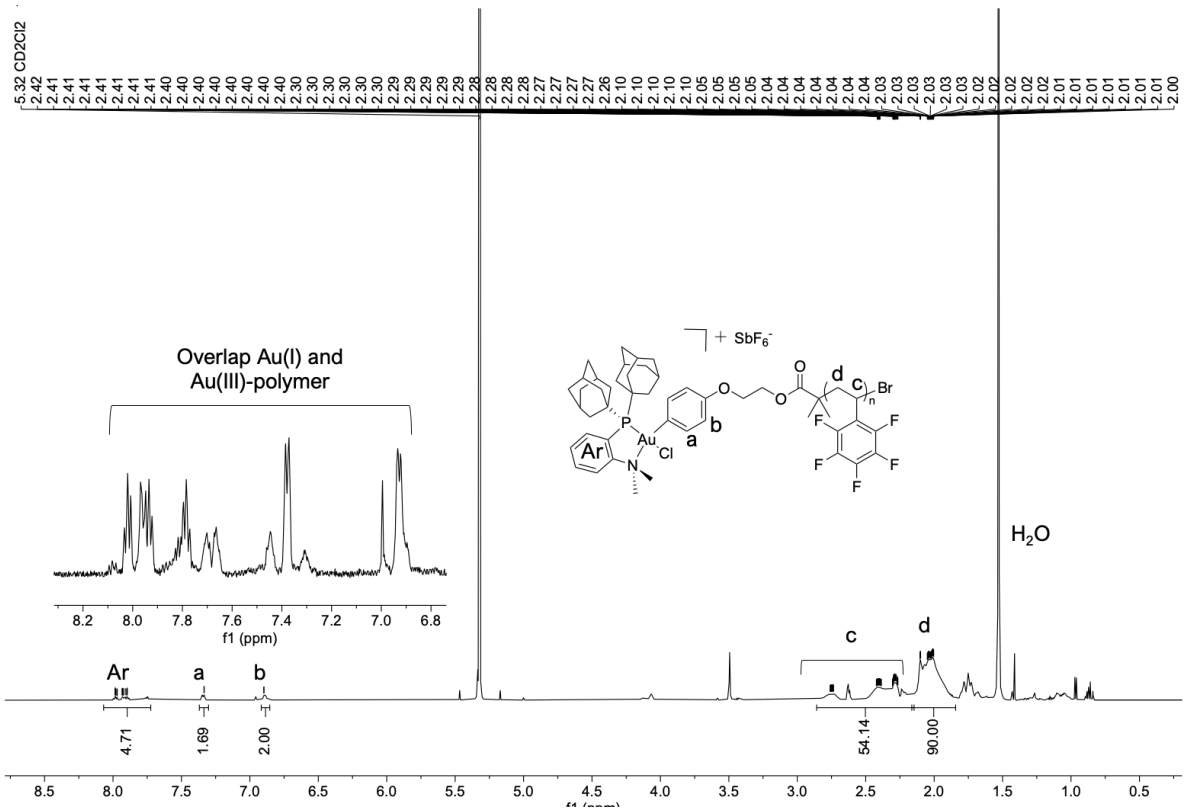


**Figure 2.48** $^1$H NMR spectrum of pPFS-Au(III) (**6a**) in $CD_2Cl_2$ at 25 ºC.

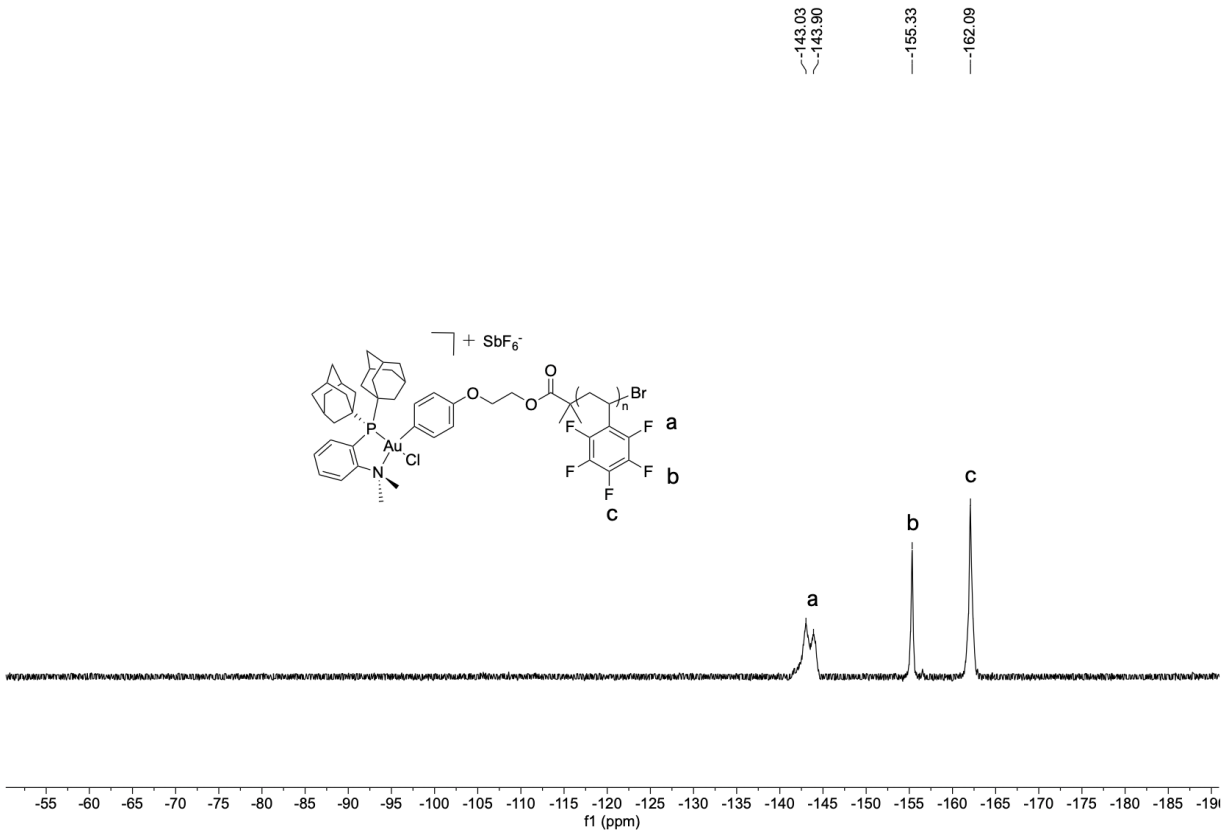


**Figure 2.49** $^{19}F\{^{1}H\}$ NMR spectrum of pPFS-Au(III) (**6a**) in $CD_2Cl_2$ at 25 ºC.

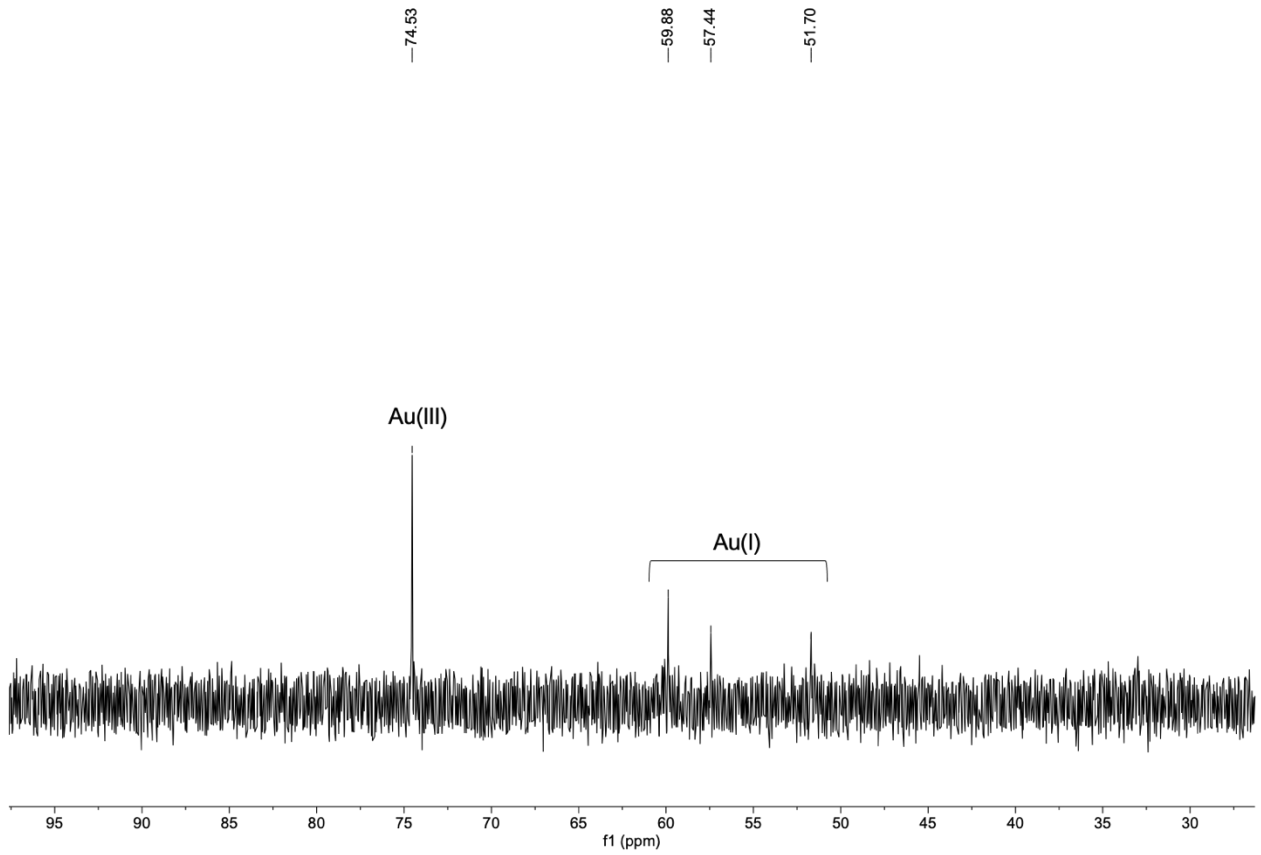


**Figure 2.50** $^{31}P\{^{1}H\}$ NMR spectrum of pPFS-Au(III) (**6a**) in $CD_2Cl_2$ at 25 ºC.

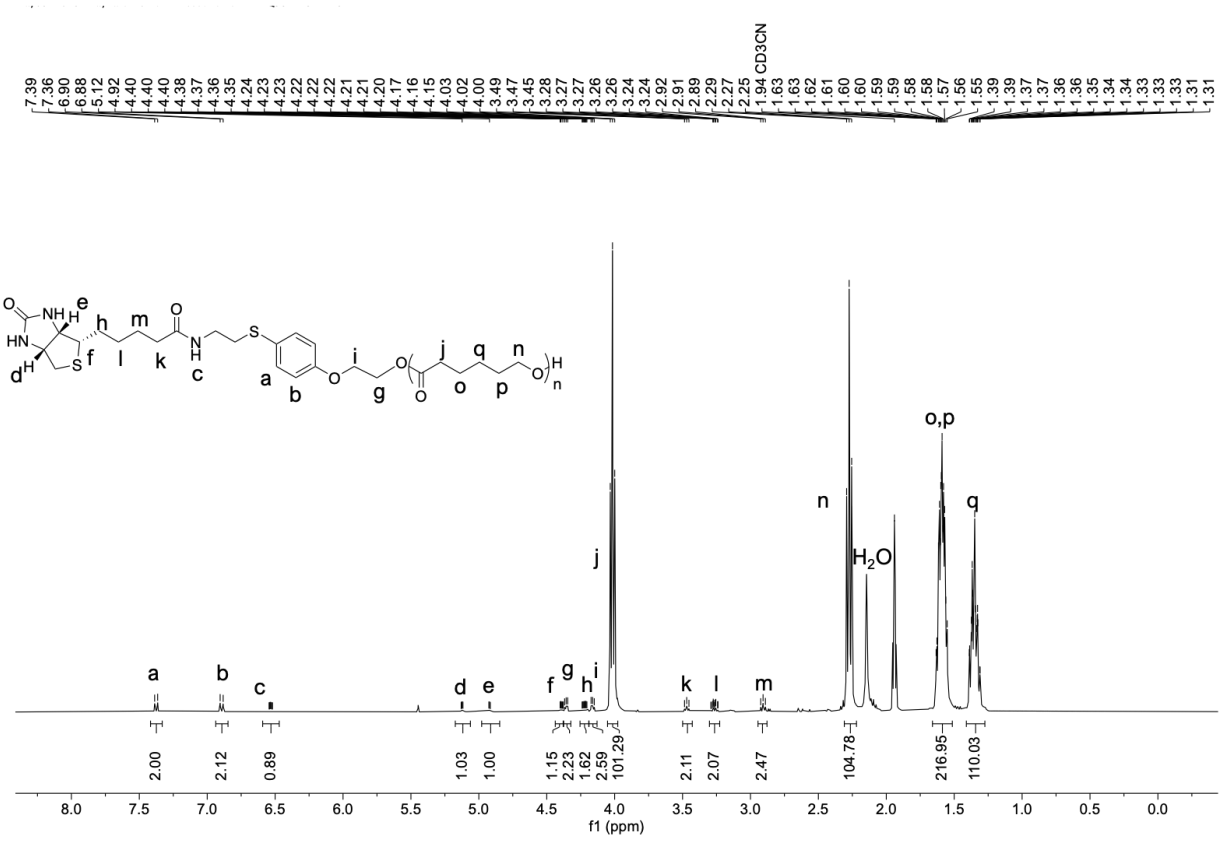


**Figure 2.51** $^{1}$H NMR spectrum of biotin-p(CL) (**1a-8a**) in $CD_3CN$ at 25 ºC.

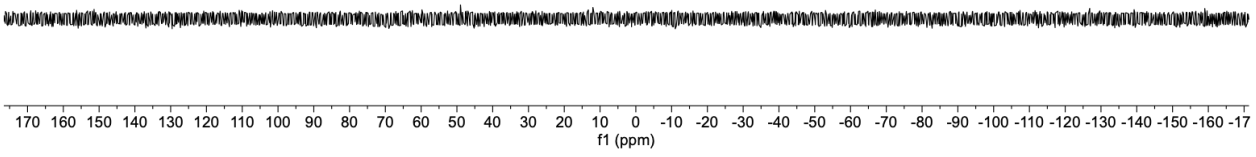


**Figure 2.52*** $^{31}P\{^{1}H\}$ NMR spectrum of biotin-p(CL) (**1a-8a**) in $CD_3CN$ at 25 ºC.

*No $^{31}$P NMR peak is expected, indicating Au(III) is eliminated.

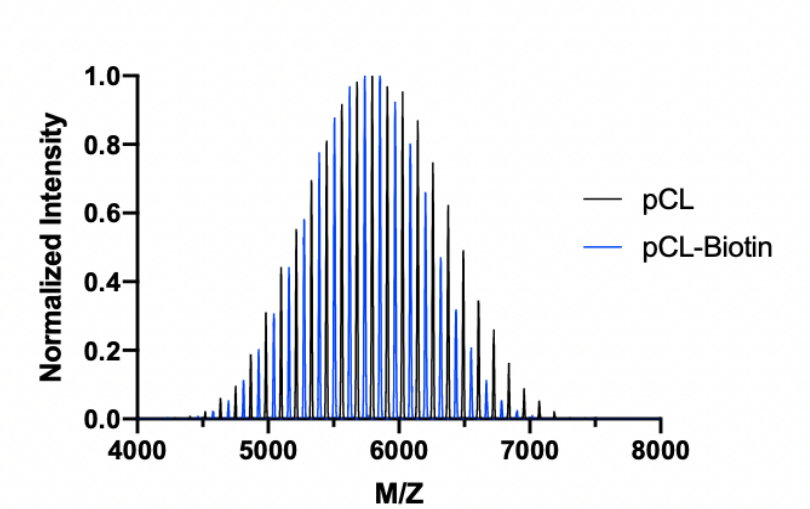


**Figure 2.53** MALDI of biotin-p(CL) (**1a-8a**). This figure is shown in chapter 2 but shown larger here for easier viewing.

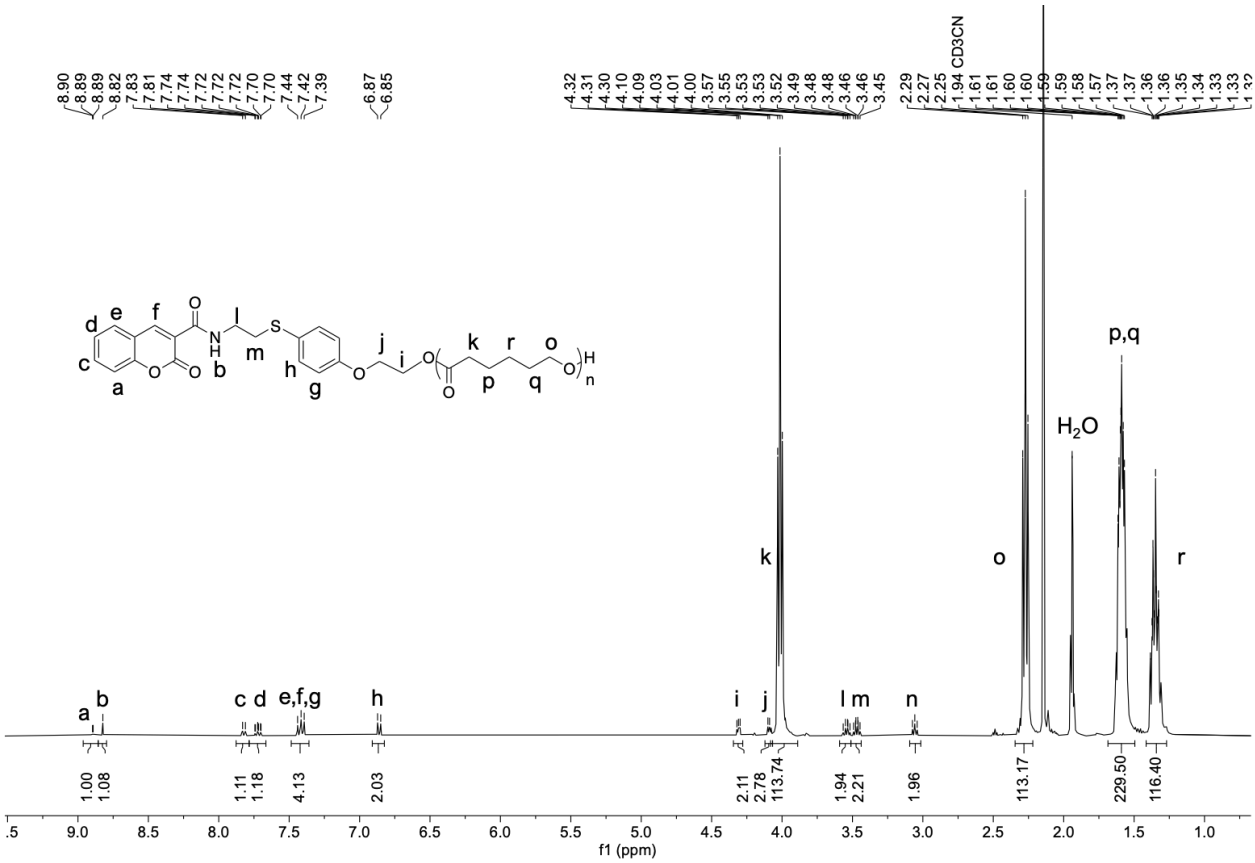


**Figure 2.54** $^{1}H$ NMR spectrum of coumarin-pCL (**1a-9a**) in $CD_3CN$ at 25 ºC.

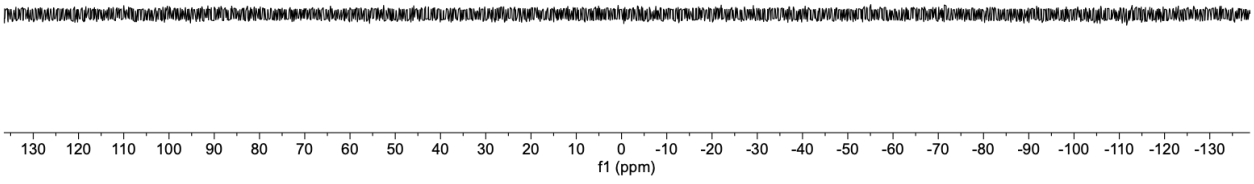


**Figure 2.55** $^{31}P\{^{1}H\}$ NMR spectrum of coumarin-p(CL) (**1a-9a**) in $CD_3CN$ at 25 ºC.

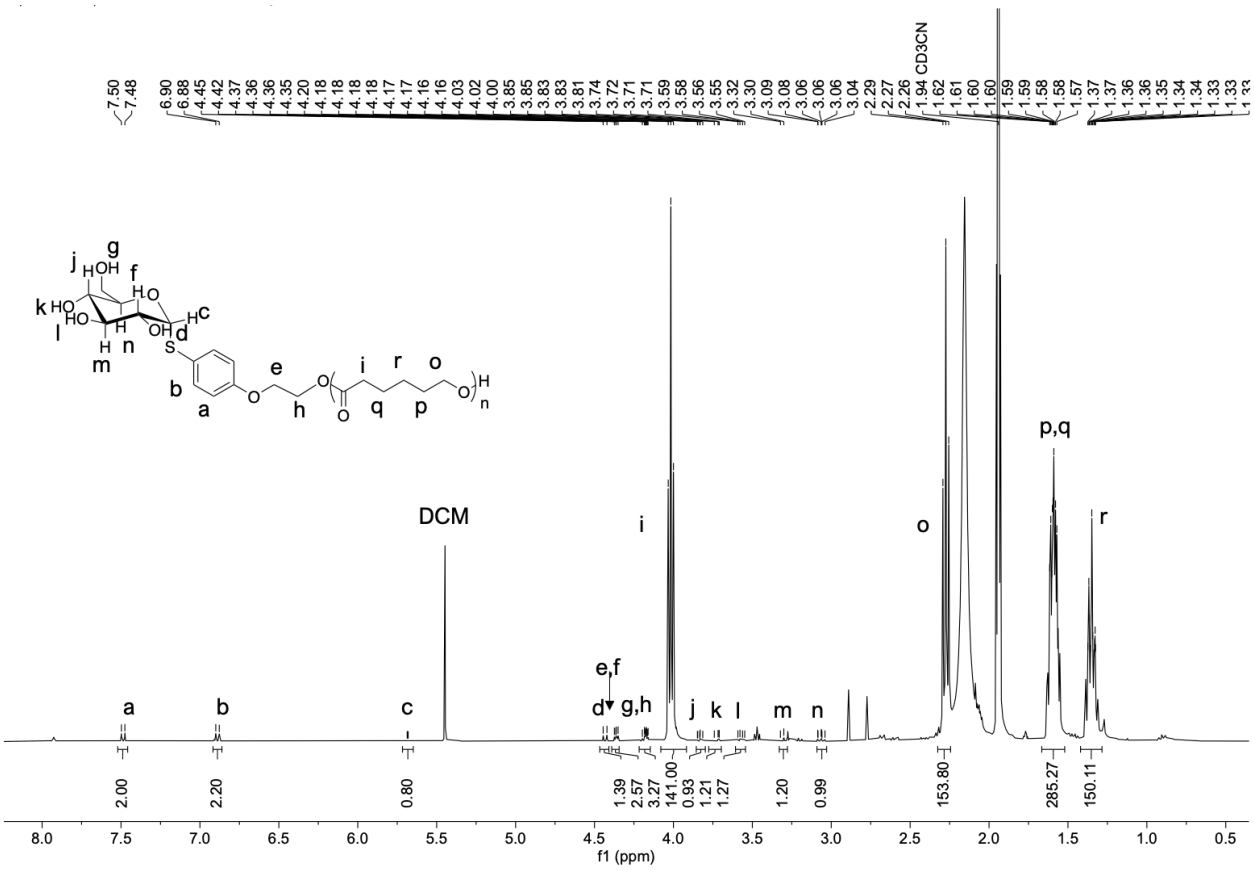


**Figure 2.56** $^{1}$H NMR spectrum of glucose-p(CL) (**1a-TG**) in $CD_3CN$ at 25 ºC.

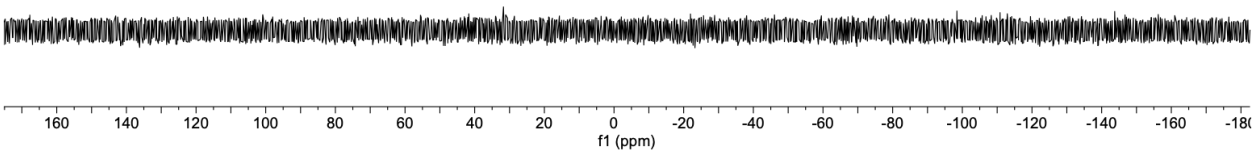


**Figure 2.57** $^{31}P\{^{1}H\}$ NMR spectrum of glucose-p(CL) (**1a-TG**) in $CD_3CN$ at 25 ºC.

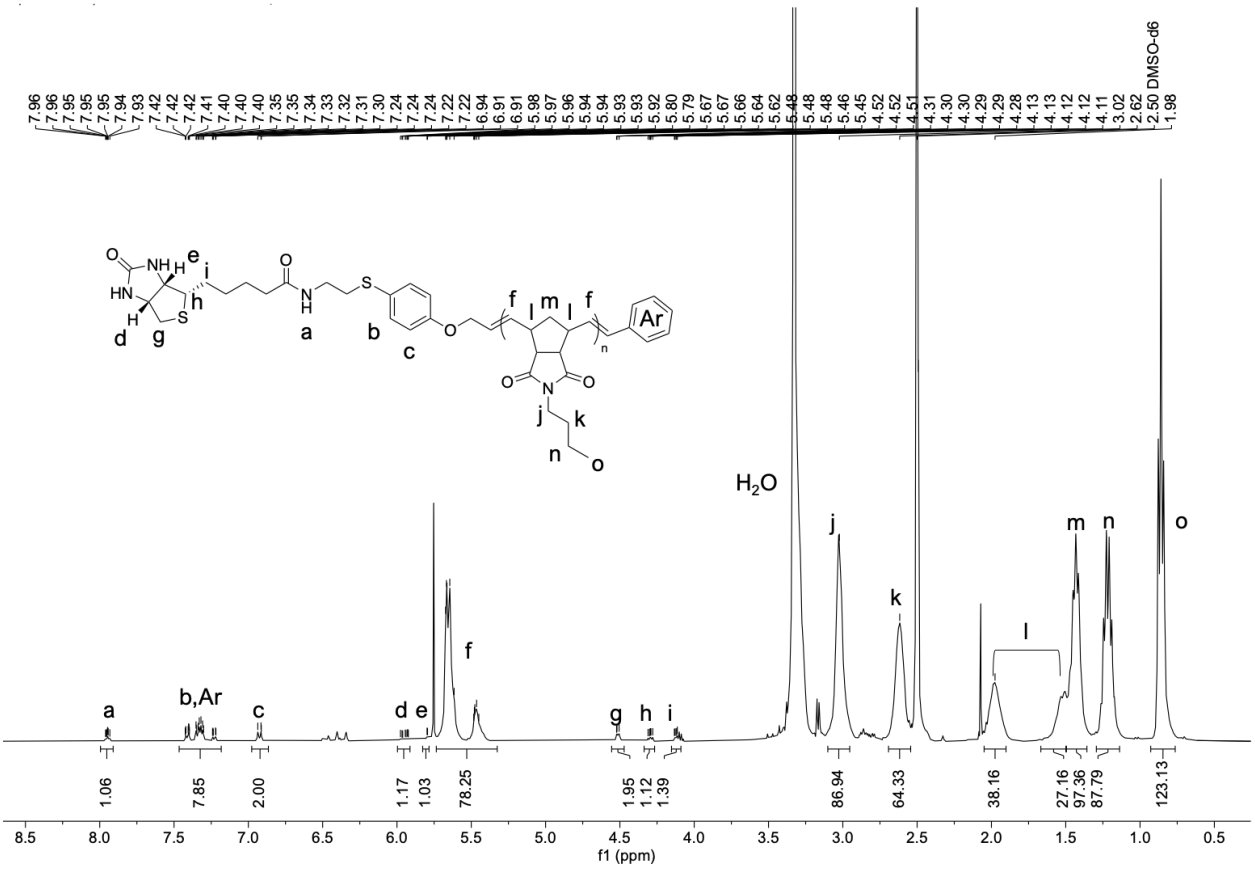


**Figure 2.58** $^{1}H$ NMR spectrum of biotin-p(BNI) (**3a-8a**) in DMSO-$d_6$ at 25 ºC.

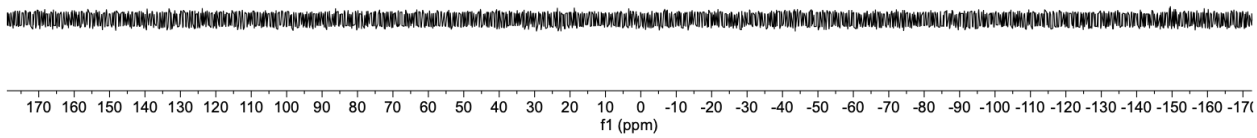


**Figure 2.59** $^{31}P\{^{1}H\}$ NMR spectrum of biotin-p(BNI) (**3a-8a**) in DMSO-$d_6$ at 25 ºC.

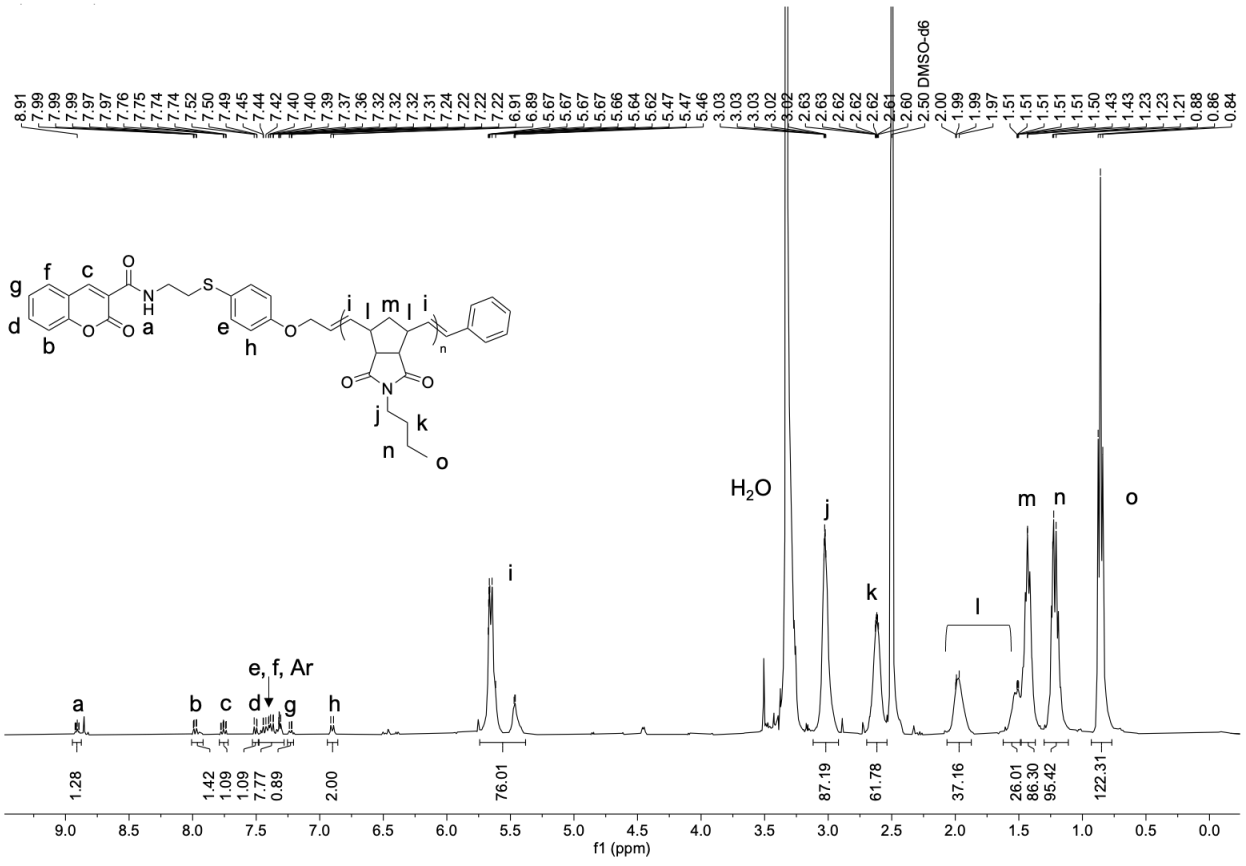


**Figure 2.60** $^{1}H$ NMR spectrum of coumarin-p(BNI) (**3a-9a**) in DMSO-$d_6$ at 25 ºC.

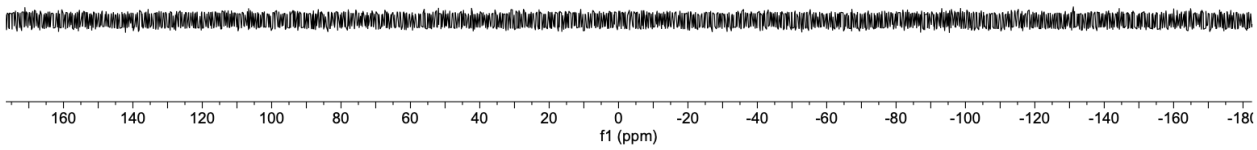


**Figure 2.61** $^{31}P\{^{1}H\}$ NMR spectrum of coumarin-p(BNI) (**3a-9a**) in DMSO-$d_6$ at 25 ºC.

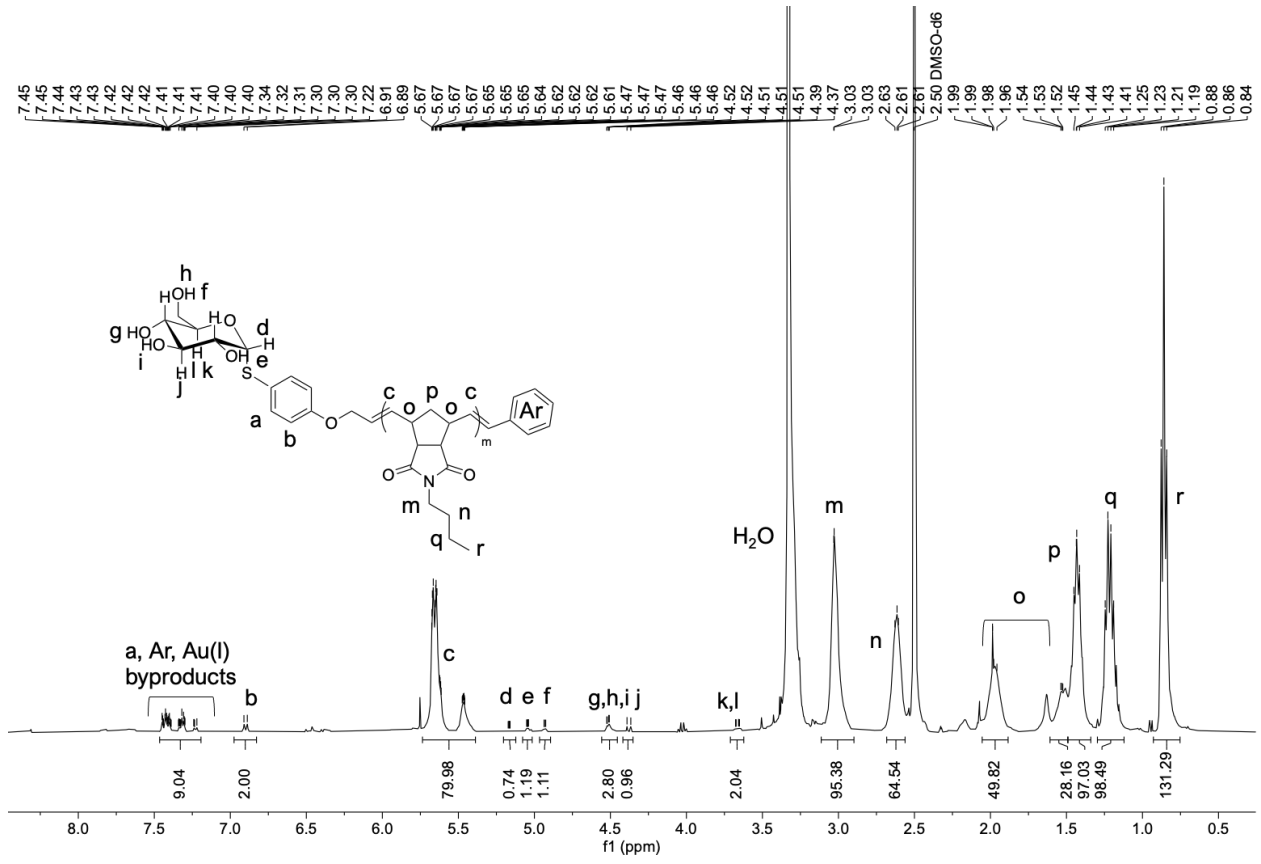


**Figure 2.62** $^{1}H$ NMR spectrum of glucose-p(BNI) (**3a-TG**) in DMSO-$d_6$ at 25 ºC.

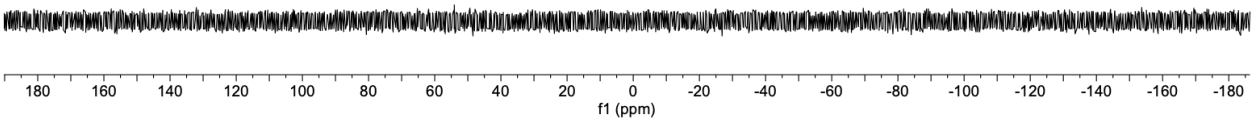


**Figure 2.63** $^{31}P\{^{1}H\}$ NMR spectrum of glucose-p(BNI) (**3a-TG**) in DMSO-$d_6$ at 25 ºC.

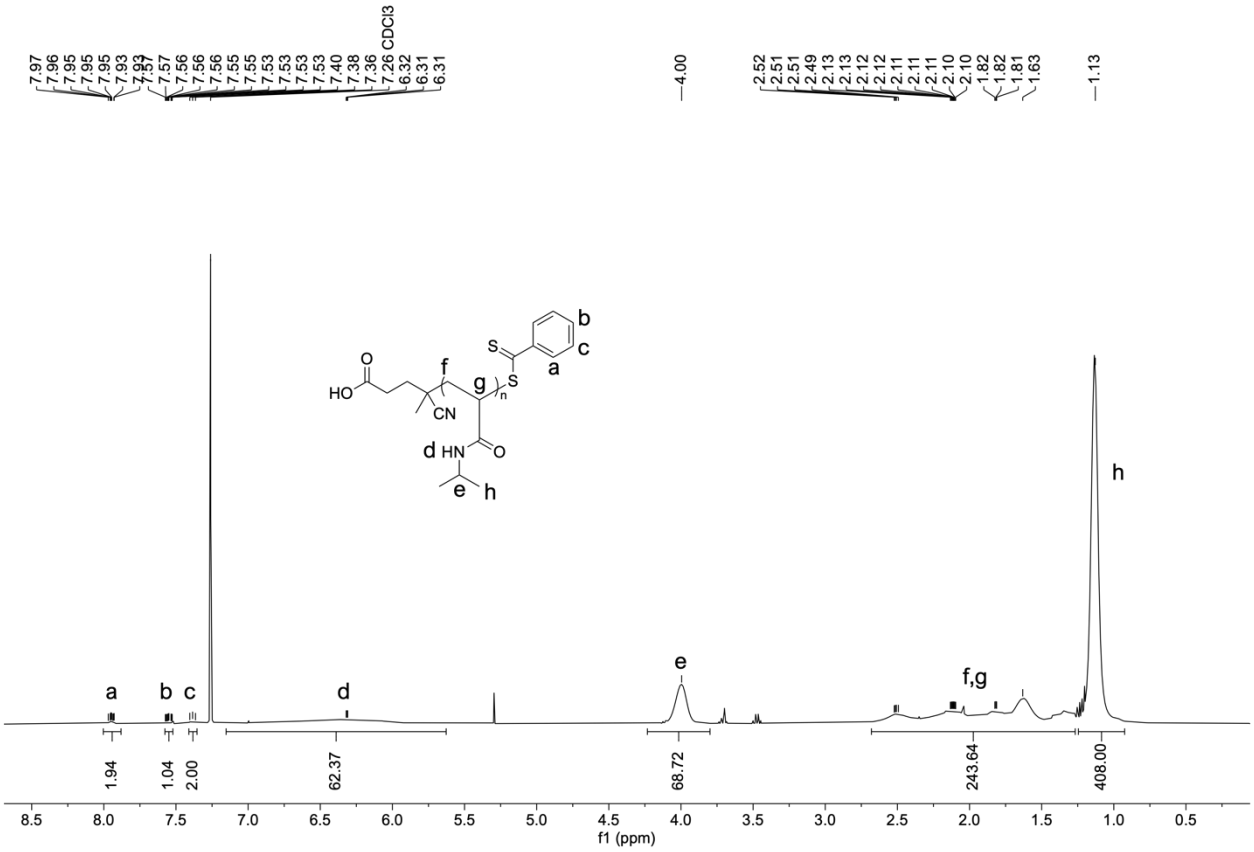


**Figure 2.64** $^{1}H$ NMR spectrum of pNIPAM (**10**) in $CDCl_3$ at 25 ºC.

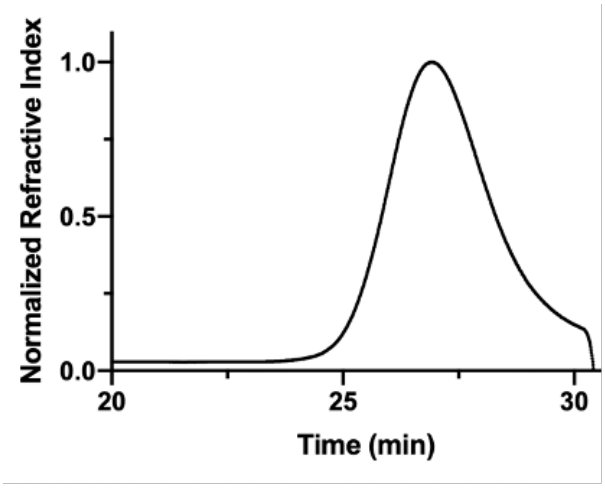


**Figure 2.65** DMF SEC trace of pNIPAM (**10**).

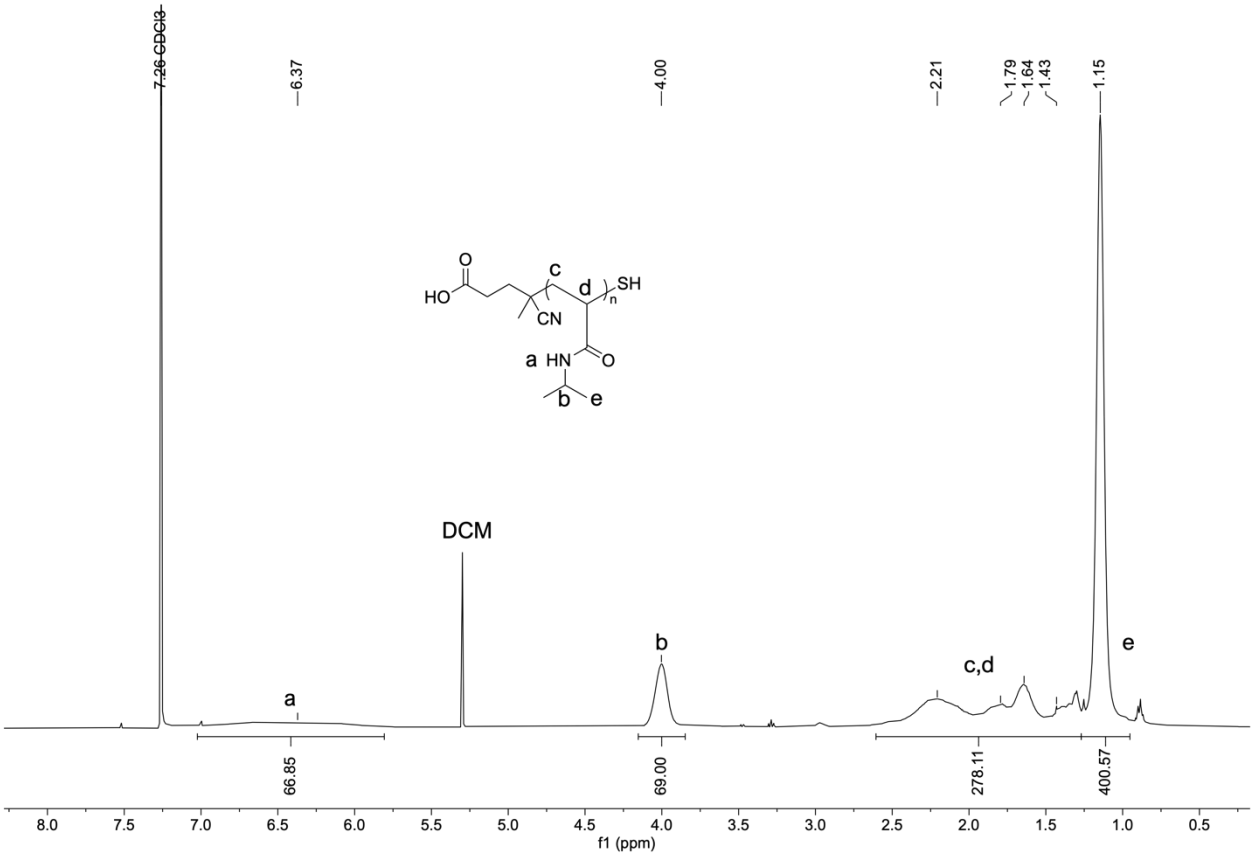


**Figure 2.66** $^{1}$H NMR spectrum of pNIPAM-SH (**10a**) in $CDCl_3$ at 25 ºC.

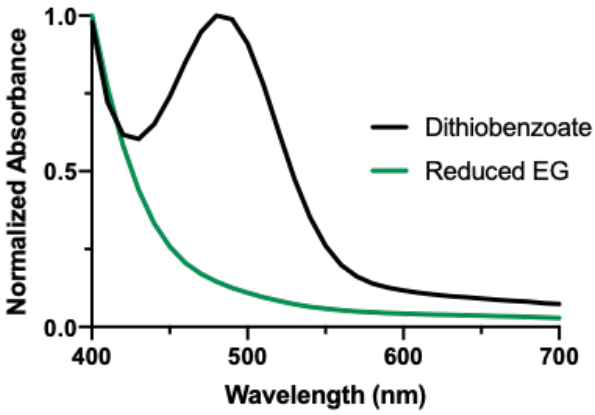


**Figure 2.67** UV-vis spectroscopy of dithiobenzoate-containing p(NIPAM) (**10**) (black) and the resulting reduced thiol end-group pNIPAM-SH (**10a**) (green).

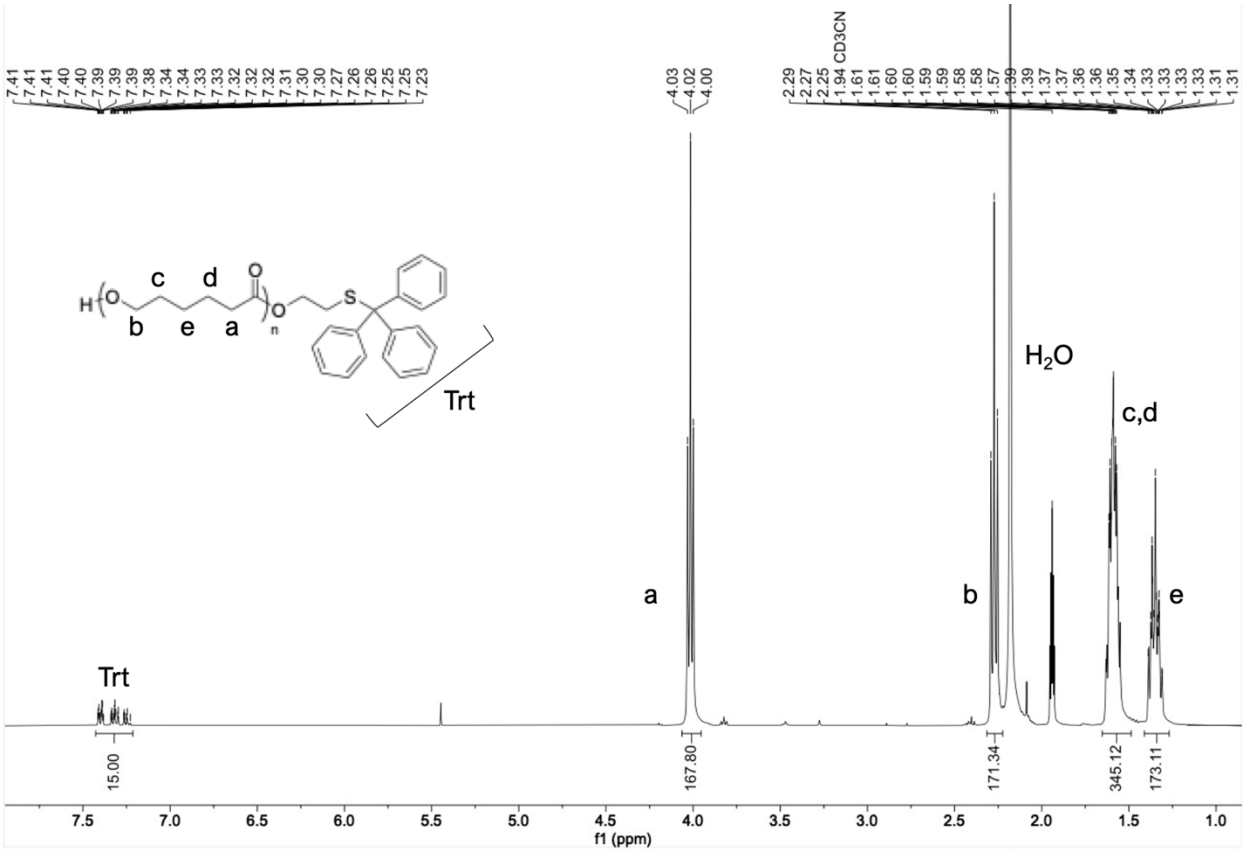


**Figure 2.68** $^{1}$H NMR spectrum of pCL-Trt (**12**) in $CD_3CN$ at 25 ºC.

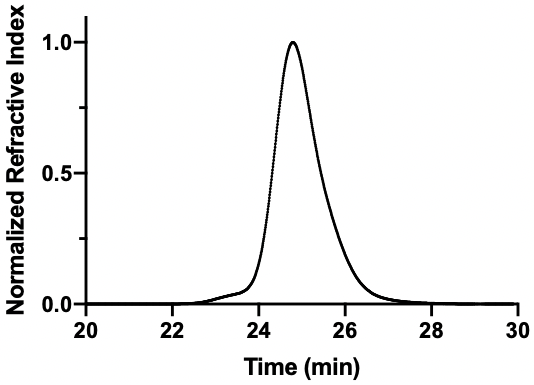


**Figure 2.69** DMF SEC trace of pCL-Trt (**12**).

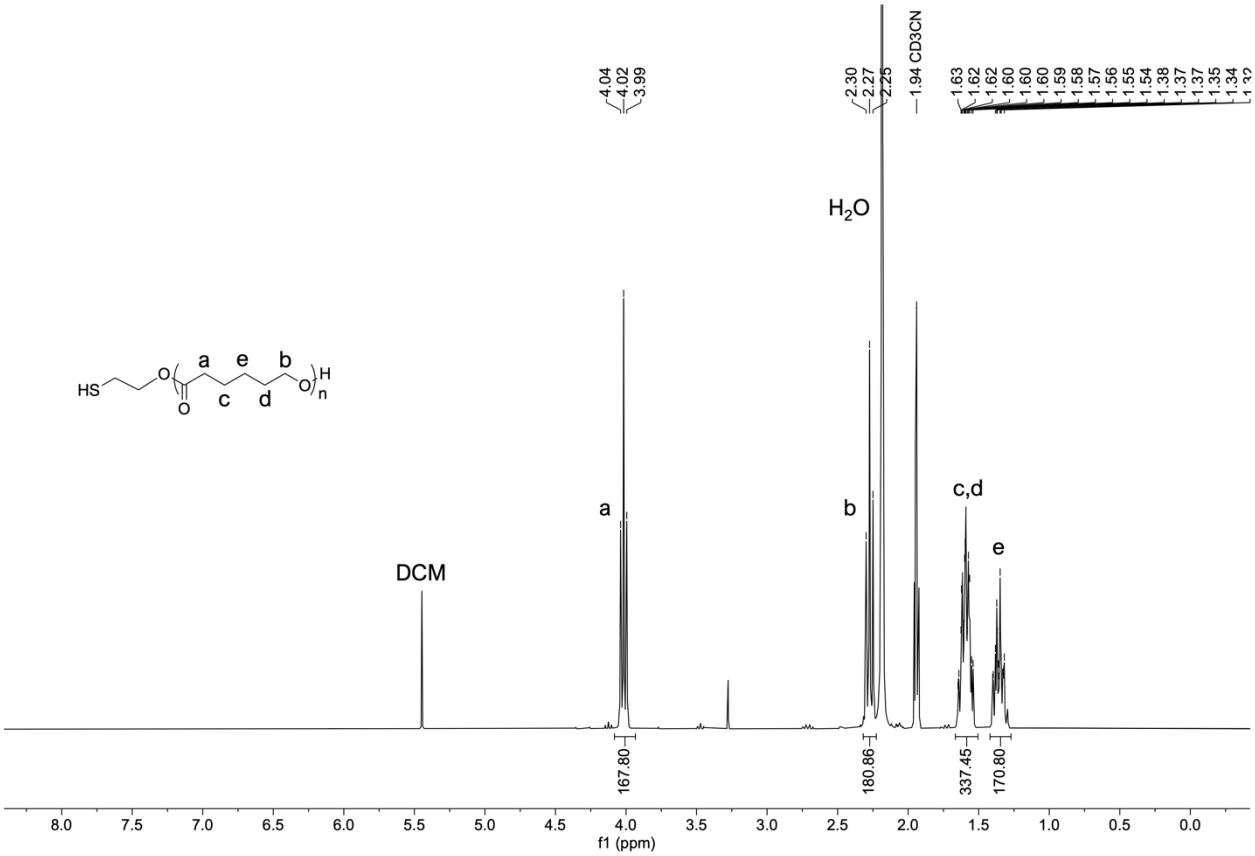


**Figure 2.70** $^{1}$H NMR spectrum of pCL-SH (**12a**) in $CD_3CN$ at 25 ºC.

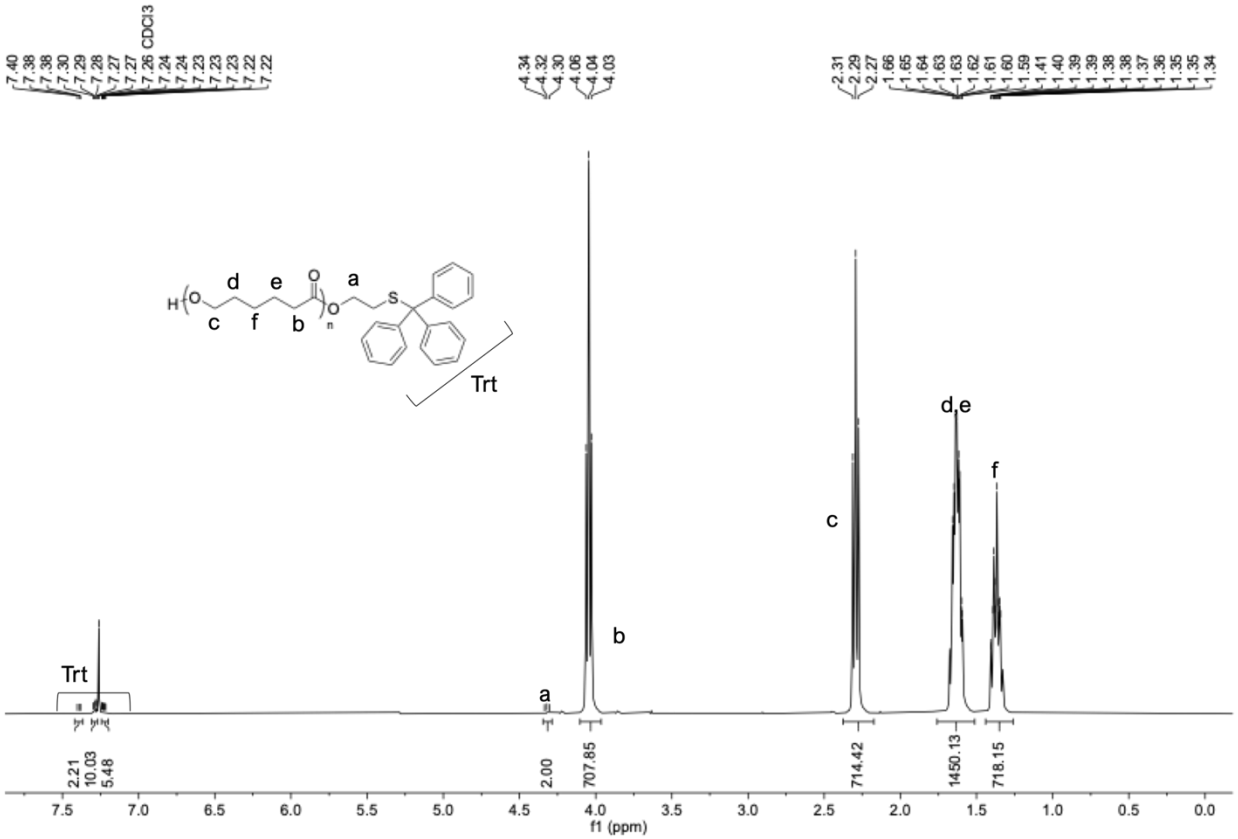


**Figure 2.71** $^{1}$H NMR spectrum of p(CL)-Trt (**17**) in $CDCl_3$ at 25 ºC.

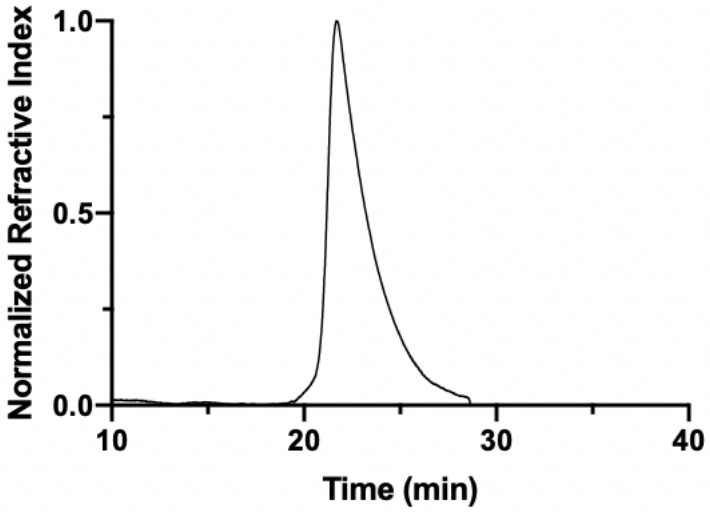


**Figure 2.72** DMF SEC trace of p(CL)-Trt (**17**).

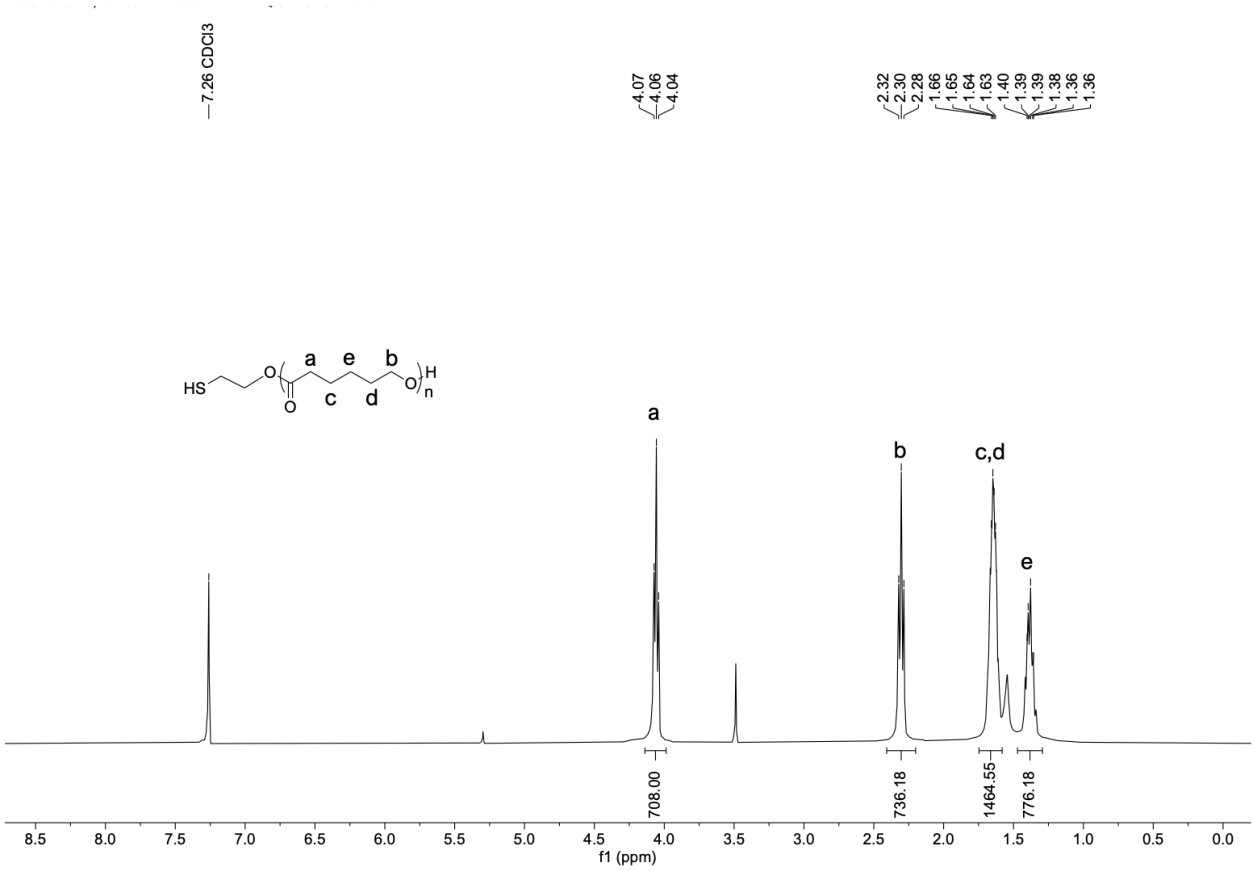


**Figure 2.73** $^{1}$H NMR spectrum of p(CL)-SH (**17a**) in $CDCl_3$ at 25 ºC.

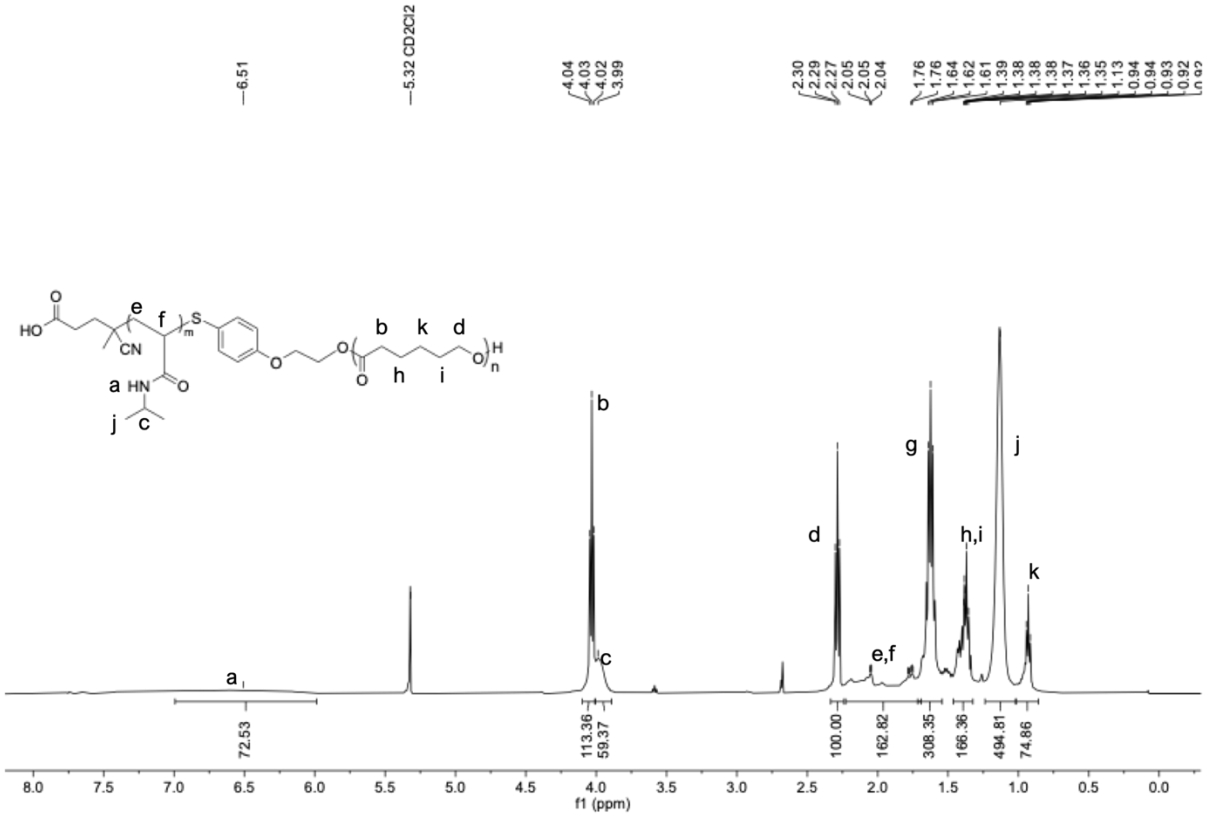


**Figure 2.74** $^{1}H$ NMR spectrum of p(NIPAM)-*b*-p(CL) (**13**) in $CD_2Cl_2$ at 25 ºC.

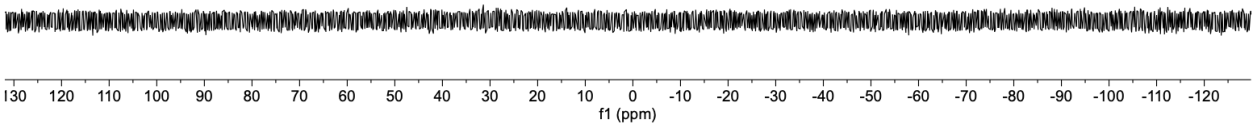


**Figure 2.75** $^{31}P\{^{1}H\}$ NMR spectrum of p(NIPAM)-*b*-p(CL) (**13**) in $CD_2Cl_2$ at 25 ºC.

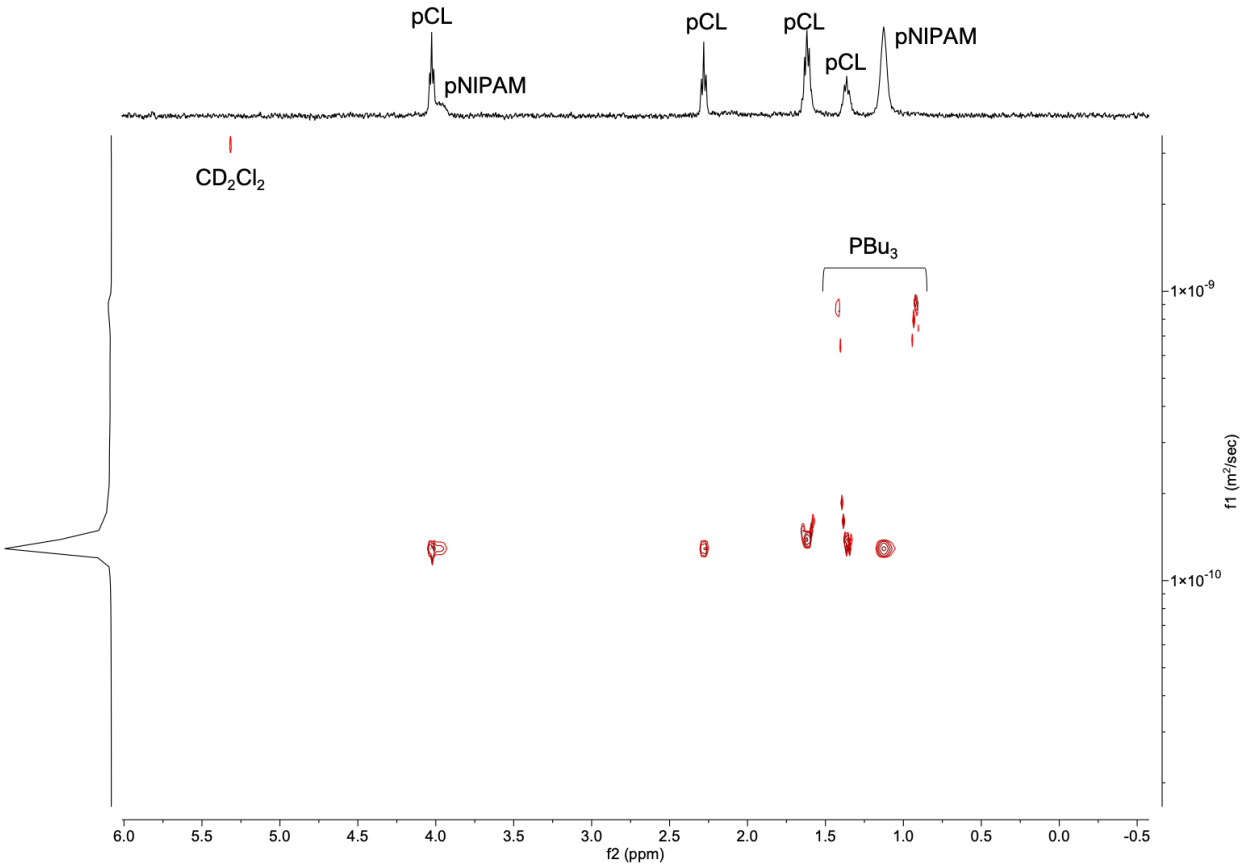


**Figure 2.76** DOSY spectrum of p(NIPAM)-*b*-p(CL) (**13**) in $CD_2Cl_2$ at 25 ºC.

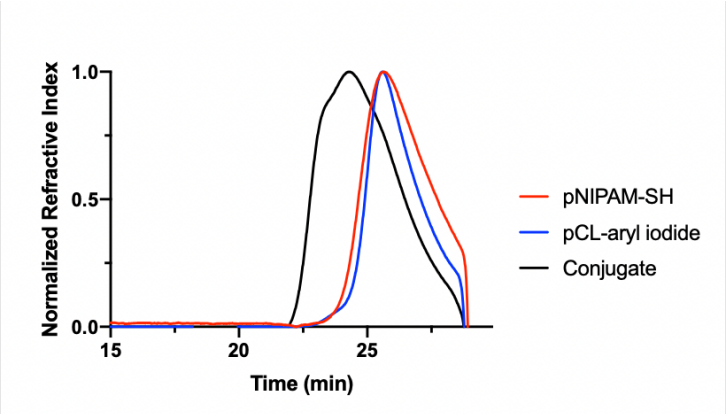


**Figure 2.77** DMF SEC trace of p(NIPAM)-*b*-p(CL) (**13**).

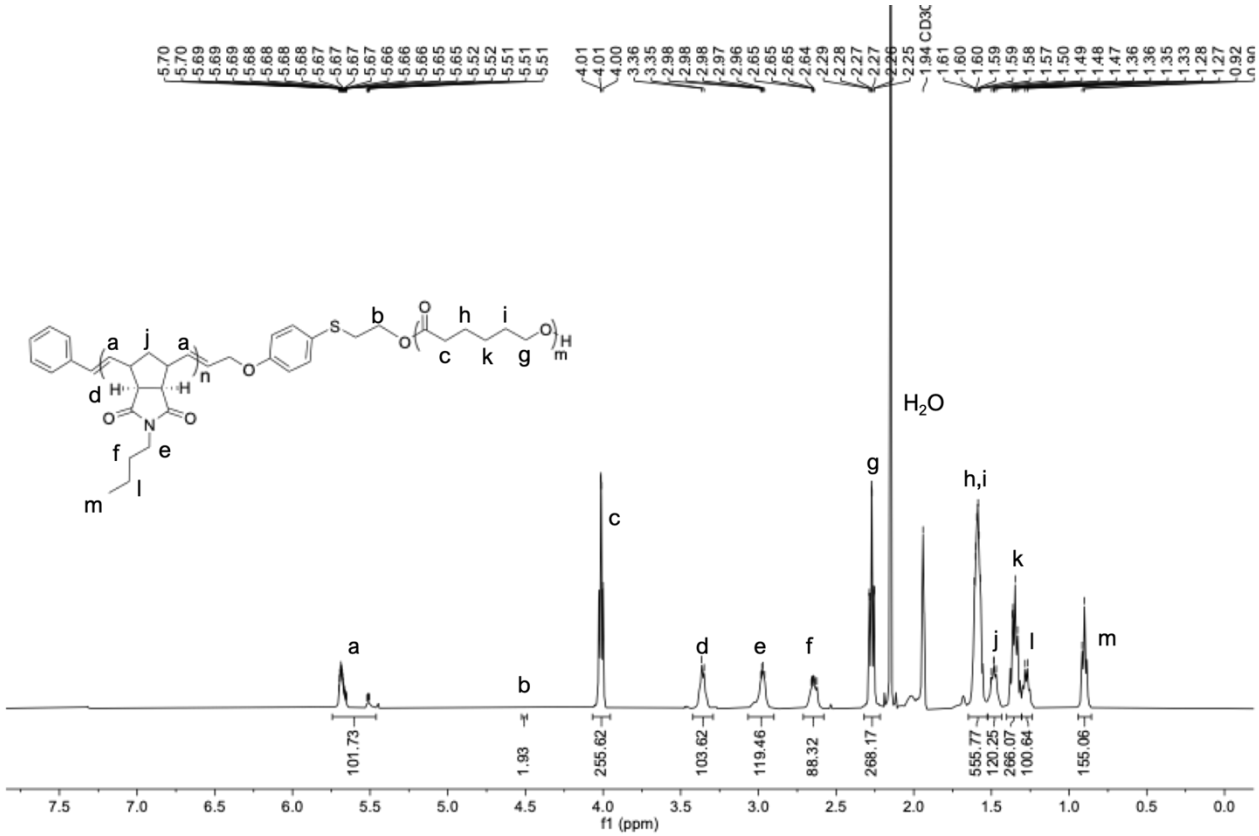


**Figure 2.78** $^{1}$H NMR spectrum of p(CL)-*b*-p(BNI) (**14**) in $CD_3CN$ at 25 ºC.

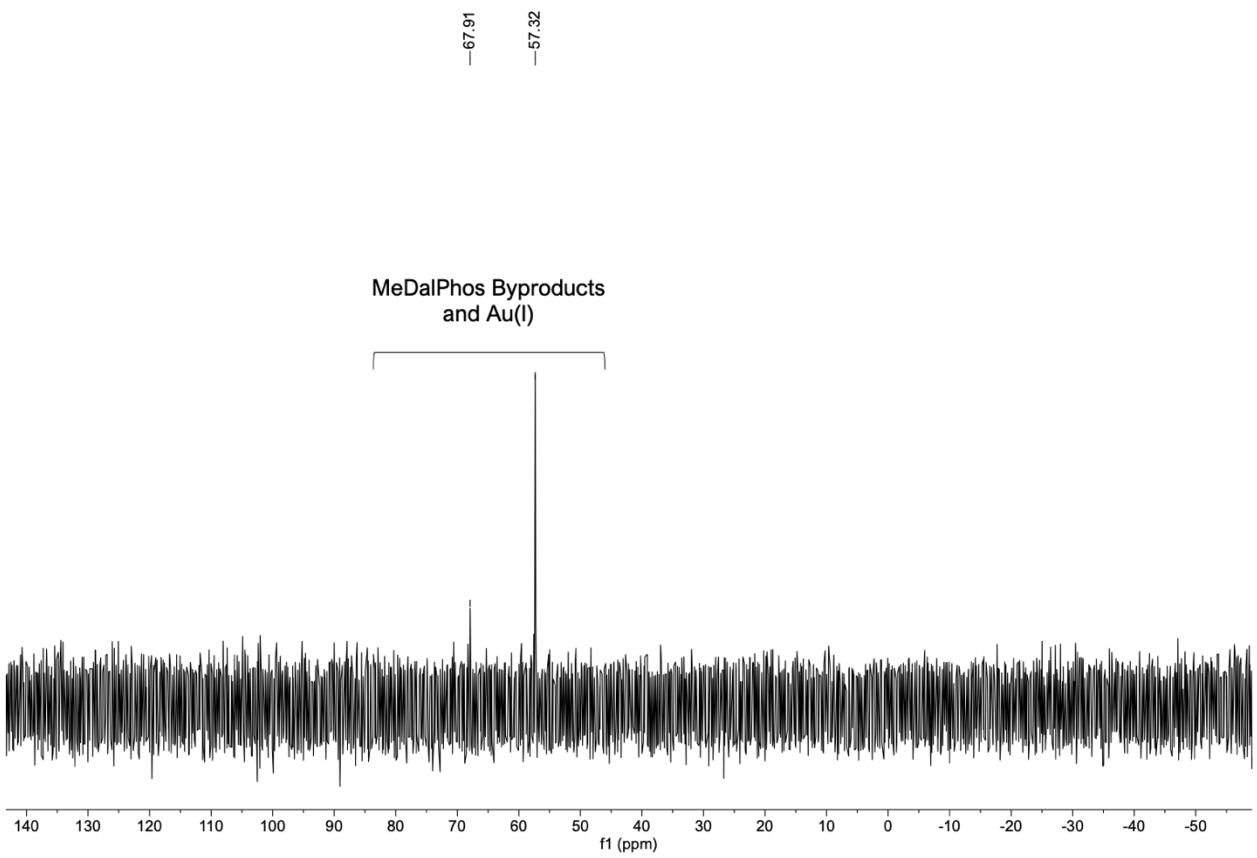


**Figure 2.79** $^{31}P\{^{1}H\}$ NMR spectrum of p(CL)-*b*-p(BNI) (**14**) in $CD_3CN$ at 25 ºC.

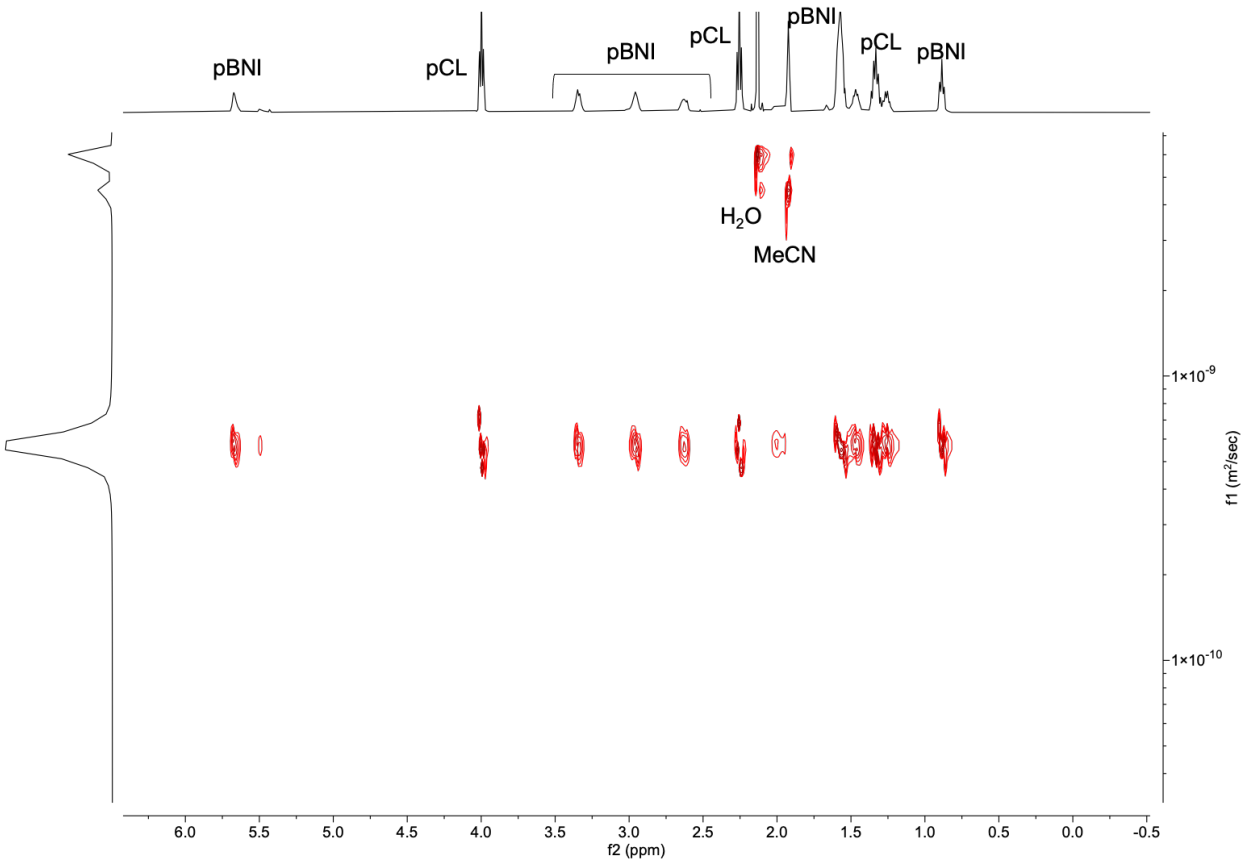


**Figure 2.80** DOSY NMR spectrum of p(CL)-*b*-p(BNI) (**14**) in $CD_3CN$ at 25 ºC.

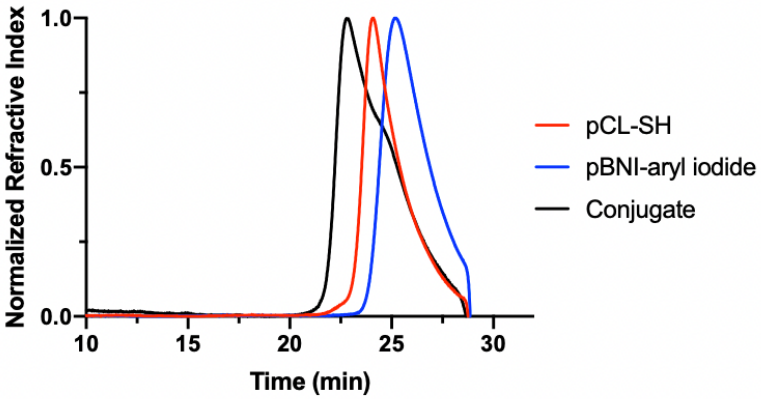


**Figure 2.81** DMF SEC trace of p(CL)-*b*-p(BNI) (**14**).

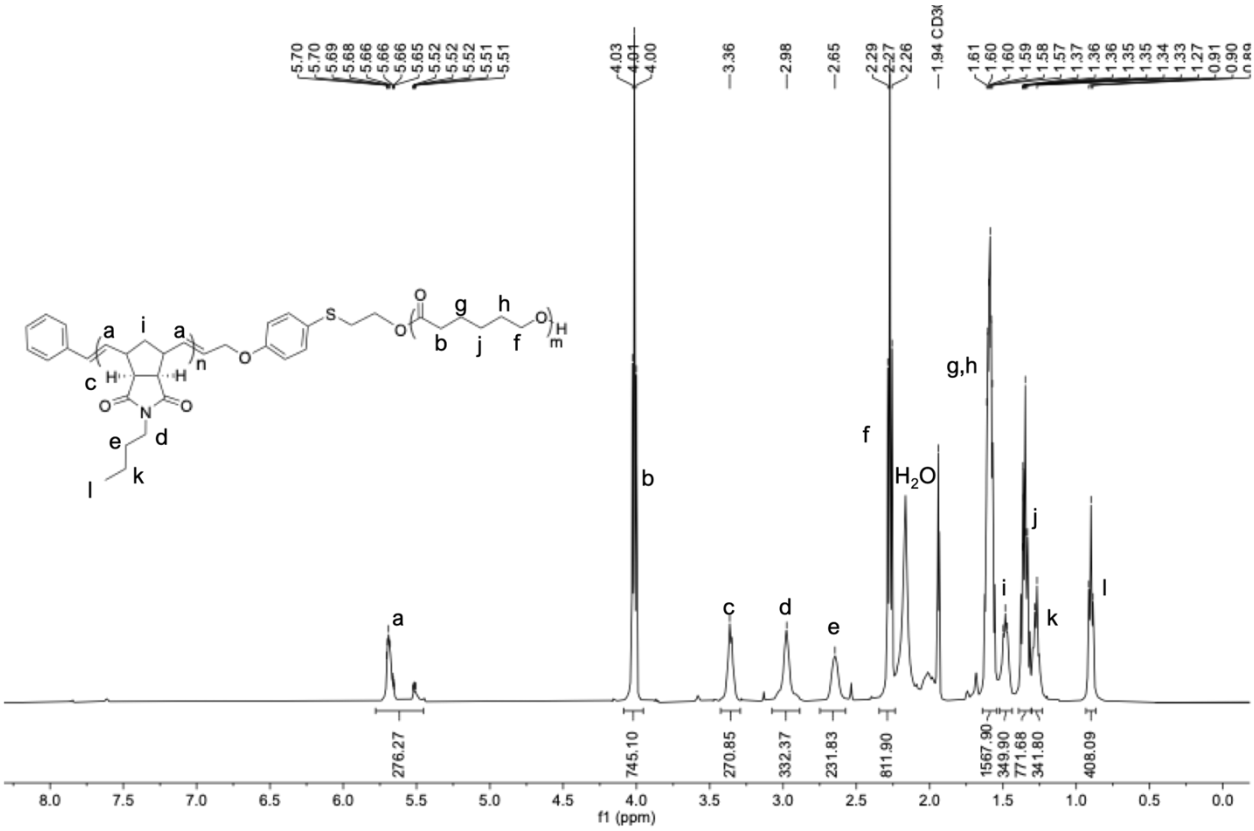


**Figure 2.82** $^{1}$H NMR spectrum of p(CL)-*b*-p(BNI) (**18**) in $CDCN_3$ at 25 ºC. Peak "a" contains both cis- and trans- alkene protons.

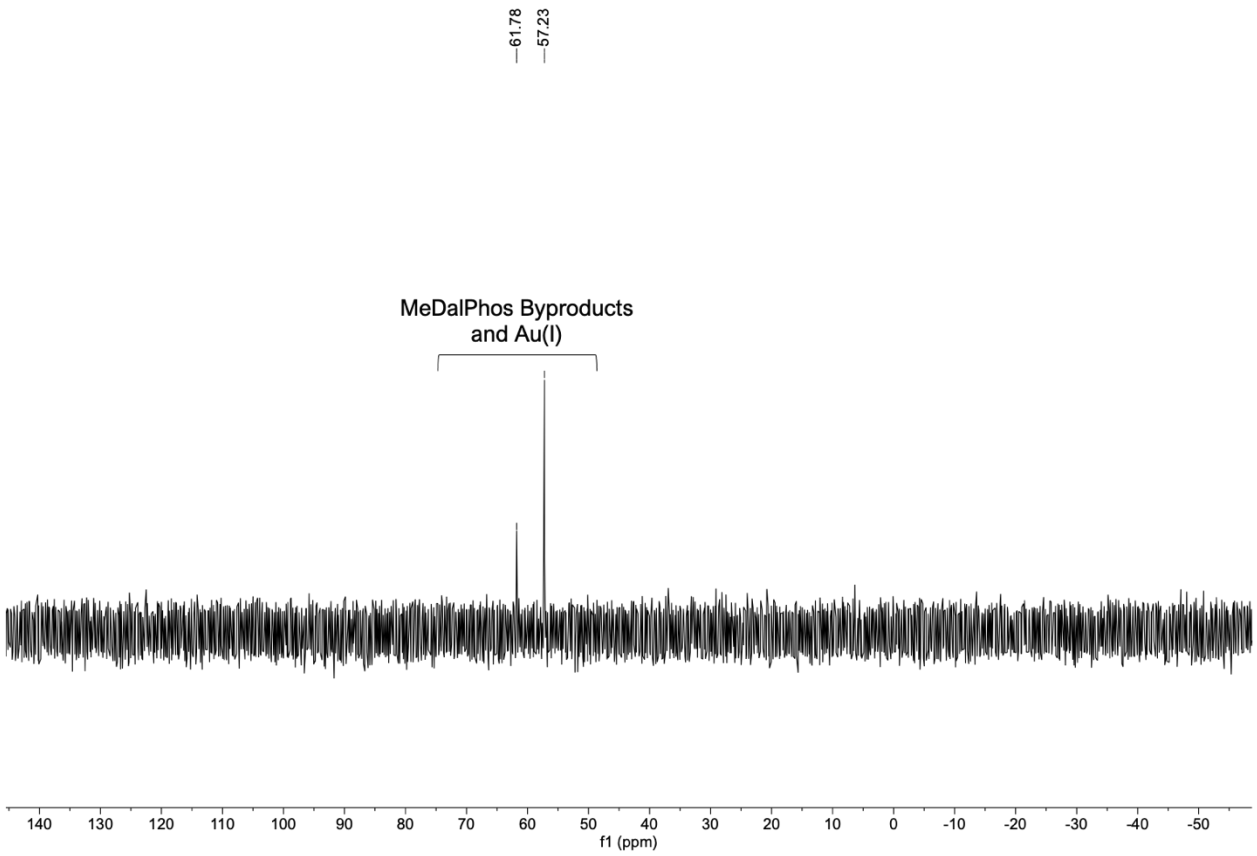


**Figure 2.83** $^{31}P\{^{1}H\}$ NMR spectrum of p(CL)-*b*-p(BNI) (**18**) in $CDCN_3$ at 25 ºC.

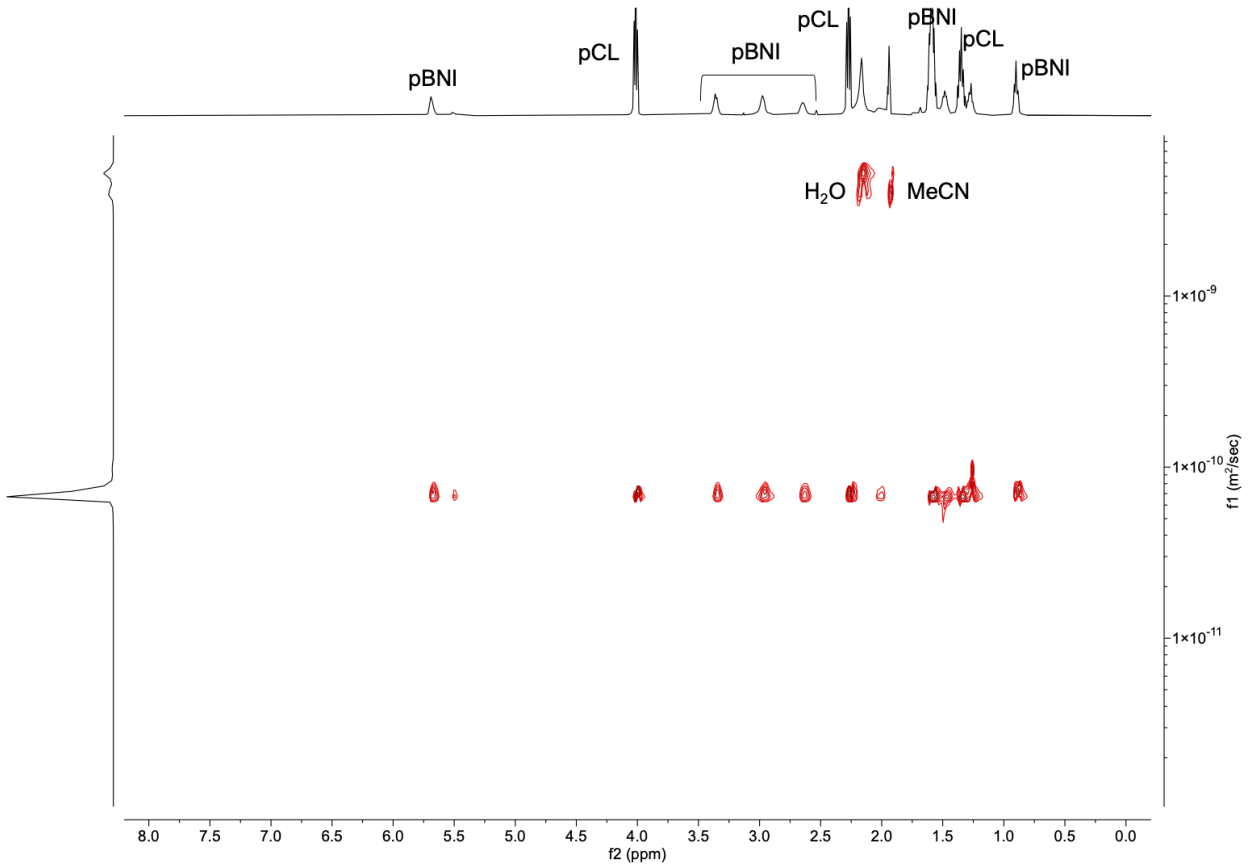


**Figure 2.84** DOSY spectrum of p(CL)-*b*-p(BNI) (**18**) in $CDCN_3$ at 25 ºC.

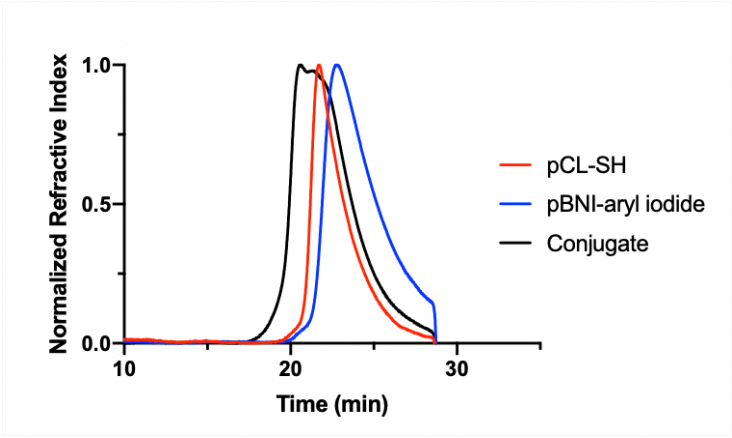


**Figure 2.85** DMF SEC trace of p(CL)-*b*-p(BNI) (**18**).

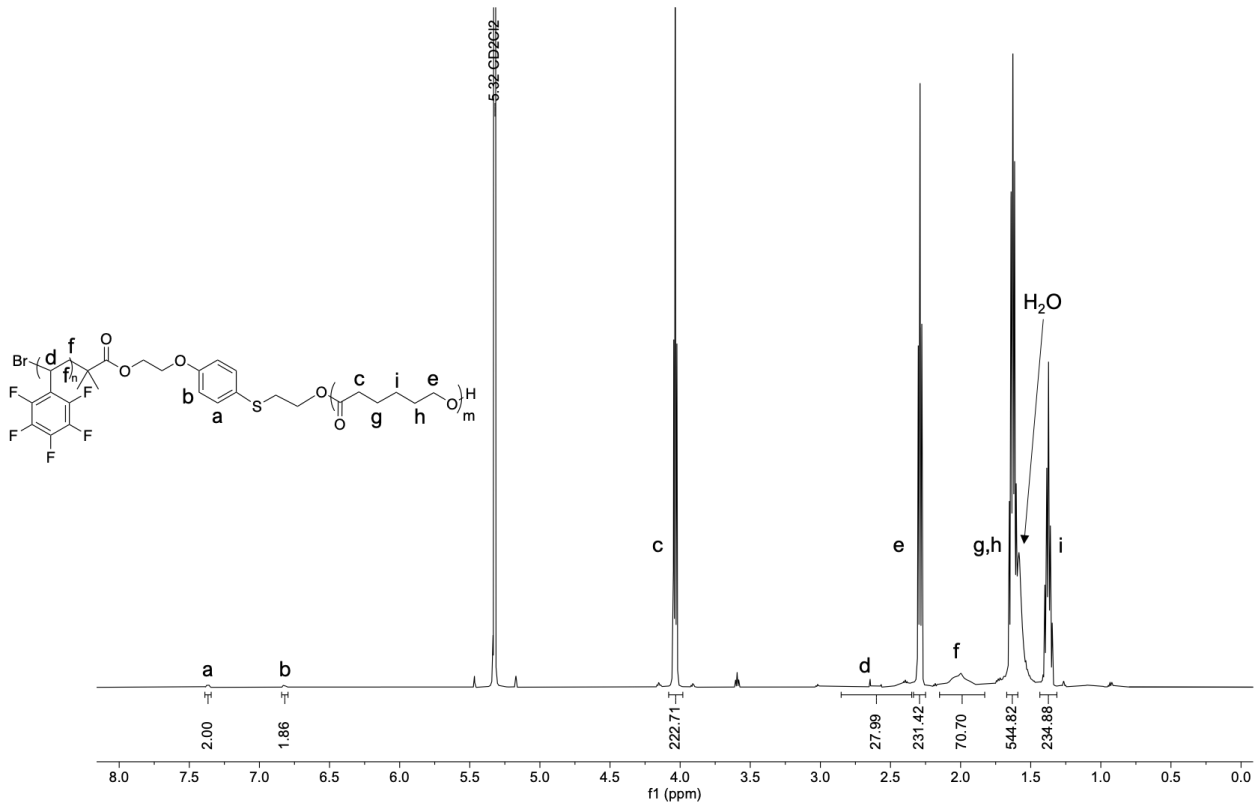


**Figure 2.86** $^{1}H$ NMR spectrum of p(CL)-*b*-p(PFS) (**15**) in $CD_2Cl_2$ at 25 ºC.

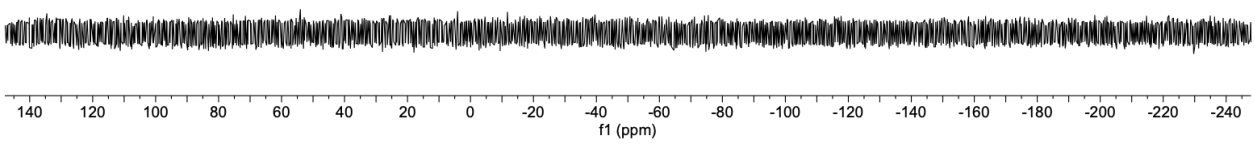


**Figure 2.87** $^{31}P\{^{1}H\}$ NMR spectrum of p(CL)-*b*-p(PFS) (**15**) in $CD_3CN$ at 25 ºC.

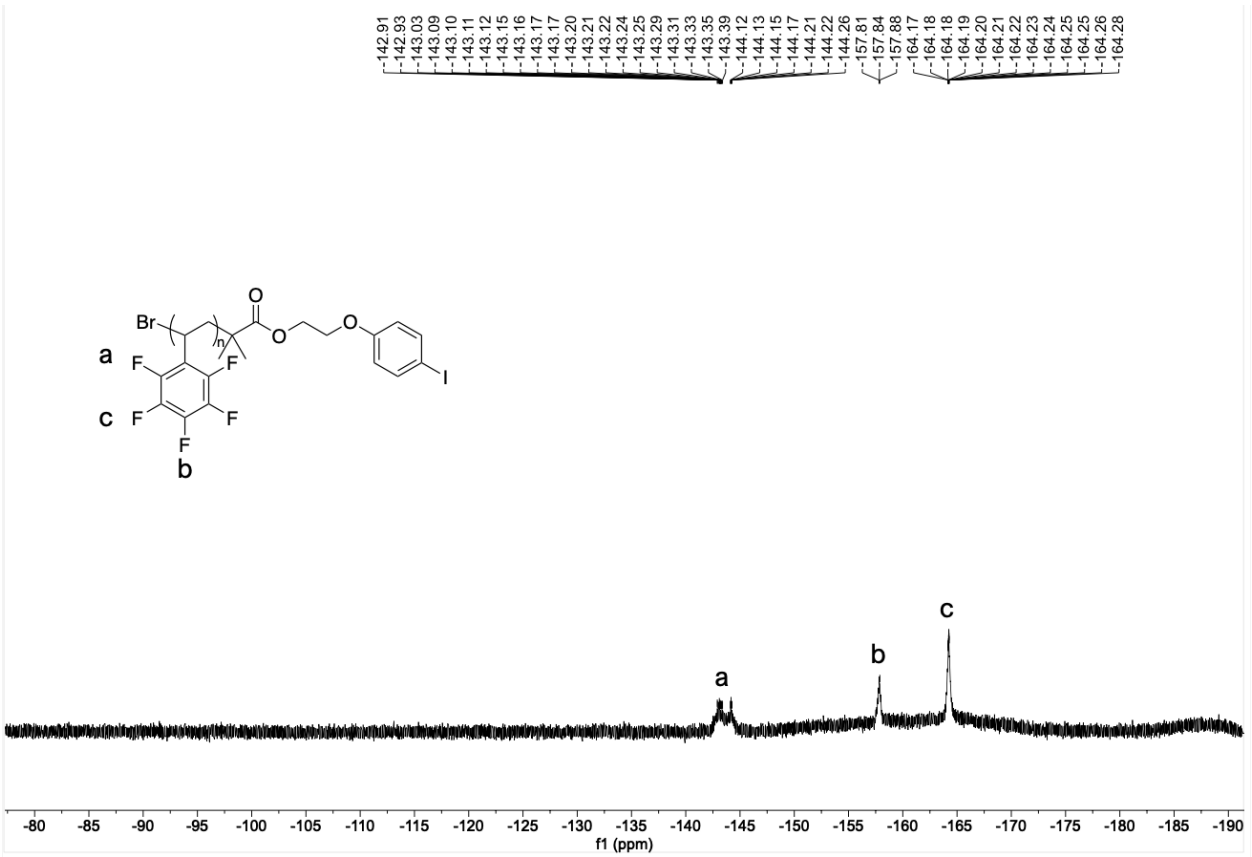


**Figure 2.88** $^{19}F\{^{1}H\}$ NMR spectrum of p(CL)-*b*-p(PFS) (**15**) in $CD_3CN$ at 25 ºC.

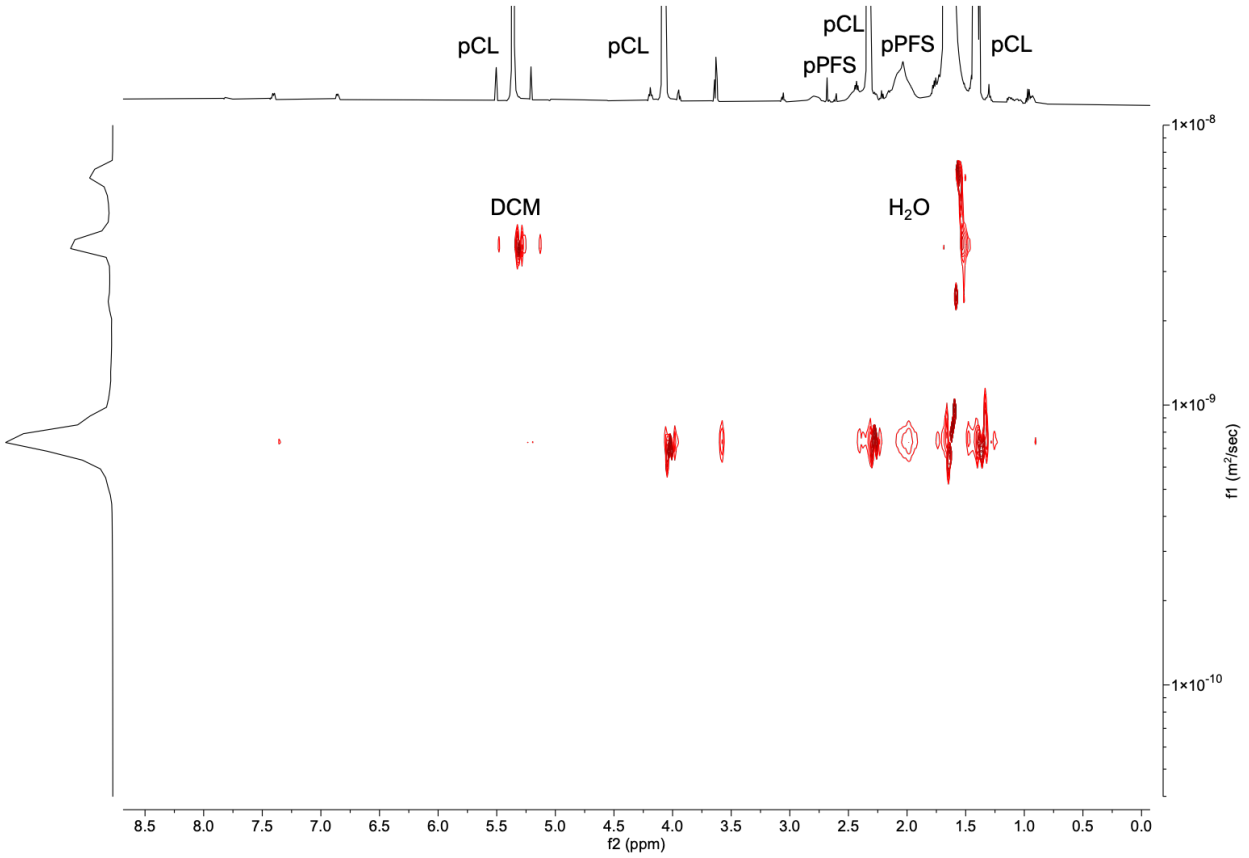


**Figure 2.89** DOSY NMR spectrum of p(CL)-*b*-p(PFS) (**15**) in $CD_2Cl_2$ at 25 ºC.

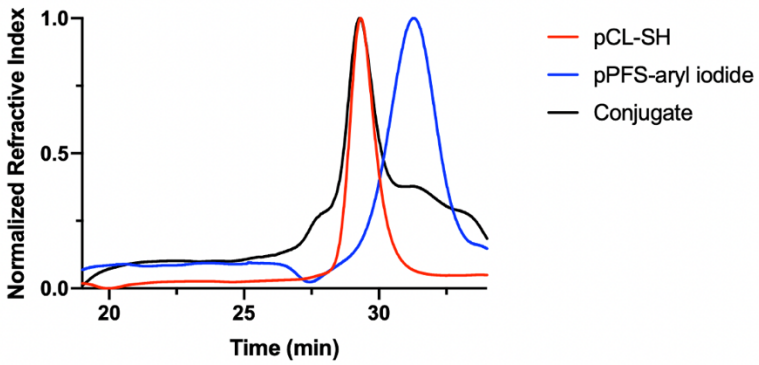


**Figure 2.90** THF SEC trace of p(CL)-*b*-p(PFS) (**15**).

## 2.5 References

†This chapter, with copyright permission from RSC, contains a paper published as:

Kunkel, G. E.; Treacy, J. W.; Montgomery, H. R.; Puente, E. G.; Doud, E. A.; Spokoyny, A. M.; Maynard, H. D. Efficient End-Group Functionalization and Diblock Copolymer Synthesis via Au(III) Polymer Reagents. *Chem. Commun.* **2023**, *60* (1), 79–82.

(1) Kim, J.; Jung, H. Y.; Park, M. J. End-Group Chemistry and Junction Chemistry in Polymer Science: Past, Present, and Future. *Macromolecules* **2020**, *53* (3), 746–763. https://doi.org/10.1021/acs.macromol.9b02293.

(2) Alconcel, S. N. S.; Kim, S. H.; Tao, L.; Maynard, H. D. Synthesis of Biotinylated Aldehyde Polymers for Biomolecule Conjugation. *Macromol. Rapid Commun.* **2013**, *34* (12), 983–989. https://doi.org/10.1002/marc.201300205.

(3) Dau, H.; Jones, G. R.; Tsogtgerel, E.; Nguyen, D.; Keyes, A.; Liu, Y.-S.; Rauf, H.; Ordonez, E.; Puchelle, V.; Basbug Alhan, H.; Zhao, C.; Harth, E. Linear Block Copolymer Synthesis. *Chem. Rev.* **2022**, *122* (18), 14471–14553. https://doi.org/10.1021/acs.chemrev.2c00189.

(4) Kolb, H. C.; Finn, M. G.; Sharpless, K. B. Click Chemistry: Diverse Chemical Function from a Few Good Reactions. *Angew. Chem. Int. Ed.* **2001**, *40* (11), 2004–2021. https://doi.org/10.1002/1521-3773(20010601)40:11<2004::AID-ANIE2004>3.0.CO;2-5.

(5) Spruell, J. M.; Levy, B. A.; Sutherland, A.; Dichtel, W. R.; Cheng, J. Y.; Stoddart, J. F.; Nelson, A. Facile Postpolymerization End-Modification of RAFT Polymers. *J. Polym. Sci. Part Polym. Chem.* **2009**, *47* (2), 346–356. https://doi.org/10.1002/pola.23138.

(6) Plank, M.; Frieß, F. V.; Bitsch, C. V.; Pieschel, J.; Reitenbach, J.; Gallei, M. Modular Synthesis of Functional Block Copolymers by Thiol–Maleimide “Click” Chemistry for

Porous Membrane Formation. *Macromolecules* **2023**, *56* (4), 1674–1687. https://doi.org/10.1021/acs.macromol.2c02255.

(7) Opsteen, J. A.; Hest, J. C. M. van. Modular Synthesis of Block Copolymers via Cycloaddition of Terminal Azide and Alkyne Functionalized Polymers. *Chem. Commun.* **2005**, No. 1, 57–59. https://doi.org/10.1039/B412930J.

(8) Agut, W.; Taton, D.; Lecommandoux, S. A Versatile Synthetic Approach to Polypeptide Based Rod−Coil Block Copolymers by Click Chemistry. *Macromolecules* **2007**, *40* (16), 5653–5661. https://doi.org/10.1021/ma070579m.

(9) Toncheva-Moncheva, N.; Bakardzhiev, P.; Rangelov, S.; Trzebicka, B.; Forys, A.; Petrov, P. D. Linear Amphiphilic Polyglycidol/Poly(ε-Caprolactone) Block Copolymers Prepared via "Click" Chemistry-Based Concept. *Macromolecules* **2019**, *52* (9), 3435–3447. https://doi.org/10.1021/acs.macromol.9b00366.

(10) Durmaz, H.; Dag, A.; Altintas, O.; Erdogan, T.; Hizal, G.; Tunca, U. One-Pot Synthesis of ABC Type Triblock Copolymers via in Situ Click [3 + 2] and Diels−Alder [4 + 2] Reactions. *Macromolecules* **2007**, *40* (2), 191–198. https://doi.org/10.1021/ma061819l.

(11) Inglis, A. J.; Sinnwell, S.; Stenzel, M. H.; Barner-Kowollik, C. Ultrafast Click Conjugation of Macromolecular Building Blocks at Ambient Temperature. *Angew. Chem. Int. Ed.* **2009**, *48* (13), 2411–2414. https://doi.org/10.1002/anie.200805993.

(12) Brendel, J. C.; Martin, L.; Zhang, J.; Perrier, S. SuFEx – a Selectively Triggered Chemistry for Fast, Efficient and Equimolar Polymer–Polymer Coupling Reactions. *Polym. Chem.* **2017**, *8* (48), 7475–7485. https://doi.org/10.1039/C7PY01636K.

(13) Iha, R. K.; Wooley, K. L.; Nyström, A. M.; Burke, D. J.; Kade, M. J.; Hawker, C. J. Applications of Orthogonal "Click" Chemistries in the Synthesis of Functional Soft Materials. *Chem. Rev.* **2009**, *109* (11), 5620–5686. https://doi.org/10.1021/cr900138t.

(14) Fournier, D.; Hoogenboom, R.; Schubert, U. S. Clicking Polymers: A Straightforward Approach to Novel Macromolecular Architectures. *Chem. Soc. Rev.* **2007**, *36* (8), 1369–1380. https://doi.org/10.1039/B700809K.

(15) Geng, Z.; Shin, J. J.; Xi, Y.; Hawker, C. J. Click Chemistry Strategies for the Accelerated Synthesis of Functional Macromolecules. *J. Polym. Sci.* **2021**, *59* (11), 963–1042. https://doi.org/10.1002/pol.20210126.

(16) Shahrokhinia, A.; Biswas, P.; Reuther, J. F. Orthogonal Synthesis and Modification of Polymer Materials. *J. Polym. Sci.* **2021**, *59* (16), 1748–1786. https://doi.org/10.1002/pol.20210345.

(17) Koo, S. P. S.; Stamenović, M. M.; Prasath, R. A.; Inglis, A. J.; Du Prez, F. E.; Barner-Kowollik, C.; Van Camp, W.; Junker, T. Limitations of Radical Thiol-Ene Reactions for Polymer–Polymer Conjugation. *J. Polym. Sci. Part Polym. Chem.* **2010**, *48* (8), 1699–1713. https://doi.org/10.1002/pola.23933.

(18) Durmaz, H.; Colakoglu, B.; Tunca, U.; Hizal, G. Preparation of Block Copolymers via Diels Alder Reaction of Maleimide- and Anthracene-End Functionalized Polymers. *J. Polym. Sci. Part Polym. Chem.* **2006**, *44* (5), 1667–1675. https://doi.org/10.1002/pola.21275.

(19) Duxbury, C. J.; Cummins, D.; Heise, A. Glaser Coupling of Polymers: Side-Reaction in Huisgens "Click" Coupling Reaction and Opportunity for Polymers with Focal Diacetylene Units in Combination with ATRP. *J. Polym. Sci. Part Polym. Chem.* **2009**, *47* (15), 3795–3802. https://doi.org/10.1002/pola.23437.

(20) Notestein, J. M.; Lee, L.-B. W.; Register, R. A. Well-Defined Diblock Copolymers via Termination of Living ROMP with Anionically Polymerized Macromolecular Aldehydes. *Macromolecules* **2002**, *35* (6), 1985–1987. https://doi.org/10.1021/ma012157x.

(21) Messina, M. S.; Stauber, J. M.; Waddington, M. A.; Rheingold, A. L.; Maynard, H. D.; Spokoyny, A. M. Organometallic Gold(III) Reagents for Cysteine Arylation. *J. Am. Chem. Soc.* **2018**, *140* (23), 7065–7069. https://doi.org/10.1021/jacs.8b04115.

(22) Doud, E.; Tilden, J.; Treacy, J.; Chao, E.; Montgomery, H.; Kunkel, G.; Adhami, N.; Kerr, T.; Rheingold, A.; Frost, C.; Houk, K.; Maynard, H.; Spokoyny, A. *Breaking Kinetic Record for Cysteine Bioconjugation with Organometallic Reagents*; preprint; Chemistry, 2023. https://doi.org/10.26434/chemrxiv-2023-brjnz.

(23) Tilden, J. A. R.; Lubben, A. T.; Reeksting, S. B.; Kociok-Köhn, G.; Frost, C. G. Pd(II)-Mediated C−H Activation for Cysteine Bioconjugation. *Chem. – Eur. J.* **2022**, *28* (11), e202104385. https://doi.org/10.1002/chem.202104385.

(24) Fastnacht, K. V.; Spink, S. S.; Dharmaratne, N. U.; Pothupitiya, J. U.; Datta, P. P.; Kiesewetter, E. T.; Kiesewetter, M. K. Bis- and Tris-Urea H-Bond Donors for Ring-Opening Polymerization: Unprecedented Activity and Control from an Organocatalyst. *ACS Macro Lett.* **2016**, *5* (8), 982–986. https://doi.org/10.1021/acsmacrolett.6b00527.

(25) Hilf, S.; Grubbs, R. H.; Kilbinger, A. F. M. End Capping Ring-Opening Olefin Metathesis Polymerization Polymers with Vinyl Lactones. *J. Am. Chem. Soc.* **2008**, *130* (33), 11040–11048. https://doi.org/10.1021/ja8022863.

(26) Madkour, A. E.; Koch, A. H. R.; Lienkamp, K.; Tew, G. N. End-Functionalized ROMP Polymers for Biomedical Applications. *Macromolecules* **2010**, *43* (10), 4557–4561. https://doi.org/10.1021/ma100330u.

(27) Coessens, V.; Pintauer, T.; Matyjaszewski, K. Functional Polymers by Atom Transfer Radical Polymerization. *Prog. Polym. Sci.* **2001**, *26* (3), 337–377. https://doi.org/10.1016/S0079-6700(01)00003-X.

(28) Tsarevsky, N. V.; Sumerlin, B. S.; Matyjaszewski, K. Step-Growth "Click" Coupling of Telechelic Polymers Prepared by Atom Transfer Radical Polymerization. *Macromolecules* **2005**, *38* (9), 3558–3561. https://doi.org/10.1021/ma050370d.

(29) Zhong, M.; Matyjaszewski, K. How Fast Can a CRP Be Conducted with Preserved Chain End Functionality? *Macromolecules* **2011**, *44* (8), 2668–2677. https://doi.org/10.1021/ma102834s.

(30) Montgomery, H. R.; Messina, M. S.; Doud, E. A.; Spokoyny, A. M.; Maynard, H. D. Organometallic S-Arylation Reagents for Rapid PEGylation of Biomolecules. *Bioconjug. Chem.* **2022**, *33* (8), 1536–1542. https://doi.org/10.1021/acs.bioconjchem.2c00280.

(31) Becer, C. R.; Babiuch, K.; Pilz, D.; Hornig, S.; Heinze, T.; Gottschaldt, M.; Schubert, U. S. Clicking Pentafluorostyrene Copolymers: Synthesis, Nanoprecipitation, and Glycosylation. *Macromolecules* **2009**, *42* (7), 2387–2394. https://doi.org/10.1021/ma9000176.

(32) Chen, Y.; Chen, J.; Zhang, N.; Ye, L.; Zhang, X.-J.; Yan, M. A New Synthesis of Indoles via Intramolecular Cyclization of o-Alkynyl N,N-Dialkylanilines Promoted by KOt-Bu/DMSO. *Tetrahedron Lett.* **2015**, *56* (2), 478–481. https://doi.org/10.1016/j.tetlet.2014.12.002.

(33) Lundgren, R. J.; Sappong-Kumankumah, A.; Stradiotto, M. A Highly Versatile Catalyst System for the Cross-Coupling of Aryl Chlorides and Amines. *Chem. – Eur. J.* **2010**, *16* (6), 1983–1991. https://doi.org/10.1002/chem.200902316.

(34) Hesp, K. D.; Stradiotto, M. Stereo- and Regioselective Gold-Catalyzed Hydroamination of Internal Alkynes with Dialkylamines. *J. Am. Chem. Soc.* **2010**, *132* (51), 18026–18029. https://doi.org/10.1021/ja109192w.

(35) Mudd, G. E.; Stanway, S. J.; Witty, D. R.; Thomas, A.; Baldo, S.; Bond, A. D.; Beswick, P.; Highton, A. Gold-Mediated Multiple Cysteine Arylation for the Construction of Highly Constrained Bicycle Peptides. *Bioconjug. Chem.* **2022**, *33* (8), 1441–1445. https://doi.org/10.1021/acs.bioconjchem.2c00288.

# Chapter 3

# Comparison of Cyclic and Linear PEG Conjugates†

## 3.1 Introduction

While researchers seek to improve therapeutic efficacy of drug treatments across several disease types, off-target effects often limit their advancement to the clinic and beyond.[93] As a result, the number of protein-based drug products approved by the US Food and Drug Administration (FDA) is steadily increasing, in part due to the specificity of their method-of-action.[94] Protein biologics are a powerful class of therapeutics toward effective disease treatment; however, they are susceptible to degradation and clearance *in vivo*. [95,96] Therefore, polymers are commonly used to provide stability and increased circulation times for biologics.[97,98] Furthermore, polymers can also provide "stealth" properties for protein therapeutics that initiate undesired immunogenic responses.[99] Currently, poly(ethylene glycol) (PEG) is the only polymer approved by the FDA for use in polymer-conjugated protein formulations. The FDA has approved over 30 PEGylated proteins that range in polymer size and linkage chemistry to tune properties such as circulation time and conjugation lability.[100] Despite these successful examples, the conjugation of PEG to proteins has led to deleterious effects, such as contributing to vacuolization *in vivo* and inducing immunogenic responses as a result of the formation of anti-PEG antibodies.[101,102] Although there has been extensive research using linear polymers other than PEG to conjugate to biologics,[103] the effects of more complex polymer architectures on protein-polymer conjugate properties is largely limited to branched and brush polymers.[104] Namely, branched and brush polymers are known to possess longer circulation times and high stability to proteolysis compared to their linear counterparts.[105,106] Brush polymers also possess lower solution viscosity compared to linear analogues due to their elongated "rod-like" structures that align with solution flow direction.[107,108] Low viscosity biologic formulations are likely to increase patient compliance, as

thinner needles can be used for injection. To date, linear and singly branched PEG polymers are the only polymer architectures available on the protein-polymer therapeutic market.[109]

Cyclic polymers are a macromolecular class known to have unique physical properties, such as a slower degradation profile and reduced hydrodynamic radius compared to their linear counterparts.[110] These features make cyclic polymers an attractive modality for biomedical applications.[111] Furthermore, most biologics are delivered *via* subcutaneous or intravenous injections, which are limited by injection volume (<1.5 mL).[112] Therefore, biologics that necessitate high dosage to reach efficacy must be highly concentrated formulations, which can lead to increased viscosity.[113] In these cases, cyclic polymers that possess inherently reduced hydrodynamic radii compared to their linear counterparts may provide equal stabilizing effects while also providing favorable physical properties to a biologic formulation such as increased circulation times *in vivo*.

Herein, we describe the first example of a cyclic protein-polymer conjugate and compare it to a linear protein-polymer conjugate of the same size. For our model study, we synthesized linear and cyclic 2 kDa PEG Au (III) oxidative addition complexes and performed *S*-arylation of each substrate to the surface-exposed cysteine of T4 lysozyme V131C (T4L).[39,114,115] We compared conformation, stability, and activity of the resulting purified conjugates. Finally, we performed molecular dynamics simulations of these conjugates to examine and quantify the effect of polymer architecture on protein-polymer conjugate behavior.

## 3.2 Results and Discussion

### 3.2.1 Synthesis of Cyclic and Linear 2 kDa PEG-Au(III) Reagents

One of the most significant barriers to the implementation of cyclic polymers in medicine is the challenge of their synthesis and purification.[110] Linear contaminants are known to profoundly

impact rheological properties,[116] and batch-to-batch heterogeneity could preclude FDA approval. Moreover, polymers to be used in bioconjugation are typically modified at their termini. The lack of chain ends in cyclic polymers represents an additional complication to their synthesis for this application.

The Au(III)-mediated *S*-arylation strategy is well-suited to mitigate these synthetic challenges; the preparation of a cyclic PEG Au(III) oxidative addition complex requires an aryl iodide precursor, which are relatively ubiquitous in organic chemistry. Aryl iodides also provide a

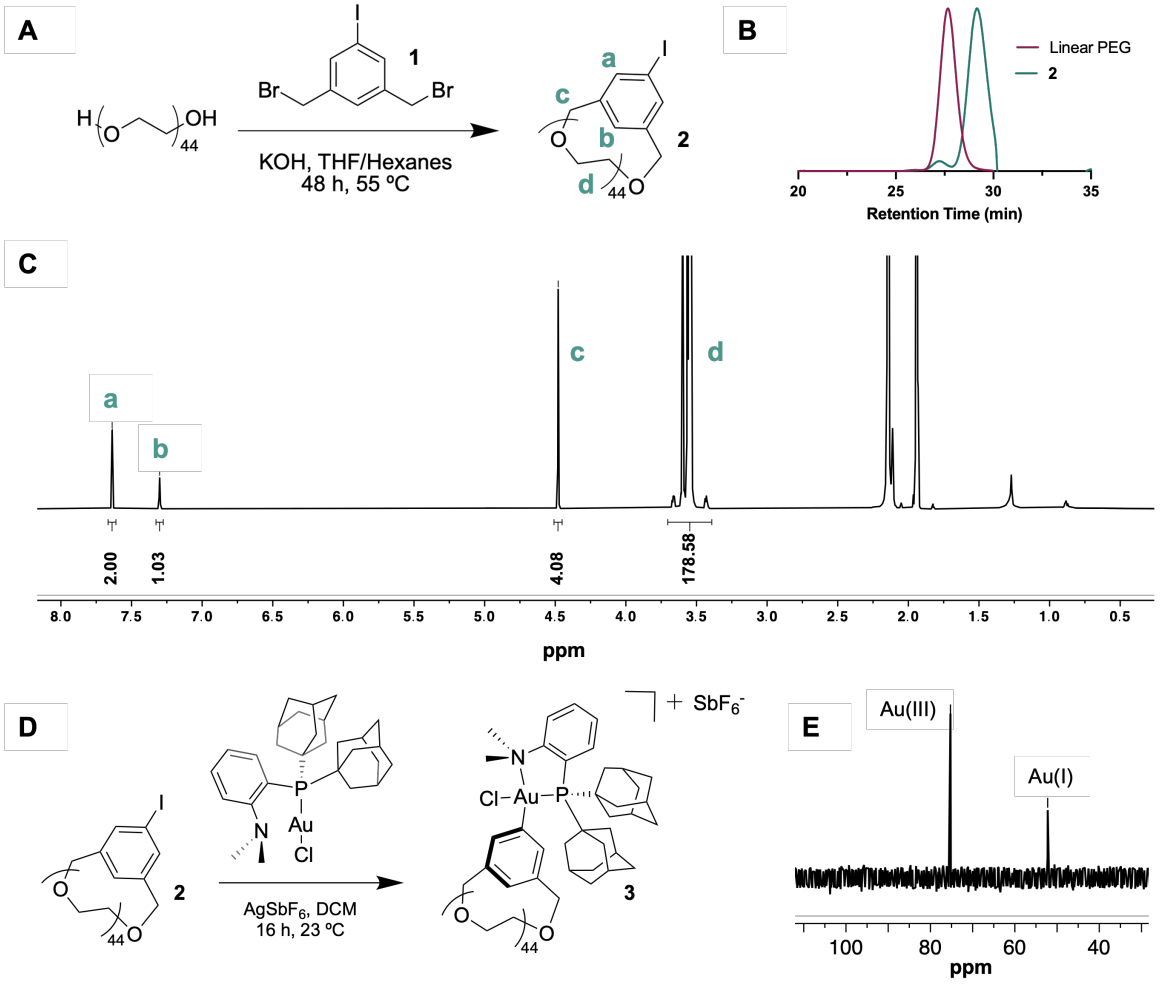


**Figure 3.1** A) Williamson ether synthesis of cyclic 2 kDa PEG-aryl iodide (2). B) DMF SEC of linear 2 kDa PEG and **2**. C) $^{1}$H NMR of **2** in $CD_3CN$. D) Oxidative addition of **2** with (Me-DalPhos)AuCl and $AgSbF_6$ to yield **3**. E) $^{31}P\{^{1}H\}$ NMR of **3** in $CD_3CN$.

convenient orthogonal functional handle, which can be carried through multiple harsh chemical synthesis steps and selectively metalated with an Au(I) precursor at late stages.[117–120] Therefore, we selected a bimolecular ring-closure strategy comprised of a homo-difunctional PEG diol and a difunctional benzyl bromide small molecule linker containing a sterically available aryl iodide (**1**). Accordingly, we used the commercially available dimethyl 5-iodoisophthalate and performed a reduction of the esters to the corresponding diol with $NaBH_4$ and $CaCl_2$, wherein the aryl iodide remained intact (**Figures 3.5 and 3.6**). Subsequent bromination of both benzyl alcohol positions afforded **1**, which contains two benzyl bromides and a sterically available aryl iodide for further functionalization (**Figures 3.7 and 3.8**). Williamson ether synthesis between a commercial 2 kDa PEG and **1** afforded the cyclic polymer **2** (**Figure 3.1A**), which is >95% pure according to $^1$H NMR and analytical high performance liquid chromatography (**Figures 3.1C, 3.9, and 3.11**).[121] Specifically, we observe aryl protons in the **2** $^1$H NMR spectrum that possess integration ratios corresponding to a high level of cyclic polymer purity. As expected, the increased retention time of **3** compared to commercial 2 kDa PEG, as observed by DMF SEC, indicates that **2** possesses a smaller hydrodynamic radius (**Figure 3.1B**). In agreement with these observations, we also measured and calculated the intrinsic viscosity (η) of **2** and its linear mPEG (2 kDa)-aryl iodide analog to be 0.003 and 0.007 mL/mg, respectively (**Figure 3.12**). Next we performed oxidative addition with (Me-DalPhos)AuCl, which afforded the bench-stable cyclic PEG-Au(III) oxidative addition complex **3** in good conversion and purity (**Figure 3.1D**, see experimental section for details). Notably, excess (Me-DalPhos)AuCl was present in the product (**Figures 3.1E and 3.14**), but it has been shown previously that it does not have deleterious effects in the subsequent *S*-arylation step.[122] Additionally, the linear 2 kDa mPEG Au(III) oxidative addition complex (**4**) was

synthesized as previously described in order to compare the effects of the polymer architecture on the protein conjugation and its subsequent properties.[39]

### 3.2.2. Preparation of PEG-T4L Conjugates

To prepare singly PEGylated T4L, a mutant T4 lysozyme containing one surface-exposed cysteine (V131C) was expressed (**Figure 3.15**).[123,124] Then, T4L was treated with 4 equivalents of tris(2-carboxyethyl)phosphinehydrochloride (TCEP•HCl) for one hour at 37 ºC to reduce the dimeric form of the protein formed by intermolecular disulfide bonds. The equivalents and

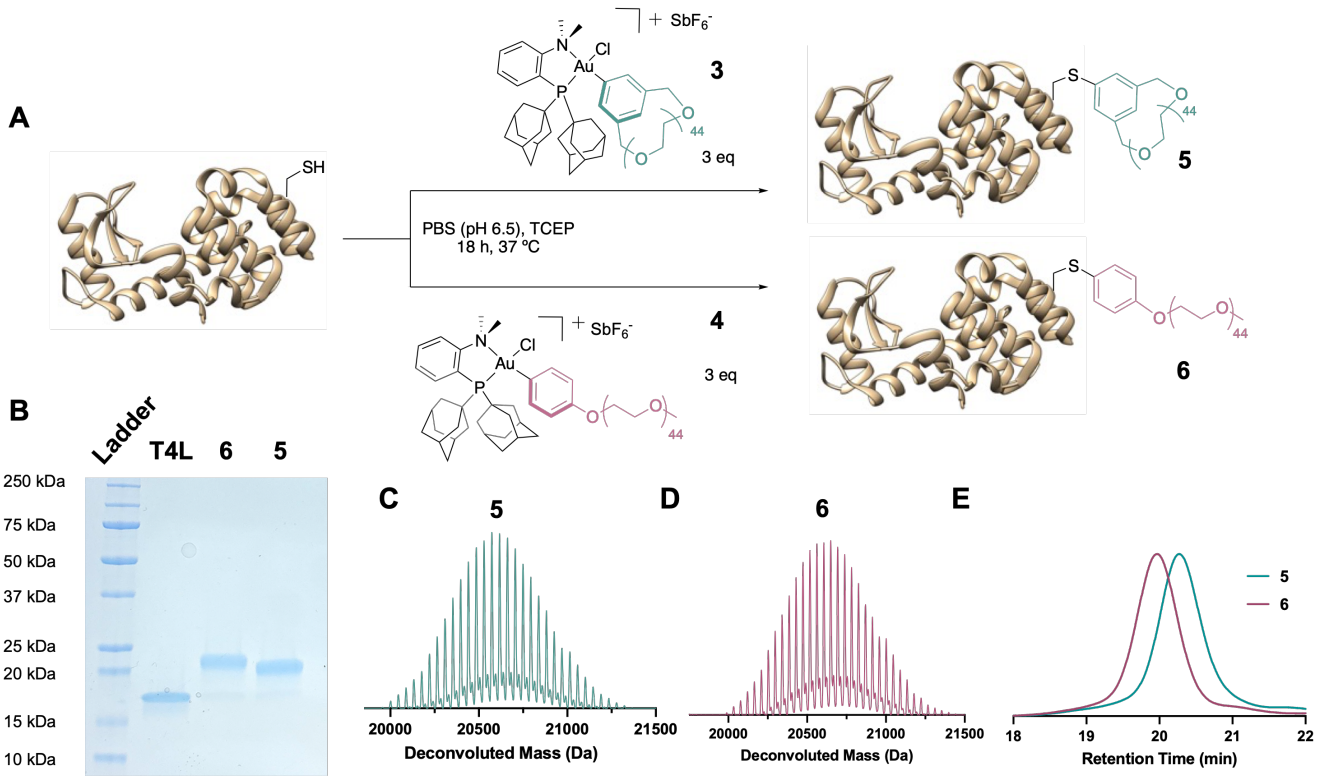


**Figure 3.2** A) Synthetic scheme representing T4L bioconjugation (PDB ID: 2HUK) to 2 kDa cyclic PEG (**3**) and 2 kDa linear mPEG (**4**), resulting in conjugates **5** and **6**, respectively. B) Coomassie-stained SDS-PAGE gel of T4L, **6**, and **5**. By ImageJ optical densitometry, **6** and **5** are 96% and 98% converted from T4L starting material, respectively. C) LCMS of **5**. Calculated mass is 20661.6 Da, observed mass is 20662.3 Da. D) LCMS of **6**. Calculated mass is 20693.6 Da, observed mass is 20694.7 Da. E) SEC FPLC spectrum for **5** and **6.**

temperature of the TCEP•HCl reduction were optimized to produce quantitative T4L monomer (**Figure 3.16**). As shown in previous work, TCEP•HCl did not negatively affect the *S*-arylation reaction and therefore did not necessitate removal.[39] Next, three equivalents of **3** and **4** were each incubated at 37 ºC with 70 μM T4L in PBS (pH 6.5) for 18 hours to produce cyclic PEG-T4L (**5**) and linear mPEG-T4L (**6**), respectively (**Figure 3.2A**). PEG equivalents, reaction time, and reaction temperature were screened (**Figures 3.17 and 3.18**) to produce nearly quantitative conversion to conjugates **5** and **6** (98% and 96%, respectively) as observed by SDS-PAGE and determined by ImageJ optical densitometry (**Figure 3.2B**). Experiments at ambient temperature (23 ºC) with all other variables held constant also resulted in high conversion to **5** and **6** (**Figure 3.19**, 84% and 80%, respectively), suggesting that this method can also be used at lower temperatures. It is important to note that kinetics of this *S*-arylation reaction are far slower than that of previous Au(III)-mediated PEGylation in a DARPin protein system,[39] which we hypothesize is due to the different local environment of the Cys residue in the protein. However, this would need to be studied. Following the *S*-arylation, **5** and **6** were purified by size exclusion fast protein liquid chromatography (SEC FPLC) to remove excess PEG reagent and Au(I) byproducts (See experimental section for details). Liquid chromatography−mass spectrometry (LCMS) of **5** and **6** produced deconvoluted mass values that correspond to each respective expected value (**Figure 3.2C** and **3.2D**). As cyclic ethers are known to effectively coordinate metal cations,[125] we aimed to ensure that this method was sufficient to remove excess Au. Accordingly, inductively coupled plasma optical emission spectroscopy (ICP-OES) was performed and determined that <50 ppb Au remained following the SEC FPLC process for both **5** and **6** (See experimental section for details).

As previously seen in their polymeric counterparts (**Figure 3.1B**), protein-polymer conjugate **5** possesses a longer SEC FPLC retention time than that of **6** (**Figure 3.2E**). Interestingly, this trend can also be observed by a smaller gel-shift of **5** compared to **6** in SDS-PAGE (**Figure 3.2B**). Therefore, as expected,[126] the smaller hydrodynamic radii of cyclic PEG compared to its linear counterpart is shown to translate to an overall smaller hydrodynamic radius of the cyclic polymer-protein conjugate. As hydrodynamic radius is known to directly correlate to viscosity, cyclic polymer-protein conjugates will likely result in a less viscous biologic formulation.[127]

### 3.2.3 Characterization of PEG-T4L Conjugates

To determine whether polymer architecture within a bioconjugate affects the secondary structure of the protein, T4L, **5**, and **6** were analyzed by circular dichroism (CD). In PBS (pH 6.5) at 23 ºC, we see no observable difference in helicity for T4L and its PEGylated conjugates (**Figure 3.3A**). Characteristic local minima are observed in each trace at 209-210 and 223 nm, which is

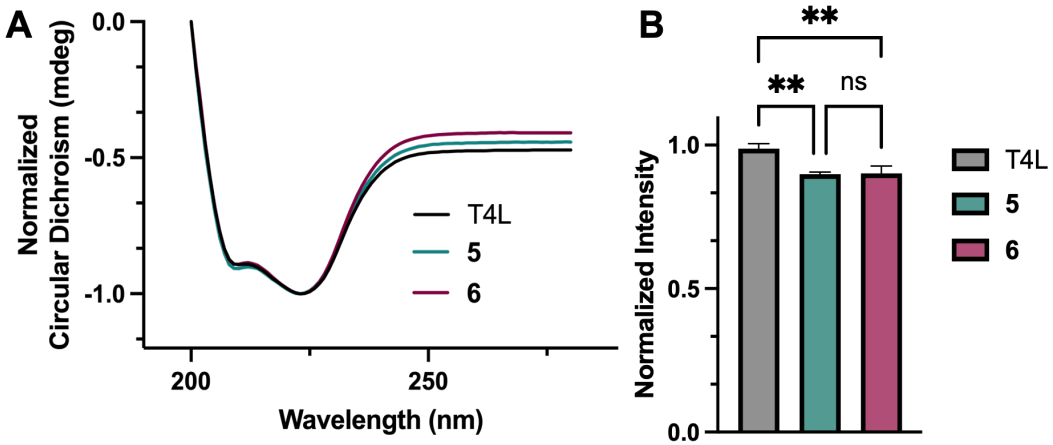


**Figure 3.3** A) Normalized CD spectrum of T4L, **5**, and **6** at 23 ºC showing no observable difference in helicity. B) Lysozyme activity fluorescence assay of T4L, **5**, and **6**. N = 3 for each group. An ordinary one-way ANOVA statistical analysis was performed. **p < 0.005. ns = not significantly different.

consistent with the protein and its conjugates adopting an alpha helical structure. Therefore, we conclude that there is no conformational difference for the protein imparted by varying the PEG architecture conjugated to T4L.

To compare the stabilizing effects of cyclic and linear PEG for T4L, CD was used to determine the experimental melting temperature ($T_m$) of T4L, **5**, and **6** (**Figure 3.23**).[128] Using a temperature ramp from 20 to 100 ºC and monitoring the relative helicity at 222 nm, we observe a $T_m$ for T4L at 56.8 ºC. **5** and **6** were determined to have a $T_m$ of 63.2 ºC and 62.6 ºC, respectively. Consequently, we conclude that cyclic PEG conjugates have the potential to stabilize T4L to a similar extent as the linear counterpart.

Modification of enzymes with PEG can have deleterious effects on their activity, often due to changes in electrostatic effects on the protein surface, modification of the protein conformation, and/or interaction of the polymer with the active site.[129,130] As we previously observed *vide supra*, there is no significant change in secondary structure of T4L after PEGylation with either **5** or **6**, though the influence on activity of T4L was still unknown. To investigate, we compared the activity of T4L, **5**, and **6** through the cell lysis of FITC-labeled Gram-positive *Micrococcus luteus* as monitored by an EnzChek™ lysozyme activity assay (See experimental section for details). Comparing the PEG conjugates (**5** and **6**) with unmodified T4L, we observe a statistically significant difference between the unmodified protein and each conjugate, wherein the conjugates are approximately 10% less active (**Figure 3.3B**). This is consistent with previous literature reports where mutations distal to the active site such as in this case have a lower effect on disruption of T4L activity.[131] However, there is no statistical significance between **5** and **6**, suggesting that the conformation of the cyclic polymer chain does not negatively affect the protein's activity compared to its linear counterpart at this molecular weight (2 kDa).

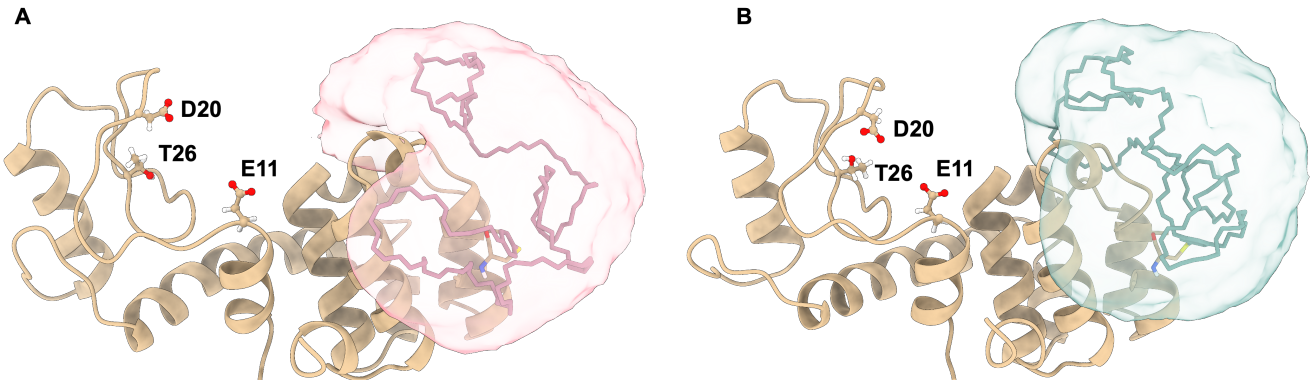


**Figure 3.4** Average polymer distribution isosurfaces resulting from three independent 1000 ns molecular dynamic simulations for A) **6** and B) **5.** Although there is no protein conformational difference induced by the polymer chain architecture, the cyclic PEG interacts less frequently with the T4L binding site compared to its linear counterpart.

To understand the behavior of the conjugate in solution, we performed three independent 1000 ns molecular dynamics simulations for conjugates **5** and **6** (See experimental section for details, **Figure 3.4**). Similar to our CD experiments, there was no significant conformational difference for T4L induced by the cyclic and linear polymer chains. However, we observe that the linear polymer of **6** interacts with the active site (E11-D20-T26) of T4L in approximately 5% of the simulations, whereas the cyclic polymer of **5** interacts with the active site in <0.1% of the simulations (**Figures 3.26-3.32**). Although these results suggest similar behavior of the polymer chains in solution, a conformationally restricted cyclic polymer may prove beneficial in the preparation of protein-polymer conjugates wherein the conjugation site is nearer to the active site of the enzyme. Additionally, we also hypothesize that utilization of a cyclic scaffold could be advantageous for longer polymers where interaction with distant active sites is spatially more likely.

## 3.3 Conclusion

Bioconjugation of polymers to proteins is a decades-long practice to impart desired functionality onto biologics. To the best of our knowledge, this report represents the first example of preparation and biophysical characterization of a cyclic polymer-protein conjugate. Herein, we describe a straightforward method (three synthetic steps) to prepare a cyclic PEG containing a bioconjugation handle with minimal linear polymer contaminants. We observed that a cyclic polymer-protein conjugate possessed a smaller hydrodynamic radius compared to its linear counterpart, despite having equal protein conformation, stability effects, and enzyme activity. We believe implementation of cyclic polymers could have a substantial impact on the rheological properties of protein-polymer bioconjugate formulations, which will be studied in the future. We recognize the significant challenge posed by introducing new polymer architectures to clinical settings, both from financial and regulatory perspectives. Nevertheless, this work highlights the cyclic polymer scaffold as an emerging modality of bioconjugation and stresses the need for continued exploration of polymer architecture for the improvement of biologic therapeutics.

## 3.4 Experimental

### 3.4.1 Materials

Unless otherwise stated, all materials were purchased and used as received from Fisher Scientific, Combi-Blocks, Alfa Aesar, Oakwood Chemicals, or Sigma Aldrich. Silver hexafluoroantimonate ($AgSbF_6$) was stored in a glovebox maintained under a nitrogen atmosphere prior to use.

### 3.4.2 Analytical Techniques

NMR spectra were recorded on the following: AV400 Bruker spectrometer at 400 ($^{1}H$) and 121 MHz ($^{31}P\{^{1}H\}$); AV300 Bruker spectrometer at 300 ($^{1}H$) and 75 MHz ($^{13}C$); NEO600 Bruker

spectrometer at 600 ($^{1}$H) and 243 ($^{31}$P{$^{1}$H}) MHz. Spectra are reported in δ (parts per million) relative to residual proteo-solvent signals for $^{1}$H and $H_3PO_4$ (δ 0.00 ppm) for $^{31}$P{$^{1}$H}. The following abbreviations were used to explain multiplicities: s = singlet, d = doublet, t = triplet, q = quartet, m = multiplet. Deuterated solvents were purchased from Cambridge Isotope Laboratories and used as received for all NMR experiments. Anhydrous DCM was prepared *via* distillation over calcium hydride and stored under a nitrogen atmosphere. Anhydrous THF was prepared using an activated alumina column and stored under an argon atmosphere.

Column chromatography was performed on a Biotage Isolera One 3.0 autocolumn instrument using KP-Sil high-performance columns repacked using Silicycle silica (P60, particle size 40–63 μm, column sizes described in experimental). TLC was performed using Millipore Sigma silica plates (60F-254) using short-wave UV light as visualizing agents. Electrospray ionization (ESI) mass spectra were obtained using an Agilent 6530 QTOF-ESI in tandem with a 1260 Infinity LC. DART mass spectra were obtained using a Thermo Exactive Plus Orbitrap with IonSense ID-CUBE DART source.

Analytical reverse-phase high performance liquid chromatography (HPLC) was carried out on a Agilent 1260 Infinity II HPLC system equipped with an autosampler and a UV detector using a Poroshell 120 2.7 μm C18 120 Å column (Analytical: 2.7 μm, 4.6 × 100 mm) with monitoring at λ = 220 and 280 nm and with a flow rate of 0.8 mL/min. Preparative HPLC purification was carried out on an Agilent 1290 Infinity II liquid chromatography system equipped with a UV detector using a Luna 5 μm C18 100 Å column (Preparatory: 5 μm, 250 × 21.2 mm) with monitoring at λ = 214 and 254 nm and with a flow rate of 20 mL/min. Individual gradients for each product purified *via* reverse phase HPLC are specified in their respective procedures.

DMF Size Exclusion Chromatography (SEC)/Gel Permeation Chromatography (GPC) was conducted on an Agilent 1260 Infinity II high performance liquid chromatography (HPLC) system with a Wyatt Optilab (RI and MALS detection), one Polymer Laboratories PLgel guard column, and two Polymer Laboratories PLgel 5 μm mixed D columns. The eluent was DMF (HPLC Grade, 99.7+%, Thermo Scientific Chemicals) containing LiBr (0.1 M) at 40 °C (Flow rate: 0.6 mL/min). Molecular weight information was determined for data collected using a PMMA (Agilent Technologies, EasiVial PMMA, preweighed calibration kit) conventional calibration analysis.

Intrinsic viscosity measurement. Polymer solutions were prepared from a stock solution of 100 mg/mL in water at different concentrations. Then, the viscosity was measured using the RheoSense HVROC-L Portable Viscometer Control Unit (USA) at 25 °C and using a constant shear rate of 8300 $s^{-1}$. The intrinsic viscosity of linear and cyclic PEG was determined using the Huggins equation by plotting the specific viscosity over concentration versus the concentration according to the following equation:

$$\frac{\eta_{sp}}{c} \cong [\eta] + k_H[\eta]^2 c$$

Where $\eta_{sp}$ is the specific viscosity, $c$ is the concentration, $[\eta]$ is the intrinsic viscosity, $k_H[\eta]^2$ is the second-order coefficient which contains the Huggins constant ($k_H$).

### 3.4.3 Methods

**Synthesis of (Me-DalPhos)AuCl Reagent**

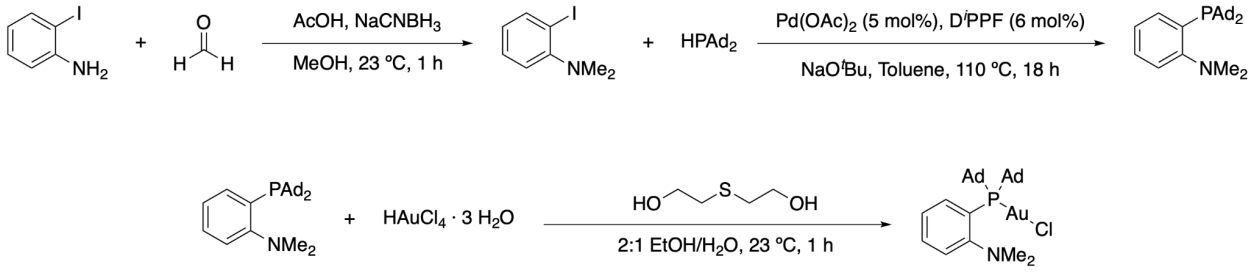


The (Me-DalPhos)AuCl reagent was synthesized as reported previously, as well as in Chapter 2.[115,122] Briefly, 2-iodoaniline was methylated using formaldehyde under reductive amination conditions. Next, the resulting 2-iodo-N,N-dimethylaniline product underwent Pd-catalyzed cross-coupling to produce Me-DalPhos (2-(diadamantylphosphinyl)-N,N-dimethylaniline).[132] Finally, this P,N ligand was metallated with chloroauric acid trihydrate and thiodiethanol to produce the (Me-DalPhos)AuCl reagent. All spectra match those of literature values.

**Synthesis of (5-iodo-1,3-phenylene)dimethanol (7)**

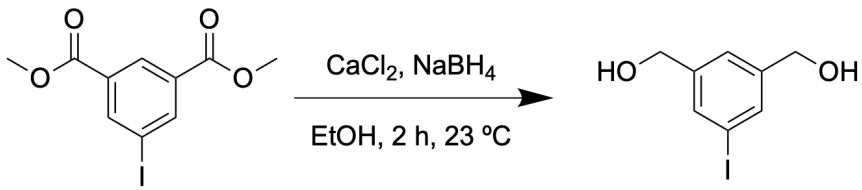


Dimethyl 5-iodoisophthalate (1.0 g, 1 eq, 3.1 mmol) was dissolved in ethanol (10 mL) in a round bottom flask charged with a stir bar. The reaction was brought to 0 ºC and sodium borohydride (485 mg, 4.1 eq, 12.8 mmol) was added slowly. Next, calcium chloride (728 mg, 2.1 eq, 6.6 mmol) in an additional 10 mL ethanol was added slowly. The reaction was allowed to warm to 23 ºC and stirred for 2 hours. Ethanol was removed under reduced pressure and the reaction was diluted with water. The crude product was extracted with ethyl acetate twice, dried over anhydrous $MgSO_4$, filtered, and concentrated under reduced pressure. The product was purified using column chromatography with a 0-10% gradient of methanol against DCM. The product was isolated as a white solid (740 mg, 2.8 mmol, 90% yield).

**Physical State:** White solid

**TLC (UV):** 0.67 (9:1 DCM-MeOH)

**$^1$H NMR (500 MHz, $CD_3CN$):** δ 7.59 (s, 2H), 7.29 (s, 1H), 4.66 – 4.23 (m, 4H), 3.27 (t, *J* = 6.0 Hz, 2H).

**$^{13}$C NMR (126 MHz, $CD_3CN$):** δ 145.75, 135.00, 125.21, 94.53, 63.77.

**HRMS (DART):** $[M-H]^-$ calculated for $C_8H_8IO_2^-$ 262.9574, observed 262.9576

**Synthesis of 1,3-bis(bromomethyl)-5-iodobenzene (1)**

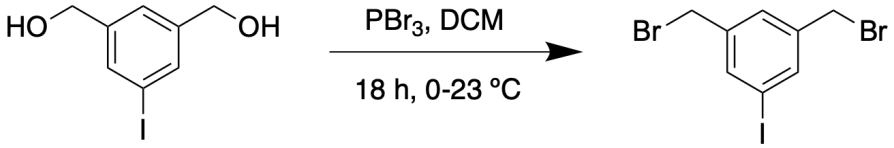


A flame dried two-neck round bottom flask was placed under argon atmosphere. (5-iodo-1,3-phenylene)dimethanol (500.0 mg, 1 eq, 1.9 mmol) was added with 10 mL anhydrous DCM. Next, the reaction was cooled to 0 ºC and phosphorus tribromide in DCM (2.1 g, 7.6 mL, 1.0 molar, 4 eq, 7.6 mmol) was added slowly. Finally, the reaction was warmed to 23 ºC and stirred for 18 hours. The crude product was concentrated under pressure and purified using column chromatography (0-100% ethyl acetate against hexanes). The product was isolated as a white solid (460 mg, 1.2 mmol, 62% yield).

**Physical State:** White solid

**TLC (UV):** 0.53 (9:1 Hexanes-EtOAc)

**$^{1}$H NMR (500 MHz, $CD_3CN$):** δ 7.75 (s, 1H), 7.49 (s, 1H), 4.49 (s, 4H).

**$^{13}$C NMR (126 MHz, $CD_3CN$):** δ 142.19, 138.72, 130.29, 94.50, 32.57.

**HRMS (DART):** $[M]^+$ calculated for $C_8H_7Br_2I^+$ 387.7959, observed 387.7945.

**Synthesis of Cyclic PEG (2 kDa)-Aryl Iodide (2)**

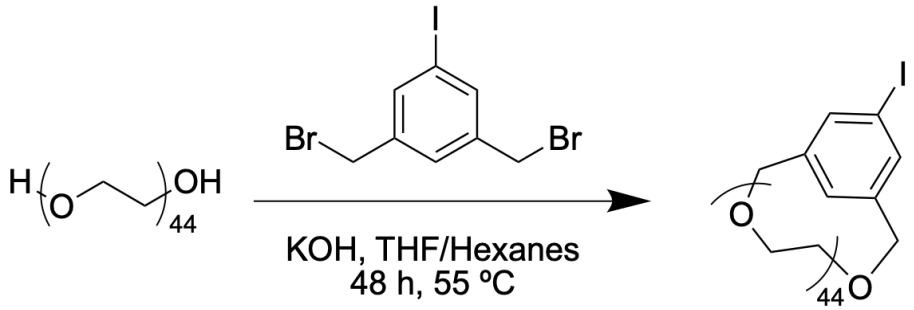


The following procedure was modified from Hadjichristidis *et al.*[121] A two-neck round bottom flask was charged with a stir bar, then finely powdered KOH (906.7 mg, 70 eq, 16.2 mmol) was added as a solid. Next, 40 mL anhydrous THF and 10 mL hexanes were added to the flask. The round bottom flask was affixed with a reflux condenser and the reaction mixture was heated to reflux (60 ºC). Separately, PEG (2 kDa) (461.8 mg, 1 eq, 230.9 μmol) and 1,3-bis(bromomethyl)-5-iodobenzene (90.0 mg, 1 eq, 230.9 μmol) were dissolved in 50 mL anhydrous THF and then added to the flask at a rate of 4.2 mL/h using a syringe pump. Then, following the completion of the precursor addition, the reaction was stirred for an additional 24 hours while refluxing (60 ºC). Next, the reaction mixture was filtered to remove KOH, then the solvents were removed under reduced pressure. The crude product was dissolved in DCM and purified by one precipitation in hexanes followed by three fractionations in toluene/hexanes as the good solvent and non-solvent, respectively. Finally, the product was purified using preparative HPLC with a 30-100% MeCN against $H_2O$ gradient (Both with 0.1% TFA additive). The product was isolated as a white solid (205.2 mg, 92.4 μmol, 40% yield).

**Physical State:** White solid

**$^1$H NMR (500 MHz, $CD_3CN$):** δ 7.64 (s, 2H), 7.30 (s, 1H), 4.48 (s, 4H), 3.70 – 3.20 (m, 179H).

**Synthesis of Cyclic PEG (2 kDa) [(Me-DalPhos)AuCl][$SbF_6$] (3)**

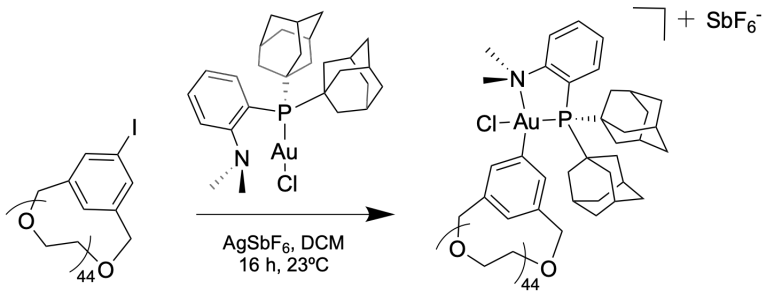


$AgSbF_6$ was removed from a dinitrogen-filled glove box prior to the reaction. (Me-DalPhos)AuCl (9.4 mg, 1.5 eq, 14.3 μmol) and $AgSbF_6$ (9.8 mg, 3 eq, 28.7 μmol) were added together with 1.5 mL DCM and stirred for 1 minute. Visible particulates crashed from the solution. Next, **3** (21.0 mg, 1 eq, 9.5 μmol) was added with an additional 500 μL DCM. The reaction was stirred for 18 hours at 23 ºC. The crude product was filtered through Celite, then the DCM was removed under reduced pressure. The product was isolated as an off-white solid (24 mg, 7.98 μmol, 84% yield). The product purity by weight was determined to be 85% by $^1$H NMR.

**Physical State:** Off-white solid

**$^1$H NMR (600 MHz, $CD_3CN$):** δ 8.10 – 7.94 (m, 3H), 7.89 – 7.80 (m, 1H), 7.58 (s, 2H), 7.24 – 7.14 (m, 1H), 4.52 (s, 4H), 3.72 – 3.40 (m, 177H), 1.82 – 1.63 (m, 26H).

**$^{31}$P{$^1$H} NMR (243 MHz, $CD_3CN$):** δ 75.25, 52.22.

**Synthesis of Linear PEG (2 kDa) [(Me-DalPhos)AuCl][$SbF_6$] (4)**

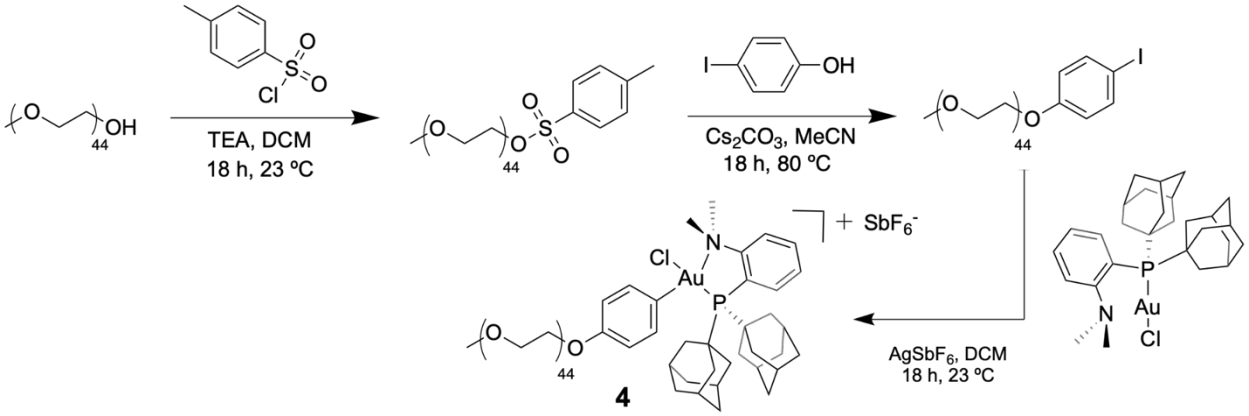


Linear mPEG (2 kDa) Au(III) reagent was synthesized as reported previously.[39] Briefly, commercial mPEG-OH (2 kDa) was tosylated under basic conditions at 23 ºC. Next, the resulting mPEG-tosyl was arylated with 4-iodophenol under refluxing conditions. Finally, the mPEG-aryl iodide underwent oxidative addition with (Me-DalPhos)AuCl to produce linear mPEG (2 kDa) [(Me-DalPhos)AuCl][$SbF_6$] (**4**). All spectra match those of literature values.

**T4 Lysozyme V131C (T4L) Protein Expression**

T4 lysozyme V131C (T4L) protein expression and purification was adapted from literature procedures.[133] T4 lysozyme V131C (T4L) Sequence (Calculated Mass: 18605.36 Da): MNIFEMLRIDEGLRLKIYKDTEGYYTIGIGHLLTKSPSLNAAKSELDKAIGRNTNGVITKD EAEKLFNQDVDAAVRGILRNAKLKPVYDSLDAVRRAALINMVFQMGETGVAGFTNSLR MLQQKRWDEAACNLAKSRWYNQTPNRAKRVITTFRTGTWDAYKNL.

*E. coli* host BL21(DE3) (Invitrogen) was used to express T4 lysozyme V131C (T4L) using an ampicillin resistant expression vector obtained from Prof. Wayne Hubbell (UCLA). To each of two 2 L flasks each containing 750 mL of previously autoclaved LB Broth (Miller) with ampicillin (50 μg/mL) was added 5 mL of a saturated 18 hour culture inoculated from a glycerol stock. The culture was grown at 37 °C with 250 rpm shaking for ca. 6 hours before the OD600 reached ~0.75 and the culture was induced with 1 mM IPTG. The culture continued to shake at 37 °C at 250 rpm for approximately 2 hours. The cultures were harvested by centrifugation at 4000 rpm for 15 min to yield a cell pellet. The pellet was resuspended in 20 mL lysis buffer (25 mM Tris, 25 mM MOPS, 0.2 mM EDTA, pH 7.6) by stirring vigorously. Spontaneous bacterial lysis occurred during resuspension as evident by increased viscosity of the suspension due to DNA release. Bacterial lysis was likely due to proteolytic activity of the lysozyme present in the bacteria. One subsequent freeze-thaw cycle ensured complete lysis of the bacteria. Benzoase (0.2 μL/mL) was then added to the solution and incubated at 25 °C for 15 min. Bacterial debris was then separated by centrifugation at 17,000 rpm for 25 min at 4 °C. The supernatant was loaded onto a 5 mL gravity SP Sepharose Fast Flow column (Cytiva) and washed with 200 mL lysis buffer. The column was then washed with two column volumes of lysis buffer with increasing NaCl content (gradient from 0 M to 0.5 M in 0.1 M steps) to elute the desired protein. SDS-PAGE was run on all fractions and

under reducing conditions with Coomassie Blue staining. Pure fractions were combined and solvent exchanged into storage buffer (20 mM PBS, pH 6.5) and concentrated to ~15 mL using an Amicon 3K Ultra-15 Centrifugal Filter (Millipore). Protein was further purified by preparative SEC-FPLC using an isocratic method in 20 mM PBS, pH 6.5. Pure fractions were concentrated and stored in storage buffer as described above. The purified protein was analyzed by LCMS and SDS-PAGE confirming sample purity and molecular weight (main text Figure 2). Concentration was determined by A280 (Extinction coefficient = 25,440 $M^{-1}$ $cm^{-1}$) The protein sample was diluted with storage buffer to 76 μM and aliquots were flash frozen and stored in a -80 °C freezer.

**General Information for T4L-PEG Conjugates**

Protein-polymer conjugates were purified by FPLC on a Bio-Rad BioLogic DuoFlow chromatography system. All purifications were carried out at 4 °C. All buffers were freshly prepared and filtered over a Thermo Scientific Nalgene 565-0020 Filter Unit, 0.2 μm PES prior to use. Size exclusion chromatography (SEC) purifications were performed using a Superdex 75 Increase 10/300 GL column. All protein purifications were monitored at wavelengths of 254 nm and 280 nm. A standard isocratic method was used for T4L: 20 mM PBS, pH 6.5 over 37 minutes.

Protein concentration measurements were determined on a NanoDrop 2000 UV-Vis spectrophotometer at 280 nm. The extinction coefficient of T4L was calculated by ProtoParam on ExPASy based on the amino acid sequence of the protein ($\varepsilon$ = 25,440 $M^{-1}cm^{-1}$).

Sodium dodecyl sulfate-polyacrylamide gel electrophoresis (SDS-PAGE) was carried out in a Mini-PROTEAN Tetra Cell system (Bio-Rad) connected to a PowerPac HC (BioRad) power supply using Bio-Rad Any kD™ Mini-PROTEAN® TGX™ Precast Gels at 195 V and 3 A for 30 minutes in a running buffer (25 mM Tris, 192 mM Glycine, 0.1% (w/v) SDS, pH 8.3). Precision Plus ProteinTM Dual Xtra Prestained Protein Standards (2 μL) were used as protein ladder in all

SDS-PAGE analysis. Laemmli 2x Concentrate (Sigma) containing 4% SDS, 20% glycerol, 0.004% bromophenol blue, and 0.125 M Tris HCl at a pH of ca. 6.8 was used to load all protein and conjugate samples. Protein bands were visualized by staining the gels in an aqueous solution (0.1% Coomassie Brilliant Blue R 250, 45% MeOH, 9% acetic acid) and microwaving for 30 seconds followed by agitation for 15 minutes. Destaining was carried out by submerging the gels in an aqueous destaining solution (10% MeOH, 14% acetic acid), microwaving for 30 seconds, and agitating for several hours until the background of the gel became fully destained.

LCMS analysis was carried out using an Agilent 6530 ESI-Q-TOF. Protein analyses were carried out using an Agilent ZORBAX 300SB C3 column (3.5 μm, 3.0 × 150 mm). Liquid chromatography method used for T4L and its conjugates: column temperature: 40 °C, flow rate: 0.6 mL/min, gradient: 90% water (0.1% formic acid (FA)) for 2 minutes; 90%-9% water (0.1% FA) 2-11 minutes; 5% water (0.1% FA) from 11-14 min with acetonitrile as the co-solvent.

**T4L-PEG Conjugation Procedure: General Conditions**

*General Reductive Elimination Procedure:* 70 μM T4L, PBS pH 6.5, 4 equiv. TCEP·HCl, 3 equiv. Au(III), 18 hours, 37 °C. To a 50 μL solution of T4L at 76 μM, 5 μL of a 3 mM TCEP·HCl (4 eq) solution in PBS was added. The protein underwent disulfide reduction for 1 hour at 37 ºC. Next, 5 μL of either **3** or **4** was added to the reaction mixture. Stock solutions of **3** and **4** were prepared in MeCN prior to the procedure (6.2 mg/mL and 5.3 mg/mL, respectively) such that 3 eq of each oxidative addition complex were added. The percent weight purity of **3** was taken into account. After 18 hours, the reaction was stopped by dilution in SDS-PAGE conditions (See below) to produce T4L-cyclic PEG (**5**) and T4L-linear PEG (**6**) conjugates.

*General SDS-PAGE Sample Preparation Procedure:* 1 μL of a given reaction mixture was added to 19 μL of Laemmli loading buffer. For samples run under reducing conditions, the

Laemmli loading buffer was prepared to contain 5% mercaptoethanol by volume and samples were heated at 90 ºC for five minutes prior to loading. Samples were loaded onto SDS-PAGE gel and run as described above in the general experimental information.

**PEG Equivalent and Temperature Screen**

To a 50 µL solution of T4L at 76 µM, 5 µL of a 3 mM TCEP·HCl (4 eq) solution in PBS was added. The protein underwent disulfide reduction for 1 hour at 37 ºC. Next, 5 µL of **3** or **4** were added to the solution at either 1.3 eq or 3 eq, with all PEG stock solutions prepared in MeCN. The reactions were allowed to proceed at either 23 ºC or 37 ºC for 3 hours. Then, the samples underwent the general SDS-PAGE sample preparation procedure as described above.

**Extended Time Screen**

To a 50 µL solution of T4L at 76 µM, 5 µL of a 3 mM TCEP·HCl (4 eq) solution in PBS was added. The protein underwent disulfide reduction for 1 hour at 37 ºC. Next, 5 µL of **3** or **4** were added to the solution at either 1.3 eq or 3 eq, with all PEG stock solutions prepared in MeCN. The reactions were allowed to proceed at either 23 ºC or 37 ºC for 18 hours, then the samples underwent the general SDS-PAGE sample preparation procedure as described above.

**Circular Dichroism (CD) and Stability Assessment**

T4L and purified **5** and **6** were diluted to 7 µM in 300 µL total volume of PBS buffer (pH 6.5). CD spectra were taken ranging from 200-280 nm at 25 °C. Thermal denaturation analysis was performed by calculating the relative helicity ((mdeg-$mdeg_{min}$)/$mdeg_{max}$) at 223 nm from 20 – 100 °C.

**Activity Assay**

The lysozyme activity assay was conducted using the Invitrogen™ ENZChek™ lysozyme assay kit with minor modifications to the manufacturer instructions. Specifically, 50 µL of T4L, **5**, and **6** at 7 µM were pipetted into a 96 well plate. Sample concentration was determined *via* A280 (Extinction coefficient = 25,440 $M^{-1}$ $cm^{-1}$). For each sample, three replicates were performed. Then, 20 µL of a 5% solution fluorescein-labeled *Micrococcus luteus* in PBS (pH 6.5) was added to each well. The plate was incubated at 37 ºC for 30 minutes. Fluorescein fluorescence from cell lysis was measured (Excitation 490 nm, emission 530 nm). All activity values are reported relative to fresh unmodified T4L activity.

**ICP-OES Analysis**

Measurements were performed on an Agilent 5110 ICP-OES (Inductively coupled plasma-optical emission spectrometer). A Sigma-Aldrich 1000 ppm (Lot value: 999 ppm ± 2 ppm, 5% w/w HCl) Gold Standard for ICP was used as a stock solution to create standards of concentrations 50 ppb, 100 ppb, and 1000 ppb. Solutions were prepared using volumetric flasks, volumetric pipettes, and an Eppendorf pipette for aliquoting of the Au stock solution. A calibration curve was generated for each standard by integrating the signal corresponding to the characteristic Au emission (242.79 nm). A Yttrium internal standard (2 ppm in 2% $HNO_3$) was run simultaneously with all samples and the characteristic Y emission was measured at 371.03 nm.

Samples **5** and **6** were each quantitatively transferred with multiple washes of MilliQ water to a 14 mL Falcon tube, acidified by the addition of 0.2 mL $HNO_3$ (FisherChemical Trace Metal Grade Nitric Acid; certified [Au] < 0.1 ppb) and diluted to a total volume of 4.0 mL with MilliQ water. This solution was sonicated for 5 minutes and then immediately analyzed. No Au was

detected within the range of the calibration curve, indicating [Au] < 50 ppb in each sample, which is near the lower detection limit for this instrument.

**Molecular Dynamics Simulations**

Molecular dynamics (MD) simulations were performed using Amber 22 program and AmberTools 23 packages.[134] For the MD simulations, the protein structure from x-ray diffraction was used for the simulations (PDB code: 2HUK).[135] Hydrogen atoms were added using Protein Plus and Protoss online server.[136,137] MD simulations in explicit water were performed using the GPU accelerated code (pmemd).[138,139] For the protein scaffold, Amber 19 force field (ff19SB) parameters were applied.[140] OPC4 parameters were assigned to water molecules.[141] The partial charges of the C131 and PEG polymer were set to fit the electrostatic potential generated at the HF/6-31G(d)[142,143] level of theory by the RESP (restrained electrostatic potential) method using models systems (Figure S16).[144] The charges were calculated according to the Merz-Singh-Kollman scheme[145,146] using Gaussian 16 program package.[147] Long-range electrostatic effects were modeled using the particle mesh Ewald method with periodic boundary conditions.[148] An 8 Å cutoff was applied to Lennard-Jones and electrostatic interactions. The polymer chain was manually attached to C131 residue. To relax the polymer conformation, the system was first minimized with a maximum cycle of 10000 under GBSA implicit solvent model[149] with positional restraints (500 kcal $mol^{-1}$ $Å^{-2}$) applied to peptide backbone atoms (C, $C_\alpha$, N), and then heated from 0 K to 300 K within 2 ns in an NVT ensemble with positional restraints (30 kcal $mol^{-1}$ $Å^{-2}$) on all peptide backbone atoms (C, $C_\alpha$, N). The system was then placed in a pre-equilibrated octahedral box with a 10 Å buffer of OPC4 water molecules using the tleap module. The systems were neutralized by addition of explicit counter ions ($Cl^-$). Molecular dynamics simulations were performed according to the following steps. (1) Each system was minimized over 5,000 steps with

positional restraints (500 kcal $mol^{-1}$ $Å^{-2}$) applied to all atoms except water molecules and chloride ions, followed by an energy minimization over 5,000 steps with positional restraints (2.0 kcal $mol^{-1}$ $Å^{-2}$) on all peptide backbone atoms (C, $C_\alpha$, N). (2) The positional restraint of the ligand was removed. A 300 ps heating process was performed with periodic boundary for constant volume (NVT) with SHAKE algorithm turned on. Positional restraints (30 kcal $mol^{-1}$ $Å^{-2}$) were applied on all peptide backbone atoms (C, $C_\alpha$, N). (3) A 2 ns equilibrium process was performed with periodic boundary for constant pressure (NPT) and with a constant temperature of 300 K with high positional restraints (30 kcal $mol^{-1}$ $Å^{-2}$) on all peptide backbone atoms (C, $C_\alpha$, N). (4) A 2 ns equilibrium process was performed with constant pressure (NPT) and with a constant temperature of 300 K with low positional restraints (0.5 kcal $mol^{-1}$ $Å^{-2}$) on all peptide backbone atoms (C, $C_\alpha$, N). (5) To further relax the polymer, we then annealed the system by heating it from 300 K to 400 K, and then cooling it back to 300 K in 400 ps. The annealing cycle was repeated 10 times. Positional restraints (30 kcal $mol^{-1}$ $Å^{-2}$) were applied on all peptide backbone atoms (C, $C_\alpha$, N). (5) Three independent 1000 ns production runs were performed applying the standard simulation condition for constant pressure (NPT) and with a constant temperature of 300 K. Structures were visualized using ChimeraX[150] and VMD.[151]

# 3.6 Appendix II

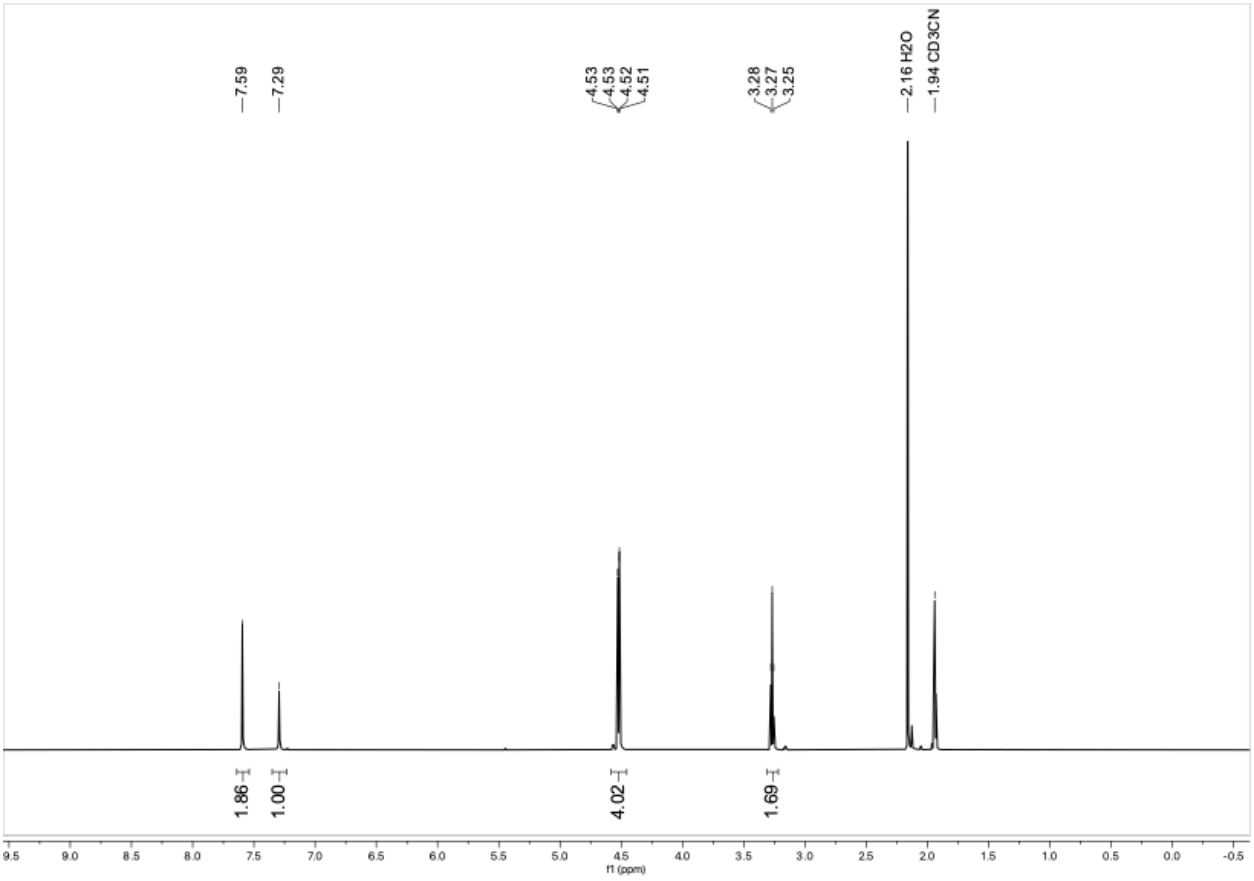


**Figure 3.5** $^{1}$H NMR of (5-iodo-1,3-phenylene)dimethanol (**7**) in $CD_3CN$ at 23 ºC.

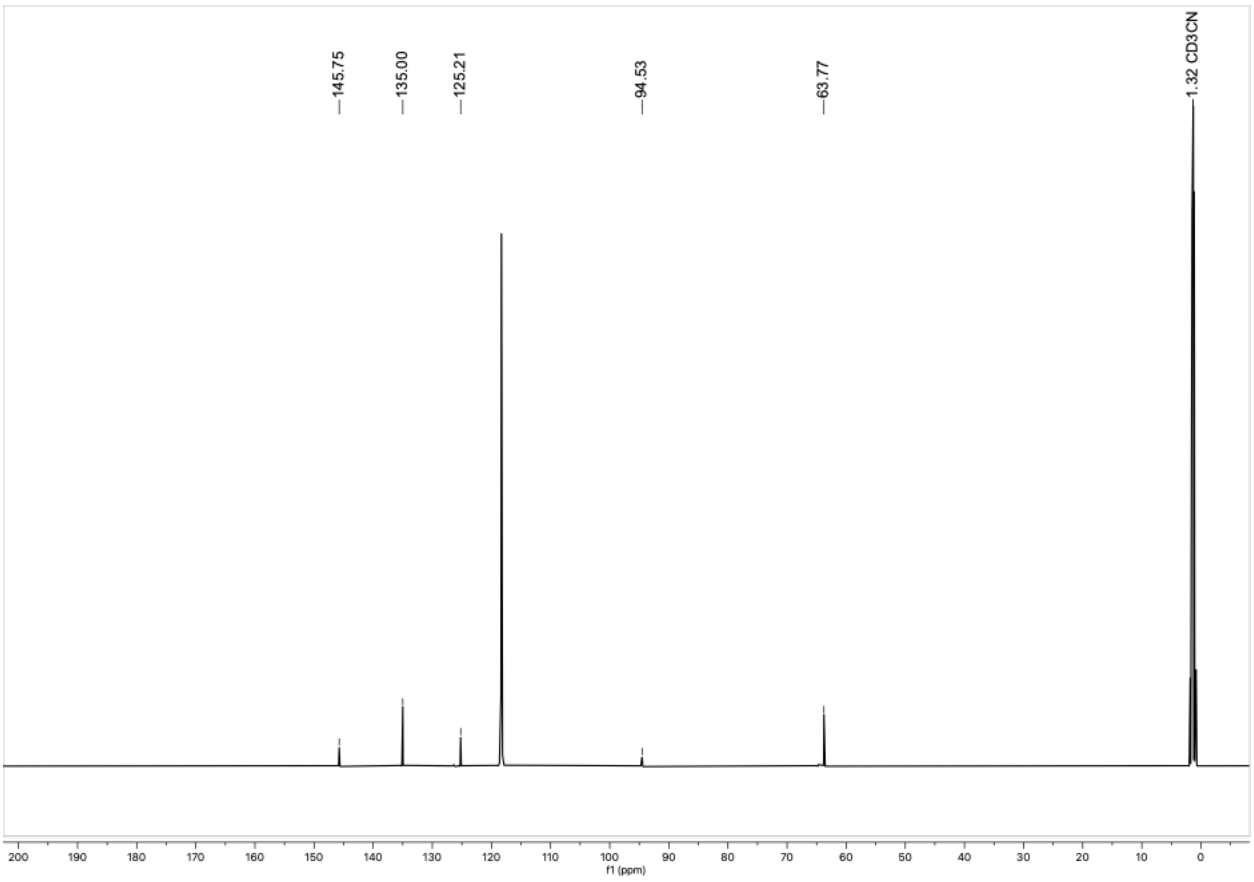


**Figure 3.6** $^{13}C$ NMR of (5-iodo-1,3-phenylene)dimethanol (**7**) in $CD_3CN$ at 23 ºC.

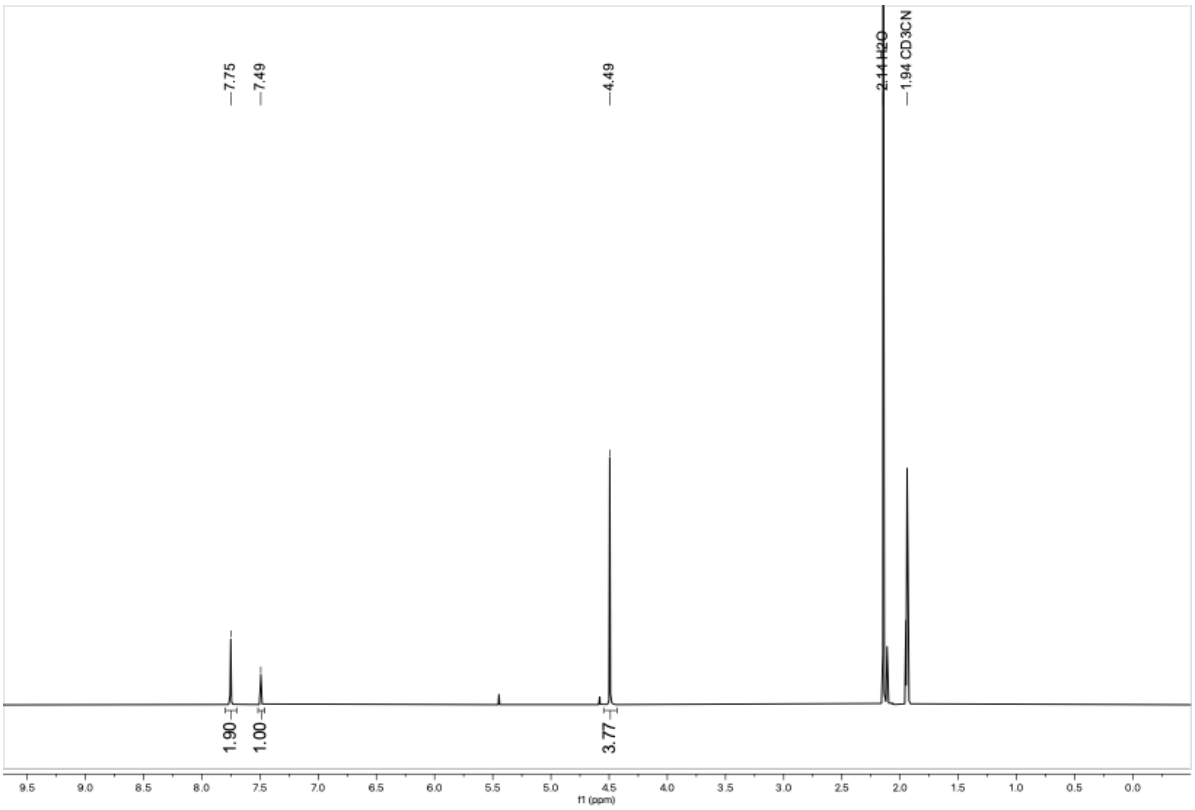


**Figure 3.7** $^{1}$H NMR of 1,3-bis(bromomethyl)-5-iodobenzene (**1**) in $CD_3CN$ at 23 ºC.

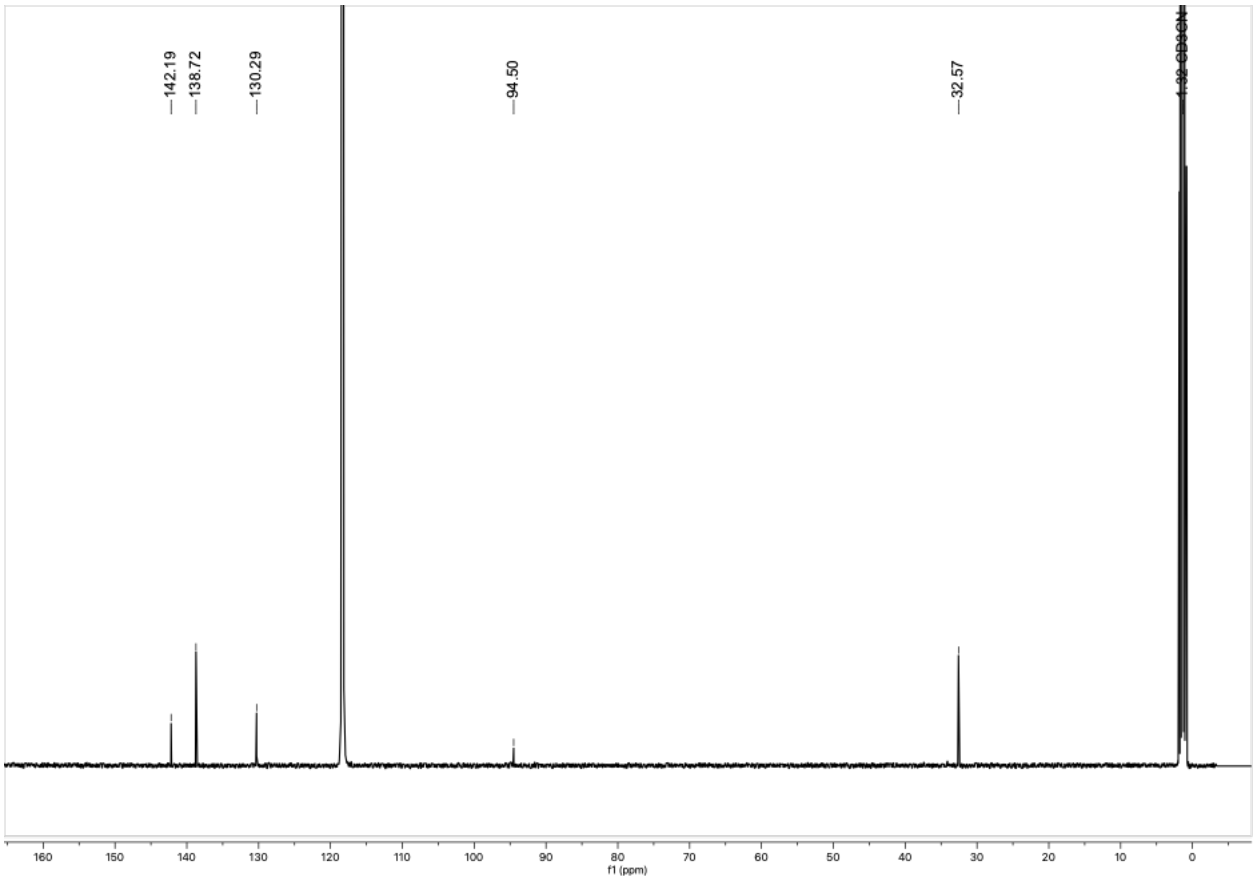


**Figure 3.8** $^{13}C$ NMR of 1,3-bis(bromomethyl)-5-iodobenzene (**1**) in $CD_3CN$ at 23 ºC.

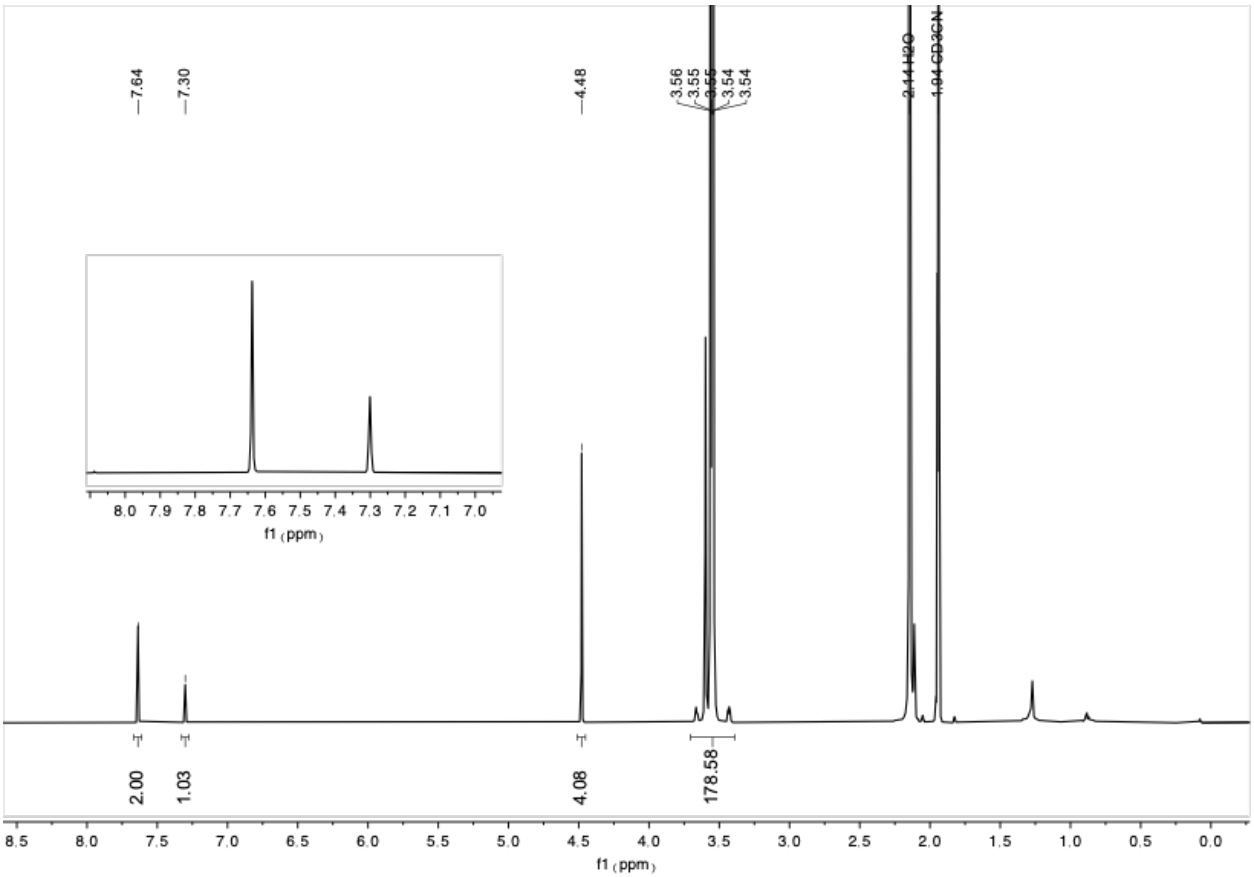


**Figure 3.9** $^{1}$H NMR of cyclic PEG (2 kDa)-aryl iodide (**2**) in $CD_3CN$ at 23 ºC. Note that this data is shown in Figure 3.1 within Chapter 3 but is also shown larger here for easier viewing.

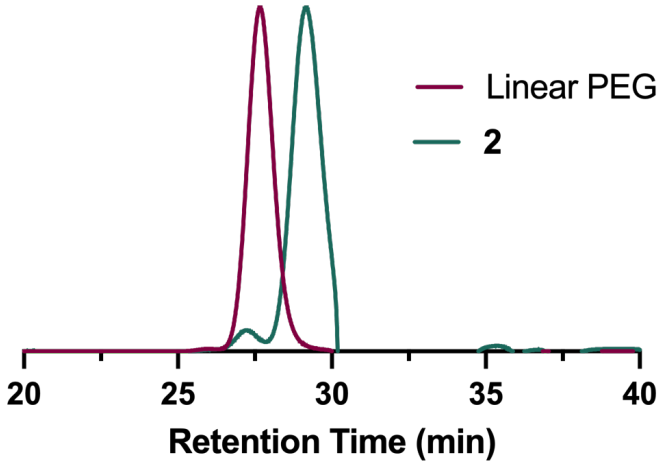


**Figure 3.10** DMF SEC of cyclic PEG (2 kDa)-aryl iodide (**2**) and commercial linear PEG (2 kDa). Note that this data is shown in Figure 3.1 within Chapter 3 but is also shown larger here for easier viewing. The SEC analysis for **2** is as follows: $M_n$ – 2.3 kDa, $M_w$ – 2.6 kDa, ~~$Đ$~~ – 1.15.

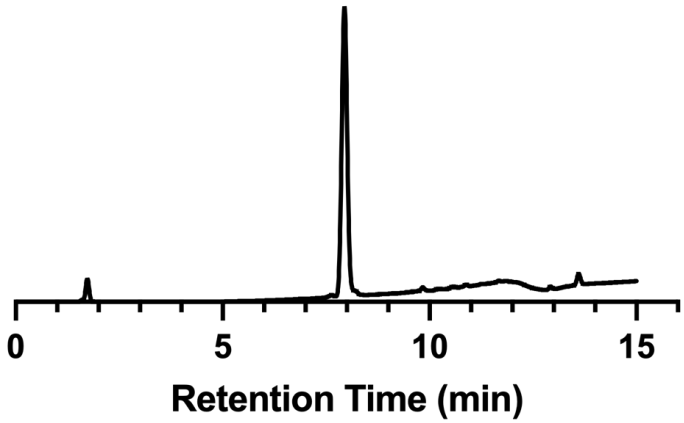


**Figure 3.11** Analytical HPLC of cyclic PEG (2 kDa)-aryl iodide (**2**) at 280 nm.

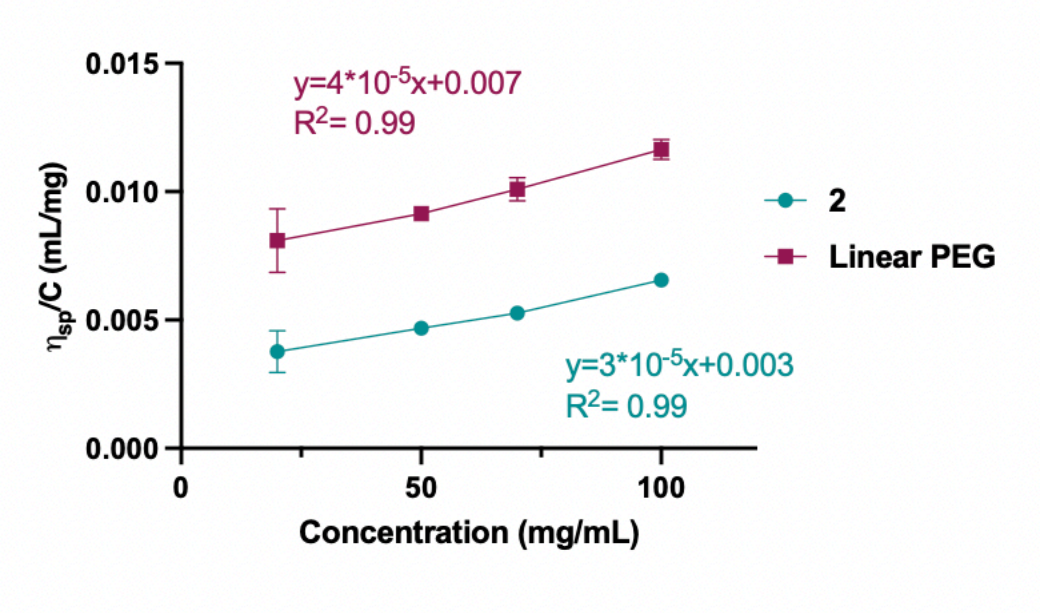


**Figure 3.12** Intrinsic viscosity of cyclic PEG (2 kDa)-aryl iodide (**2**) and linear mPEG (2 kDa)-aryl iodide. The y-intercepts represent the intrinsic viscosity [η] for **2** and linear mPEG (2 kDa)-aryl iodide as 0.003 and 0.007 mL/mg, respectively.

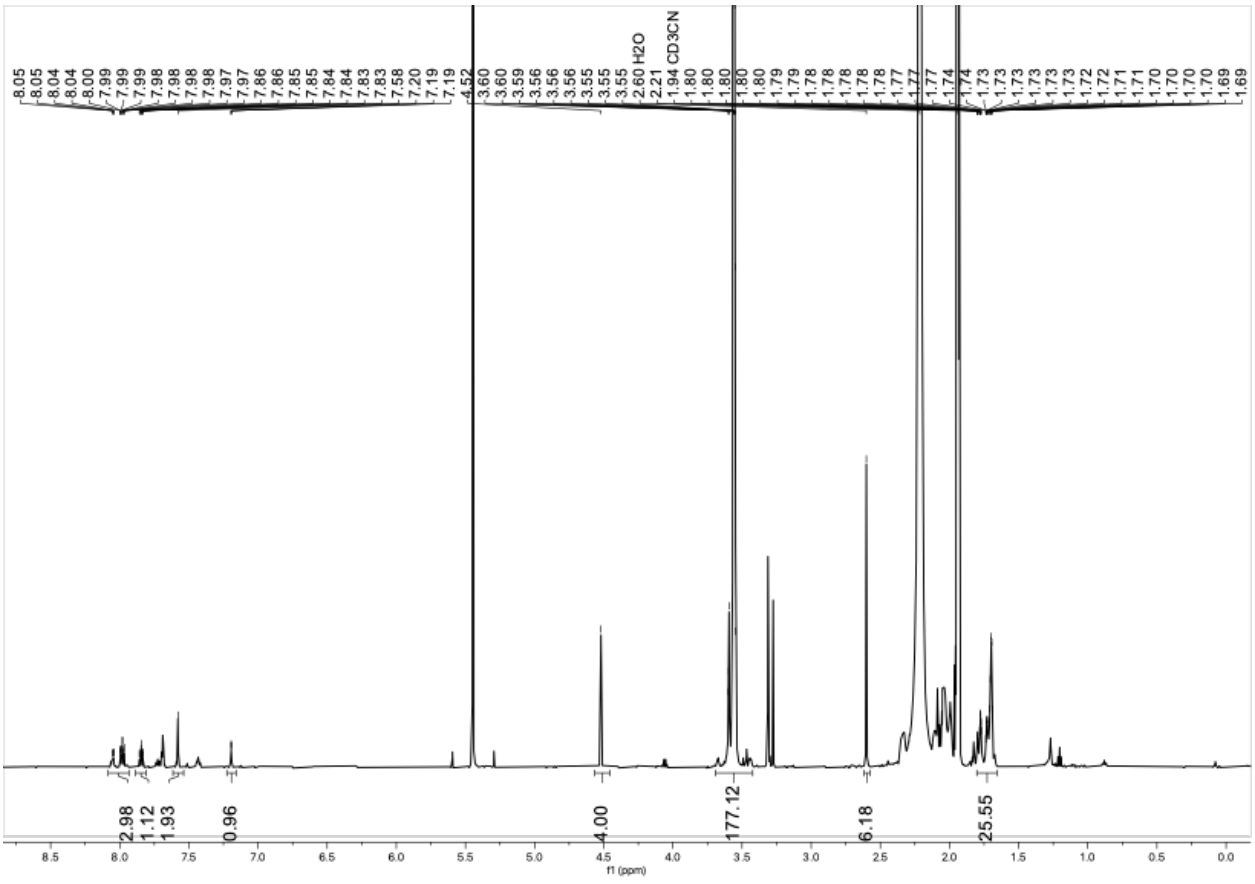


**Figure 3.13** $^{1}$H NMR of cyclic PEG (2 kDa) [(Me-DalPhos)AuCl][$SbF_6$] (**3**) in $CD_3CN$ at 23 ºC.

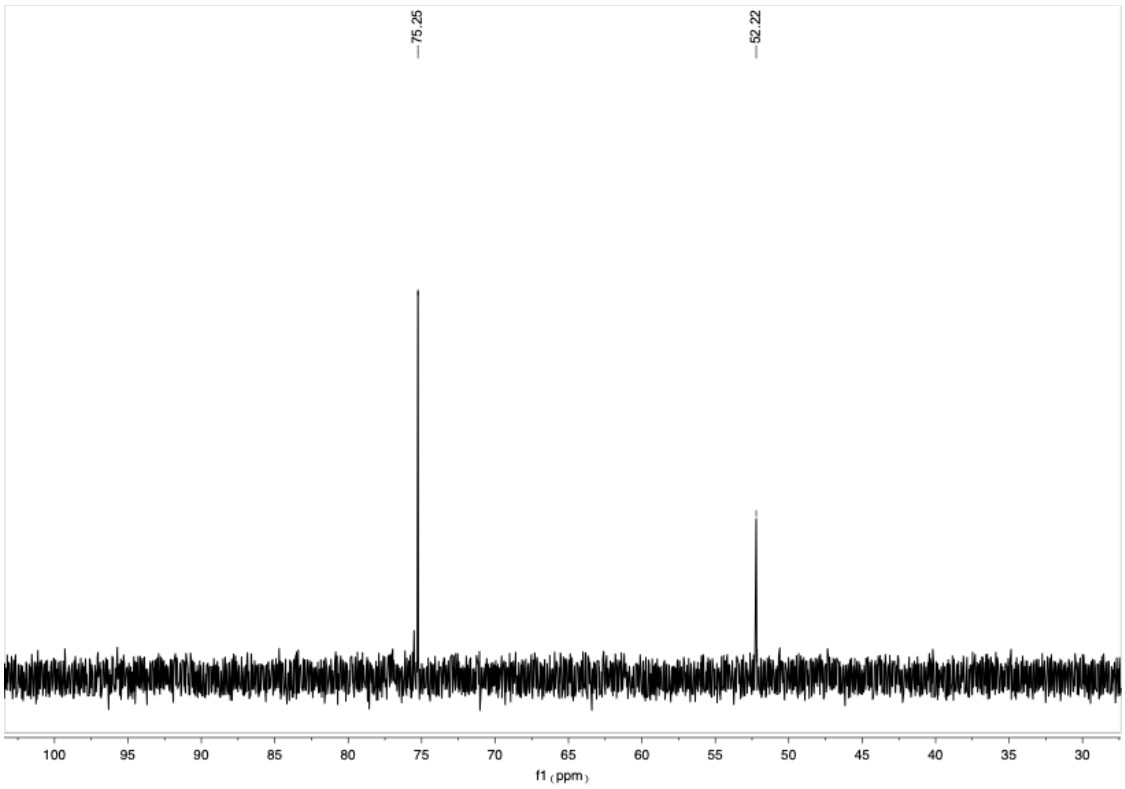


**Figure 3.14** $^{31}P\{^{1}H\}$ NMR of cyclic PEG (2 kDa) [(Me-DalPhos)AuCl][$SbF_6$] (**3**) in $CD_3CN$ at 23 ºC. The desired Au(III) resonance occurs at 75 ppm. The resonance at 52 ppm corresponds to residual (Me-DalPhos)Au(I)Cl starting material. Note that this data is shown in Figure 3.1 of within Chapter 3 but is also shown larger here for easier viewing.

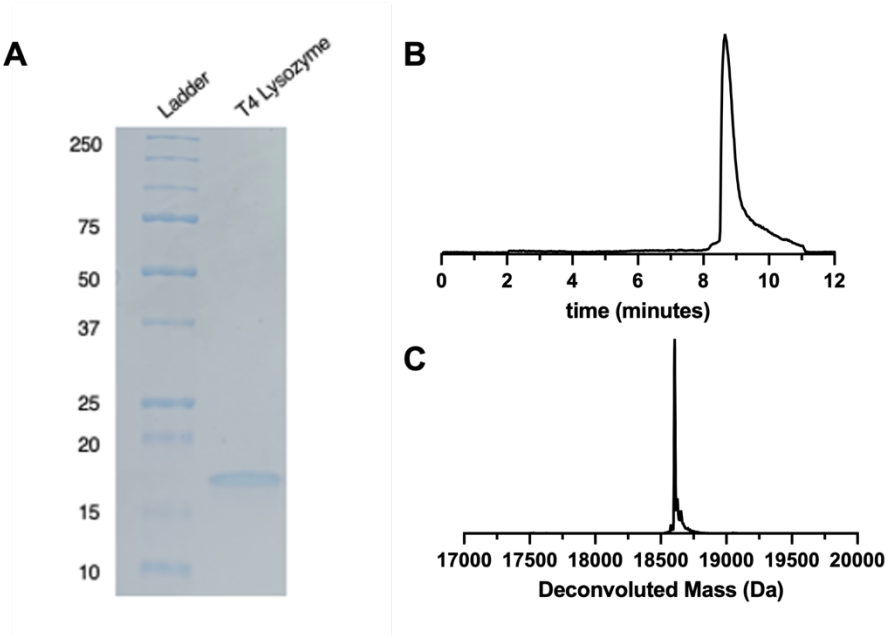


**Figure 3.15** A) SDS-PAGE gel of T4 lysozyme following purification. B) LCMS total ion chromatogram (TIC) of T4 lysozyme following purification. C) LCMS deconvoluted mass of T4 lysozyme following purification. Expected mass: 18605.27 Da. Observed mass: 18604.95 Da.

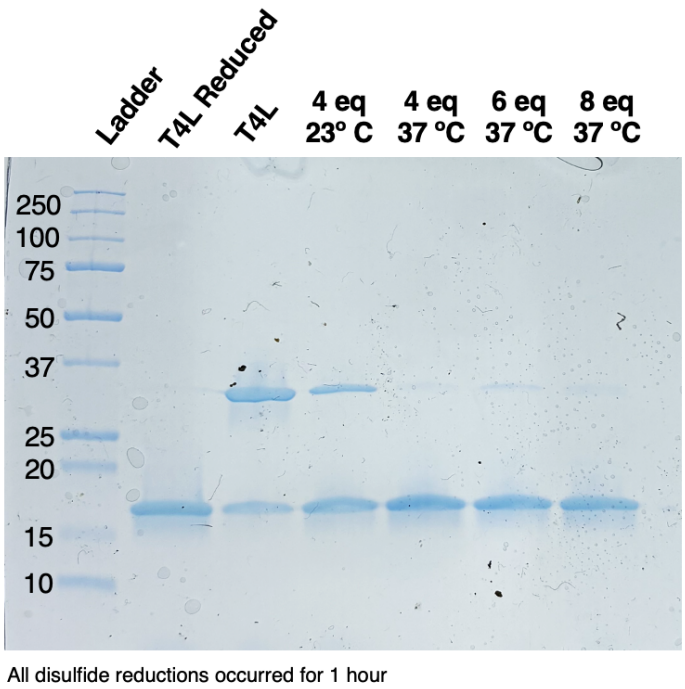


**Figure 3.16** SDS-PAGE of T4 lysozyme (T4L) in PBS buffer (pH 6.5) reduced with 4, 6, or 8 eq TCEP·HCl for 1 hour at either 23 ºC or 37 ºC. These samples were run in conventional Laemmli buffer (non-reducing).

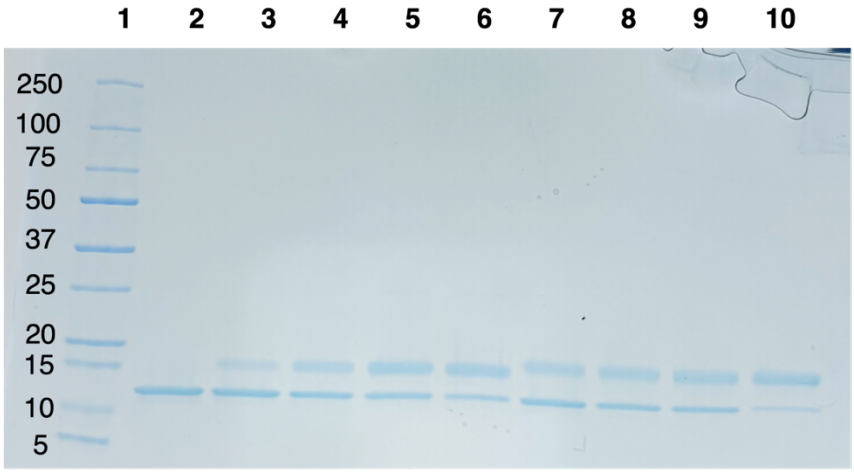


| Lane | Condition |
|---|---|
| 1 | Ladder |
| 2 | T4L-reduced |
| 3 | Cyclic PEG (**3**,1.3 eq), 23 ºC |
| 4 | Cyclic PEG (**3**,1.3 eq), 37 ºC |
| 5 | Cyclic PEG (**3**, 3 eq), 23 ºC |
| 6 | Cyclic PEG (**3**, 3 eq), 37 ºC |
| 7 | Linear mPEG (**4**, 1.3 eq), 23 ºC |
| 8 | Linear mPEG (**4**, 1.3 eq), 37 ºC |
| 9 | Linear mPEG (**4**, 3 eq), 23 ºC |
| 10 | Linear mPEG (**4**, 3 eq), 37 ºC |

All reductive eliminations occurred for 3 hours

**Figure 3.17** SDS-PAGE of crude T4L-PEG conjugates synthesized in PBS buffer (pH 6.5) for 3 hours, utilizing either 1.3 or 3 equivalents of **3** and **4** at either 23 ºC or 37 ºC. These samples were run in a reducing Laemmli buffer.

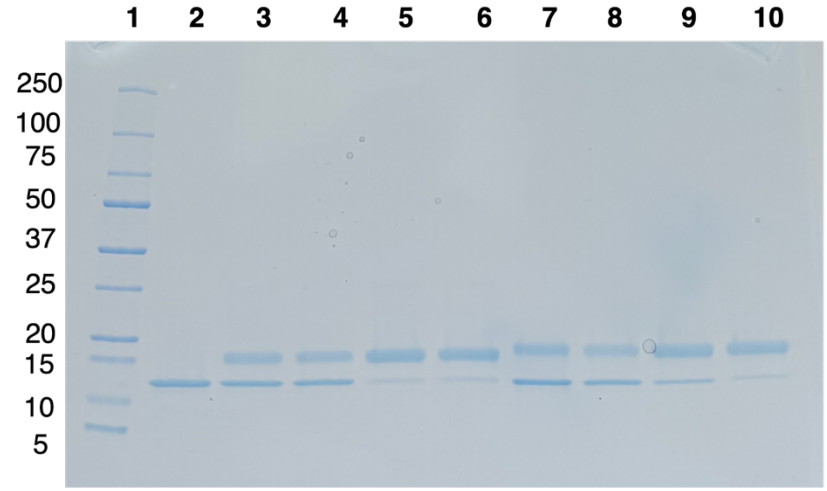


| Lane | Condition |
|---|---|
| 1 | Ladder |
| 2 | T4L-reduced |
| 3 | Cyclic PEG (**3**,1.3 eq), 23 ºC |
| 4 | Cyclic PEG (**3**,1.3 eq), 37 ºC |
| 5 | Cyclic PEG (**3**, 3 eq), 23 ºC |
| 6 | Cyclic PEG (**3**, 3 eq), 37 ºC |
| 7 | Linear mPEG (**4**, 1.3 eq), 23 ºC |
| 8 | Linear mPEG (**4**, 1.3 eq), 37 ºC |
| 9 | Linear mPEG (**4**, 3 eq), 23 ºC |
| 10 | Linear mPEG (**4**, 3 eq), 37 ºC |

All reductive eliminations occurred for 18 hours

**Figure 3.18** SDS-PAGE of crude T4L-PEG conjugates synthesized in PBS buffer (pH 6.5) for 18 hours, utilizing 1.3 or 3 equivalents of **3** and **4** at either 23 ºC or 37 ºC. These samples were run in a reducing Laemmli buffer.

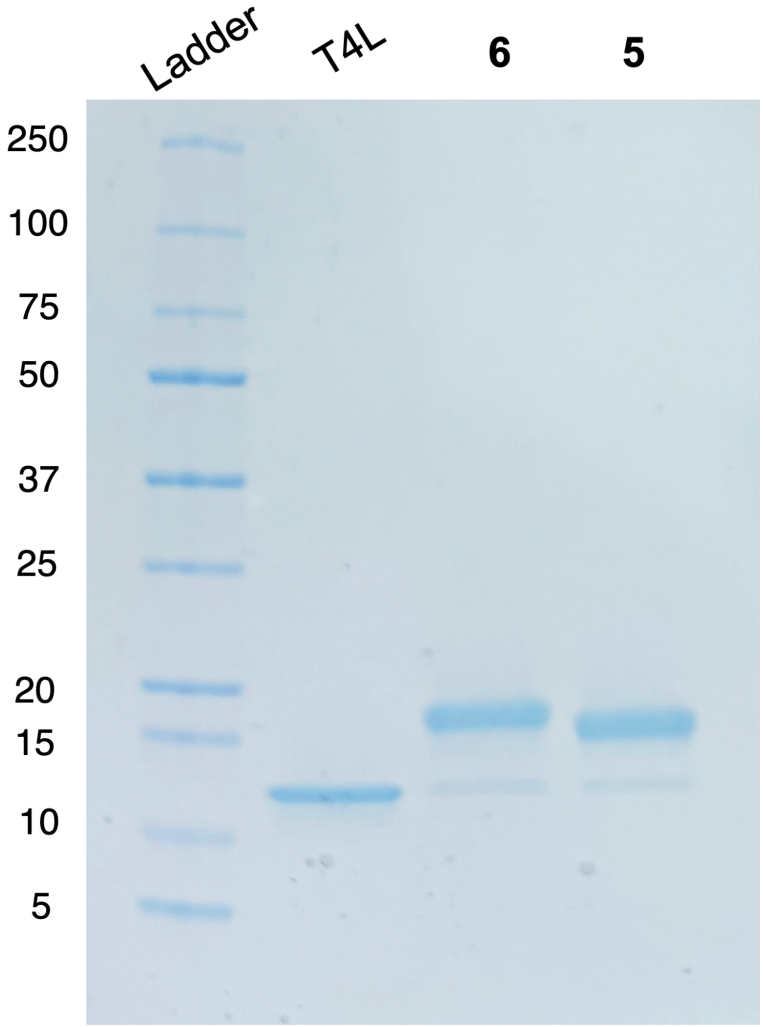


**Figure 3.19** SDS-PAGE of crude T4L-PEG conjugates **6** and **5** synthesized in PBS buffer (pH 6.5) for 18 hours at 23 ºC, utilizing 3 equivalents of **4** and **3**, respectively. These samples were run in a reducing Laemmli buffer. Based on ImageJ optical densitometry, conversion to conjugate **6** is 80% and conversion to **5** is 84%.

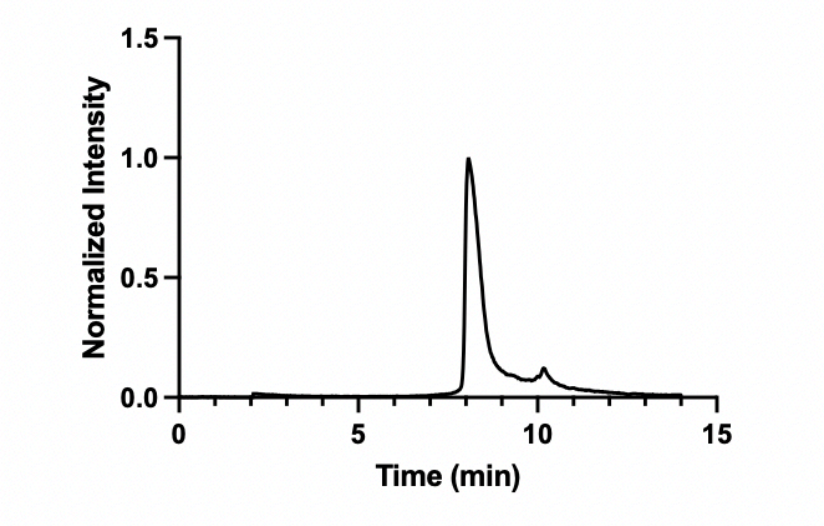


**Figure 3.20** LCMS total ion chromatogram (TIC) of T4L-cyclic PEG (**5**) following purification. The major peak at 8 min corresponds to the deconvoluted mass spectra shown in Figure 3.2 C. The minor peak at 10 min corresponds to 2 kDa PEG.

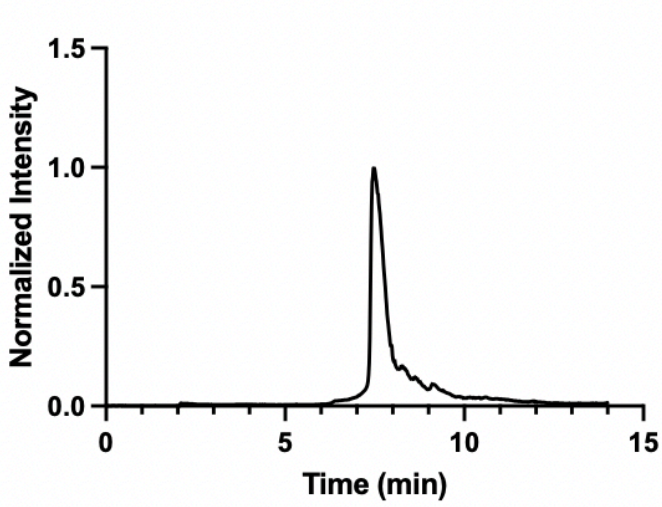


**Figure 3.21** LCMS total ion chromatogram (TIC) of T4L-linear PEG (**6**) following purification. The major peak at 7.5 min corresponds to the deconvoluted mass spectra shown in Figure 3.2 D.

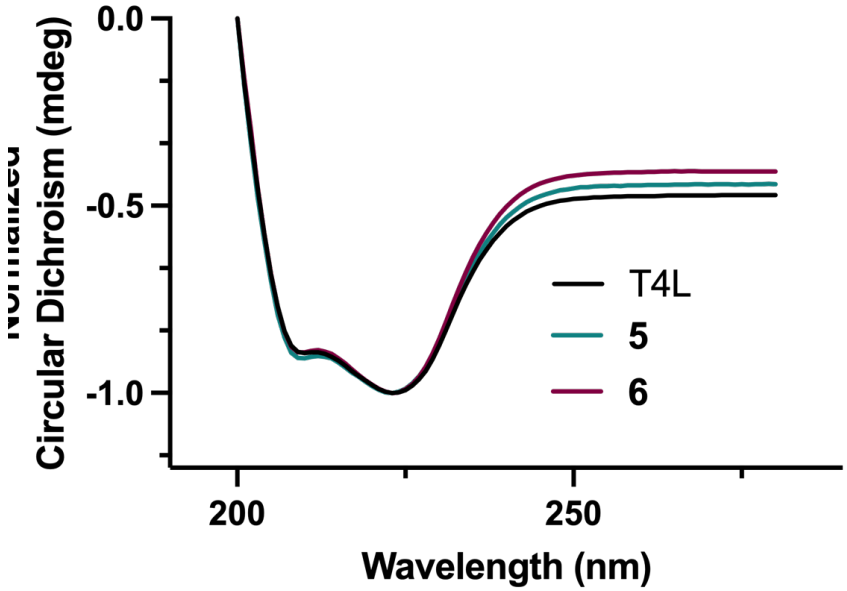


**Figure 3.22** CD spectrum of T4L and T4L conjugates (**5** and **6**) at 25 ºC showing no significant difference in helicity. Data has been normalized to the global minimum for each sample. Local minima for each sample are as follows – T4L: 210 and 223 nm, **5**: 209 and 223 nm, **6**: 210 and 223 nm. Note that this data is shown in Figure 3.3 but is also shown larger here for easier viewing.

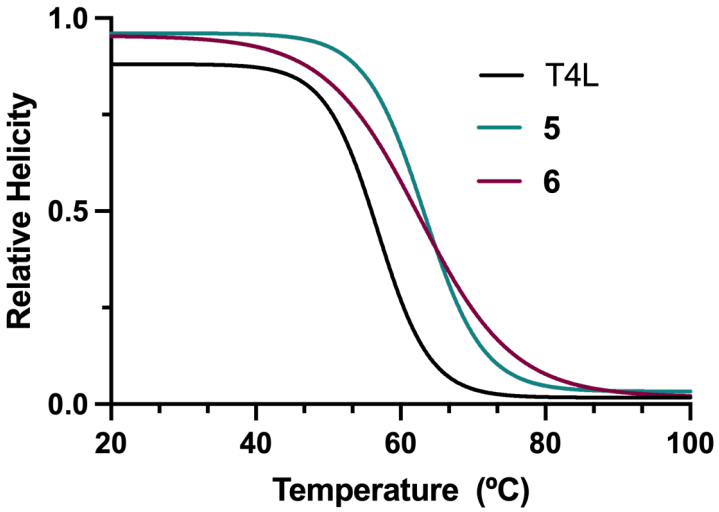


**Figure 3.23** CD thermal denaturation curves at 223 nm of T4L and T4L conjugates (**5** and **6**) showing no significant difference in melting temperature ($T_m$) between 20 – 100 °C. Specifically, $T_m$ values for each sample are as follows – T4L: 56.8 ºC, **5**: 63.2 ºC, **6**: 62.6 ºC.

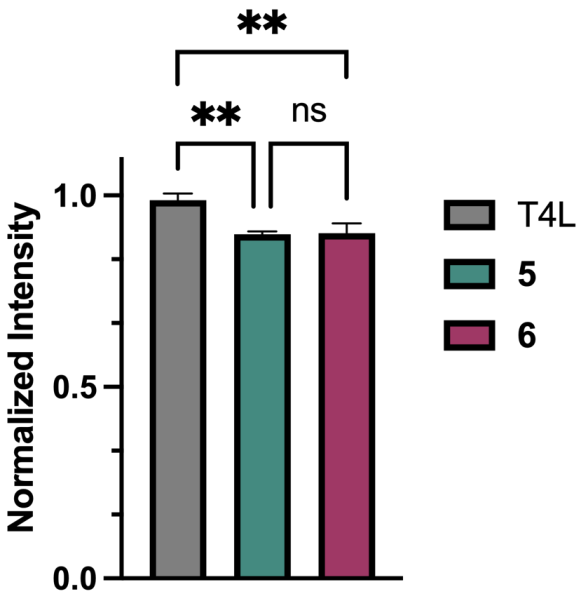


**Figure 3.24** Lysozyme activity assay fluorescence output of T4L, **5**, and **6**. N = 3 for each group. Ordinary one-way ANOVA statistical analysis was performed. **p < 0.005. ns = not significantly different. Note that this data is shown in Figure 3.4 but is also shown larger here for easier viewing.

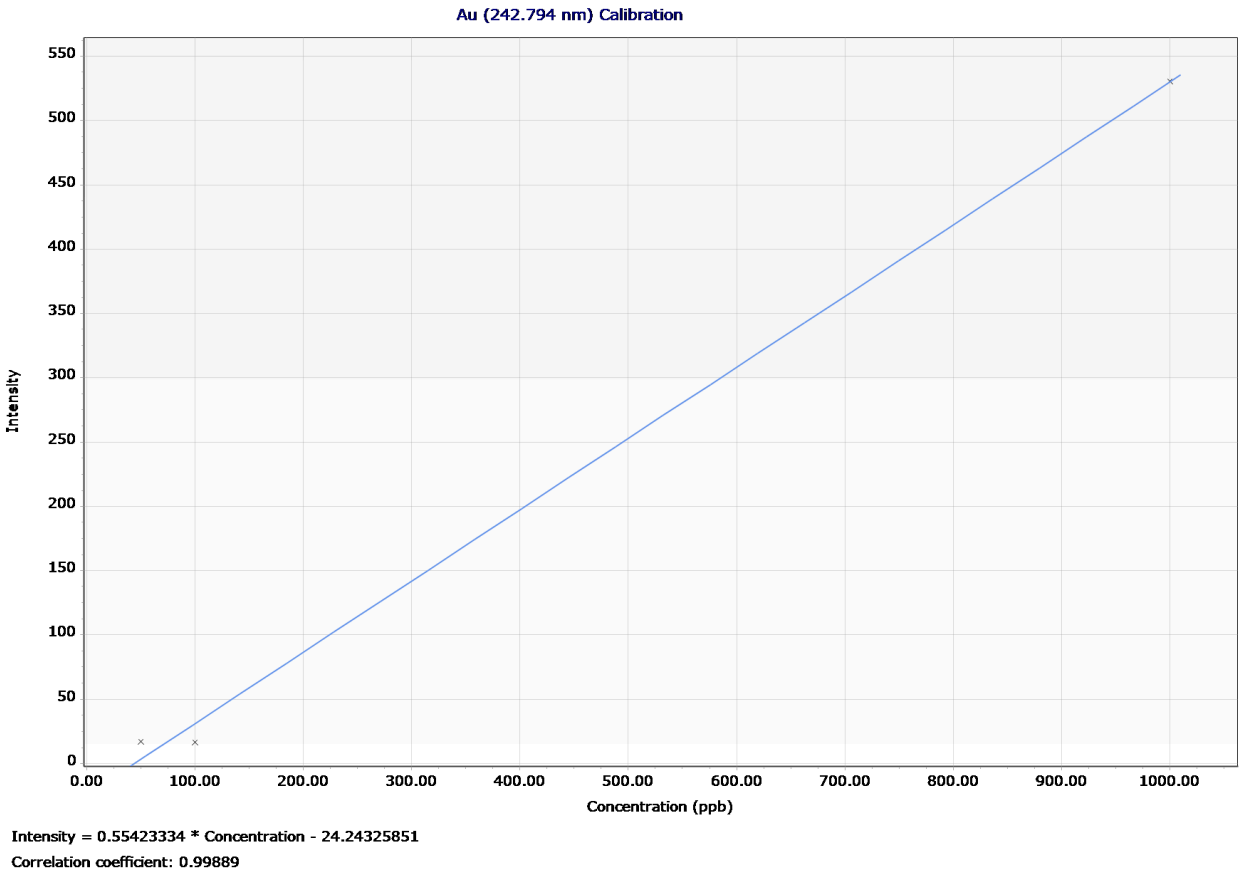


**Figure 3.25** ICP-OES Au calibration curve.

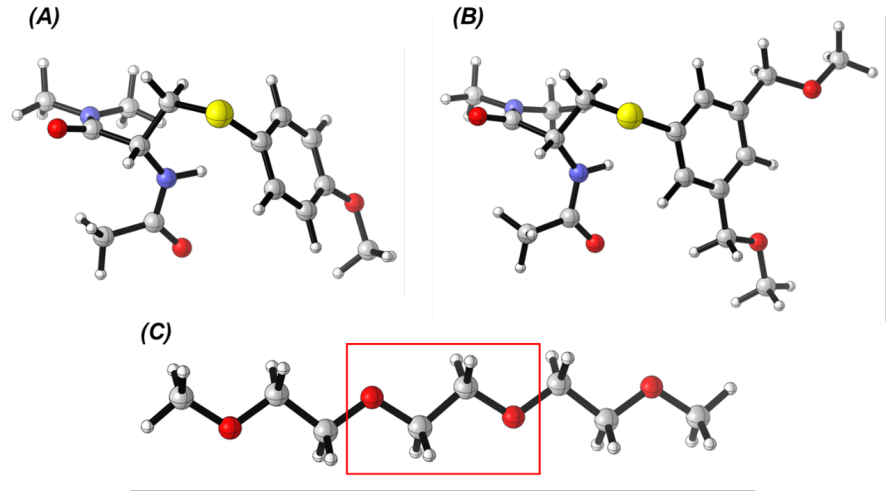


**Figure 3.26** Model systems used for RESP charge calculations. (A) Model system for C131 and phenyl linker in simulations for **6**. (B) Model system for C131 and phenyl linker in simulations for **5**. (C) Model system for PEG polymer. The RESP charges of the two units in the middle (shown in red box) were average and assigned to all the PEG units in the system. All the structures are optimized with B3LYP-D3/6-31G(d).

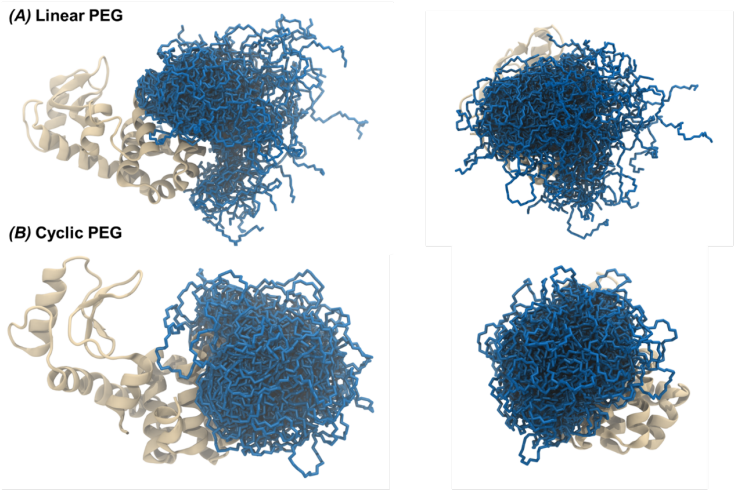


**Figure 3.27** Overlay of the trajectories. (A) Trajectories for **6**. (B) Trajectories for **5**. Left: front view, right: side view. Linear PEG polymer demonstrates more conformational flexibility in MD simulations compared to cyclic PEG conjugate.

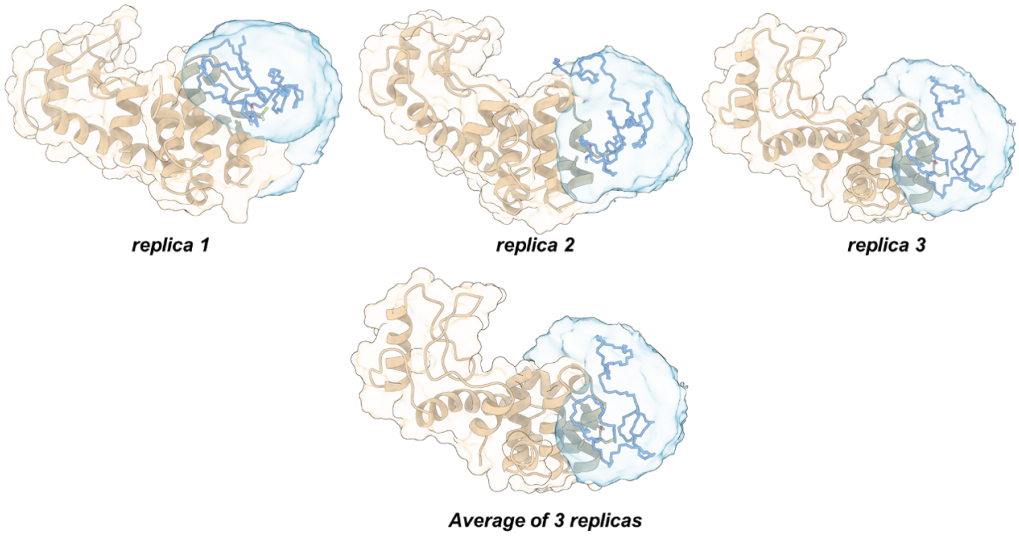


**Figure 3.28** Spatial distribution functions of linear PEG (Shown in light blue isosurface) and representative structures of simulations for **6**.

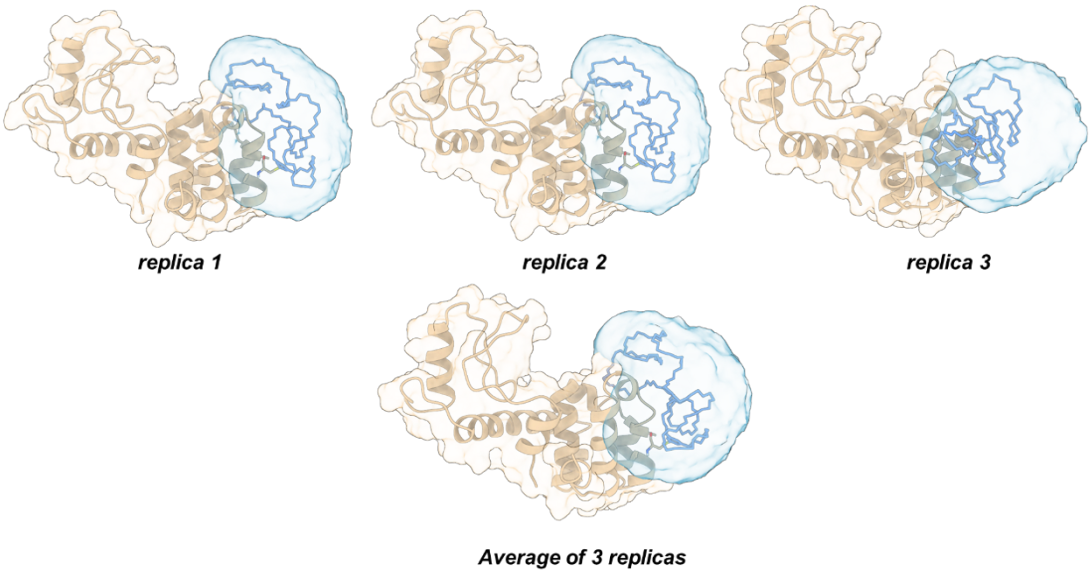


**Figure 3.29** Spatial distribution functions of cyclic PEG (Shown in light blue isosurface) and representative structures of simulations for **5**.

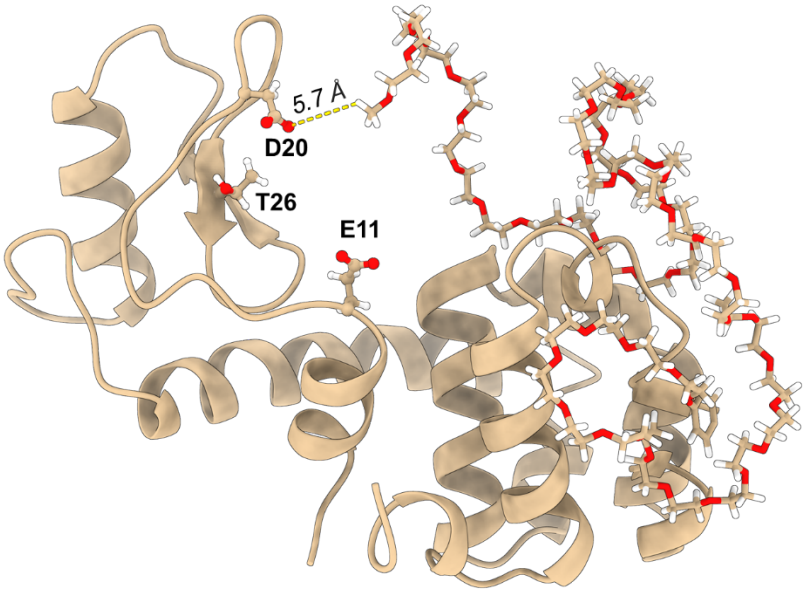


**Figure 3.30** Illustration of the minimum distance studied in Figures 3.28 and 3.29. The minimum distance is defined as the smallest distance between any pair of atoms from the active site and PEG polymer. As the picture shows, the minimum distance for this structure is the distance between the carboxylic oxygen in D20 and a hydrogen in PEG (labeled by yellow dashed line).

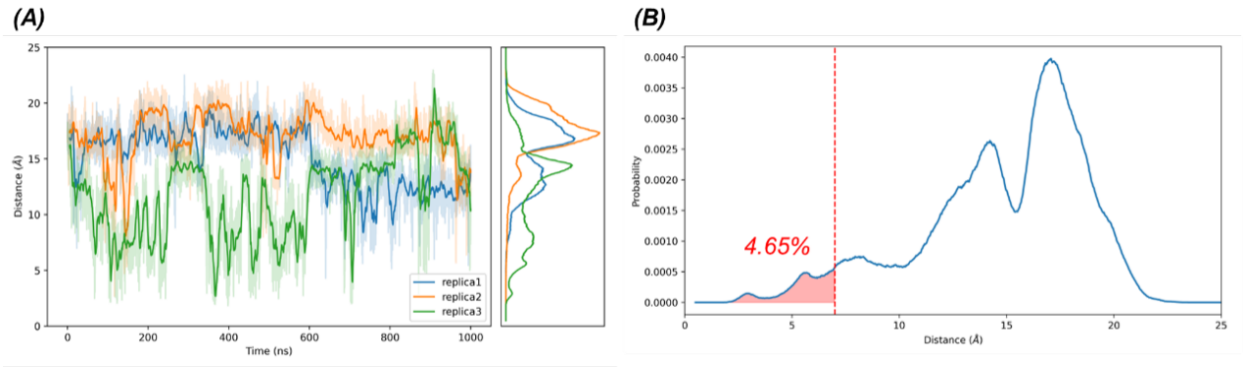


**Figure 3.31** (A) Minimum distance between active site (E11, D20, and T26) and PEG polymer along the simulations of **6**. Distribution of each is shown in the right panel. (B) Averaged distance distribution of three replicas, where 4.65% of the frames are considered having interaction between active site and PEG polymer (Minimum distance < 7.0 Å).

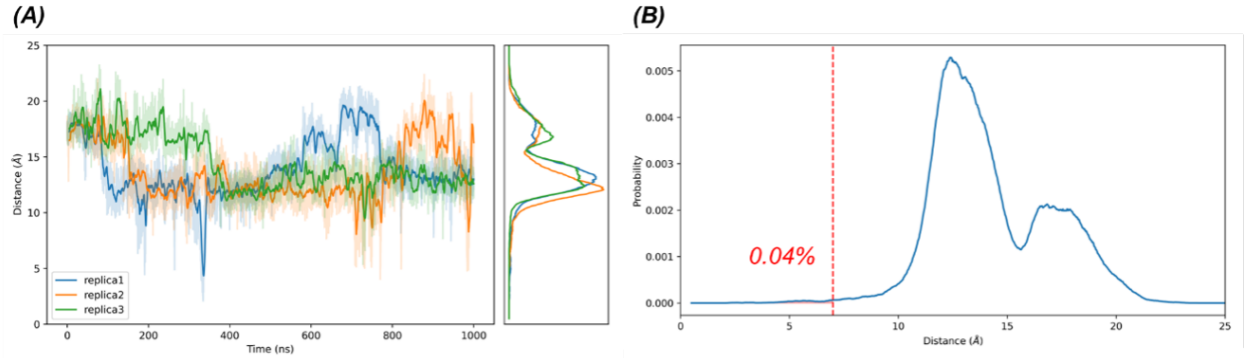


**Figure 3.32** (A) Minimum distance between active site (E11, D20, and T26) and PEG polymer along the simulations of **5**. Distribution of each replica is shown in the right panel. (B) Averaged distance distribution of three replicas, where 0.04% of the frames are considered having interaction between active site and PEG polymer (Minimum distance < 7.0 Å).

## 3.5 References

†This chapter, with copyright permission from ACS, contains a paper published as: **Kunkel, G. E.**; Zhou, Q.; Treacy, J. W.; Montgomery, H. R.; Salas-Ambrosio, P.; Ready, A. D.; Spokoyny, A. M.; Houk, K. N.; Maynard, H. D. Comparison of Cyclic and Linear PEG Conjugates. *Bioconjugate Chem.* **2024**, *35* (6), 744–749.

Molecular dynamics simulations can be accessed from the citation above.

(1) Lin, A.; Giuliano, C. J.; Palladino, A.; John, K. M.; Abramowicz, C.; Yuan, M. L.; Sausville, E. L.; Lukow, D. A.; Liu, L.; Chait, A. R.; Galluzzo, Z. C.; Tucker, C.; Sheltzer, J. M. Off-Target Toxicity Is a Common Mechanism of Action of Cancer Drugs Undergoing Clinical Trials. *Sci. Transl. Med.* **2019**, *11* (509), eaaw8412. https://doi.org/10.1126/scitranslmed.aaw8412.

(2) Senior, M. Fresh from the Biotech Pipeline: Fewer Approvals, but Biologics Gain Share. *Nat. Biotechnol.* **2023**, *41* (2), 174–182. https://doi.org/10.1038/s41587-022-01630-6.

(3) Xu, X.; Vugmeyster, Y. Challenges and Opportunities in Absorption, Distribution, Metabolism, and Excretion Studies of Therapeutic Biologics. *AAPS J.* **2012**, *14* (4), 781–791. https://doi.org/10.1208/s12248-012-9388-8.

(4) Zhao, L.; Ren, T.; Wang, D. D. Clinical Pharmacology Considerations in Biologics Development. *Acta Pharmacol. Sin.* **2012**, *33* (11), 1339–1347. https://doi.org/10.1038/aps.2012.51.

(5) Ko, J. H.; Maynard, H. D. A Guide to Maximizing the Therapeutic Potential of Protein–Polymer Conjugates by Rational Design. *Chem. Soc. Rev.* **2018**, *47* (24), 8998–9014. https://doi.org/10.1039/C8CS00606G.

(6) Wright, T. A.; Page, R. C.; Konkolewicz, D. Polymer Conjugation of Proteins as a Synthetic Post-Translational Modification to Impact Their Stability and Activity. *Polym. Chem.* **2019**, *10* (4), 434–454. https://doi.org/10.1039/C8PY01399C.

(7) Ozer, I.; Chilkoti, A. Site-Specific and Stoichiometric Stealth Polymer Conjugates of Therapeutic Peptides and Proteins. *Bioconjug. Chem.* **2017**, *28* (3), 713–723. https://doi.org/10.1021/acs.bioconjchem.6b00652.

(8) Gao, Y.; Joshi, M.; Zhao, Z.; Mitragotri, S. PEGylated Therapeutics in the Clinic. *Bioeng. Transl. Med.* **2024**, *9* (1), e10600. https://doi.org/10.1002/btm2.10600.

(9) Bendele, A.; Seely, J.; Richey, C.; Sennello, G.; Shopp, G. Short Communication: Renal Tubular Vacuolation in Animals Treated with Polyethylene-Glycol-Conjugated Proteins. *Toxicol. Sci.* **1998**, *42* (2), 152–157. https://doi.org/10.1093/toxsci/42.2.152.

(10) Chen, B.-M.; Cheng, T.-L.; Roffler, S. R. Polyethylene Glycol Immunogenicity: Theoretical, Clinical, and Practical Aspects of Anti-Polyethylene Glycol Antibodies. *ACS Nano* **2021**, *15* (9), 14022–14048. https://doi.org/10.1021/acsnano.1c05922.

(11) Pelegri-O'Day, E. M.; Lin, E.-W.; Maynard, H. D. Therapeutic Protein–Polymer Conjugates: Advancing Beyond PEGylation. *J. Am. Chem. Soc.* **2014**, *136* (41), 14323–14332. https://doi.org/10.1021/ja504390x.

(12) Liu, B.; Rodriguez, J.; Kilgallon, L. J.; Wang, W.; Wang, Y.; Wang, A.; Dai, Y.; Nguyen, H. V.-T.; Pentelute, B. L.; Johnson, J. A. An Organometallic Swap Strategy for Bottlebrush Polymer–Protein Conjugate Synthesis. *Chem. Commun.* **2024**, *60* (31), 4238–4241. https://doi.org/10.1039/D4CC00293H.

(13) Magnusson, J. P.; Bersani, S.; Salmaso, S.; Alexander, C.; Caliceti, P. In Situ Growth of Side-Chain PEG Polymers from Functionalized Human Growth Hormone—A New

Technique for Preparation of Enhanced Protein−Polymer Conjugates. *Bioconjug. Chem.* **2010**, *21* (4), 671–678. https://doi.org/10.1021/bc900468v.

(14) Monfardini, C.; Schiavon, O.; Caliceti, P.; Morpurgo, M.; Harris, J. M.; Veronese, F. M. A Branched Monomethoxypoly(Ethylene Glycol) for Protein Modification. *Bioconjug. Chem.* **1995**, *6* (1), 62–69. https://doi.org/10.1021/bc00031a006.

(15) Dutta, S.; Wade, M. A.; Walsh, D. J.; Guironnet, D.; Rogers, S. A.; Sing, C. E. Dilute Solution Structure of Bottlebrush Polymers. *Soft Matter* **2019**, *15* (14), 2928–2941. https://doi.org/10.1039/C9SM00033J.

(16) Gürel, U.; Giuntoli, A. Shear Thinning from Bond Orientation in Model Unentangled Bottlebrush Polymer Melts. *Macromolecules* **2023**, *56* (15), 5708–5717. https://doi.org/10.1021/acs.macromol.3c01061.

(17) Turecek, P. L.; Bossard, M. J.; Schoetens, F.; Ivens, I. A. PEGylation of Biopharmaceuticals: A Review of Chemistry and Nonclinical Safety Information of Approved Drugs. *J. Pharm. Sci.* **2016**, *105* (2), 460–475. https://doi.org/10.1016/j.xphs.2015.11.015.

(18) Haque, F. M.; Grayson, S. M. The Synthesis, Properties and Potential Applications of Cyclic Polymers. *Nat. Chem.* **2020**, *12* (5), 433–444. https://doi.org/10.1038/s41557-020-0440-5.

(19) Tu, X.-Y.; Liu, M.-Z.; Wei, H. Recent Progress on Cyclic Polymers: Synthesis, Bioproperties, and Biomedical Applications. *J. Polym. Sci. Part Polym. Chem.* **2016**, *54* (11), 1447–1458. https://doi.org/10.1002/pola.28051.

(20) Shire, S. J.; Shahrokh, Z.; Liu, J. Challenges in the Development of High Protein Concentration Formulations. *J. Pharm. Sci.* **2004**, *93* (6), 1390–1402. https://doi.org/10.1002/jps.20079.

(21) Pham, N. B.; Meng, W. S. Protein Aggregation and Immunogenicity of Biotherapeutics. *Int. J. Pharm.* **2020**, *585*, 119523. https://doi.org/10.1016/j.ijpharm.2020.119523.

(22) Messina, M. S.; Stauber, J. M.; Waddington, M. A.; Rheingold, A. L.; Maynard, H. D.; Spokoyny, A. M. Organometallic Gold(III) Reagents for Cysteine Arylation. *J. Am. Chem. Soc.* **2018**, *140* (23), 7065–7069. https://doi.org/10.1021/jacs.8b04115.

(23) Montgomery, H. R.; Messina, M. S.; Doud, E. A.; Spokoyny, A. M.; Maynard, H. D. Organometallic S-Arylation Reagents for Rapid PEGylation of Biomolecules. *Bioconjug. Chem.* **2022**, *33* (8), 1536–1542. https://doi.org/10.1021/acs.bioconjchem.2c00280.

(24) Doud, E. A.; Tilden, J. A. R.; Treacy, J. W.; Chao, E. Y.; Montgomery, H. R.; Kunkel, G. E.; Olivares, E. J.; Adhami, N.; Kerr, T. A.; Chen, Y.; Rheingold, A. L.; Loo, J. A.; Frost, C. G.; Houk, K. N.; Maynard, H. D.; Spokoyny, A. M. Ultrafast Au(III)-Mediated Arylation of Cysteine. *J. Am. Chem. Soc.* **2024**, *146* (18), 12365–12374. https://doi.org/10.1021/jacs.3c12170.

(25) Jeong, Y.; Jin, Y.; Chang, T.; Uhlik, F.; Roovers, J. Intrinsic Viscosity of Cyclic Polystyrene. *Macromolecules* **2017**, *50* (19), 7770–7776. https://doi.org/10.1021/acs.macromol.7b01511.

(26) Akram, M. O.; Das, A.; Chakrabarty, I.; Patil, N. T. Ligand-Enabled Gold-Catalyzed C(Sp2)–N Cross-Coupling Reactions of Aryl Iodides with Amines. *Org. Lett.* **2019**, *21* (19), 8101–8105. https://doi.org/10.1021/acs.orglett.9b03082.

(27) McCallum, T. Heart of Gold: Enabling Ligands for Oxidative Addition of Haloorganics in Au(I)/Au(III) Catalysed Cross-Coupling Reactions. *Org. Biomol. Chem.* **2023**, *21* (8), 1629–1646. https://doi.org/10.1039/D3OB00002H.

(28) Zeineddine, A.; Estévez, L.; Mallet-Ladeira, S.; Miqueu, K.; Amgoune, A.; Bourissou, D. Rational Development of Catalytic Au(I)/Au(III) Arylation Involving Mild Oxidative Addition of Aryl Halides. *Nat. Commun.* **2017**, *8* (1), 565. https://doi.org/10.1038/s41467-017-00672-8.

(29) Muratov, K.; Zaripov, E.; Berezovski, M. V.; Gagosz, F. DFT-Enabled Development of Hemilabile (P∧N) Ligands for Gold(I/III) RedOx Catalysis: Application to the Thiotosylation of Aryl Iodides. *J. Am. Chem. Soc.* **2024**, *146* (6), 3660–3674. https://doi.org/10.1021/jacs.3c08943.

(30) Sharma, S.; Ntetsikas, K.; Ladelta, V.; Bhaumik, S.; Hadjichristidis, N. Well-Defined Cyclic Polymer Synthesis via an Efficient Etherification-Based Bimolecular Ring-Closure Strategy. *Polym. Chem.* **2021**, *12* (45), 6616–6625. https://doi.org/10.1039/D1PY01337H.

(31) Kunkel, G. E.; Treacy, J. W.; Montgomery, H. R.; Puente, E. G.; Doud, E. A.; Spokoyny, A. M.; Maynard, H. D. Efficient End-Group Functionalization and Diblock Copolymer Synthesis *via* Au( III ) Polymer Reagents. *Chem. Commun.* **2024**, 10.1039.D3CC05350D. https://doi.org/10.1039/D3CC05350D.

(32) Columbus, L.; Kálai, T.; Jekö, J.; Hideg, K.; Hubbell, W. L. Molecular Motion of Spin Labeled Side Chains in α-Helices: Analysis by Variation of Side Chain Structure. *Biochemistry* **2001**, *40* (13), 3828–3846. https://doi.org/10.1021/bi002645h.

(33) Mchaourab, H. S.; Lietzow, M. A.; Hideg, K.; Hubbell, W. L. Motion of Spin-Labeled Side Chains in T4 Lysozyme. Correlation with Protein Structure and Dynamics. *Biochemistry* **1996**, *35* (24), 7692–7704. https://doi.org/10.1021/bi960482k.

(34) Pedersen, C. J. Cyclic Polyethers and Their Complexes with Metal Salts. *J. Am. Chem. Soc.* **1967**, *89* (10), 2495–2496. https://doi.org/10.1021/ja00986a052.

(35) Aboudzadeh, M. A.; Iturrospe, A.; Arbe, A.; Grzelczak, M.; Barroso-Bujans, F. Cyclic Polyethylene Glycol as Nanoparticle Surface Ligand. *ACS Macro Lett.* **2020**, *9* (11), 1604–1610. https://doi.org/10.1021/acsmacrolett.0c00730.

(36) Dunstan, D. E. The Viscosity-Radius Relationship for Concentrated Polymer Solutions. *Sci. Rep.* **2019**, *9* (1), 543. https://doi.org/10.1038/s41598-018-36596-6.

(37) Becktel, W. J.; Baase, W. A. Thermal Denaturation of Bacteriophage T4 Lysozyme at Neutral pH. *Biopolymers* **1987**, *26* (5), 619–623. https://doi.org/10.1002/bip.360260505.

(38) Veronese, F. M.; Mero, A. The Impact of PEGylation on Biological Therapies. *BioDrugs* **2008**, *22* (5), 315–329. https://doi.org/10.2165/00063030-200822050-00004.

(39) Fishburn, C. S. The Pharmacology of PEGylation: Balancing PD with PK to Generate Novel Therapeutics. *J. Pharm. Sci.* **2008**, *97* (10), 4167–4183. https://doi.org/10.1002/jps.21278.

(40) Wilding, K. M.; Smith, A. K.; Wilkerson, J. W.; Bush, D. B.; Knotts, T. A. I.; Bundy, B. C. The Locational Impact of Site-Specific PEGylation: Streamlined Screening with Cell-Free Protein Expression and Coarse-Grain Simulation. *ACS Synth. Biol.* **2018**, *7* (2), 510–521. https://doi.org/10.1021/acssynbio.7b00316.

(41) Lundgren, R. J.; Sappong-Kumankumah, A.; Stradiotto, M. A General Catalyst System for Amination of Aryl Chlorides. *Synfacts* **2010**, *2010* (05), 0580–0580. https://doi.org/10.1055/s-0029-1219677.

(42) Lorenzo, M. M.; Decker, C. G.; Kahveci, M. U.; Paluck, S. J.; Maynard, H. D. Homodimeric Protein–Polymer Conjugates via the Tetrazine–Trans-Cyclooctene Ligation. *Macromolecules* **2016**, *49* (1), 30–37. https://doi.org/10.1021/acs.macromol.5b02323.

(43) Case, D. A.; Aktulga, H. M.; Belfon, K.; Cerutti, D. S.; Cisneros, G. A.; Cruzeiro, V. W. D.; Forouzesh, N.; Giese, T. J.; Götz, A. W.; Gohlke, H.; Izadi, S.; Kasavajhala, K.; Kaymak,

M. C.; King, E.; Kurtzman, T.; Lee, T.-S.; Li, P.; Liu, J.; Luchko, T.; Luo, R.; Manathunga, M.; Machado, M. R.; Nguyen, H. M.; O'Hearn, K. A.; Onufriev, A. V.; Pan, F.; Pantano, S.; Qi, R.; Rahnamoun, A.; Risheh, A.; Schott-Verdugo, S.; Shajan, A.; Swails, J.; Wang, J.; Wei, H.; Wu, X.; Wu, Y.; Zhang, S.; Zhao, S.; Zhu, Q.; Cheatham, T. E. I.; Roe, D. R.; Roitberg, A.; Simmerling, C.; York, D. M.; Nagan, M. C.; Merz, K. M. Jr. AmberTools. *J. Chem. Inf. Model.* **2023**, *63* (20), 6183–6191. https://doi.org/10.1021/acs.jcim.3c01153.

(44) Banatao, D. R.; Cascio, D.; Crowley, C. S.; Fleissner, M. R.; Tienson, H. L.; Yeates, T. O. An Approach to Crystallizing Proteins by Synthetic Symmetrization. *Proc. Natl. Acad. Sci.* **2006**, *103* (44), 16230–16235. https://doi.org/10.1073/pnas.0607674103.

(45) Fährrolfes, R.; Bietz, S.; Flachsenberg, F.; Meyder, A.; Nittinger, E.; Otto, T.; Volkamer, A.; Rarey, M. ProteinsPlus: A Web Portal for Structure Analysis of Macromolecules. *Nucleic Acids Res.* **2017**, *45* (Web Server issue), W337–W343. https://doi.org/10.1093/nar/gkx333.

(46) Bietz, S.; Urbaczek, S.; Schulz, B.; Rarey, M. Protoss: A Holistic Approach to Predict Tautomers and Protonation States in Protein-Ligand Complexes. *J. Cheminformatics* **2014**, *6* (1), 12. https://doi.org/10.1186/1758-2946-6-12.

(47) Götz, A. W.; Williamson, M. J.; Xu, D.; Poole, D.; Le Grand, S.; Walker, R. C. Routine Microsecond Molecular Dynamics Simulations with AMBER on GPUs. 1. Generalized Born. *J. Chem. Theory Comput.* **2012**, *8* (5), 1542–1555. https://doi.org/10.1021/ct200909j.

(48) Salomon-Ferrer, R.; Götz, A. W.; Poole, D.; Le Grand, S.; Walker, R. C. Routine Microsecond Molecular Dynamics Simulations with AMBER on GPUs. 2. Explicit Solvent Particle Mesh Ewald. *J. Chem. Theory Comput.* **2013**, *9* (9), 3878–3888. https://doi.org/10.1021/ct400314y.

(49) Tian, C.; Kasavajhala, K.; Belfon, K. A. A.; Raguette, L.; Huang, H.; Migues, A. N.; Bickel, J.; Wang, Y.; Pincay, J.; Wu, Q.; Simmerling, C. ff19SB: Amino-Acid-Specific Protein Backbone Parameters Trained against Quantum Mechanics Energy Surfaces in Solution. *J. Chem. Theory Comput.* **2020**, *16* (1), 528–552. https://doi.org/10.1021/acs.jctc.9b00591.

(50) Izadi, S.; Anandakrishnan, R.; Onufriev, A. V. Building Water Models: A Different Approach. *J. Phys. Chem. Lett.* **2014**, *5* (21), 3863–3871. https://doi.org/10.1021/jz501780a.

(51) Ditchfield, R.; Hehre, W. J.; Pople, J. A. Self-Consistent Molecular-Orbital Methods. IX. An Extended Gaussian-Type Basis for Molecular-Orbital Studies of Organic Molecules. *J. Chem. Phys.* **1971**, *54* (2), 724–728. https://doi.org/10.1063/1.1674902.

(52) Hehre, W. J.; Ditchfield, R.; Pople, J. A. Self—Consistent Molecular Orbital Methods. XII. Further Extensions of Gaussian—Type Basis Sets for Use in Molecular Orbital Studies of Organic Molecules. *J. Chem. Phys.* **1972**, *56* (5), 2257–2261. https://doi.org/10.1063/1.1677527.

(53) Bayly, C. I.; Cieplak, P.; Cornell, W.; Kollman, P. A. A Well-Behaved Electrostatic Potential Based Method Using Charge Restraints for Deriving Atomic Charges: The RESP Model. *J. Phys. Chem.* **1993**, *97* (40), 10269–10280. https://doi.org/10.1021/j100142a004.

(54) Besler, B. H.; Merz Jr., K. M.; Kollman, P. A. Atomic Charges Derived from Semiempirical Methods. *J. Comput. Chem.* **1990**, *11* (4), 431–439. https://doi.org/10.1002/jcc.540110404.

(55) Singh, U. C.; Kollman, P. A. An Approach to Computing Electrostatic Charges for Molecules. *J. Comput. Chem.* **1984**, *5* (2), 129–145. https://doi.org/10.1002/jcc.540050204.

(56) Frisch, M. J.; Trucks, G. W.; Schlegel, H. B.; Scuseria, G. E.; Robb, M. A.; Cheeseman, J. R.; Scalmani, G.; Barone, V.; Petersson, G. A.; Nakatsuji, H.; Li, X.; Caricato, M.;

Marenich, A. V.; Bloino, J.; Janesko, B. G.; Gomperts, R.; Mennucci, B.; Hratchian, H. P.; Ortiz, J. V.; Izmaylov, A. F.; Sonnenberg, J. L.; Williams; Ding, F.; Lipparini, F.; Egidi, F.; Goings, J.; Peng, B.; Petrone, A.; Henderson, T.; Ranasinghe, D.; Zakrzewski, V. G.; Gao, J.; Rega, N.; Zheng, G.; Liang, W.; Hada, M.; Ehara, M.; Toyota, K.; Fukuda, R.; Hasegawa, J.; Ishida, M.; Nakajima, T.; Honda, Y.; Kitao, O.; Nakai, H.; Vreven, T.; Throssell, K.; Montgomery Jr., J. A.; Peralta, J. E.; Ogliaro, F.; Bearpark, M. J.; Heyd, J. J.; Brothers, E. N.; Kudin, K. N.; Staroverov, V. N.; Keith, T. A.; Kobayashi, R.; Normand, J.; Raghavachari, K.; Rendell, A. P.; Burant, J. C.; Iyengar, S. S.; Tomasi, J.; Cossi, M.; Millam, J. M.; Klene, M.; Adamo, C.; Cammi, R.; Ochterski, J. W.; Martin, R. L.; Morokuma, K.; Farkas, O.; Foresman, J. B.; Fox, D. J. Gaussian 16 Rev. C.01, 2016.

(57) Darden, T.; York, D.; Pedersen, L. Particle Mesh Ewald: An N·log(N) Method for Ewald Sums in Large Systems. *J. Chem. Phys.* **1993**, *98* (12), 10089–10092. https://doi.org/10.1063/1.464397.

(58) Onufriev, A.; Bashford, D.; Case, D. A. Exploring Protein Native States and Large-Scale Conformational Changes with a Modified Generalized Born Model. *Proteins* **2004**, *55* (2), 383–394. https://doi.org/10.1002/prot.20033.

(59) Pettersen, E. F.; Goddard, T. D.; Huang, C. C.; Meng, E. C.; Couch, G. S.; Croll, T. I.; Morris, J. H.; Ferrin, T. E. UCSF ChimeraX: Structure Visualization for Researchers, Educators, and Developers. *Protein Sci. Publ. Protein Soc.* **2021**, *30* (1), 70–82. https://doi.org/10.1002/pro.3943.

(60) Humphrey, W.; Dalke, A.; Schulten, K. VMD: Visual Molecular Dynamics. *J. Mol. Graph.* **1996**, *14* (1), 33–38, 27–28. https://doi.org/10.1016/0263-7855(96)00018-5.

# Chapter 4

# Access to Biomacromolecular Heterodimers *via* Regioselective Au(III) *S*-Arylation PEG Reagents

## 4.1 Introduction

Selective chemical labeling of proteins remains among the most popular tools used by researchers to probe and manipulate protein behavior across several fields such as molecular biology, proteomics, and biomedical chemistry.[4,152,153] As the specificity and tunability of these labeling techniques improves, complex macromolecular heterostructures become more accessible, thereby allowing researchers to study deeper intricacies of the protein space.[154] Cysteine residues are common targets for protein modification, due to their nucleophilicity and low proteomic abundance, which allows for more specific labeling.[37,152,155,156] Conventional cysteine modification techniques, such as Michael additions or pyridyl disulfide exchange are useful, but the reversibility of the forged bond can be non-ideal.[157–159] Alkylation of cysteine residues is generally irreversible, however, the kinetics of the reaction are relatively slow.[160] Alternatively, *S*-arylation chemistry provides a straightforward path toward hydrolytically resistant bioconjugate formation.[38,57]

Notably, palladium oxidative addition complexes (OACs) have been used to forge protein homo- and heterodimers with stable *S*-aryl linkages.[161,162] This two-step reaction relies on reinsertion of the Pd metal into a second, nearby aryl halide/pseudohalide after the first reaction to regenerate the OAC. To form the protein heterodimers, the OAC can then complete the second *S*-arylation with a cysteine from a separate protein. Alternatively, Pd(II) reagents containing an N-hydroxysuccinimide (NHS) ester underwent amine acylation followed by *S*-arylation at a cysteine residue of a second protein to generate protein heterodimers.[163] In a similar linker strategy that utilizes multiple orthogonal nucleophiles, ortho-pyridinium sulfones have been used to rapidly undergo cysteine arylation while a pendant fluoride performed SNAr with a phenol on a dye

payload.[164] In each of the examples noted above, hetero-conjugate linkers were limited to small molecules.

Recently, Pd has been used to mediate catalyst transfer polymerization (CTP) for the formation of protein-polymer conjugates, wherein polymerization could be terminated by addition of thiol-containing species, including a second protein.[165] This innovative graft-from strategy represented one of the first reports of a macromolecular linker that forged hydrolytically stable *S*-aryl bonds between two distinct proteins. CTP is typically limited to aromatic monomer groups, which limited the degree of polymerization accessible in water in this example.

Our group has reported Au(III) OACs as a facile handle for cysteine PEGylation, providing nearly quantitative conversion to PEGylated product in one minute (**Figure 4.1A**).[39] Recently, we kinetically investigated various Au(III) OACs, finding that dicyclohexylphosphine ($PCy_2$) ligated OACs performed S-arylation more rapidly than the previously used di-1-adamantylphosphine ($PAd_2$) and di-tert-butylphosphine ligated OACs.[114,166,167] This acceleration was due to the ultrarapid coordination of the thiol to the cationic Au(III) center with the smaller diphosphine substituent. This provided more rapid *S*-arylation despite the faster reductive elimination induced by the larger diphosphine reagents. In this study, we also demonstrated that we could slow coordination to the Au(III) center to prepare protein-oligonucleotide conjugates using a small molecule linker with two, sterically distinct Au(III) sites (**Figure 4.1B**).[166] However, full conversion to hetero-conjugates was not achieved, the linkers were limited to small molecules, and OACs were comprised of the kinetically slower $PAd_2$ ligand. We hypothesized that the Au(III) OAC linkers developed previously could be optimized to provide better regioselectivity resulting in improved conversion to discrete hetero-conjugates. Furthermore, we sought to demonstrate that

this selectivity could be achieved across macromolecular linker scaffolds and while using the ultrafast $PCy_2$ ligand. Therefore, we prepared a heterotelechelic polymer such that the terminal $PCy_2$ Au(III) OACs possessed differentiated rates of S-arylation with thiol coupling partners (**Figure 4.1C**). Computational modeling of both the electronics and sterics of this system guided the substrate design to maximize regioselectivity. The regioselectivity of small molecule model substrates were verified by reductive elimination competition experiments and monitored by LCMS. Ultimately, these substrates were incorporated into linkers that can mediate the one-pot formation of ABC block macromolecules including a protein block copolymer conjugate and a protein heterodimer. The computational and small molecule competition portions of this work were performed by Dr. Joseph (Billy) Treacy and are therefore excluded from this chapter.

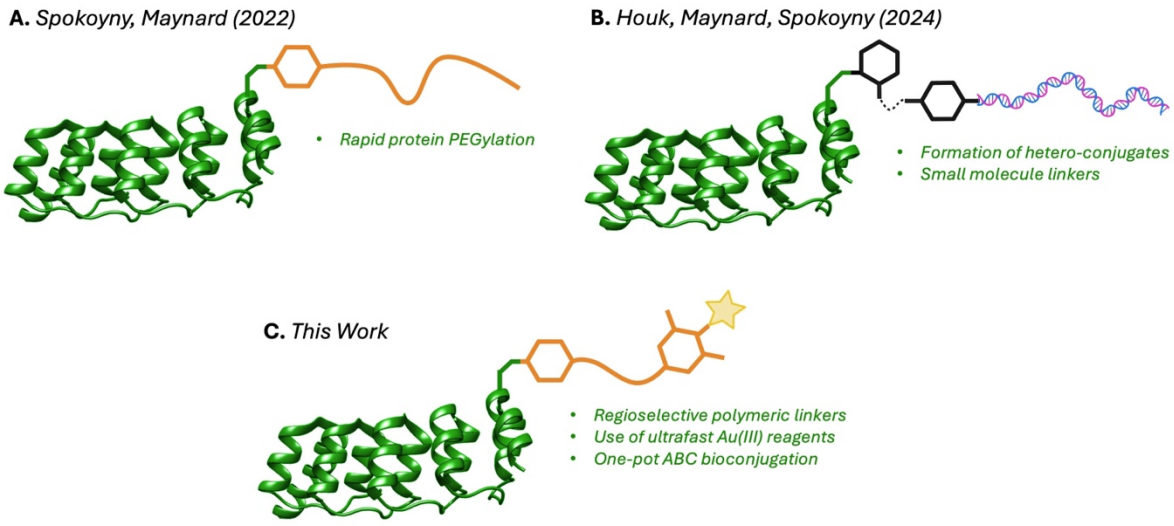


**Figure 4.1** A) Rapid PEGylation of DARPin using organometallic Au(III) PEG reagents. B) Construction of hetero-conjugates using bis-Au(III) reagents. C) Formation of heterodimeric block copolymer protein conjugates using polymeric bis-Au(III) reagents. Star indicates payloads of interest including a polymer, a therapeutic peptide, and small molecule targets.

## 4.2 Results and Discussion

### 4.2.1 Synthesis of a PEG (2 kDa) Heterobifunctional Linker

Based on computational and small molecule LCMS competition studies performed by Dr. Joseph (Billy) Treacy, we hypothesized that the observed regioselectivity between a *para* and *meta* xylene aryl iodide would allow for incorporation of these groups into a heterotelechelic polymer linker that would be capable of mediating sequential and selective *S*-arylation reactions (**Figure 4.2**). Therefore, we performed a Mitsunobu reaction with sub-stoichiometric 4-iodophenol and commercial 2 kDa PEG to achieve mono-arylation (**1**). Unreacted PEG starting material and di-arylated byproducts were removed *via* preparative high-performance liquid chromatography to produce **1** in high purity. Next, the remaining terminal PEG alcohol was tosylated to produce **2** and subsequently arylated with 4-iodo-3,5-dimethylphenol to yield **3** (**Figures 4.5-4.7**). Finally, oxidative addition of **3** with [($PCy_2$)Me-DalPhos]AuCl (and silver hexafluoroantimonate as a halide scavenger resulted in the heterotelechelic PEG OAC (**4**).

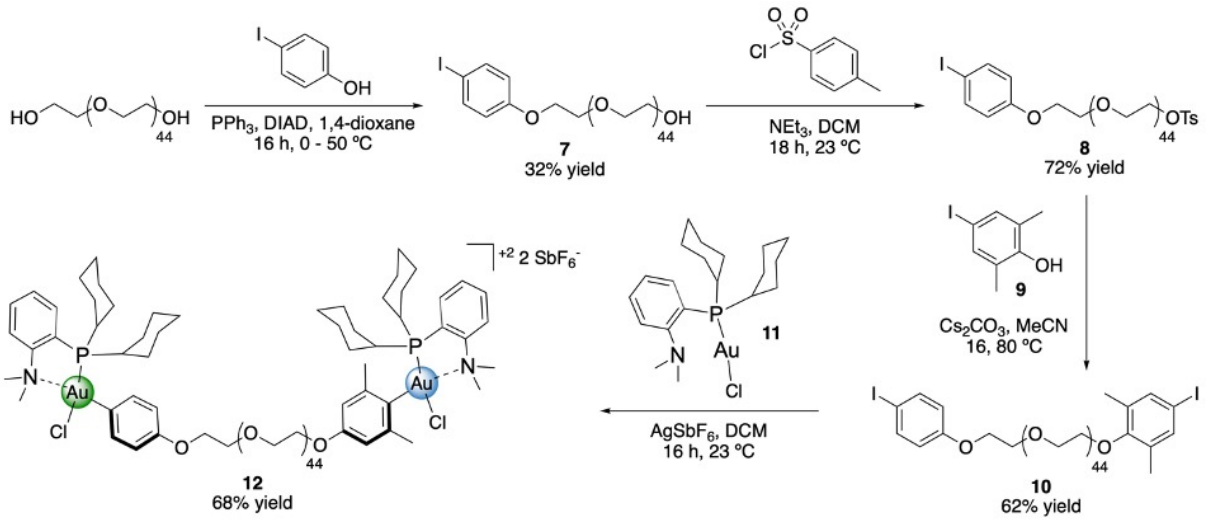


**Figure 4.2** Synthetic scheme for the preparation of the heterobifunctional Au(III) PEG linker **4**. Additional synthetic detail can be obtained in experimental section.

### 4.2.2 Construction of Block Copolymer-Protein Conjugates and Protein Heterodimers

With **4** in hand, we sought to verify that regioselectivity could be achieved with these sterically distinct aryl substituents with a polymeric linker. In previous work, our group has performed PEGylation of a designed ankyrin repeat protein (DARPin) which contained a single surface exposed cysteine at 70 μM with 1.3 equivalents of PEG reagent.[39] Continuing with DARPin as our model protein, we performed *S*-arylation of **4** using these conditions (see the experimental section for details). We observed formation of DARPin-PEG-DARPin homodimer as a significant byproduct along with incomplete conversion of DARPin monomer (**Figure 4.14**). Therefore, we sought to optimize reaction conditions such that conversion to mono-PEGylated product **5** was maximized while the formation of a DARPin homodimer, which would indicate a lack of regioselectivity, was minimized. As we propose that the bimolecular coordination is the selectivity-determining step, we hypothesized that decreasing the concentration of the reaction would improve the selectivity of the reaction. By diluting the conjugation to 35 μM and using 3 equivalents of **4**, we observe 95% conversion to **5** after one hour by SDS-PAGE with no observable formation of homodimer product (**Figure 4.3**). This confirms that the regioselectivity in the small molecule experiments translated to the macromolecular context. The formation of **5** was also verified *via* LCMS (**Figure 4.5B**), indicating that the *meta*-xylene Au(III) portion of **4** remains intact and available for further conjugation following the completion of the first *S*-arylation reaction. Therefore, **5** was used in the following experiments without purification, highlighting the practicality of this one-pot method.

It is well known that protein-polymer conjugates can undergo self-assembly to generate new structure-function relationships.[168,169] By adding a second polymer block to an existing protein-polymer conjugate, additional structures with unique properties could become attainable.

Therefore, to obtain a second macromolecular block of interest, we prepared p(NIPAM)-SH (**6**) *via* reversible addition fragmentation chain transfer polymerization (RAFT) and subsequent aminolysis (see the experimental section for details). Polymer **6** (200 eq) was directly to **5** to yield **7** (**Figure 4.4A**). Conjugate formation was observed by SDS-PAGE, showing good conversion to the hetero-conjugate (**Figure 4.4B**). The modular graft-to preparation of discrete block-copolymer protein conjugates such as **7** can be amenable to many polymer classes and sizes.

As an alternative target, we aimed to prepare a polymerically-linked protein heterodimer. This type of macromolecular scaffold is known to be influential for improving the pharmacokinetics and in vivo activity of protein dimers by allowing flexibility between receptors to improve receptor targeting and binding.[170,171] Therefore, we added a thiolated glucagon (**GCG-SH**) (18 eq) to **5** to produce **8** (**Figure 4.4A**), wherein the corresponding molecular weight could

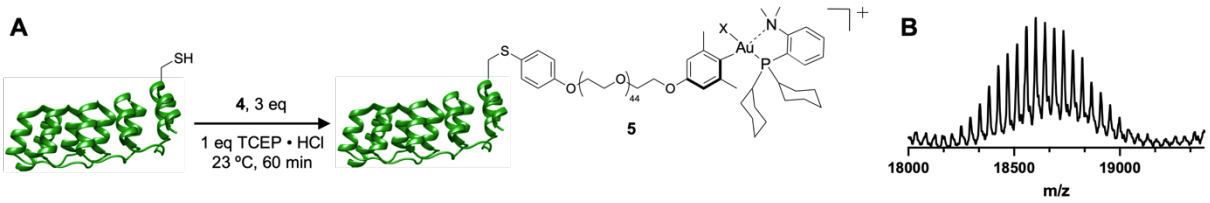


**Figure 4.3** A) Synthetic scheme of regioselective DARPin PEGylation with **4**. X = Cl or $HCO_2$ due to formic acid in the LC-MS mobile phase. B) Extracted total ion chromatogram of **5**. Calculated mass is 18602.0 Da with formate anion exchange. Observed mass is 18602.1 Da.

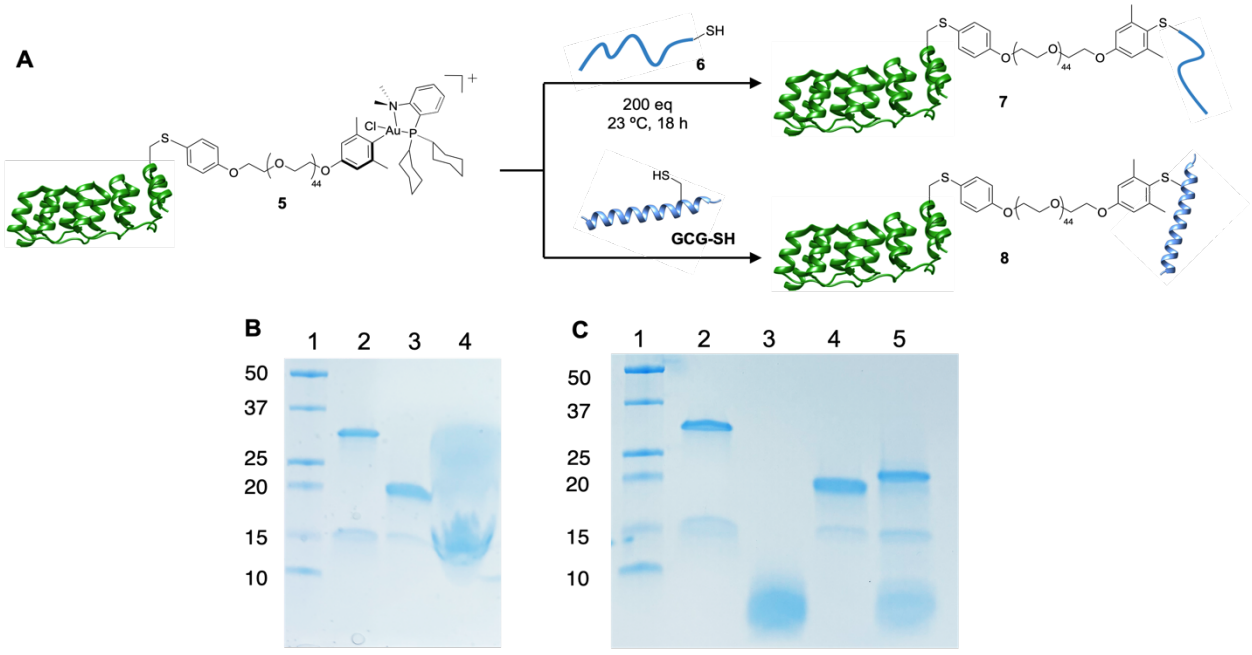


**Figure 4.4** A) Reductive elimination scheme of **5** with p(NIPAM) (**6**) or thiolated glucagon (**GCG-SH**). B) SDS-PAGE gel of *S*-arylation of **5** with **6** to produce a DARPin block copolymer conjugate. Lane 1 - protein ladder. Lane 2 - DARPin (non-reducing conditions). Lane 3 - **5**. Lane 4 - **7**. C) SDS-PAGE gel of *S*-arylation of **5** with **GCG-SH** to produce a DARPin-GCG heterodimer. Lane 1 - protein ladder. Lane 2 - DARPin (non-reducing conditions). Lane 3 - **GCG-SH**. Lane 4 - **5**. Lane 5 - **8**. Unless otherwise noted, all gel lanes were prepared under reducing conditions (5% mercaptoethanol v/v). See the experimental section for additional details.

again be observed by SDS-PAGE (**Figure 4.4B**). This one-pot formation of a protein heterodimer was performed without the use of any unnatural amino acids and resulted in strong *S*-aryl linkages which are resistant to hydrolysis and reversibility. The second *S*-arylation occurred at 11 μM, demonstrating the robustness of this transformation even at low concentrations. Furthermore, the length of PEG linker can be easily modulated, offering a straightforward method to spatially tune

protein-protein interactions. Additionally, this modular approach can be used for polymer end-group modification of PEGylated protein bioconjugates with biologically relevant small molecules such as DOTA (metal chelator), glucose (saccharide), and coumarin (fluorophore).

## 4.3 Conclusion

In this work, we incorporated sterically differentiated end-groups on a heterotelechelic PEG linker for regioselective functionalization. Control of kinetics on these end groups allowed for the one-pot construction of block copolymer-protein conjugates and protein heterodimers with excellent selectivity and good kinetics. This report showcases the utility of organometallic reagents in the modification and construction of biomolecular conjugates due to their rapid kinetics, tunable selectivity, and stable linkages.

## 4.4 Experimental

### 4.4.1 Materials

For the sake of simplicity, Au(III) oxidative complexes are defined herein as [((PCy$_2$)Me-DalPhos)Au$^{III}$(Aryl)Cl]$^+$ SbF$_6^-$ where the aryl group is a benzene ring with denoted substituents relative to the Au center. The synthesis of ((PCy$_2$)Me-DalPhos)Au$^{I}$Cl can be found in previously published work.[166]

All chemicals were used as purchased unless otherwise noted from Acros, Alfa Aesar, Chem-Impex, Combi-Blocks, Fisher Scientific, Oakwood Chemical, Strem Chemicals, TCI Chemicals, or Sigma Aldrich. Hydrogen tetrachloroaurate(III) trihydrate was stored in a desiccator under an argon atmosphere in a sealed scintillation vial. Thiolated glucagon (**GCG-SH**, sequence: HSQGTFTSDYSKYLDSRRAQDFVCWLMNT) was purchased from Biomatik at >90% purity. Anhydrous toluene was distilled over CaH$_2$ and stored under argon. Anhydrous 1,4-dioxane

(>99.8%) was purchased and used as received. Silver hexafluoroantimonate ($AgSbF_6$) and dicyclohexylphosphine were stored in a Vacuum Atmospheres Genesis stainless steel glove box under nitrogen atmosphere. Representative procedures are provided for each reaction.

### 4.4.2 Analytical Techniques

NMR spectra were recorded on the following: AV400 Bruker spectrometer at 400 ($^{1}H$) and 121 MHz ($^{31}P\{^{1}H\}$); AV300 Bruker spectrometer at 300 ($^{1}H$) and 75 MHz ($^{13}C$); NEO600 Bruker spectrometer at 600 ($^{1}H$), 151 ($^{13}C$), 565 ($^{19}F$), and 243 ($^{31}P\{^{1}H\}$) MHz. Spectra are reported in δ (parts per million) relative to residual proteo-solvent signals for $^{1}H$ and $H_3PO_4$ (δ 0.00 ppm) for $^{31}P\{^{1}H\}$. The following abbreviations were used to explain multiplicities: s = singlet, d = doublet, t = triplet, q = quartet, m = multiplet. Deuterated solvents were purchased from Cambridge Isotope Laboratories and used as received for all NMR experiments. Column chromatography was performed on a Biotage Isolera One 3.0 autocolumn instrument. All silica chromatography was carried out on the Biotage using KP-Sil high-performance columns repacked using the Silicycle silica (P60, particle size 40–63 μm, column sizes described in experimental). Reverse phase purification was carried out on a Agilent 1290 Infinity II liquid chromatography system equipped with a UV detector using a Luna 5 μm C18 100 Å column (Preparatory: 5 μm, 250 × 21.2 mm) with monitoring at λ = 215 and 254 nm and with a flow rate of 20 mL/min.

DMF Size Exclusion Chromatography (SEC)/Gel Permeation Chromatography (GPC) was conducted on an Agilent 1260 Infinity II high performance liquid chromatography (HPLC) system with a Wyatt Optilab (RI and MALS detection), one Polymer Laboratories PLgel guard column, and two Polymer Laboratories PLgel 5 μm mixed D columns. The eluent was DMF (HPLC Grade, 99.7+%, Thermo Scientific Chemicals) containing LiBr (0.1 M) at 40 °C (Flow rate: 0.6 mL/min).

Molecular weight information was determined for data collected using a PMMA (Agilent Technologies, EasiVial PMMA, preweighed calibration kit) conventional calibration analysis.

### 4.4.3 Methods

**Monoarylation of 2 kDa PEG (1)**

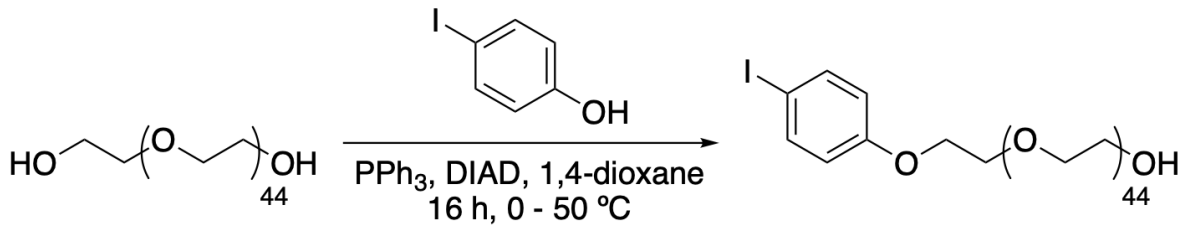


Prior to the reaction, PEG was washed three times with toluene in a flame-dried flask, with toluene removed in an azeotrope with water under vacuum between each wash. Then, triphenylphosphine (1.57 g, 1.2 eq, 6.0 mmol) was dissolved in 500 µL anhydrous 1,4-dioxane in a flame-dried two-neck flask equipped with a stir bar. The reaction was cooled to 0 ºC in an ice bath and placed under an argon environment. Diisopropyl (E)-diazene-1,2-dicarboxylate (DIAD) (1.28 g, 1.24 mL, 95% wt, 1.2 eq, 6.0 mmol) was diluted with 100 µL dry dioxane and added to the reaction flask. The reaction stirred for 30 minutes, wherein it turned from yellow to dark orange. Then, PEG (2 kDa) (10.0 g, 1 eq, 5.00 mmol) was dissolved in 3 mL anhydrous 1,4-dioxane and added to the round bottom flask. The solution was cloudy and remained orange in color. The reaction was allowed to stir for 1.5 hours. Then, 4-iodophenol (1.32 g, 1.2 eq, 6.00 mmol) was added as a solid and the mixture became yellow and less cloudy. The reaction was allowed to return to ambient temperature and removed from argon. The reaction was then heated to 50 ºC for 17 hours. 1,4-dioxane was removed under reduced pressure. The crude produce was then diluted with MeCN and filtered with a 0.2 µm PTFE filter. The resulting viscous mixture was purified by

preparative HPLC (10-100% MeCN against water gradient, 0.1% TFA). Pure fractions were concentrated under vacuum and subsequently lyophilized to yield **7** as a white powder (3.5 g, 1.6 mmol, 32% yield).

**$^1$H NMR (500 MHz, $CD_3CN$):** δ 7.59 (d, *J* = 9.0 Hz, 2H), 6.76 (d, *J* = 9.0 Hz, 2H), 4.07 (d, 2H), 3.76 (d, 2H), 3.67 – 3.37 (m, 228H).

**Tosylation of Monoarylated 2 kDa PEG (2)**

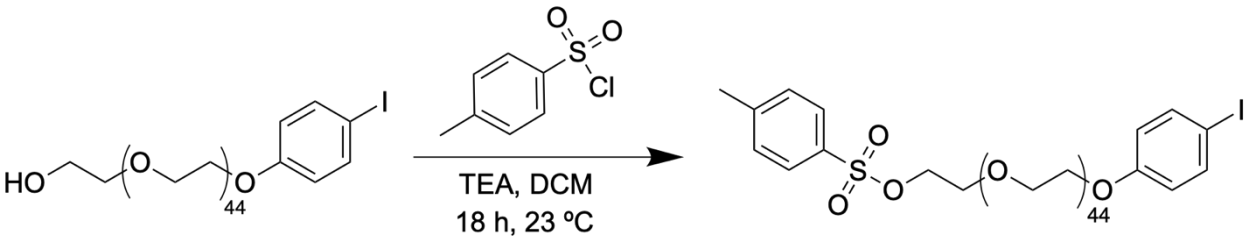


PEG 2 kDa aryl iodide (**1**) (500.0 mg, 1 eq, 218.3 μmol) was added to a round bottom flask equipped with a stir bar and dissolved in 8 mL DCM. Next, 4-methylbenzenesulfonyl chloride (249.7 mg, 6 eq, 1.3 mmol) and TEA (220.9 mg, 304 μL, 10 eq, 2.2 mmol) were added to the reaction. After 16 hours, the reaction solution was concentrated under reduced pressure. The crude product was further purified by flash column chromatography (25 g silica gel, 0-10% gradient of methanol against DCM) and subsequently precipitated three times in cold diethyl ether and dried under reduced pressure to produce **2** as a white powder (384 mg, 218 μmol, 72% yield).

**$^1$H NMR (600 MHz, $CD_3CN$):** δ 7.79 (d, *J* = 8.3 Hz, 2H), 7.59 (d, *J* = 8.9 Hz, 2H), 7.44 (d, *J* = 8.1 Hz, 2H), 6.76 (d, *J* = 8.9 Hz, 2H), 4.13 – 4.10 (m, 2H), 4.08 – 4.05 (m, 2H), 3.79 – 3.73 (m, 2H), 3.55 (s, 216H).

**Arylation of Monoarylated 2 kDa PEG (3)**

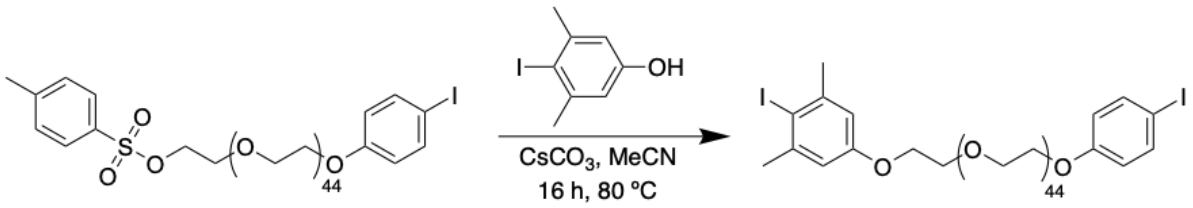


4-iodo-3,5-dimethylphenol (466 mg, 1 eq, 191 μmol) was added to a round bottom flask with a stir bar and dissolved in 4 mL MeCN. Next, cesium carbonate (310 mg, 5 eq, 952 μmol) and **2** (236 mg, 5 eq, 952 μmol) were added as solid powders to the flask. The reaction was refluxed at 80 ºC for 16 hours. Next, the MeCN was removed under reduced pressure. The crude product was further purified by flash column chromatography (25 g silica gel, 0-10% gradient of methanol against DCM) and subsequently precipitated in cold diethyl ether three times to produce **3** a white powder (298 mg, 191 μmol, 62% yield).

**$^1$H NMR (500 MHz, $CD_3CN$):** δ 7.59 (d, *J* = 8.5 Hz, 2H), 6.89 – 6.59 (m, 4H), 4.21 – 3.97 (m, 4H), 3.91 – 3.67 (m, 4H), 3.55 (s, 195H), 2.41 (s, 6H).

**Oxidative Addition of Heteroarylated 2 kDa PEG (4)**

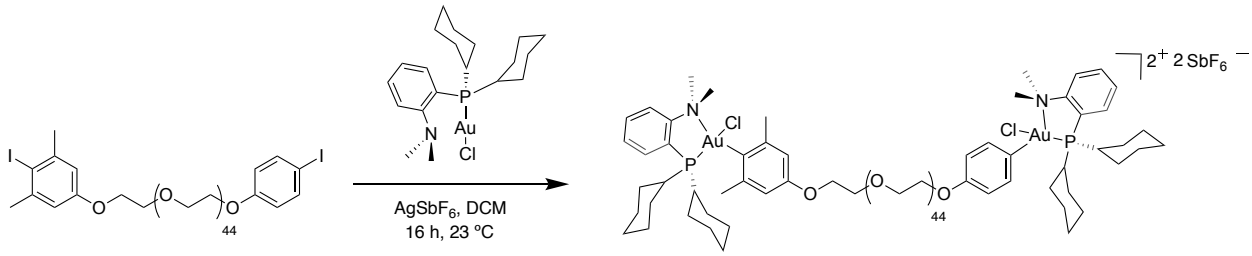


Silver hexafluorostibate(V) (8.2 mg, 3.0 eq, 23.8 μmol) removed from a nitrogen atmosphere glove box in a dram vial and blocked from light. **3** (20.0 mg, 1 eq, 7.9 μmol) was weighed into a dram vial equipped with a stir bar and (Me-CyDalPhos)AuCl (13.1 mg, 3.0 eq, 23.8 μmol) was added. 250 μL of DCM was added to each vial. The vials were placed in a -20 ºC freezer for ca. 1 minute. Next, the solutions were added together with an additional 500 μL DCM. The reaction was stirred while blocked from light for 21 hours. The reaction solution was filtered through a pad of Celite with DCM. The solvent was removed under reduced pressure. Next, the crude product was triturated once in diethyl ether, triturated three times in 3.5:1.5 diethyl ether/THF (v/v), and finally triturated once more in diethyl ether to produce **4** as a yellow oil (20.7 mg, 7.9 μmol, 68% yield).

**$^{1}$H NMR (600 MHz, $CD_3CN$):** δ 8.09 – 7.99 (m, 2H), 7.98 – 7.91 (m, 2H), 7.85 – 7.68 (m, 4H), 7.25 (d, *J* = 8.8 Hz, 2H), 7.01 (d, *J* = 8.8 Hz, 2H), 6.80 – 6.69 (m, 2H), 4.21 – 4.00 (m, 4H), 3.87 – 3.73 (m, 4H), 3.55 (s, 225H), 3.41 (d, *J* = 2.5 Hz, 12H), 1.40 – 1.14 (m, 44H).

**$^{31}$P{$^{1}$H} NMR (243 MHz, $CD_3CN$):** δ 60.10, 58.75.

**Protein Expression and Purification**

DARPin-Cys protein expression and purification was adapted from literature procedures.[39] DARPin-Cys Sequence (Calculated Mass: 15996.84 Da): MGSDKIHHHHHHHENLYFQGGCGGSDLGKKLLEAARAGQDDEVRILMANGADVNAYDD NGVTPLHLAAFLGHLEIVEVLLKYGADVNAADSWGTTPLHLAATWGHLEIVEVLLKHG ADVNAQDKFGKTAFDISIDNGNEDLAEILQKLN.

The plasmid was designed to have an *N*-terminal His6 tag followed by a TEV protease cleavage site which was left on for our purposes (Model bioconjugation protein). The plasmid purchased from Twist Bioscience is a pET29b(+) vector with kanamycin resistance and the DARPin-Cys gene was cloned in via NdeI and XhoI restriction sites. Prior to expression, the plasmid was transformed into BL21-Gold cells (Agilent) using the standard manufacturer's procedure. Overnight cultures were grown and from these, two glycerol stocks were made and stored in the -80 °C freezer. Two 2-liter flasks were filled with 750 mL of previously autoclaved LB Broth (Miller) containing kanamycin (50 μg/mL) each. Then, 5 mL of a saturated overnight culture inoculated from one of the aforementioned glycerol stocks were added to each flask. The culture was grown at 37 °C with 250 rpm shaking for ca. 4 hours before the OD600 reached ~0.4 and the culture was induced with 1 mM IPTG. The temperature was lowered, and the culture was shaken at 30 °C at 250 rpm for approximately 20 hours. The cultures were harvested by centrifugation at 6000 rpm for 30 min to yield a cell pellet. The pellet was resuspended in lysis buffer containing 20 mM Tris and 150 mM NaCl (pH 7.5), 15 mg lysozyme, and 0.5 tablet of protease inhibitor cocktail. The resulting suspension was homogenized (Avestin Emulsiflex C-3) and centrifuged at 17,000 rpm for 30 min to remove cell debris. The supernatant was loaded onto a 5 mL gravity Ni-NTA column (Qiagen) and washed with 30 mL (3 x 10 mL) 5 mM imidazole,

20 mL (2 x 10 mL) 20 mM imidazole and eluted with 25 mL (5 x 5 mL) 200 mM imidazole all in 20 mM Tris 150 mM NaCl pH 8.5 buffer. SDS-PAGE was run on all fractions and under reducing conditions with Coomassie Blue staining. Pure fractions were combined, and solvent exchanged into storage buffer (20 mM Tris, 150 mM NaCl, pH 7.5) and concentrated using a Amicon 3 kDa MWCO Ultra-15 Centrifugal Filter (Millipore). The purified protein was analyzed by LC-MS and SDS-PAGE confirming sample purity and molecular weight. Protein concentration was determined by a NanoDrop 2000 UV-Vis spectrophotometer at 280 nm (Extinction coefficient = 15470 $M^{-1}$ $cm^{-1}$). The protein sample was diluted with storage buffer (20 mM Tris and 150 mM NaCl (pH 7.5)) to 76 μM and aliquots were flash frozen and stored in a –80 °C freezer.

**Synthesis of p(NIPAM) (7)**

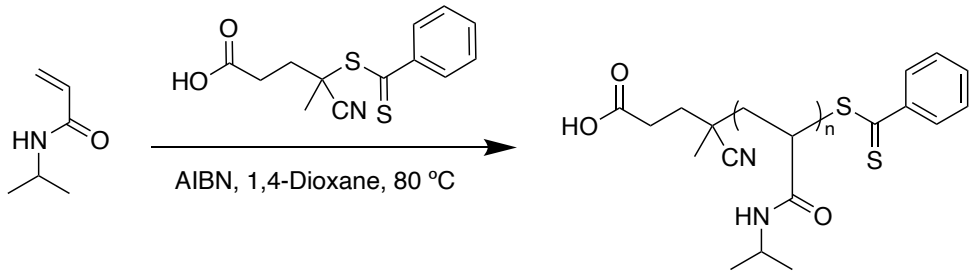


N-isopropylacrylamide (700.0 mg, 140.0 eq, 6.2 mmol) and 4-cyano-4-((phenylcarbonothioyl)thio)pentanoic acid (12.3 mg, 1 eq, 44.2 μmol), and azobisisobutyronitrile (2.2 mg, 0.3 eq, 13.3 μmol) were dissolved in a Schlenk flask with 3 mL of anhydrous 1,4-dioxane. The reaction underwent three freeze-pump-thaw cycles. The reaction was then exposed to an argon atmosphere. The reaction progressed at 80 °C while stirring for 4.5 hours. The polymer was precipitated three times into cold diethyl ether and the solvent was removed under reduced pressure to produce **7** as a pink powder (70 % conversion, 117 mg, 300 μmol, 17% yield).

**$^1$H NMR (300 MHz, $CDCl_3$):** δ 8.02 – 7.87 (m, 2H), 7.58 – 7.49 (m, 1H), 7.44 – 7.33 (m, 2H), 4.00 (s, 98H), 2.65 – 1.27 (m, 341H), 1.30 – 0.90 (m, 613H).

**DMF SEC:** $M_n$ is 10.6 kDa, $M_w$ is 14.0 kDa, $Đ$ is 1.32.

**Reduction of pNIPAM-Dithiobenzoate (6)**

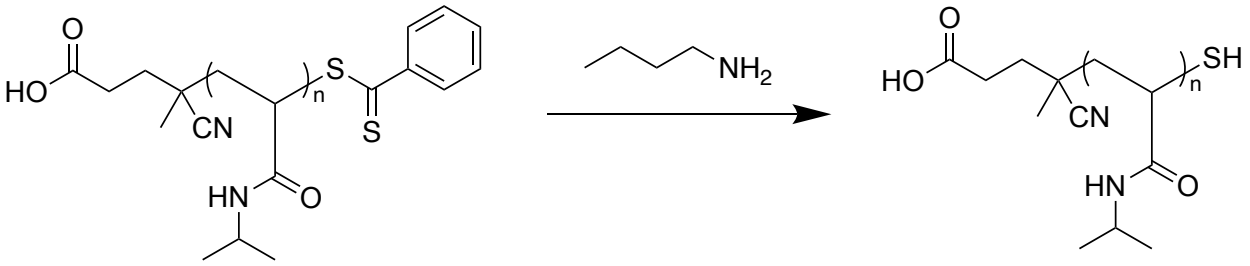


pNIPAM (**7**) (100.0 mg, 1 eq) was dissolved in 1 mL DCM in a dram vial charged with a stir bar. *n*-Butylamine (115.4 mg, 0.16 mL, 250 eq, 1.6 mmol) was added. The reaction proceeded for 20 minutes, then precipitated in cold diethyl ether to produce **6** as a white powder (62 mg, 9.2 μmol, 62% yield). Refer to Chapter 2 for UV-Visible spectroscopy of the cleaved CTA end group. **$^1$H NMR (300 MHz, $CDCl_3$)** δ 4.00 (s, 98H), 2.64 – 1.29 (m, 460H), 1.31 – 0.98 (m, 601H).

**General Information for Conjugation Experiments**

Protein concentration was determined by a NanoDrop 2000 UV-Vis spectrophotometer at 280 nm (Extinction coefficient = 15470 $M^{-1}$ $cm^{-1}$). Sodium dodecyl sulfate-polyacrylamide gel electrophoresis (SDS-PAGE) was carried out in a Mini-PROTEAN Tetra Cell system (Bio-Rad) connected to a PowerPac HC (BioRad) power supply using Bio-Rad Any kDTM Mini-PROTEAN® TGXTM Precast Gels at 195 V and 3 A for 30 minutes in a running buffer (25 mM Tris, 192 mM Glycine, 0.1% (w/v) SDS, pH 8.3). Precision Plus ProteinTM Dual Xtra Prestained Protein Standards (2 μL) were used as protein ladder in all SDS-PAGE analysis. Laemmli 2x Concentrate (Sigma) containing 4% SDS, 20% glycerol, 0.004% bromophenol blue, and 0.125 M Tris HCl at a pH of ca. 6.8 was used to load all protein and conjugate samples. Protein bands were visualized by staining the gels in an aqueous solution (0.1% Coomassie Brilliant Blue R 250, 45% MeOH, 9% acetic acid) and microwaving for 30 seconds followed by agitation for 15 minutes.

Destaining was carried out by submerging the gels in an aqueous destaining solution (10% MeOH, 14% acetic acid), microwaving for 30 seconds, and agitating for several hours until the background of the gel became fully destained.

LCMS analysis was carried out using an Agilent 6530 ESI-Q-TOF. Protein analyses were carried out using an Agilent ZORBAX 300SB C3 column (3.5 μm, 3.0 × 150 mm). Liquid chromatography method used for DARPin and its conjugates: column temperature: 40 °C, flow rate: 0.6 mL/min, gradient: 90% water (0.1% formic acid (FA)) for 2 minutes; 90%-9% water (0.1% FA) 2-11 minutes; 5% water (0.1% FA) from 11-14 min with acetonitrile as the co-solvent.

**Initial DARPin PEGylation Conditions**[39]

To a 50 μL solution of DARPin at 76 μM in storage buffer, 5 μL of a 0.076 mM TCEP·HCl (0.218 mg/mL, 1 eq) solution in storage buffer was added. Therefore, PEGylation would occur at a protein concentration of 70 μM. The protein underwent disulfide reduction for 1 hour at 37 ºC. Next, 5 μL of **4** was added to the reaction mixture. A stock solution of **4** was prepared in MeCN prior to the procedure (3.83 mg/mL) such that 1.3 eq of **4** was added. After 1 hour at 23 ºC, the reaction was stopped by dilution in SDS-PAGE conditions (see below).

*General SDS-PAGE Sample Preparation Procedure:* 1 μL of a given reaction mixture was added to 19 μL of Laemmli loading buffer. For samples run under reducing conditions, the Laemmli loading buffer was prepared to contain 5% mercaptoethanol by volume and samples were heated at 90 ºC for five minutes prior to loading. Samples were loaded onto SDS-PAGE gel and run as described above in the general experimental information.

**Optimized PEGylation Conditions (5)**

To a 50 µL solution of DARPin at 76 µM in storage buffer, 50 µL of additional storage buffer was added to bring the protein concentration to 38 µM. Then, 5 µL of a 0.076 mM TCEP·HCl (0.218 mg/mL, 1 eq) solution in storage buffer was added to the reaction. Therefore, PEGylation would occur at a protein concentration of 35 µM. The protein underwent disulfide reduction for 1 hour at 37 ºC. Next, 5 µL of **4** was added to the reaction mixture. A stock solution of **4** was prepared in MeCN prior to the procedure (8.84 mg/mL) such that 3 eq of **4** was added. After 1 hour at 23 ºC, the reaction was stopped by dilution in SDS-PAGE conditions (see above) or carried forward for additional one-pot conjugation reactions without further purification (see below). PEGylation was observed *via* SDS-PAGE and LC-MS (see **Figure 4.3**).

**NIPAM Conjugation Conditions (7)**

To a 60 µL solution of **5** from above at a protein concentration of 32 µM, 5 µL of **6** was added. A stock solution of **6** (1.5 g/mL) was prepared in storage buffer prior to the reaction, such that 200 eq of **6** was added. The reaction proceeded for 18 hours at 4 ºC, wherein the low temperature aided in the dissolution of **6**. Conjugation was observed *via* SDS-PAGE gel (see **Figure 4.4**).

**Glucagon Conjugation Conditions (8)**

To a 60 µL solution of **5** from above at a protein concentration of 32 µM, 140 µL of GCG-SH was added. A stock solution of GCG-SH (1 mg/mL) was prepared in storage buffer at pH 4 prior to the reaction, such that 20 eq of GCG-SH was added. The reaction proceeded for 18 hours at 23 ºC. Conjugation was observed *via* SDS-PAGE gel (See **Figure 4.4**).

# 4.6 Appendix III

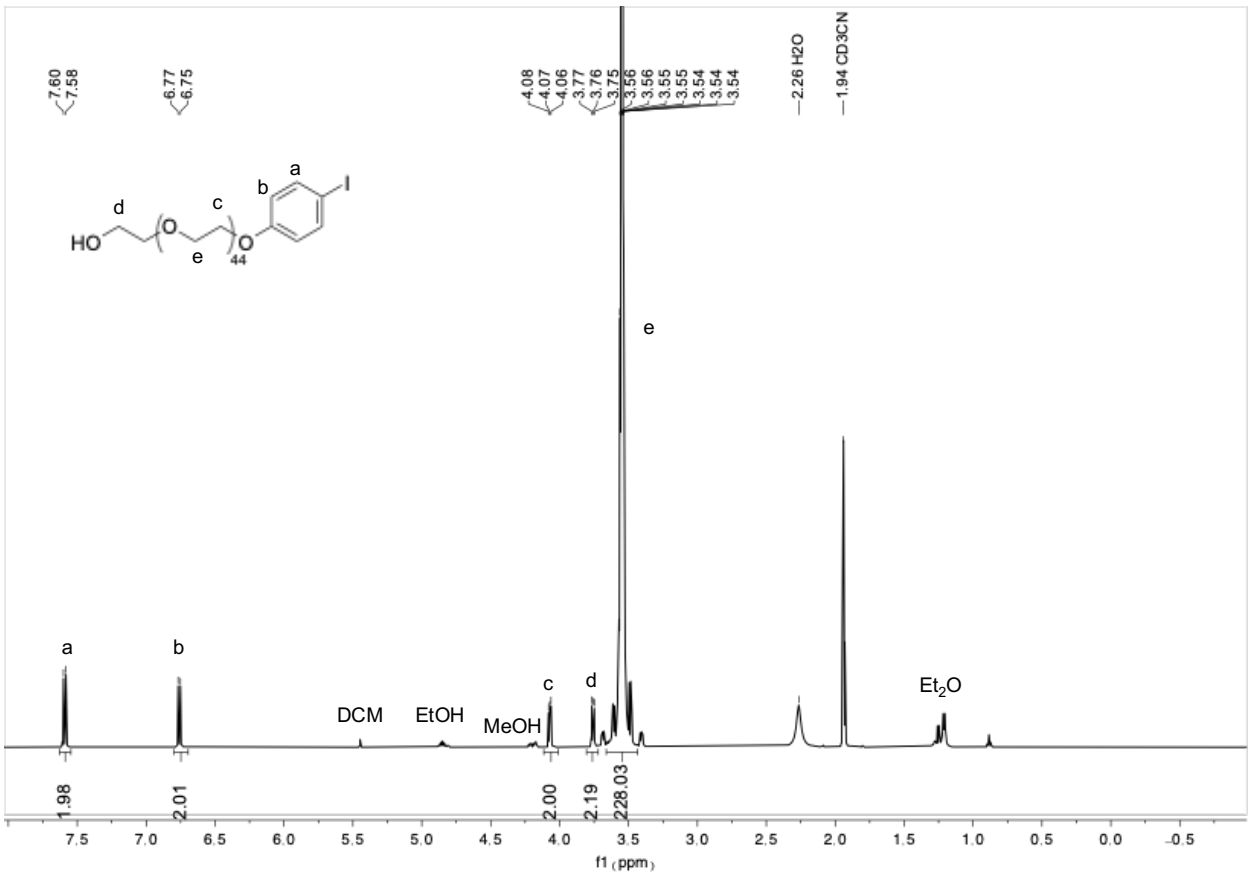


**Figure 4.5** $^{1}H$ NMR of **1** in $CD_3CN$ at 298 K.

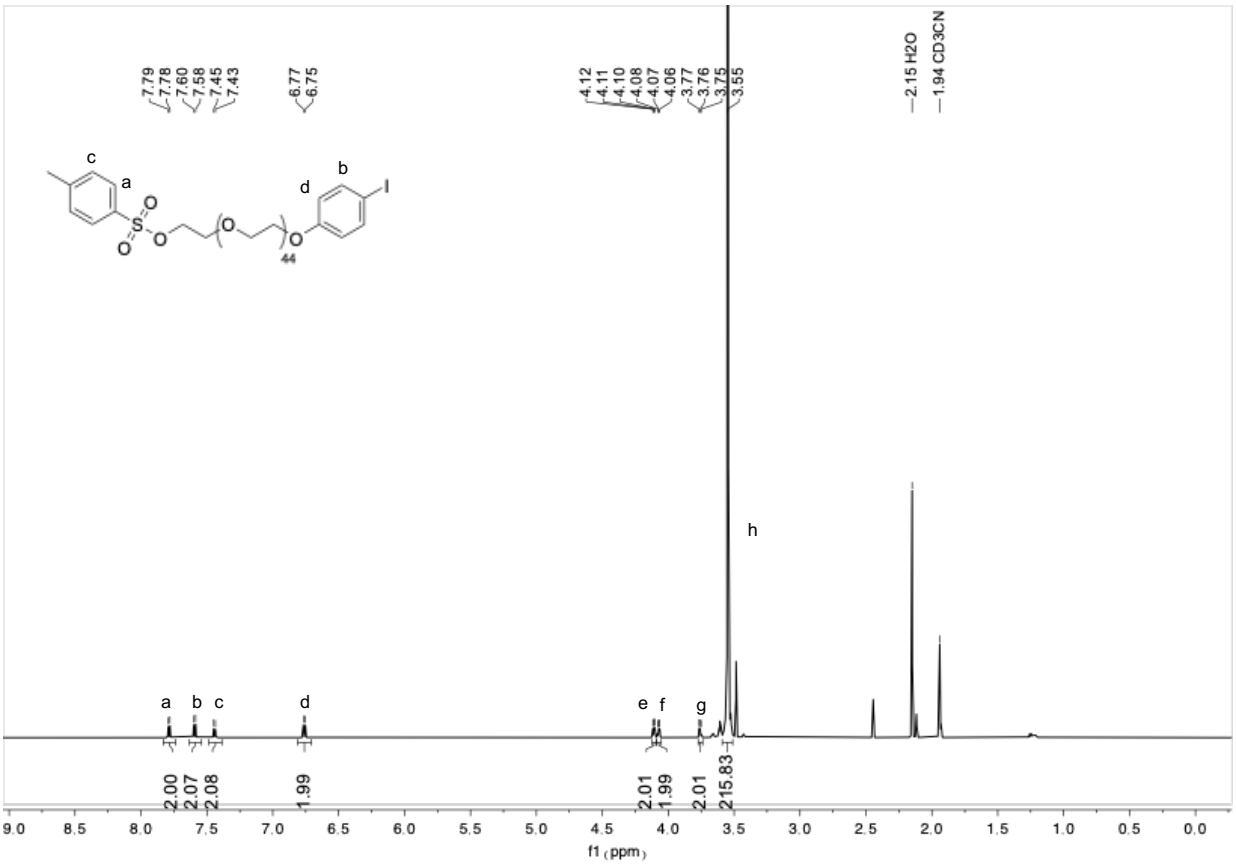


**Figure 4.6** $^{1}$H NMR of **2** in $CD_3CN$ at 298 K.

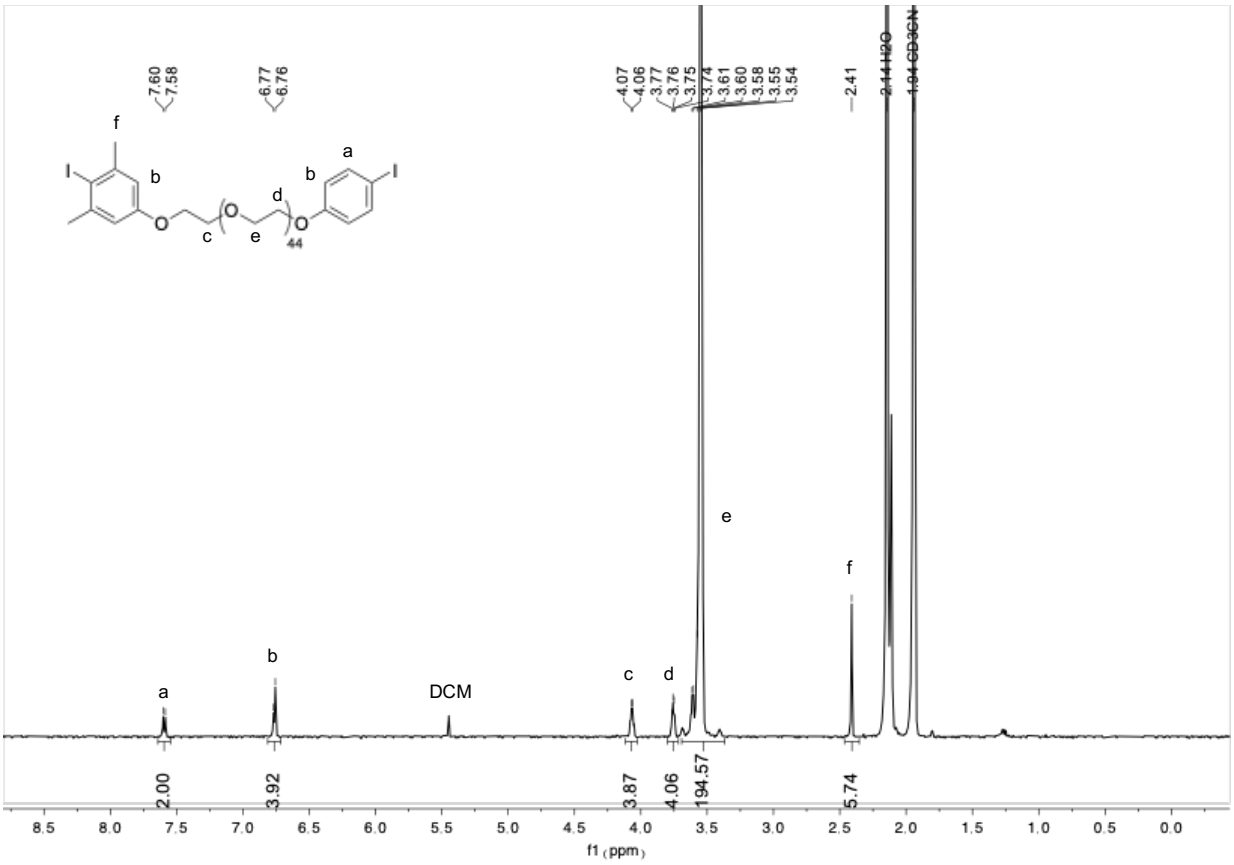


**Figure 4.7** $^{1}$H NMR of **3** in $CD_3CN$ at 298 K

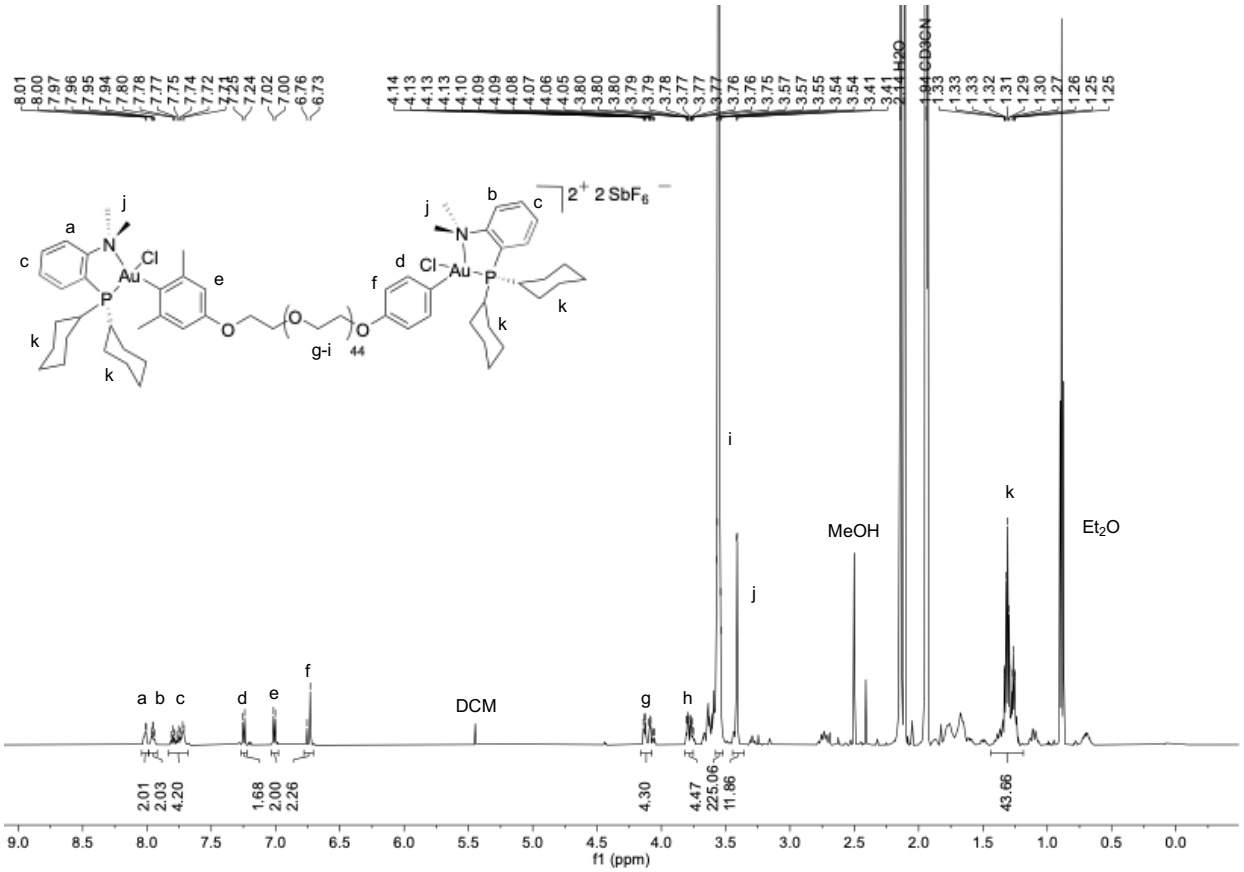


**Figure 4.8** $^{1}$H NMR of **4** in $CD_3CN$ at 298 K.

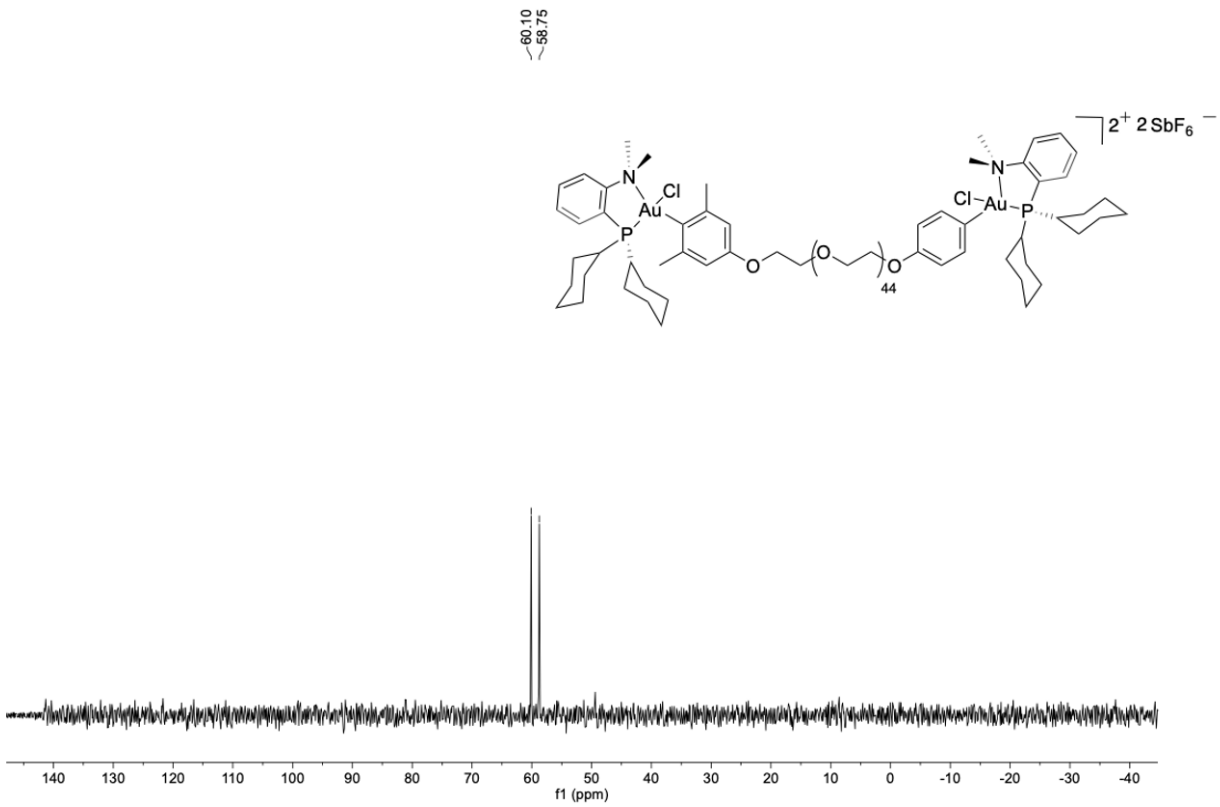


**Figure 4.9** $^{31}P\{^{1}H\}$ NMR of **4** in $CD_3CN$ at 298 K.

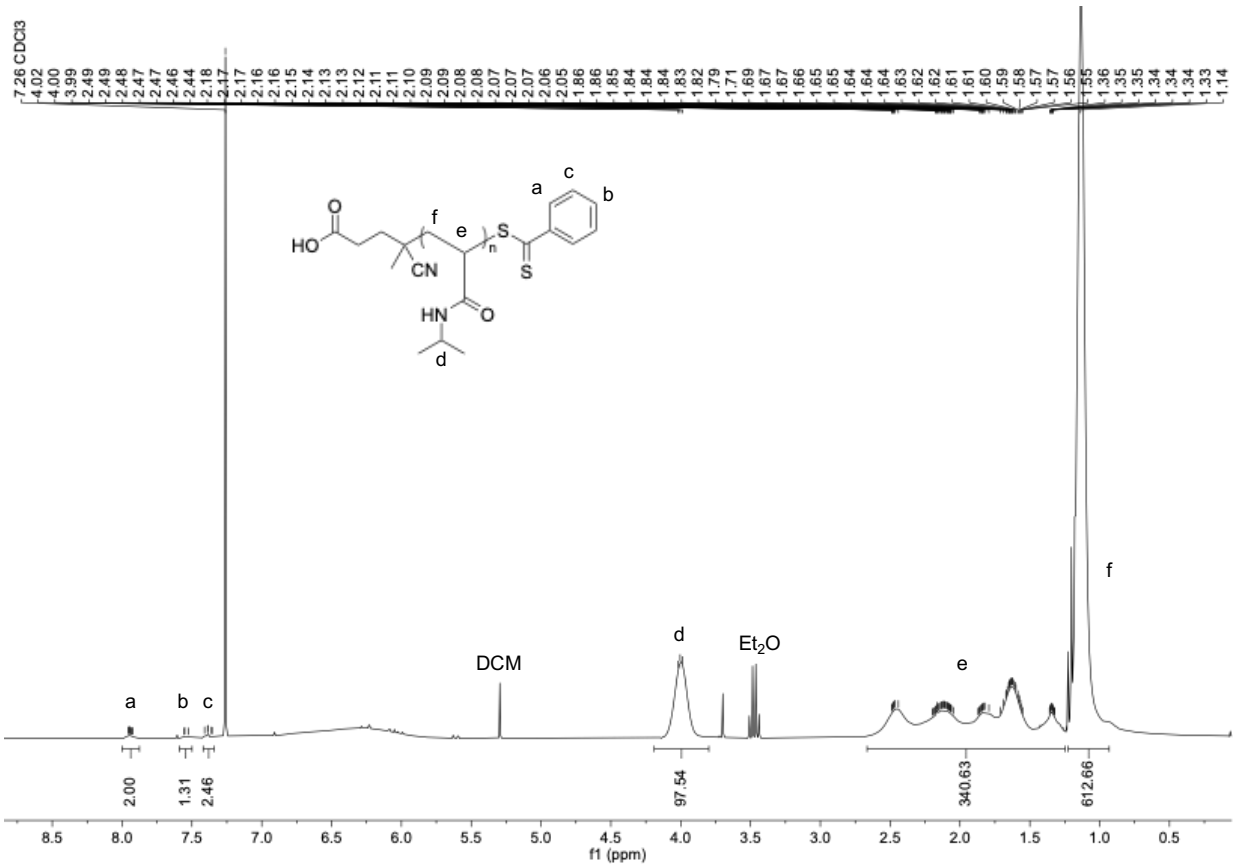


**Figure 4.10** $^{1}$H NMR of **7** in $CDCl_3$ at 298 K.

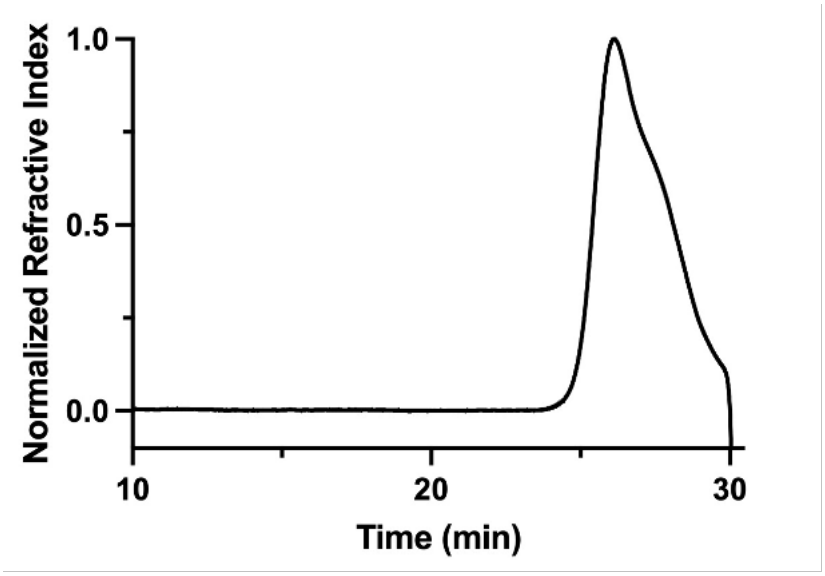


**Figure 4.11** DMF SEC spectrum of **7**. $M_n$ is 10.6 kDa, $M_w$ is 14.0 kDa, $Đ$ is 1.32.

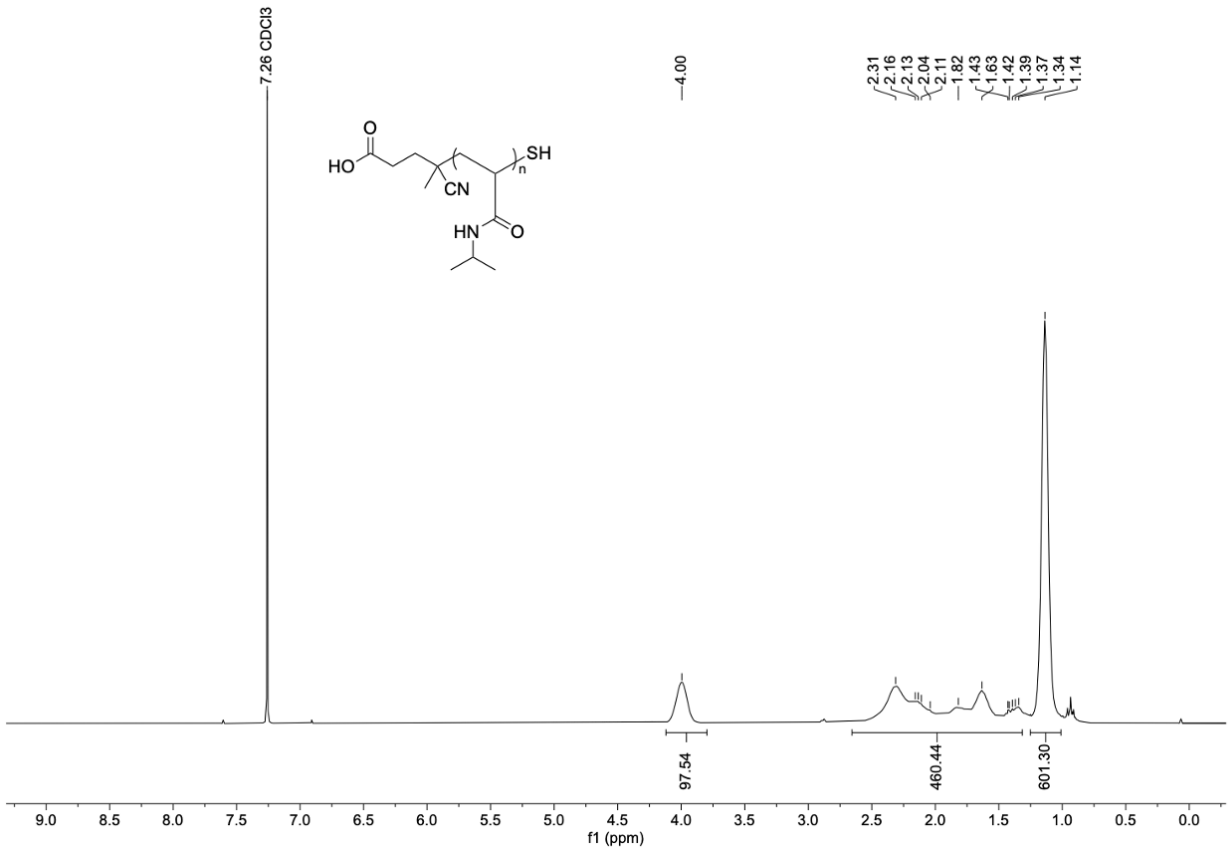


**Figure 4.12** $^{1}$H NMR of **6** in $CDCl_3$ at 298 K.

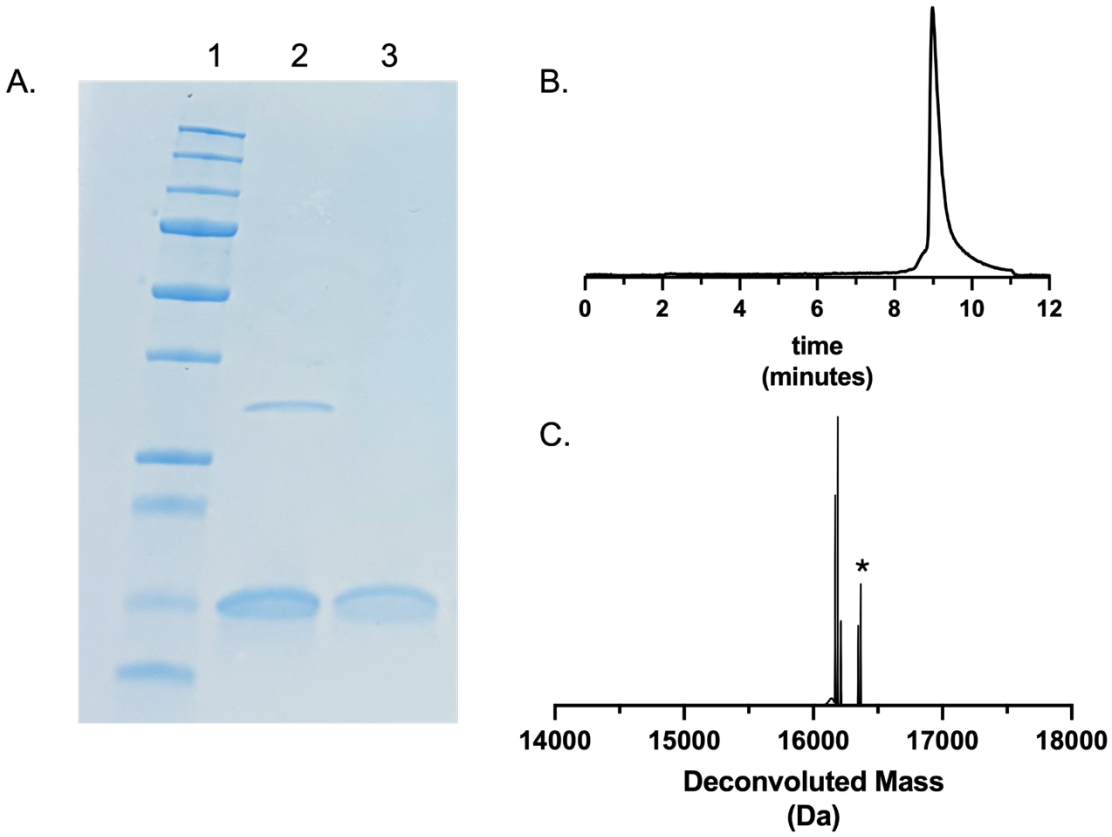


**Figure 4.13** A) SDS-PAGE gel of DARPin following purification. Lane 1 - protein ladder. Lane 2 - DARPin (non-reducing conditions). Lane 3 - DARPin (reducing conditions, 5% mercaptoethanol by volume). B) LCMS total ion chromatogram (TIC) of DARPin following purification. C) LCMS deconvoluted mass of DARPin following purification. Expected mass: 15,866.84 Da. Observed mass: 15,866.23 Da. * denotes the parent mass.

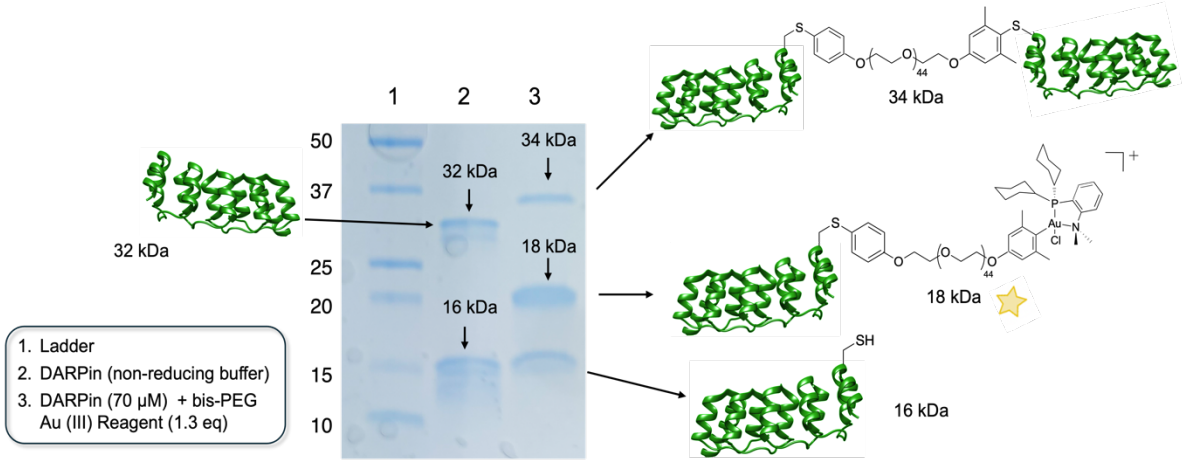


**Figure 4.14** A) Regioselective DARPin PEGylation scheme. B) SDS-PAGE gel results from conventional Au(III)-mediated PEGylation conditions (70 µM DARPin, 1.3 eq Au(III) reagent) and the corresponding products. Lane 1 - protein ladder. Lane 2 - DARPin (non-reducing conditions). Lane 3 - DARPin PEGylation with **4**. Desired product (monoPEGylated DARPin, 18 kDa) is indicated with a star.

## 4.5 References


(1) Spicer, C. D.; Davis, B. G. Selective Chemical Protein Modification. *Nat. Commun.* **2014**, *5* (1), 4740. https://doi.org/10.1038/ncomms5740.

(2) Rawale, D. G.; Thakur, K.; Adusumalli, S. R.; Rai, V. Chemical Methods for Selective Labeling of Proteins. *Eur. J. Org. Chem.* **2019**, *2019* (40), 6749–6763. https://doi.org/10.1002/ejoc.201900801.

(3) Shiraiwa, K.; Cheng, R.; Nonaka, H.; Tamura, T.; Hamachi, I. Chemical Tools for Endogenous Protein Labeling and Profiling. *Cell Chem. Biol.* **2020**, *27* (8), 970–985. https://doi.org/10.1016/j.chembiol.2020.06.016.

(4) Zhu, J.; Avakyan, N.; Kakkis, A.; Hoffnagle, A. M.; Han, K.; Li, Y.; Zhang, Z.; Choi, T. S.; Na, Y.; Yu, C.-J.; Tezcan, F. A. Protein Assembly by Design. *Chem. Rev.* **2021**, *121* (22), 13701–13796. https://doi.org/10.1021/acs.chemrev.1c00308.

(5) Chen, F.-J.; Gao, J. Fast Cysteine Bioconjugation Chemistry. *Chem. – Eur. J.* **2022**, *28* (66), e202201843. https://doi.org/10.1002/chem.202201843.

(6) Ochtrop, P.; Hackenberger, C. P. R. Recent Advances of Thiol-Selective Bioconjugation Reactions. *Curr. Opin. Chem. Biol.* **2020**, *58*, 28–36. https://doi.org/10.1016/j.cbpa.2020.04.017.

(7) You, J.; Zhang, J.; Wang, J.; Jin, M. Cysteine-Based Coupling: Challenges and Solutions. *Bioconjug. Chem.* **2021**, *32* (8), 1525–1534. https://doi.org/10.1021/acs.bioconjchem.1c00213.

(8) Renault, K.; Fredy, J. W.; Renard, P.-Y.; Sabot, C. Covalent Modification of Biomolecules through Maleimide-Based Labeling Strategies. *Bioconjug. Chem.* **2018**, *29* (8), 2497–2513. https://doi.org/10.1021/acs.bioconjchem.8b00252.

(9) Woghiren, C.; Sharma, B.; Stein, S. Protected Thiol-Polyethylene Glycol: A New Activated Polymer for Reversible Protein Modification. *Bioconjug. Chem.* **1993**, *4* (5), 314–318. https://doi.org/10.1021/bc00023a002.

(10) Gong, Y.; Leroux, J.-C.; Gauthier, M. A. Releasable Conjugation of Polymers to Proteins. *Bioconjug. Chem.* **2015**, *26* (7), 1172–1181. https://doi.org/10.1021/bc500611k.

(11) Sechi, S.; Chait, B. T. Modification of Cysteine Residues by Alkylation. A Tool in Peptide Mapping and Protein Identification. *Anal. Chem.* **1998**, *70* (24), 5150–5158. https://doi.org/10.1021/ac9806005.

(12) Zhang, C.; Vinogradova, E. V.; Spokoyny, A. M.; Buchwald, S. L.; Pentelute, B. L. Arylation Chemistry for Bioconjugation. *Angew. Chem. Int. Ed.* **2019**, *58* (15), 4810–4839. https://doi.org/10.1002/anie.201806009.

(13) Montgomery, H. R.; Spokoyny, A. M.; Maynard, H. D. Organometallic Oxidative Addition Complexes for S-Arylation of Free Cysteines. *Bioconjug. Chem.* **2024**. https://doi.org/10.1021/acs.bioconjchem.4c00222.

(14) Jbara, M.; Pomplun, S.; Schissel, C. K.; Hawken, S. W.; Boija, A.; Klein, I.; Rodriguez, J.; Buchwald, S. L.; Pentelute, B. L. Engineering Bioactive Dimeric Transcription Factor Analogs via Palladium Rebound Reagents. *J. Am. Chem. Soc.* **2021**. https://doi.org/10.1021/jacs.1c05666.

(15) Dhanjee, H. H.; Saebi, A.; Buslov, I.; Loftis, A. R.; Buchwald, S. L.; Pentelute, B. L. Protein–Protein Cross-Coupling via Palladium–Protein Oxidative Addition Complexes

from Cysteine Residues. *J. Am. Chem. Soc.* **2020**, *142* (20), 9124–9129. https://doi.org/10.1021/jacs.0c03143.

(16) Dhanjee, H. H.; Buslov, I.; Windsor, I. W.; Raines, R. T.; Pentelute, B. L.; Buchwald, S. L. Palladium–Protein Oxidative Addition Complexes by Amine-Selective Acylation. *J. Am. Chem. Soc.* **2020**, *142* (51), 21237–21242. https://doi.org/10.1021/jacs.0c09180.

(17) Lipka, B. M.; Honeycutt, D. S.; Bassett, G. M.; Kowal, T. N.; Adamczyk, M.; Cartnick, Z. C.; Betti, V. M.; Goldberg, J. M.; Wang, F. Ultra-Rapid Electrophilic Cysteine Arylation. *J. Am. Chem. Soc.* **2023**, *145* (43), 23427–23432. https://doi.org/10.1021/jacs.3c10334.

(18) Rodriguez, J.; Dhanjee, H. H.; Pentelute, B. L.; Buchwald, S. L. Palladium Mediated Synthesis of Protein–Polyarene Conjugates. *J. Am. Chem. Soc.* **2022**, *144* (26), 11706–11712. https://doi.org/10.1021/jacs.2c03492.

(19) Montgomery, H. R.; Messina, M. S.; Doud, E. A.; Spokoyny, A. M.; Maynard, H. D. Organometallic S-Arylation Reagents for Rapid PEGylation of Biomolecules. *Bioconjug. Chem.* **2022**, *33* (8), 1536–1542. https://doi.org/10.1021/acs.bioconjchem.2c00280.

(20) Doud, E. A.; Tilden, J. A. R.; Treacy, J. W.; Chao, E. Y.; Montgomery, H. R.; Kunkel, G. E.; Olivares, E. J.; Adhami, N.; Kerr, T. A.; Chen, Y.; Rheingold, A. L.; Loo, J. A.; Frost, C. G.; Houk, K. N.; Maynard, H. D.; Spokoyny, A. M. Ultrafast Au(III)-Mediated Arylation of Cysteine. *J. Am. Chem. Soc.* **2024**. https://doi.org/10.1021/jacs.3c12170.

(21) Messina, M. S.; Stauber, J. M.; Waddington, M. A.; Rheingold, A. L.; Maynard, H. D.; Spokoyny, A. M. Organometallic Gold(III) Reagents for Cysteine Arylation. *J. Am. Chem. Soc.* **2018**, *140* (23), 7065–7069. https://doi.org/10.1021/jacs.8b04115.

(22) Stauber, J. M.; Rheingold, A. L.; Spokoyny, A. M. Gold(III) Aryl Complexes as Reagents for Constructing Hybrid Peptide-Based Assemblies via Cysteine S-Arylation. *Inorg. Chem.* **2021**. https://doi.org/10.1021/acs.inorgchem.1c00087.

(23) Stevens, Corey. A.; Kaur, K.; Klok, H.-A. Self-Assembly of Protein-Polymer Conjugates for Drug Delivery. *Adv. Drug Deliv. Rev.* **2021**, *174*, 447–460. https://doi.org/10.1016/j.addr.2021.05.002.

(24) Hamley, I. W. Protein Assemblies: Nature-Inspired and Designed Nanostructures. *Biomacromolecules* **2019**, *20* (5), 1829–1848. https://doi.org/10.1021/acs.biomac.9b00228.

(25) Stefano, J. E.; Bird, J.; Kyazike, J.; Cheng, A. W.-M.; Boudanova, E.; Dwyer, M.; Hou, L.; Qiu, H.; Matthews, G.; O'Callaghan, M.; Pan, C. Q. High-Affinity VEGF Antagonists by Oligomerization of a Minimal Sequence VEGF-Binding Domain. *Bioconjug. Chem.* **2012**, *23* (12), 2354–2364. https://doi.org/10.1021/bc300301m.

(26) Decker, C. G.; Wang, Y.; Paluck, S. J.; Shen, L.; Loo, J. A.; Levine, A. J.; Miller, L. S.; Maynard, H. D. Fibroblast Growth Factor 2 Dimer with Superagonist in Vitro Activity Improves Granulation Tissue Formation during Wound Healing. *Biomaterials* **2016**, *81*, 157–168. https://doi.org/10.1016/j.biomaterials.2015.12.003.

# Chapter 5

# Functionalization of Electrospun Polymer Fibers *via* Organometallic Au(III) Reagents

## 5.1 Introduction

Electrospun fibers are a unique class of functional materials due to the synthetic accessibility of tunable features such as degradability, surface area, pore size, and mechanical performance. As a result, electrospun fibers are utilized in a wide variety of applications including tissue engineering, filtration, and energy storage. To impart additional functionality to these materials in a biological context, the optimization of robust modification strategies with biomolecules of interest is a growing research topic.[172–174] Several classes of bioactive materials can be considered as candidates to improve the biological performance of electrospun fibers, such as peptides for specific cell adhesion,[175] heparin to aid in wound healing,[176] and small molecule drugs for implantable controlled-release cancer treatments.[177]

Physical incorporation is a straightforward method to achieve functionalized fibers. One strategy involves co-spinning a bioactive material with a conventional polymer that is suitable for electrospinning, such as a polyester. However, this method is limited to materials stable to high voltage conditions. Additionally, co-spinning materials must be produced at large molecular weights to avoid undesired electrospraying processes.[178] Another common technique for physical incorporation of bioactive modalities is adsorption *via* electrostatic interactions.[179] Ultimately, all physically incorporated functionalization targets are subject to reversibility due the lability of the relatively weaker intermolecular bonds, which are highly susceptible to the chemical complexities of a biological setting.

The specific and covalent conjugation of targets, rather than simple adhesion, to electrospun fiber networks requires highly efficient chemistry due to the steric hindrance caused by polymer chains. Therefore, “click” type chemistries such as strain-promoted azide-alkyne cycloaddition (SPAAC), maleimide thiol-ene conjugations, and copper (I)-catalyzed azide-alkyne

cycloadditions (CuAAC) have been utilized for this purpose.[180–182] As observed by Sanyal and coworkers, the application of orthogonal "click" chemistries for the fabrication of electrospun fibers can provide access to modularly functional materials, both with respect to functionalization target identity and ratio.[182] Therefore, we hypothesized that our previously developed Au(III) *S*-arylation strategy would be an impactful addition to a growing toolbox for electrospun fiber functionalization due its chemoselective and rapid nature.[114] This work represents the first example of applying this Au(III)-mediated strategy to a heterogenous reaction solution wherein the forged *S*-aryl bond would occur on a material surface. Although chemistry on the solid phase can reduce the time-intensiveness of purification steps, it has also been shown to reduce the yield and purity of macromolecular products.[183] Ultimately, the purpose of this work was to design electrospun fibers such that Au(III) oxidative addition complexes (OAC) could be effective mediators of fiber functionalization *via S*-arylation. Through reaction optimization, we sought to determine whether the reaction robustness of Au(III) OACs in solution would translate to the solid phase. To achieve this, we prepared aryl iodide polymer precursors for electrospinning, to be followed by oxidative

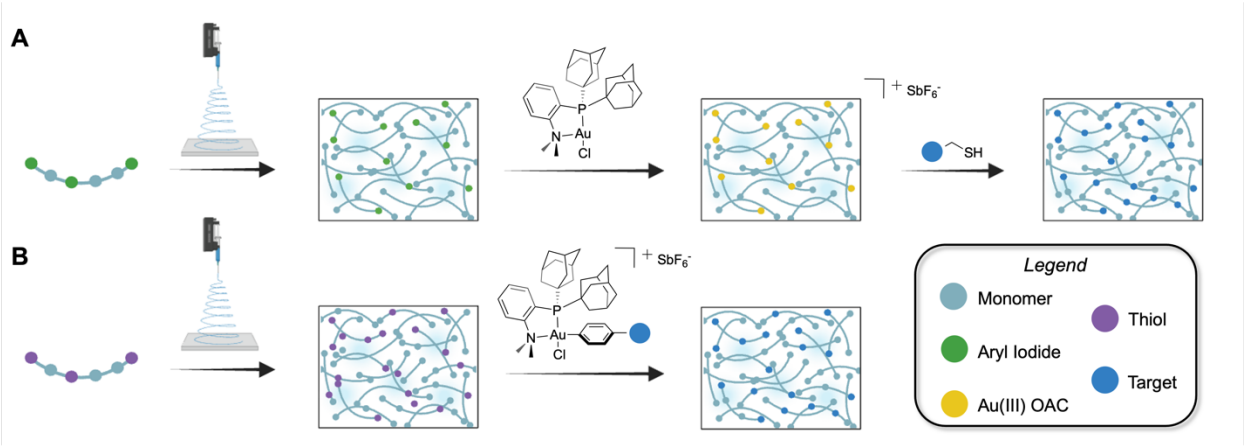


**Figure 5.1** A) Aryl-I polymerization scheme for Au(III)-mediated electrospun fiber functionalization. B) Thiol polymerization scheme for Au(III)-mediated electrospun fiber functionalization.

addition on the fiber surfaces (**Figure 5.1 A**). Separately, we prepared thiol-containing polymer precursors for electrospinning, which would be followed by reductive elimination with Au(III) OAC functionalization targets (**Figure 5.1 B**).

## 5.2 Results and Discussion

### 5.2.1. Preparation of Au(III) Functionalized Electrospun Fibers via Aryl Iodide Polyesters

The first strategy toward Au(III)-mediated fiber functionalization involved the synthesis of aryl iodide (aryl-I) initiated p(caprolactone) (pCL) *via* ring-opening polymerization (ROP) (**Figure 5.2 A**). We selected pCL as an idea candidate for electrospinning, as it is well known to form uniform fibers.[184] In our initial attempts, we synthesized pCL-aryl iodide (**1**), which reached a $M_w$ of 11 kDa by DMF SEC. This molecular weight is considered low for typical electrospinning conditions. However, attempts to increase the molecular weight of **1** resulted in polymer back-biting, which prevented large molecular weights from being reached. Therefore, **1** was mixed with a commercial pCL (80 kDa) at a ratio of 2:1, respectively, prior to electrospinning (see experimental section for further detail). p(Valerolactone) (pVL) (**2**) was also prepared by ROP, reaching a molecular weight of 60 kDa (**Figure 5.2 A**). We hypothesize that the faster kinetics afforded by the smaller ring size of the valerolactone monomer enabled higher molecular weights to be reached, allowing fibers of **2** to be prepared without the addition of a commercial co-polymer.

Fibers were electrospun by collaborators at the University of Auckland in the group of Professor Jadranka Travas-Sejdic (**Figure 5.2 B**, see experimental section for further detail). Although fiber mats containing **1** and **2** could be processed and handled (**Figure 5.2 C**), undesired beading of the polymer materials was observed *via* scanning electron microscopy (SEM) (**Figure 5.2 D-E**). Nevertheless, initial conditions for oxidative addition were screened using these materials. Oxidative addition to form Au(III) reagents is typically performed in DCM,[114] however fiber mats of both **1** and **2** are solubilized by DCM which eliminated the desired fiber morphology. Attempts to reproducibly perform oxidative addition in other solvents, such as acetone and methanol, were unsuccessful and led to the formation of gold nanoparticles or disturbed fiber morphology by SEM.

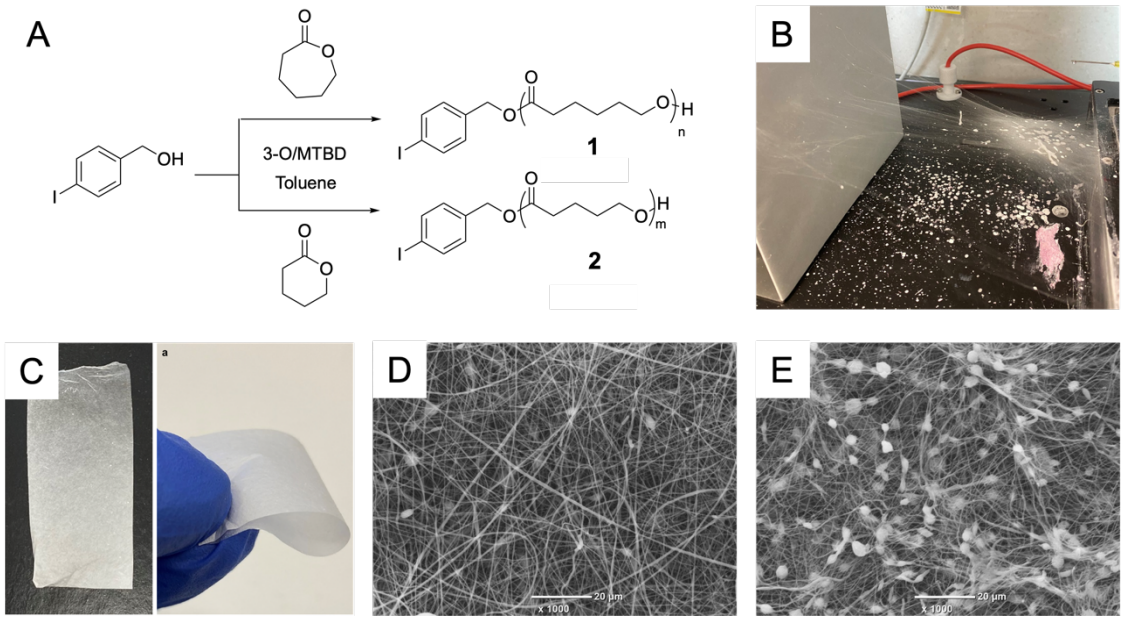


**Figure 5.2** A) ROP scheme for aryl iodide initiated **1** and **2**. B) Electrospinning process. C) Fiber mat consisting of **1** and commercial pCL (80 kDa) D) SEM of **1** and commercial pCL (80 kDa) co-spun fibers. Scale bar is 20 µm. E) SEM of **2** fiber mats. Scale bar is 20 µm. SEM images in this figure were collected by collaborators from the University of Auckland.

### 5.2.2. Preparation of Au(III) Functionalized Electrospun Fibers *via* Aryl Iodide Polynorbornene Imides

From the initial studies using pCL and pVL, it was understood that an ideal polymer candidate for Au(III)-mediated fiber functionalization would reach high molecular weight and be insoluble in DCM. With respect to the former, ring opening metathesis polymerization (ROMP) is an attractive strategy as it is well known to rapidly produce polymers of high molecular weight due to the highly active nature of the third generation Grubbs catalyst (G3).[185] However, ROMP is conventionally performed in DCM, which was undesirable for the oxidative addition process post-electrospinning as polymers soluble in DCM during polymerization would likely dissolve during the electrospinning process. Therefore, we designed a Boc-protected norbornene imide amine derivative (**3**), wherein the Boc protection would provide solubility in DCM during ROMP and the

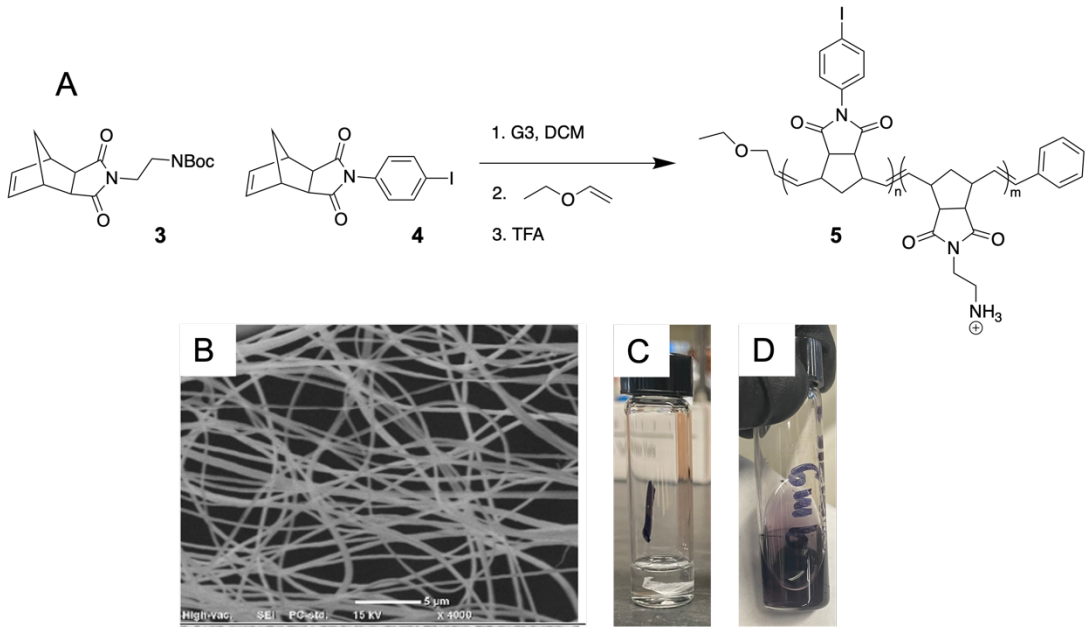


**Figure 5.3** A) ROMP of **3** and **4** to produce random copolymer **5**. B) SEM of **5** fiber mats. Scale bar is 5 µm. C) **5** fiber mats suspended in DCM. D) **5** fiber mats suspended in DCM under oxidative addition conditions (see experimental section for additional detail). SEM images in this figure were collected by collaborators from the University of Auckland.

subsequent deprotection with TFA would prevent its dissolution in DCM during the conjugation post-electrospinning by producing a free amine norbornene imide derivative ($\mathbf{3_{NH2}}$). To improve the accessible degree of functionalization in this second-generation polymer, we also co-polymerized with an aryl-I norbornene imide derivative (**4**) *via* ROMP (**Figure 5.3 A**).

These monomers were polymerized at a ratio of 1 to 4 using **4** and **3**, respectively, and a $M_n$ of >100 kDa was reached (**5**) (see experimental section for further detail). Next, **5** was successfully electrospun into a fiber mat without the inclusion of any additives (**Figure 5.3 B**, see experimental section for further details). As expected, the fiber mat was completely insoluble in DCM (**Figure 5.3 C**). However, oxidative addition was unsuccessful and resulted in a significant formation of gold nanoparticles (**Figure 5.3 D**). We hypothesize that oxidative addition at the solid-liquid interface is sluggish, thus causing the intermediate and unstable Au(I) cation to degrade before the Au(III) complex can be formed.

### 5.2.3. Preparation of Au(III)-mediated Functionalized Electrospun Fibers *via* Thiol Polynorbornene Imides

As an alternative approach, we sought to utilize ROMP to produce thiol-containing high molecular weight polymers. This strategy would allow functionalization at the solid-liquid interface to occur *via* reductive elimination, which is more rapid than oxidative addition.[115]

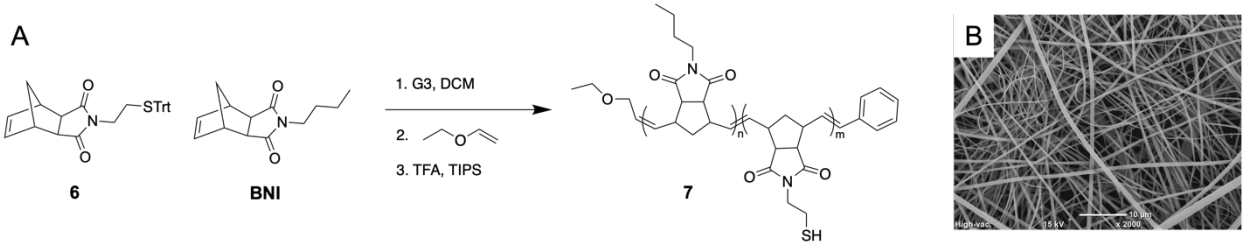


**Figure 5.4** A) ROMP of **6** and **BNI** to produce random copolymer **7**. B) SEM of **7** fiber mats. Scale bar is 10 μm. Images in this figure were collected by collaborators from the University of Auckland.

Separately, oxidative addition of selected functional targets could be performed entirely in the liquid phase, subverting the challenge of the unstable Au(I) cation intermediate. In this case, the resultant fiber mat solubility is only limited to reductive elimination conditions, such that fibers must be insoluble in aqueous buffer. Therefore, Trt-protected thiol nobornene imide derivative (**6**) was synthesized for incorporation in ROMP polymers. Then, **6** was then co-polymerized at a ratio of 1:10 with hydrophobic **BNI** (see Chapter 1 for **BNI** synthetic details) to produce p(BNI-*co*-$NI_{SH}$) (**7**) (**Figure 5.4 A**). Next, **7** was electrospun and fiber morphology was verified by SEM (**Figure 5.4 B**). Following Trt deprotection, a free thiol norbornene imide derivative is hypothesized to be available for *S*-arylation ($NI_{SH}$).

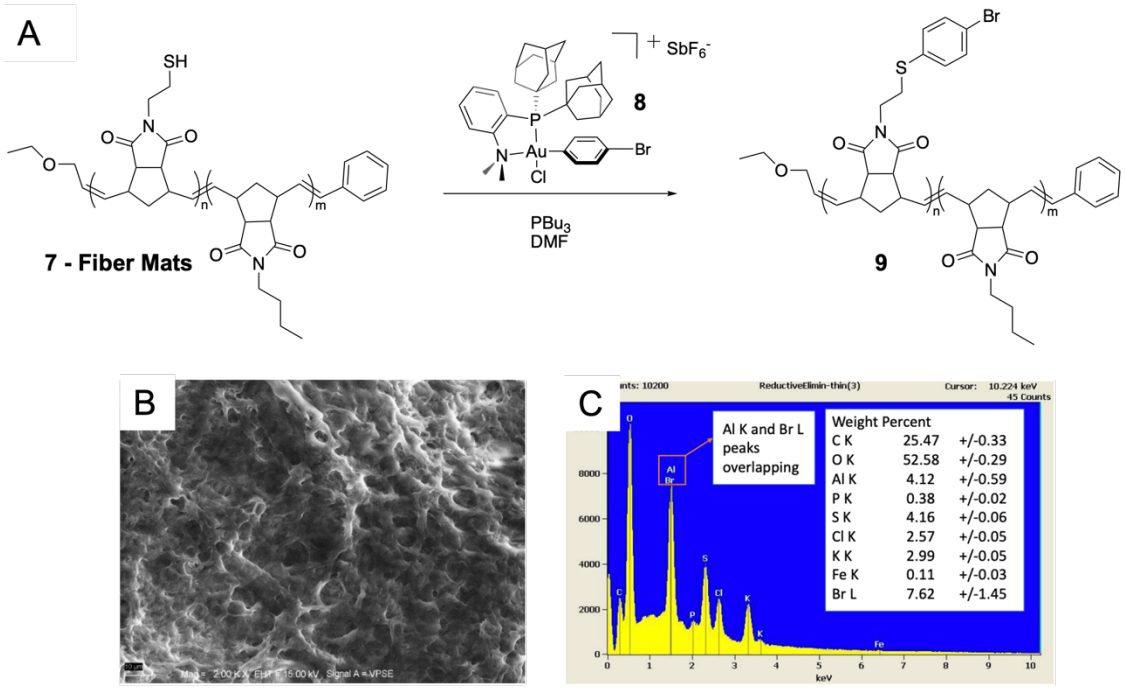


**Figure 5.5** A) Reductive elimination of **8** with **7** fiber mats to produce functionalized fiber mat **9**. B) SEM of **9** fiber mats. Scale bar is 10 µm. C) EDS spectrum of **9** fiber mats. SEM and EDS images in this figure were collected by staff from UCLA CNSI.

As a model substrate, 1-bromo-4-iodobenzene underwent oxidative addition with Au(I)-$Ad_2$ (see Chapter 2 for Au(I)-$Ad_2$ synthetic details) to produce an aryl bromide Au(III) OAC (**8**). Next, reductive elimination of **8** with **7** fiber mats was performed using standard conditions (**Figure 5.5 A**, see experimental section for additional detail). This reaction was initially deemed successful as observed by an appearance of aryl peaks by $^1$H NMR of dissolved fibers (**Figure 5.14**). Further characterization of these functionalized electrospun fibers was conducted by staff scientists at the California NanoSystems Institute (CNSI) at UCLA. Unexpectedly, fiber morphology was significantly disrupted by conventional reductive elimination conditions, as observed by SEM (**Figure 5.5 B**). Furthermore, energy dispersive X-ray spectroscopy (EDS) was inconclusive, as the signal corresponding to bromine overlapped with aluminum and potassium (**Figure 5.5 C**). Therefore, alternative functionalization targets and further reaction optimization was required.

Dye functionalized fibers are known to be well-characterized by UV-visible spectroscopy and fluorescence microscopy.[176] Therefore, we synthesized a BODIPY-Au(III) OAC (**10**) as a model substrate. Reductive elimination with **10** and **7** fiber mats in water hypothetically produced functionalized fibers (**11**). We subjected **11** to significant washing steps with DCM (**Figure 5.6 A**,

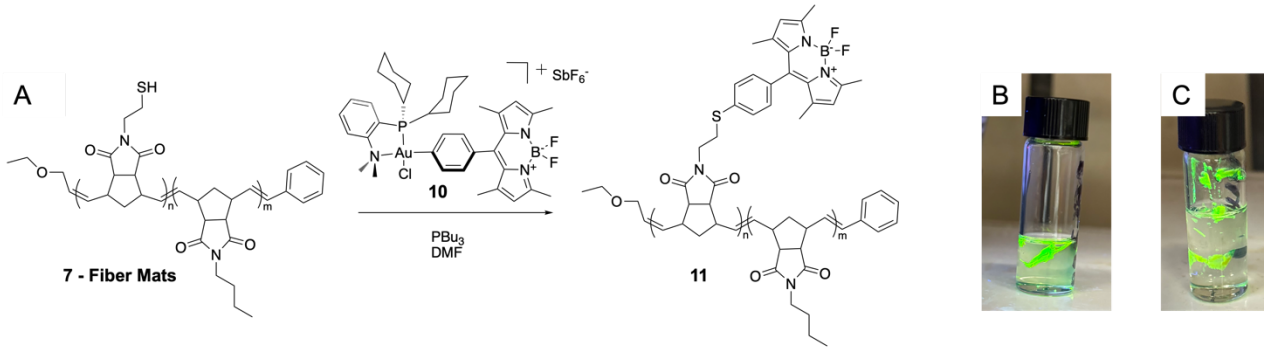


**Figure 5.6** A) Reductive elimination of **10** with **7** fiber mats to produce functionalized fiber mat **11**. B) Fluorescence image of **11**. C) Fluorescence image of Trt-protected **11**.

see experimental section for additional detail) to remove excess **10** that had physically adsorbed to the fiber surface. As a control, reductive elimination conditions using **10** were performed for Trt-protected **7** fiber mats, wherein no *S*-arylation was expected to occur due to the lack of free thiols present at the solid-liquid interface. However, significant fluorescence was observed for both **7** and Trt-protected **7** fiber mats (**Figure 5.6 B-C**). We hypothesize that the DCM washing steps employed for this reaction were not sufficient to remove adsorbed dye from fiber surfaces. Due to these findings, it was challenging to determine whether **11** was successfully prepared, and further optimization is needed. Future work will involve screening additional washing conditions, such as the use of alternative organic solvents, to successfully obtain a negative control.

## 5.3 Conclusion

In this work, we designed several polymer iterations that underwent electrospinning to produce polymer fibers with the intention of using Au(III) OACs to robustly functionalize these materials. Fiber morphology was difficult to retain in conditions suitable for oxidative addition and reductive elimination. The instability of Au(I) cations proved detrimental to reaction progress during slow reaction steps, such as oxidative addition at the solid-liquid interface. Furthermore, characterization of these fibers to determine whether functionalization occurred was not conclusive or reproducible. Therefore, fiber functionalization *via* Au(III) OACs merits further optimization, either by expanding the scope of solvents that can be successful for oxidative addition such that morphology is retained or by using additional tools to investigate reaction conversion, such as FT-IR or Raman spectroscopy.

## 5.4 Experimental

### 5.4.1 Materials

Unless otherwise stated, all materials were purchased and used as received from Fisher Scientific, Combi-Blocks, Alfa Aesar, Oakwood Chemicals, or Sigma Aldrich. Silver hexafluoroantimonate ($AgSbF_6$) was stored in a glovebox maintained under a nitrogen atmosphere prior to use. Polymer **2** was synthesized by Dr. Jane Yang. Polymer **5** and monomers **3** and **4** were synthesized by Dr. Panagiotis Georgiou. Au(I)-$Cy_2$ was prepared by coauthors of a previous publication.[115] Accordingly, the individual characterization data for these materials were not included in this supporting information. Anhydrous DCM and toluene were prepared by distillation over calcium hydride under an argon atmosphere.

### 5.4.2 Analytical Techniques

NMR spectra were recorded on the following: AV400 Bruker spectrometer at 400 ($^1$H); AV300 Bruker spectrometer at 300 ($^1$H); NEO600 Bruker spectrometer at 600 ($^1$H). Spectra are reported in δ (parts per million) relative to residual proteo-solvent signals for $^1$H. The following abbreviations were used to explain multiplicities: s = singlet, d = doublet, t = triplet, q = quartet, m = multiplet. Deuterated solvents were purchased from Cambridge Isotope Laboratories and used as received for all NMR experiments.

DMF Size Exclusion Chromatography (SEC)/Gel Permeation Chromatography (GPC) was conducted on an Agilent 1260 Infinity II high performance liquid chromatography (HPLC) system with a Wyatt Optilab (RI and MALS detection), one Polymer Laboratories PLgel guard column, and two Polymer Laboratories PLgel 5 μm mixed D columns. The eluent was DMF (HPLC Grade, 99.7+%, Thermo Scientific Chemicals) containing LiBr (0.1 M) at 40 °C (Flow rate: 0.6 mL/min).

Molecular weight information was determined for data collected using a PMMA (Agilent Technologies, EasiVial PMMA, preweighed calibration kit) conventional calibration analysis.

Column chromatography was performed on a Biotage Isolera One 3.0 autocolumn instrument using KP-Sil high-performance columns repacked using Silicycle silica (P60, particle size 40–63 μm, column sizes described in experimental). TLC was performed using Millipore Sigma silica plates (60F-254) using short-wave UV light or $KMnO_4$ as visualizing agents.

General electrospinning procedure: each electrospinning solution was loaded into a 3 mL glass syringe equipped with a 21G metal needle. The syringe was then mounted on a syringe pump to provide a steady flow rate of 1 mL $h^{-1}$. A stainless-steel collector plate (20 × 20 cm) was covered with paper and placed 15 cm from the needle tip and grounded. Electrospinning was performed at dark by applying a 15 kV positive potential to the syringe needle. Specific solution details for each sample are provided in Appendix IX (**Table 5.1**). All solutions were prepared in 1:1 DMF:THF v/v.

Scanning electron microscopy (SEM) images were collected by both collaborators from the University of Auckland and staff scientists from UCLA CNSI, and the origin of each image is noted in each figure caption. For SEM images collected from the University of Auckland, the following procedure was followed: samples were fixed on glass slides using carbon tape. A SEM (JCM-6000 Versatile Benchtop SEM) was used to observe the morphology of fiber mats at an accelerating voltage of 15 kV and a magnification of ≥ 800 ×. For SEM and energy dispersive X-ray spectroscopy (EDS) images collected from UCLA CNSI, the following procedure was followed: A SEM (Supra 40VP, Zeiss) at an accelerating voltage of 15 kV with an SE2 detector was used to collect SEM images. Samples were fixed on SEM stubs using carbon tape. EDS maps

were collected at an accelerating voltage of 20 kV using a Proza (Phi-Rho-Z) sigma correction method and a take-off angle of 29.0 degrees.

### 5.4.3 Methods

**ROP of ε-caprolactone to prepare pCL (1)**

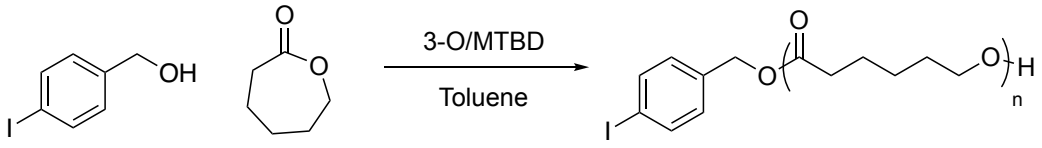


This reaction was performed at 23ºC within a nitrogen filled glovebox. 3-O catalyst (see Chapter 2 for synthetic details) (20.0 mg, 1.2 eq, 21.9 μmol) was weighed in a vial and a stir bar was added. Caprolactone (200.0 mg, 194 μL, 95 eq, 1.8 mmol) was added to a second vial. In a third vial, (4-iodophenyl)methanol (4.3 mg, 1 eq, 18.4 μmol) was measured and added to the 3-O vial using toluene to transfer. Next, MTBD (3.4 mg, 3.1 μL, 1.2 eq, 21.9 μmol) was added to the 3-O vial. Finally, the contents of the caprolactone vial were added to the 3-O reaction vial to initiate the reaction using toluene to transfer. A total of 5 mL anhydrous toluene was added to the reaction mixture. After 60 min, the reaction was quenched with acetic acid outside of the glovebox and monomers were removed *via* precipitation with 45 mL of a cold MeOH/hexanes mixture (20:1 v/v) four times to produce a white powder (Yield: 89 %).

**$^1$H NMR (300 MHz, $CDCl_3$)** δ 7.69 (d, *J* = 8.3 Hz, 2H), 7.09 (d, *J* = 8.3 Hz, 2H), 4.06 (t, *J* = 6.7 Hz, 171H), 2.30 (t, *J* = 7.5 Hz, 173H), 1.83 – 1.53 (m, 391H), 1.51 – 1.21 (m, 176H).

**DMF SEC:** $M_n$=10.4 kDa, $M_w$=10.5 kDa, ~~*Đ*~~= 1.01

**General Oxidative Addition Procedure of Polyester Fiber Mats (Polymers 1 and 2)**

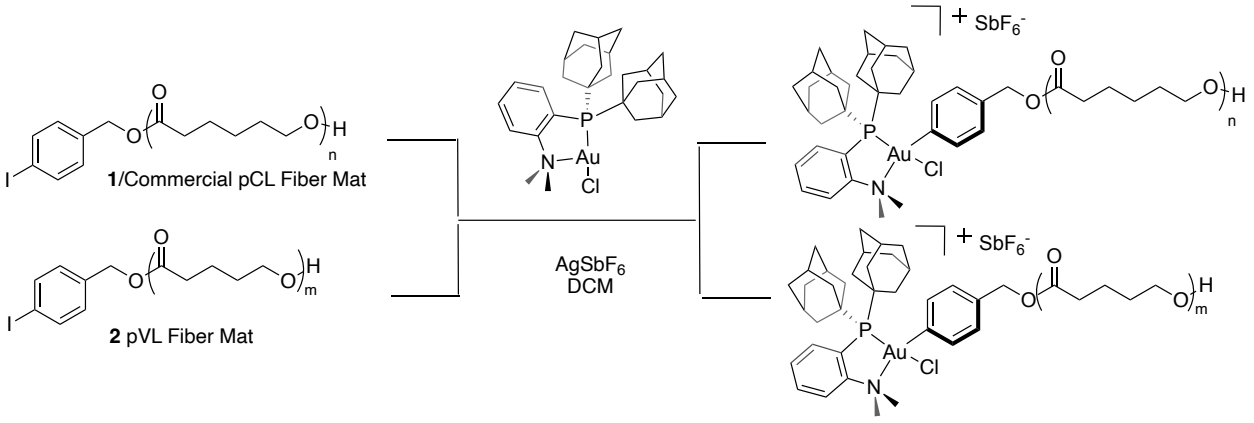


$AgSbF_6$ was removed from a dinitrogen-filled glove box prior to the reaction. (Me-DalPhos)AuCl (see Chapter 2 for synthetic detail) and $AgSbF_6$ were added together with 1 mL DCM and stirred for 1 minute. Visible particulates crashed from the solution. Next, polyester fiber mats were added with an additional 500 µL DCM. The polyester fiber mats dissolved in DCM and the reaction could not proceed. No other solvents (acetone, methanol, DMSO) provided suitable conditions for successful oxidative addition to occur.

**Oxidative Addition Procedure of Polynorbornene imide Fiber Mats (Polymer 5)**

$AgSbF_6$ was removed from a dinitrogen-filled glove box prior to the reaction. Next, (Me-DalPhos)AuCl (see Chapter 2 for synthetic detail) (1.0 mg, 600 eq, 1.5 µmol) was dissolved in 500 µL DCM. 5 (0.51 mg, 1 eq, 0.003 µmol) was added to the solution with 500 µL additional DCM. Finally, $AgSbF_6$ (0.13 mg, 150 eq, 0.4 µmol) was added to the reaction. Significant participates crashed out, but the fibers remained intact. The fibers were agitated by a stir bar for 24 hours. The solution and fibers became purple, indicative of the formation of nanoparticles.

**Synthesis of Trt-protected Thiol Norbornene Imide Monomer (6)**

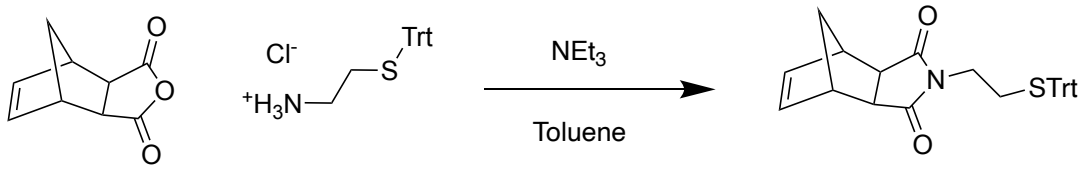


This procedure was adapted from report by Grubbs and coworkers.[17] An oven dried 100 mL pressure tube was charged with a stir bar; cis-5-Norbornene-exo-2,3-dicarboxylic anhydride (400 mg, 1 eq, 2.4 mmol) and 2-(tritylthio)ethan-1-aminium chloride (867 mg, 1 eq, 2.4 mmol) (see Chapter 2 for synthetic detail) were added. The solids were dissolved in 5 mL of toluene and triethylamine (2.0 g, 2.7 mL, 8 eq, 19.5 mmol) was added. The flask was sealed and heated to 160 °C for 2 hours. The solids went into solution completely and resulted in a light-yellow solution. The reaction was cooled to 23 ºC and the solution was added to a separatory funnel and diluted with ethyl acetate. The organic layer was washed with 0.1 M HCl twice. The organic layer was then collected and dried over magnesium sulfate and filtered. The organic layer was concentrated under reduced pressure to yield a sticky light brown oil. This mixture was purified by column chromatography using 0-100% EtOAc in hexanes gradient to produce a white solid (Yield: 44 %).

**$^1$H NMR (400 MHz, DMSO)** δ 7.49 – 7.07 (m, 15H), 6.39 – 6.14 (m, 2H), 3.31 (d, *J* = 6.8 Hz, 2H), 3.05 (t, *J* = 1.9 Hz, 2H), 2.63 (d, *J* = 1.3 Hz, 2H), 2.32 (t, *J* = 6.9 Hz, 2H), 1.37 – 1.12 (m, 2H).

**Synthesis of p(BNI-*co*-NI$_{SH}$) (7)**

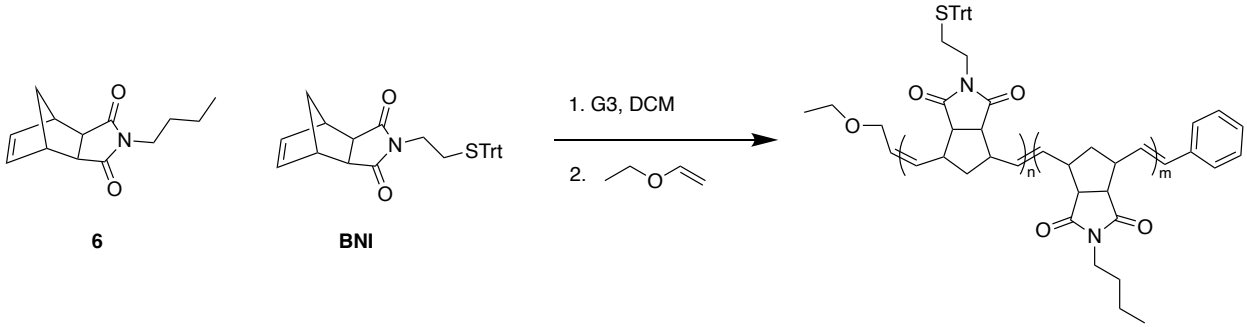


6 (841.3 mg, 566 eq, 3.8 mmol) and BNI (see Chapter 2 for synthetic detail) (357 mg, 113.2 eq, 767 μmol) were added to a schlenk flask with 1 mL anhydrous DCM and underwent three freeze-pump-thaw cycles. Next, Grubbs 3$^{rd}$ Generation Catalyst (G3) (6.0 mg, 1 eq, 6.8 μmol) was added with 0.2 mL anhydrous DCM under argon. Ethyl vinyl ether (244 mg, 322 μL, 500 eq, 3.4 mmol) was added to quench the reaction. The quenched reaction stirred for 15 hours, followed by three precipitations in cold diethyl ether to produce a tan solid (Yield: 33 %).

**$^1$H NMR (400 MHz, DMSO)** δ 7.46 – 7.05 (m, 15H), 5.69 – 5.28 (m, 23H), 3.02 (s, 35H), 1.58 – 1.31 (m, 32H), 1.28 – 1.07 (m, 22H), 0.94 – 0.72 (m, 31H). * Note that in the absence of a defined end-group, the trityl group is integrated to 15 to observe the ratio between the monomer types (~10:1 BNI to **6**, respectively).

**DMF SEC:** $M_n$=160.0 kDa, $M_w$=190.1 kDa, ~~$Đ$~~= 1.19

**Synthesis of *para*-bromobenzene Au(III)-Ad$_2$ OAC (8)**

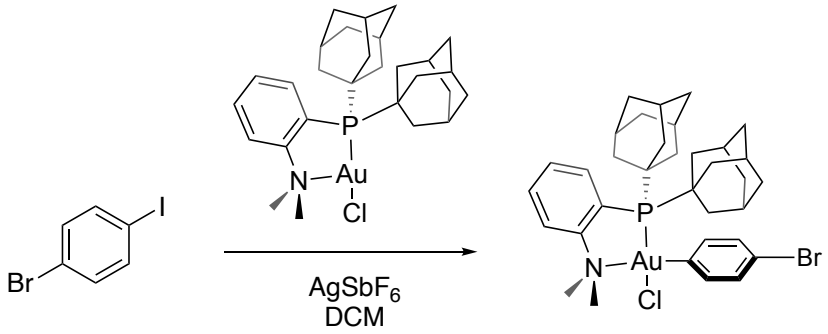


$AgSbF_6$ was removed from a dinitrogen-filled glove box prior to the reaction. (Me-DalPhos)AuCl (20.0 mg, 1 eq, 30.6 μmol) and $AgSbF_6$ (10.5 mg, 1 eq, 30.6 μmol) were added together with 1.5 mL DCM and stirred for 1 minute. Visible particulates crashed from the solution. Next, 1-bromo-4-iodobenzene (43.3 mg, 5 eq, 152.9 μmol) was added with an additional 500 μL DCM. The reaction was stirred for 18 hours at 23 ºC. The crude product was filtered through Celite and precipitated in 1:3 THF to $Et_2O$. Finally, the solvents were removed under reduced pressure. The product was isolated as an off-white solid (Yield 63 %).

**$^1$H NMR (600 MHz, $CD_2Cl_2$)** δ 8.05 – 7.85 (m, 3H), 7.81 – 7.72 (m, 1H), 7.56 – 7.46 (m, 2H), 7.42 – 7.32 (m, 2H), 3.47 – 3.33 (m, 6H), 2.31 – 2.23 (m, 6H), 2.19 – 2.01 (m, 13H), 1.77 (d, $J$ = 29.1 Hz, 12H).

**$^{31}$P NMR (243 MHz, $CD_2Cl_2$)** δ 76.50.

**Synthesis of p(BNI-*co*-NI$_{\text{Aryl Br}}$) Fiber Mats (9)**

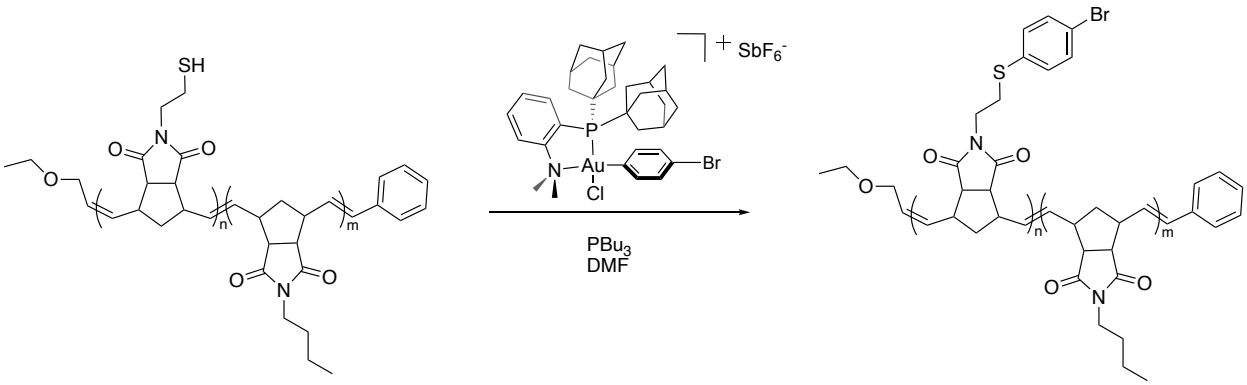


**7** fiber mats (1.2 mg, 1 eq, 0.006 μmol) was reduced with tributyl phosphine (199 μg, 245 nL, 160 eq, 1.0 μmol) for 1 hour in 250 μL MilliQ $H_2O$ at 23 ºC. **7** was insoluble and floated freely in solution. **7** was agitated using a small stir bar. 8 (399 μg, 80 eq, 0.5 μmol) and potassium carbonate (85.1 μg, 100 eq, 0.6 μmol) was added to the solution with an additional 250 μL MilliQ $H_2O$. The reaction progressed for 20 hours at 23 ºC. The resulting fiber was removed from the water solution and washed several times with a stream of DCM.

**$^1$H NMR (600 MHz, DMSO)** δ 8.17 – 8.10 (m, 2H), 7.66 – 7.38 (m, 2H), 5.79 – 5.27 (m, 23H), 3.12 – 2.96 (m, 32H), 1.60 – 1.29 (m, 47H), 1.26 – 1.10 (m, 32H), 0.89 – 0.65 (m, 48H). Note that in the absence of a defined end-group, an aryl Br peak is integrated to 2 to observe the ratio between BNI and aryl Br (~8:1 BNI to Aryl Br, respectively).

**Synthesis of BODIPY-Au(III) OAC (10)**

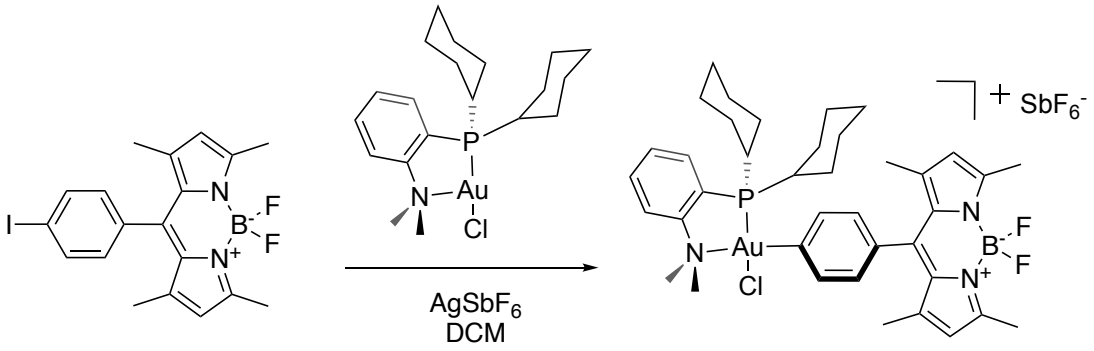


$AgSbF_6$ was removed from a dinitrogen-filled glove box prior to the reaction. Au(I)-$Cy_2$ (see Chapter 4 for synthetic details) (16.3 mg, 1 eq, 29.6 μmol) and $AgSbF_6$ (110.2 mg, 1 eq, 29.6 μmol) were added together with 1.5 mL DCM and stirred for 1 minute. Visible particulates crashed from the solution. Next, BODIPY (20.0 mg, 1.5 eq, 44.4 μmol) was added with an additional 500 μL DCM. The reaction was stirred for 18 hours at 23 ºC. The crude product was filtered through Celite and triturated in 3:4 hexanes to EtOAc. Finally, the solvents were removed under reduced pressure. The product was isolated as an off-white solid (Yield 59 %).

**$^1$H NMR (600 MHz, $CD_2Cl_2$)** δ 8.09 – 7.98 (m, 1H), 7.96 – 7.89 (m, 1H), 7.86 – 7.78 (m, 2H), 7.45 (d, *J* = 8.2 Hz, 2H), 7.39 (d, *J* = 8.2 Hz, 2H), 6.07 (s, 2H), 3.49 (s, 6H), 2.84 – 2.72 (m, 2H), 2.54 (s, 6H), 1.97 – 1.74 (m, 12H), 1.57 – 1.26 (m, 13H), 1.20 – 0.99 (m, 7H).

**$^{31}$P NMR (243 MHz, $CD_2Cl_2$)** δ 60.01.

**Synthesis of p(BNI-*co*-NI$_{BODIPY}$) Fiber Mats (11)**

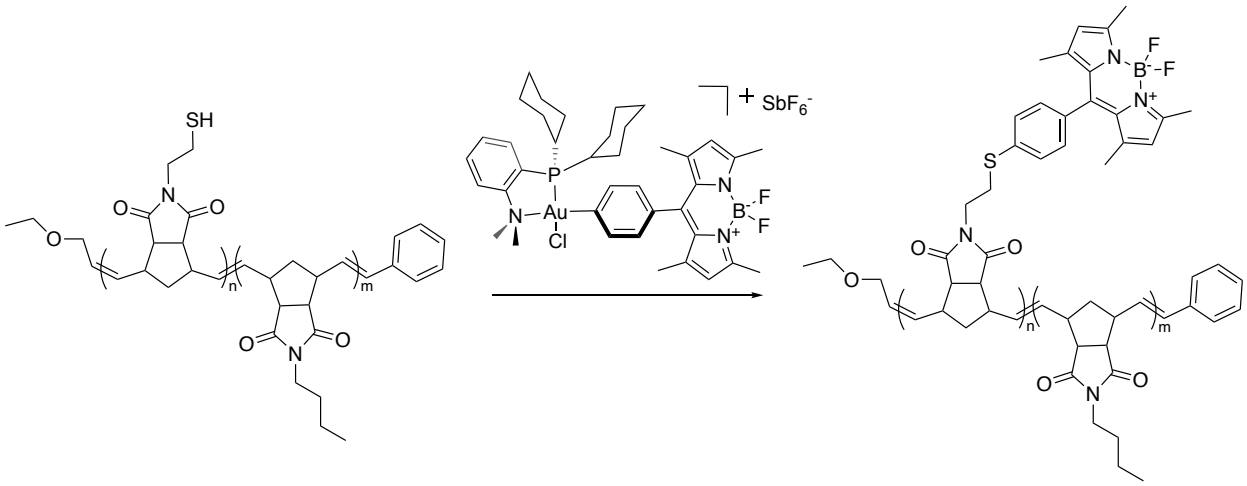

**7** fiber mats (1.2 mg, 1 eq, 0.006 μmol) was reduced with tributyl phosphine (199 μg, 245 nL, 160 eq, 1.0 μmol) for 1 hour in 250 μL MilliQ $H_2O$ at 23 ºC. **7** was insoluble and floated freely in solution. **7** was agitated using a small stir bar. 10 (568 μg, 80 eq, 0.5 μmol) and potassium carbonate (85.1 μg, 100 eq, 0.6 μmol) was added to the solution with an additional 250 μL MilliQ $H_2O$. The reaction progressed for 22 hours at 23 ºC. The resulting fiber was removed from the water solution and washed several times with a stream of DCM.

# 5.6 Appendix IV

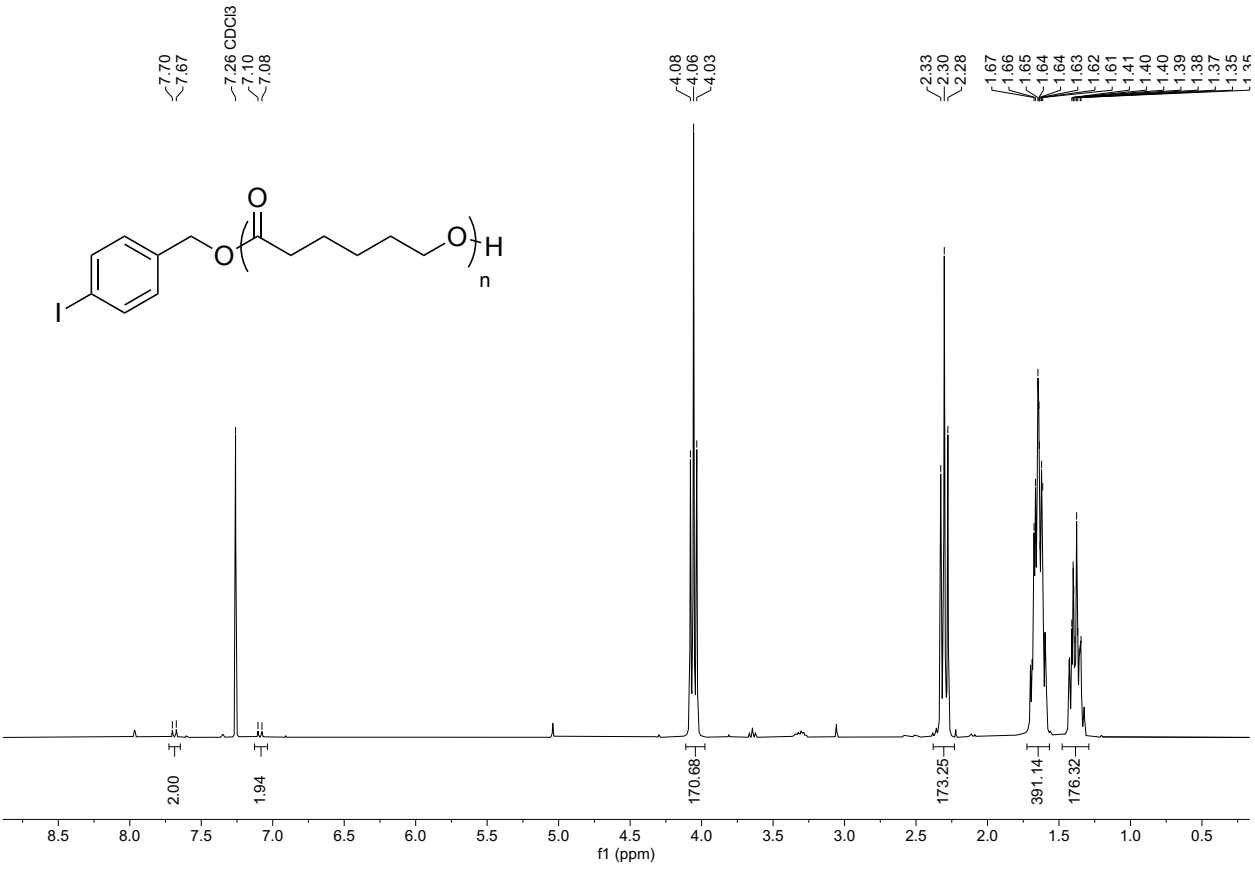


**Figure 5.7** $^{1}$H NMR of pCL-aryl I (**1**) in $CDCl_3$ at 23 ºC.

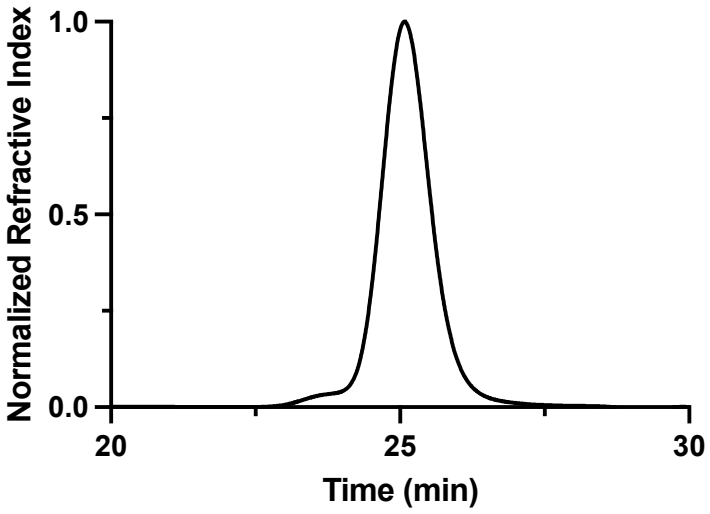


**Figure 5.8** DMF SEC of pCL-aryl I (**1**).

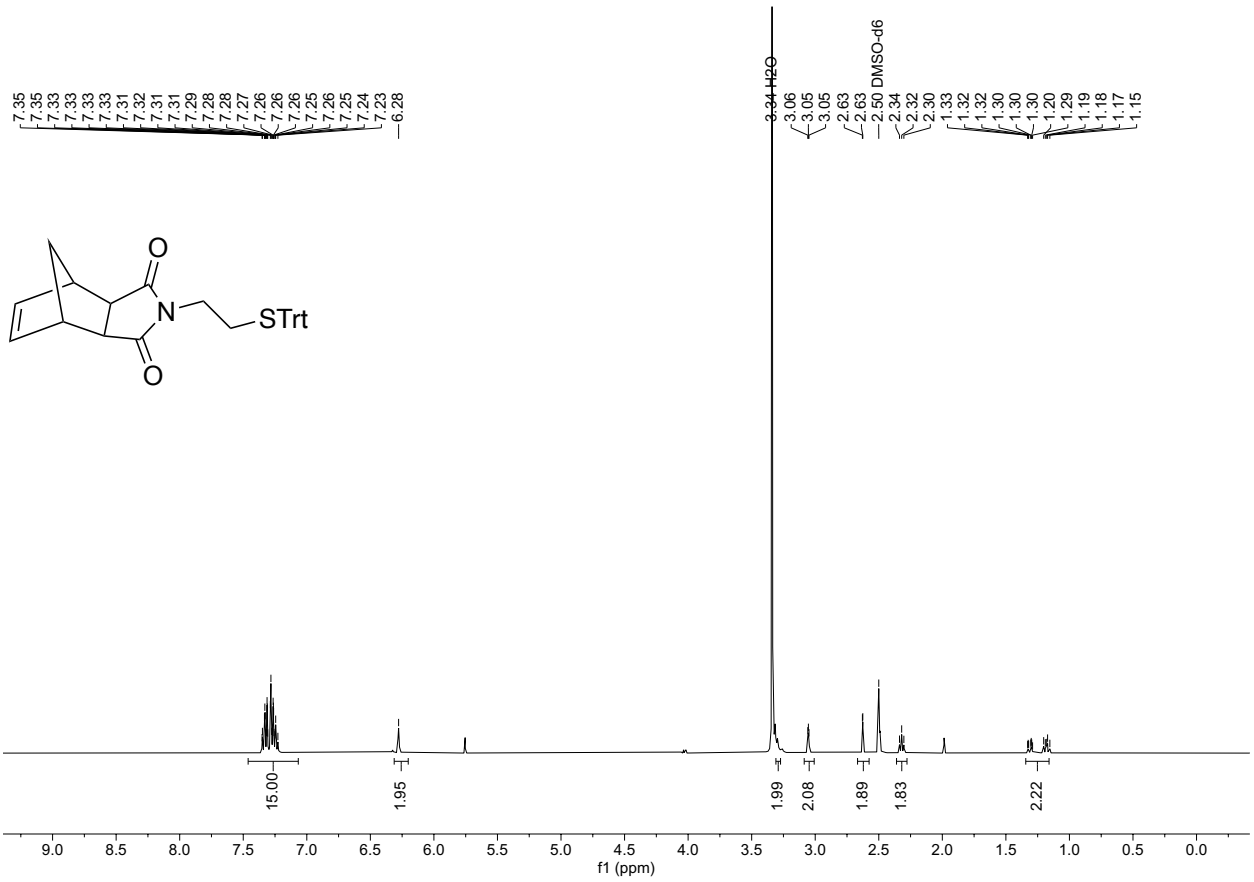


**Figure 5.9** $^{1}$H NMR of Trt-protected thiol norbornene imide monomer (**6**) in DMSO-$d_6$ at 23 ºC.

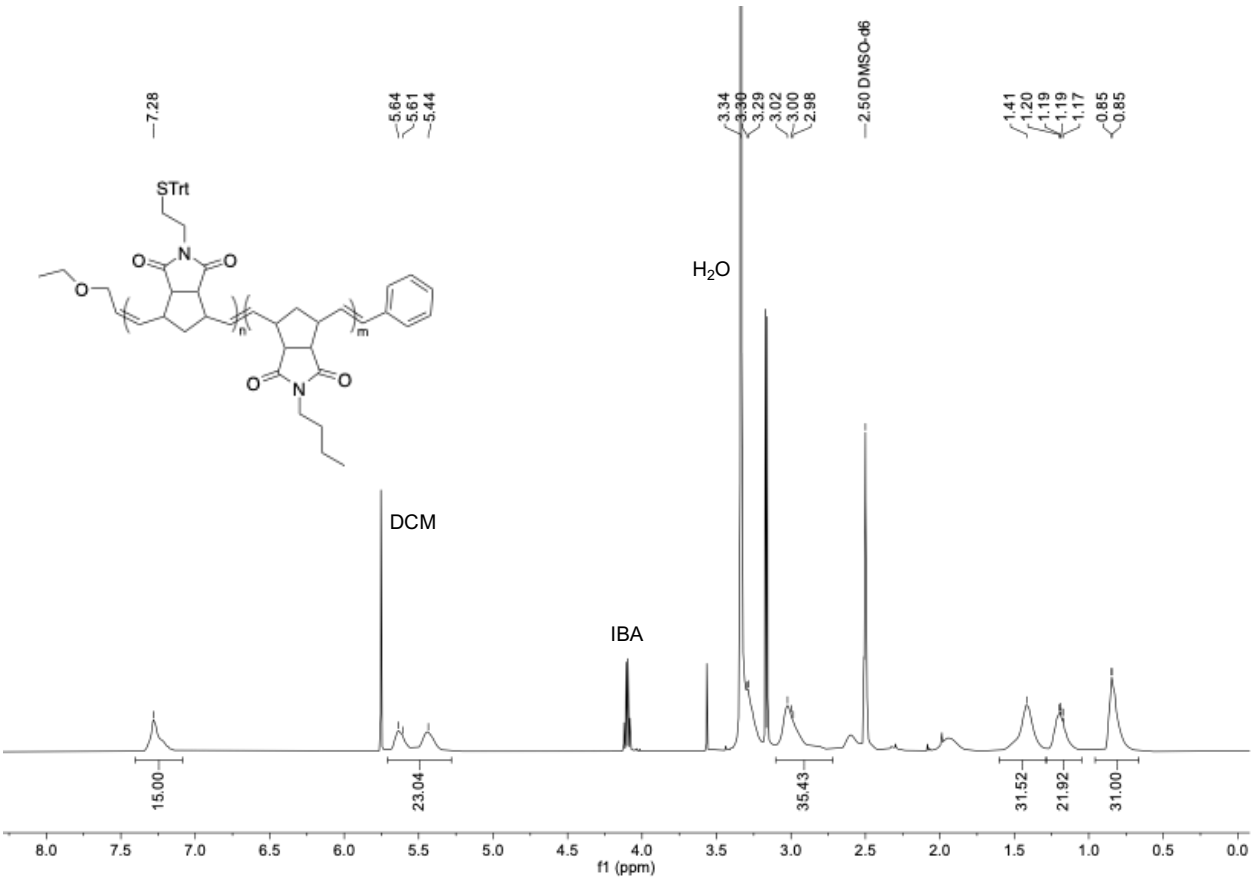


**Figure 5.10** $^{1}$H NMR of p(BNI-*co*-NI$_{SH}$) (**7**) in DMSO-d$_6$ at 23 ºC. Note that in the absence of a defined end-group, the trityl group is integrated to 15 to observe the ratio between the monomer types (~10:1 BNI to **6**, respectively).

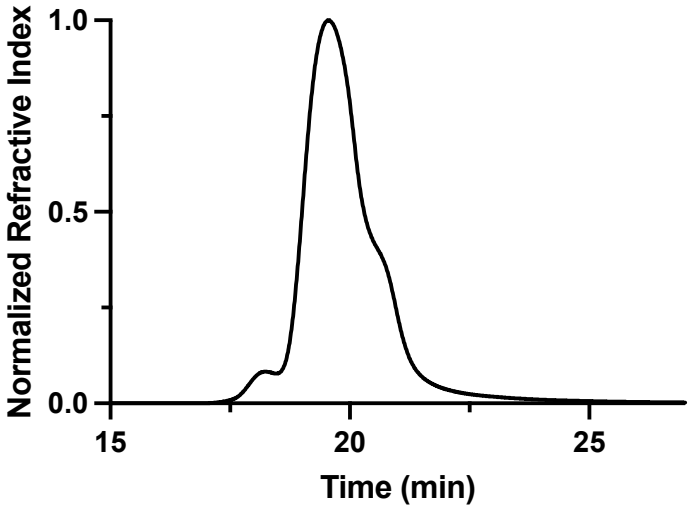


**Figure 5.11** DMF SEC of p(BNI-*co*-$NI_{SH}$) (**7**)**.**

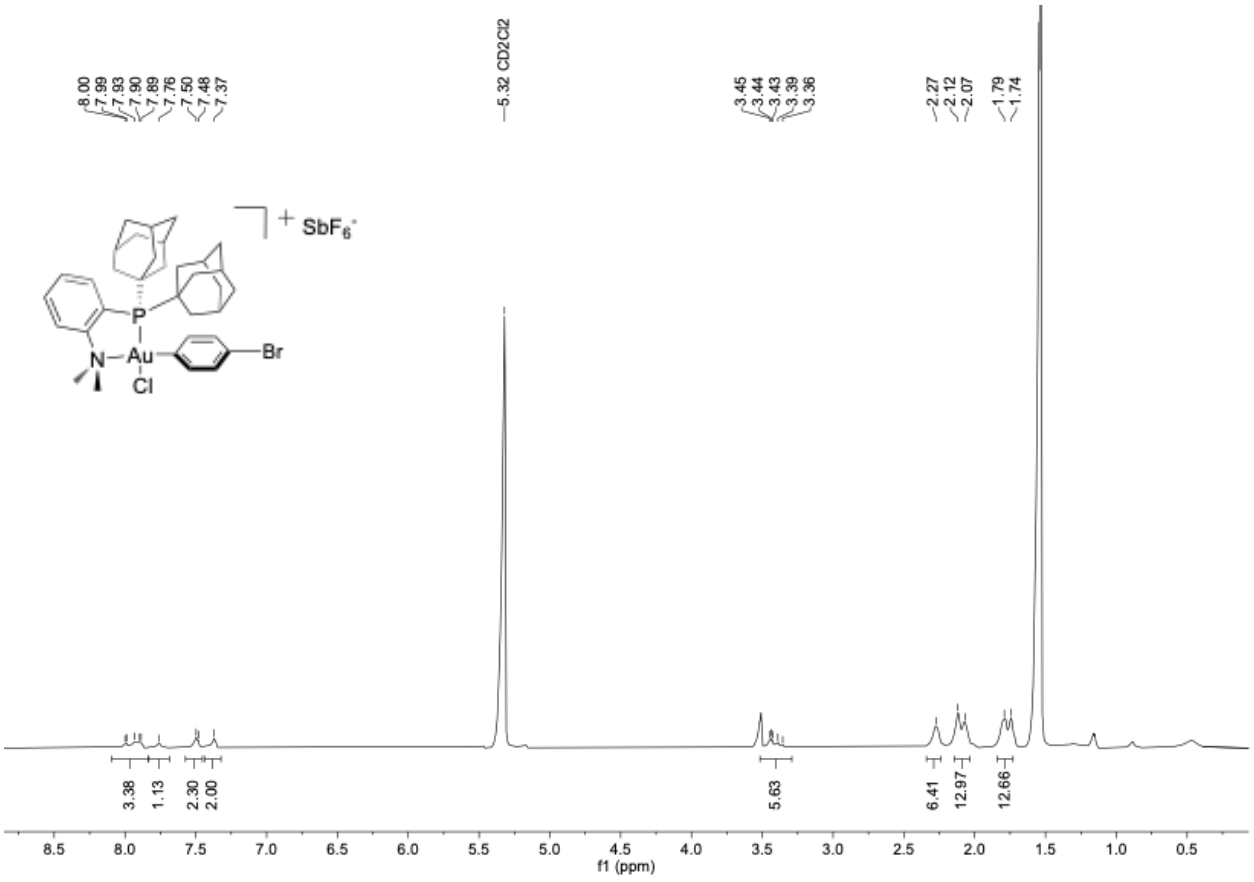


**Figure 5.12** $^{1}$H NMR of *para*-bromobenzene Au(III)-Ad$_2$ OAC (**8**) in $CD_2Cl_2$ at 23 ºC.

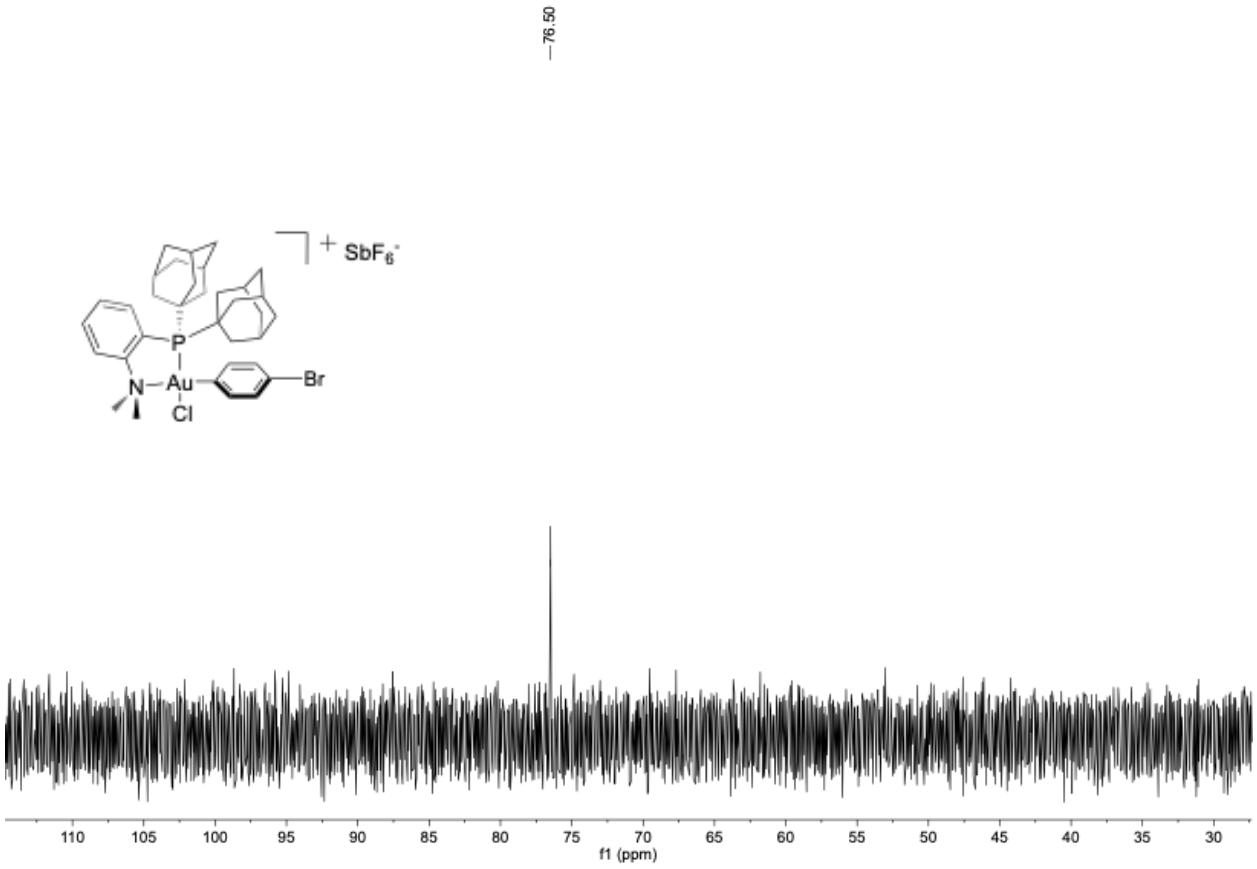


**Figure 5.13** $^{31}P\{^{1}H\}$ NMR of *para*-bromobenzene Au(III)-$Ad_2$ OAC (**8**) in $CD_2Cl_2$ at 23 ºC.

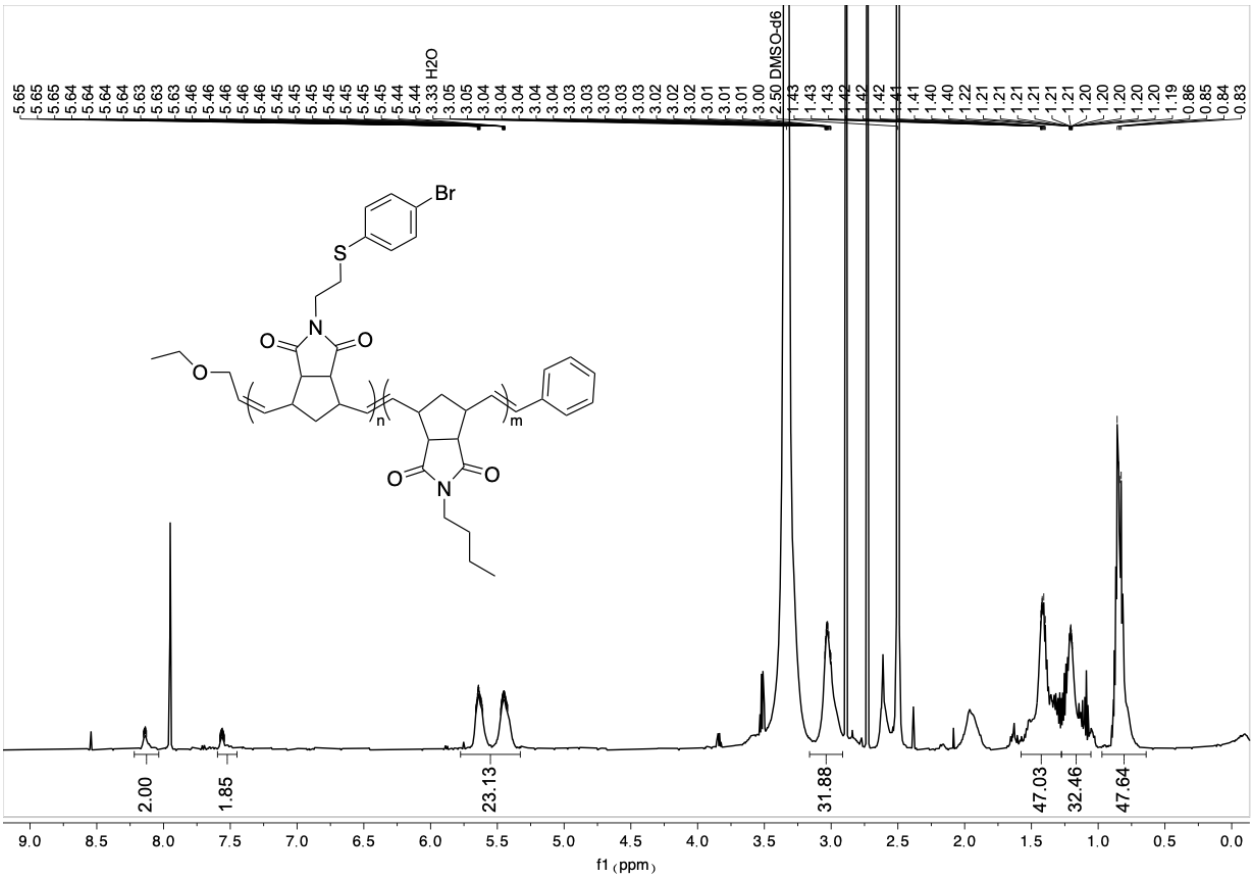


**Figure 5.14** $^{1}$H NMR of p(BNI-*co*-NI$_{\text{Aryl Br}}$) (**9**) in $CD_2Cl_2$ at 23 ºC. Note that in the absence of a defined end-group, an aryl Br peak is integrated to 2 to observe the ratio between BNI and aryl Br (~8:1 BNI to Aryl Br, respectively).

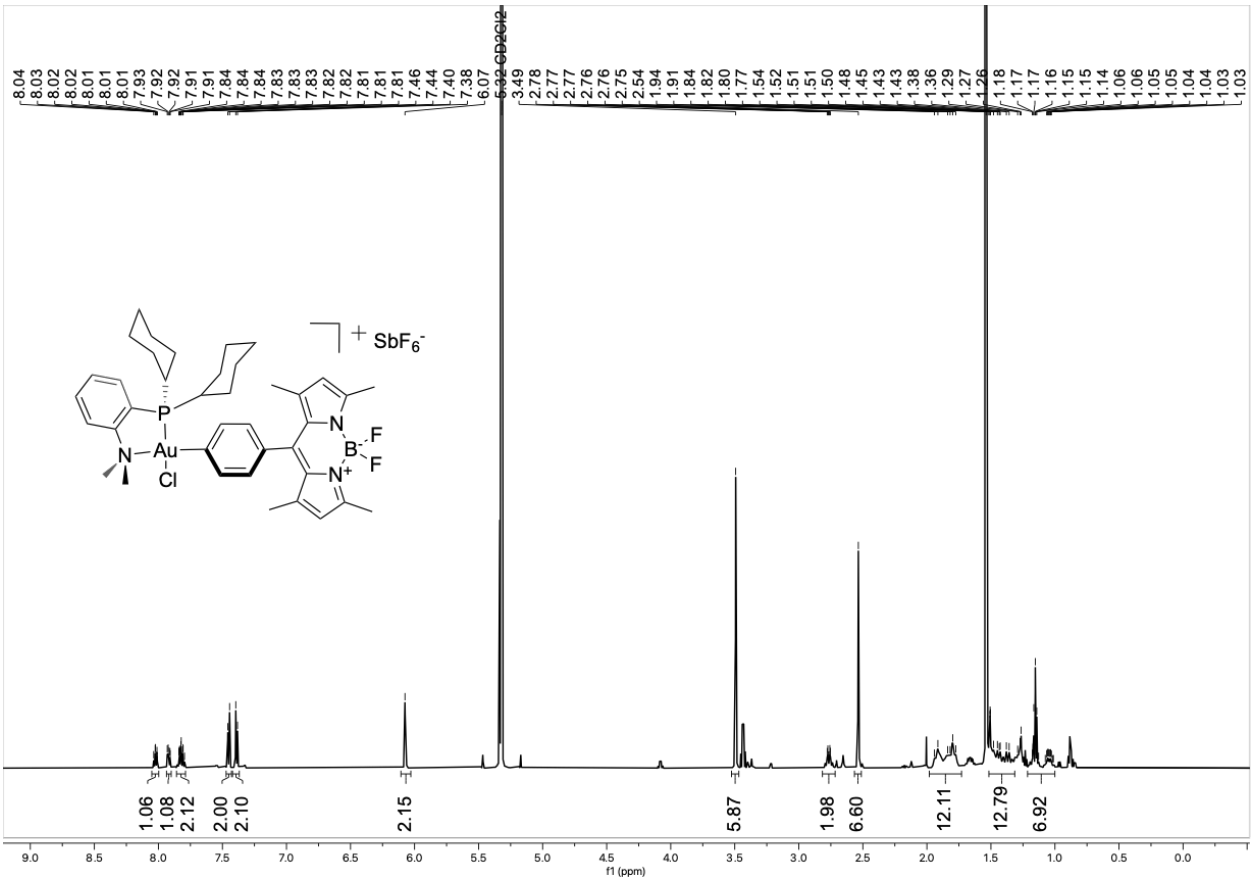


**Figure 5.15** $^{1}$H NMR of BODIPY-Au(III) OAC **(10)** in $CD_2Cl_2$ at 23 ºC.

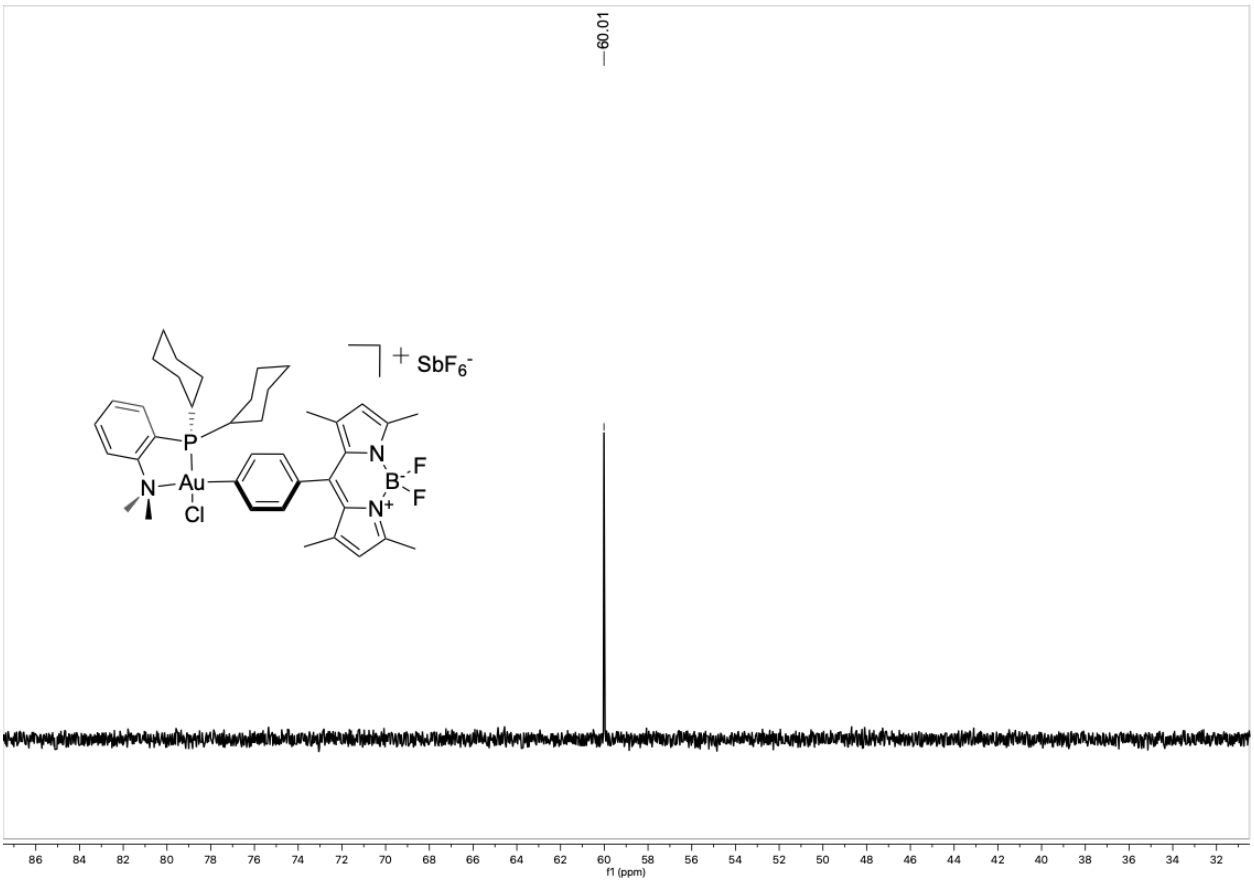


**Figure 5.16** $^{31}P\{^{1}H\}$ NMR of BODIPY-Au(III) OAC **(10)** in $CD_2Cl_2$ at 23 ºC.

**Table 5.1:** Electrospinning Solution Conditions

| Polymer | Aryl-I Polymer Concentration (g/mL) | Commercial pCL Concentration (g/mL) | Total Concentration (g/mL) | Aryl-I to Commercial Polymer Ratio |
|---|---|---|---|---|
| **1** | 10 | 5 | 15 | 2:1 |
| **2** | 15 | 0 | 15 | -- |
| **7** | 10 | 0 | 10 | -- |

## 5.5 References


(1) Jordan, A. M.; Viswanath, V.; Kim, S.-E.; Pokorski, J. K.; Korley, L. T. J. Processing and Surface Modification of Polymer Nanofibers for Biological Scaffolds: A Review. *J. Mater. Chem. B* **2016**, *4* (36), 5958–5974. https://doi.org/10.1039/C6TB01303A.

(2) Taskin, M. B.; Ahmad, T.; Wistlich, L.; Meinel, L.; Schmitz, M.; Rossi, A.; Groll, J. Bioactive Electrospun Fibers: Fabrication Strategies and a Critical Review of Surface-Sensitive Characterization and Quantification. *Chem. Rev.* **2021**, *121* (18), 11194–11237. https://doi.org/10.1021/acs.chemrev.0c00816.

(3) Sagitha, P.; Reshmi, C. R.; Sundaran, S. P.; Sujith, A. Recent Advances in Post-Modification Strategies of Polymeric Electrospun Membranes. *Eur. Polym. J.* **2018**, *105*, 227–249. https://doi.org/10.1016/j.eurpolymj.2018.05.033.

(4) Kaur, G.; Kumari, S.; Saha, P.; Ali, R.; Patil, S.; Ganesh, S.; Verma, S. Selective Cell Adhesion on Peptide–Polymer Electrospun Fiber Mats. *ACS Omega* **2019**, *4* (2), 4376–4383. https://doi.org/10.1021/acsomega.8b03494.

(5) Casper, C. L.; Yamaguchi, N.; Kiick, K. L.; Rabolt, J. F. Functionalizing Electrospun Fibers with Biologically Relevant Macromolecules. *Biomacromolecules* **2005**, *6* (4), 1998–2007. https://doi.org/10.1021/bm050007e.

(6) Sasikala, A. R. K.; Unnithan, A. R.; Yun, Y.-H.; Park, C. H.; Kim, C. S. An Implantable Smart Magnetic Nanofiber Device for Endoscopic Hyperthermia Treatment and Tumor-Triggered Controlled Drug Release. *Acta Biomater.* **2016**, *31*, 122–133. https://doi.org/10.1016/j.actbio.2015.12.015.

(7) Anu Bhushani, J.; Anandharamakrishnan, C. Electrospinning and Electrospraying Techniques: Potential Food Based Applications. *Trends Food Sci. Technol.* **2014**, *38* (1), 21–33. https://doi.org/10.1016/j.tifs.2014.03.004.

(8) He, L.; Tang, S.; Prabhakaran, M. P.; Liao, S.; Tian, L.; Zhang, Y.; Xue, W.; Ramakrishna, S. Surface Modification of PLLA Nano-Scaffolds with Laminin Multilayer by LbL Assembly for Enhancing Neurite Outgrowth. *Macromol. Biosci.* **2013**, *13* (11), 1601–1609. https://doi.org/10.1002/mabi.201300177.

(9) Lancuški, A.; Fort, S.; Bossard, F. Electrospun Azido-PCL Nanofibers for Enhanced Surface Functionalization by Click Chemistry. *ACS Appl. Mater. Interfaces* **2012**, *4* (12), 6499–6504. https://doi.org/10.1021/am301458y.

(10) Kalaoglu-Altan, O. I.; Sanyal, R.; Sanyal, A. Reactive and 'Clickable' Electrospun Polymeric Nanofibers. *Polym. Chem.* **2015**, *6* (18), 3372–3381. https://doi.org/10.1039/C5PY00098J.

(11) Kalaoglu-Altan, O. I.; Sanyal, R.; Sanyal, A. Orthogonally "Clickable" Biodegradable Nanofibers: Tailoring Biomaterials for Specific Protein Immobilization. *ACS Omega* **2019**, *4* (1), 121–129. https://doi.org/10.1021/acsomega.8b03041.

(12) Messina, M. S.; Stauber, J. M.; Waddington, M. A.; Rheingold, A. L.; Maynard, H. D.; Spokoyny, A. M. Organometallic Gold(III) Reagents for Cysteine Arylation. *J. Am. Chem. Soc.* **2018**, *140* (23), 7065–7069. https://doi.org/10.1021/jacs.8b04115.

(13) O. Holloway, J.; S. Wetzel, K.; Martens, S.; Prez, F. E. D.; R. Meier, M. A. Direct Comparison of Solution and Solid Phase Synthesis of Sequence-Defined Macromolecules. *Polym. Chem.* **2019**, *10* (28), 3859–3867. https://doi.org/10.1039/C9PY00558G.

(14) Cipitria, A.; Skelton, A.; Dargaville, T. R.; Dalton, P. D.; Hutmacher, D. W. Design, Fabrication and Characterization of PCL Electrospun Scaffolds—a Review. *J. Mater. Chem.* **2011**, *21* (26), 9419–9453. https://doi.org/10.1039/C0JM04502K.

(15) Hyatt, M. G.; Walsh, D. J.; Lord, R. L.; Andino Martinez, J. G.; Guironnet, D. Mechanistic and Kinetic Studies of the Ring Opening Metathesis Polymerization of Norbornenyl Monomers by a Grubbs Third Generation Catalyst. *J. Am. Chem. Soc.* **2019**, *141* (44), 17918–17925. https://doi.org/10.1021/jacs.9b09752.

(16) Doud, E. A.; Tilden, J. A. R.; Treacy, J. W.; Chao, E. Y.; Montgomery, H. R.; Kunkel, G. E.; Olivares, E. J.; Adhami, N.; Kerr, T. A.; Chen, Y.; Rheingold, A. L.; Loo, J. A.; Frost, C. G.; Houk, K. N.; Maynard, H. D.; Spokoyny, A. M. Ultrafast Au(III)-Mediated Arylation of Cysteine. *J. Am. Chem. Soc.* **2024**, *146* (18), 12365–12374. https://doi.org/10.1021/jacs.3c12170.

(17) Matson, J. B.; Grubbs, R. H. Synthesis of Fluorine-18 Functionalized Nanoparticles for Use as in Vivo Molecular Imaging Agents. *J. Am. Chem. Soc.* **2008**, *130* (21), 6731–6733. https://doi.org/10.1021/ja802010d.